Optimal sizing and energy management of storage systems for renewable sources deployment, design of a LVDC microgrid

Jérémy Dulout

THÈSE

En vue de l'obtention du

DOCTORAT DE L'UNIVERSITÉ DE TOULOUSE

Délivré par :

Université Toulouse 3 Paul Sabatier (UT3 Paul Sabatier)

Présentée et soutenue par :
Jérémy DULOUT

le vendredi 8 décembre 2017

Titre :

Dimensionnement et gestion optimaux d'éléments de stockage pour le déploiement de sources renouvelables, réalisation d'un micro-réseau LVDC.

Optimal sizing and energy management of storage systems for renewable sources deployment, design of a LVDC microgrid.

École doctorale et discipline ou spécialité :
ED GEET : Génie Électrique

Unité de recherche :
LAAS-CNRS (UPR 8001) - Équipe Intégration de Systèmes de Gestion de l'énergie (ISGE)

Directeur/trice(s) de Thèse :
Mme Corinne ALONSO, Prof. Université Toulouse 3 Paul Sabatier – LAAS-CNRS
M. Bruno JAMMES, MdC. Université Toulouse 3 Paul Sabatier – LAAS-CNRS

Jury :

M. Jean-Michel VINASSA, Prof. Bordeaux INP – IMS, Rapporteur
M. J. Marcos ALONSO, Prof. Université d'Oviedo (Espagne), Rapporteur
Mme Marise BAFLEUR, Directrice de recherche LAAS-CNRS, Examinatrice
M. Carlos Eduardo CARREJO GONZALES, Dr. Ing. Vestas Wind Systems A/S, Examinateur
M. Josep M. GUERRERO, Prof. Université d'Aalborg (Danemark), Invité

Résumé

Dimensionnement et gestion optimaux d'éléments de stockage pour le déploiement de sources renouvelables, réalisation d'un micro-réseau LVDC

La forte consommation des énergies fossiles au niveau mondial entraine une raréfaction de ces ressources et met en danger l'équilibre environnemental global du fait de la pollution qu'elle engendre. D'autres sources d'énergie dites renouvelables se développent afin de proposer un mix énergétique très diversifié et progressivement décarboné. Par exemple, dans un contexte urbain, le solaire photovoltaïque présente de nombreux atouts comme la possibilité de produire de l'électricité de façon décentralisée, l'intégration aisée dans les bâtiments et infrastructures publiques, la réduction des pertes liées au transport de l'électricité, pas de pollution sonore, pas ou peu d'impact sur l'écosystème environnant, etc. Cependant, cette source est très intermittente et difficilement prédictible (diverses échelles de temps liées au passage de nuages, cycle diurne ou cycle saisonnier) et doit être implantée dans des endroits sans ombrage d'infrastructure pour assurer la meilleure production et durée de vie. De plus, sa production n'est généralement pas temporellement en phase avec des profils de consommation de type résidentiel ou tertiaire.

Afin de répondre à la problématique d'intégration des énergies renouvelables dans nos réseaux électriques conventionnels, l'usage de moyens de stockage, par exemple de type électrochimique, semble aujourd'hui la meilleure solution, en considérant le coût, la sécurité d'approvisionnement, la maturité technologique et la facilité de mise en œuvre. Ainsi, de nouveaux micro-réseaux constitués de sources décentralisées et d'éléments de stockage apparaissent en concurrence du réseau centralisé conventionnel ou en complément de ce dernier afin d'atteindre de nouveaux objectifs (stabilité accrue du réseau, mode isolé de secours en cas de panne avec possibilité d'aider le redémarrage du réseau principal, remplacement de générateurs diesel auxiliaires, etc.). Parmi les grandes transformations actuelles, les consommateurs de plus en plus acteurs et peuvent injecter tout ou partie du surplus d'énergie produit vers le réseau ou choisir de consommer de l'énergie du réseau selon leurs souhaits. Un nouveau modèle économique se dessine avec la possibilité de voir apparaître de nouvelles tarifications de l'électricité notamment liées aux prestations assurant une plus grande robustesse du réseau.

Durant cette thèse, plusieurs années de données de production et de consommation d'un bâtiment photovoltaïque ont été analysées pour définir les contraintes imposées à l'unité de stockage assurant l'équilibre du micro-réseau électrique. Un modèle de performance et de vieillissement a été élaboré pour trois technologies de stockage: batteries plomb-acide, batteries lithium-ion et supercondensateurs. Celui-ci permet le dimensionnement, l'association d'éléments de stockage et la gestion optimale des flux énergétiques au sein du micro-réseau. Divers critères permettant d'évaluer le fonctionnement des micro-réseaux ont également été étudiés comme le coût annuel de l'unité de stockage, le taux d'autoconsommation de l'énergie photovoltaïque, la quantité d'énergie qui n'a pas été fournie au consommateur, etc. Une approche multi-objective, basée sur le concept d'optimum de Pareto, a été mise en œuvre afin d'optimiser les aspects économique, environnemental et d'autonomie de fonctionnement des futurs réseaux électriques distribués. Un démonstrateur basse tension continue de quelques kilowatts a été développé pour valider les différents points étudiés dans cette thèse.

Mots clefs : Micro-réseau; Éléments de stockage; Gestion d'énergie électrique; Dimensionnement optimal; Commande bus DC; Modélisation de batteries et supercondensateurs.

Abstract

Optimal sizing and energy management of storage systems for renewable sources deployment, design of a LVDC microgrid

Because of our global high consumption of fossil fuels, these resources are becoming scarce and the environmental equilibrium of the Earth is endangered. Other energy sources are developed in order to build a new diversified and decarbonised energy mix. For example, in an urban context, the solar photovoltaic system has many assets such as the decentralized production of electricity, easy integration in buildings, transportation losses reduction, no sound during production, low environmental impact, etc. However, the production of this energy source is highly varying, difficult to predict (several timescales, from the cloud shadows to seasonal meteorological variations) and not correlated across time with our consumption needs.

In order to enable a massive penetration of renewable energy sources in our conventional grid, the use of energy storage systems (e.g. electrochemical storage) seems a promising solution, taking into account the costs, supply security, technological maturity and ease of set up. Hence, new microgrids constituted by decentralized energy sources and energy storage systems have been developed in order to replace or complement the main centralized grid by ensuring some support functions (i.e. enhancement of the grid stability, black-start operation, replacement of diesel generators, etc.). The consumers become actors able to inject a part of all their surplus energy to the main grid, if the operation is accepted by the transmission system operator. A new business model is to define, especially in the case of putting a valuation on the functions that can help the main grid.

During this thesis, several years of data from production and consumption of a photovoltaic building have been analysed in order to define the operating profile of an energy storage system that ensures the equilibrium of the microgrid. A behavioural model taking into account the ageing has been made for three storage technologies: lead-acid batteries, lithium-ion batteries, and supercapacitors. It enables the optimal sizing, the hybrid association of storage systems, and the optimal energy management of the microgrid. Several criteria assessing the operation of microgrids have been studied (e.g. annual cost of the storage system, self-consumption rate, loss of load probability, etc.). A multi-objective methodology, based on Pareto optimality, has been developed in order to optimize economic, environmental, and autonomy aspects. A low voltage DC prototype of some kilowatts has been developed for validating the different concepts presented in this thesis.

Keywords : Microgrid; Energy storage systems; Energy management; Optimal sizing; DC bus control; Batteries and supercapacitors modelling.

Remerciements – Acknowledgments

Quelle aventure! Trois années de belles rencontres et tellement de discussions à réinventer le monde. Par amour pour les sciences mais aussi par amour pour la femme qui partage ma vie depuis presque huit ans, nous nous sommes tous deux investis, plus que de raison sans doute, dans une thèse de doctorat. Je tiens d'ailleurs à remercier très sincèrement mes familles de sang et de cœur qui m'ont apporté tout le soutien nécessaire à la réussite de mes projets professionnels et personnels. Merci à mes grands-parents, papa, maman, Émilie, Valentin et à toute ma grande famille (c'est toujours un plaisir de discuter des sciences avec toi, tonton Franck!).

Je conseille vivement à tous les curieux d'explorer cette voie qu'est la thèse. J'ai pris beaucoup de plaisir à travailler à Toulouse, notamment au sein de l'Université Toulouse III Paul Sabatier avec sa très accueillante bibliothèque universitaire et ses salles de travaux pratiques bien outillées. Je remercie l'école doctorale de Génie Électrique Électronique Télécommunications (GEET) qui m'a accordé une bourse de thèse agrémentée de nombreuses formations transverses et qui m'a donné la possibilité de travailler à l'étranger pour découvrir comment fonctionne la recherche ailleurs. Enfin, je remercie le Laboratoire d'Analyse et d'Architecture des Systèmes (LAAS-CNRS) et l'équipe d'Intégration de Systèmes de Gestion de l'Énergie (ISGE) qui m'ont accueilli dans de très bonnes conditions tant sur le plan matériel qu'humain.

Évidemment, je dois beaucoup à mes directeurs de thèse, Corinne et Bruno, qui m'ont proposé ce très intéressant sujet et qui m'ont accompagné avec bienveillance dans toutes mes démarches. Je remercie chaleureusement Lionel pour m'avoir épaulé tout au long de ma thèse et appris énormément en électronique (signal et puissance). Tous les quatre, nous avons fait un grand nombre de réunions, plus ou moins efficaces, pour en arriver là, et j'espère qu'à l'avenir nous aurons de nouveau l'occasion de travailler ensemble.

Un grand merci aux membres du jury de thèse qui se sont intéressés à ces travaux.

Merci aux collègues du laboratoire LAPLACE à Toulouse, Angel, Georges et Pascal, de m'avoir fait découvrir l'univers des éclairages à LEDs. Merci aux professeurs, Alexandre, Pascal, Damien et Bruno, avec qui je co-encadrais notamment des projets et bureaux d'études. Merci aux chefs d'équipes successifs de l'équipe ISGE, Fred et David. Un très grand merci aux secrétaires, notamment Ascension, qui m'ont aidé dans les démarches administratives pour aller présenter mes travaux dans des conférences un peu partout dans le monde. Merci au service du personnel, au service de gestion et au service d'impression du LAAS qui ont été vraiment au top tout au long de ma thèse.

Je remercie également mes collègues de galère, qui ne comptaient pas les heures à travailler, toujours prêts à donner un coup de main, Margot, Zaki, Wiem, Alonso, Adem et Hiba, merci à vous! Merci aux anciens qui m'ont partagé leur expérience, Michael, Youssef et Luiz. Je souhaite bonne chance aux prochains qui se prépareront bientôt à soutenir Kolja, Ilias, Luis et Firdaous. Une pensée pour tous les stagiaires qui ont travaillé dans l'aquarium d'à côté avec peu de lumière du jour et une climatisation plus ou moins fonctionnelle, bravo à vous.

I am also very grateful to the people I met in Aalborg. It was a great pleasure to work in the Microgrid team for four months. Thank you Josep, Juan, Medhi, Amjad, Adriana, Nelson, Enrique, Jingpeng, Ionela, Hrvoje, Tomislav, Abderezak, Ramy and everyone I met there. You are doing a wonderful job that can be a game changer to achieve a more sustainable future.

Enfin, j'espère avoir la chance de continuer ma carrière avec de nouveaux projets me permettant de satisfaire ma curiosité avec autant de joies.

Jérémy DULOUT

Abbreviations and acronyms

BESS	Battery Energy Storage System
BOS	Balance Of the System
CAES	Compressed Air Energy Storage
CC	Constant Current
CCS	Carbon Capture and Storage
DC	Direct Current
DOE	Department Of Energy
DOD	Depth Of Discharge
EIS	Electrochemical Impedance Spectroscopy
EPBT	Energy Pay-Back Time
ESS	Energy Storage System
EU	European Union
GHG	Greenhouse Gas
HESS	Hybrid Energy Storage System
IEA	International Energy Agency
LCA	Life Cycle Analysis
LCOE	Levelized Cost Of Electricity
LED	Light Emitting Diode
MG	Microgrid
O&M	Operation and Maintenance
OCV	Open-Circuit Voltage
OECD	Organisation for Economic Co-operation and Development
OPA	Open Platform for the ADREAM building (name of a project)
PCB	Printed Circuit Board
PHES	Pumped Hydropower Energy Storage
PV	Photovoltaic
SC	Supercapacitor
SEI	Solid Electrolyte Interface
SMES	Superconducting Magnetic Energy Storage
SOC	State Of Charge
SOH	State Of Health
T&D	Transmission and Distribution

« Rien n'est solitaire, tout est solidaire. L'homme est solidaire avec la planète, la planète est solidaire avec le soleil, le soleil est solidaire avec l'étoile, l'étoile est solidaire avec la nébuleuse, la nébuleuse, groupe stellaire, est solidaire avec l'infini. Ôtez un terme de cette formule, le polynôme se désorganise, l'équation chancelle, la création n'a plus de sens dans le cosmos et la démocratie n'a plus de sens sur la terre. Donc, solidarité de tout avec tout, et de chacun avec chaque chose. La solidarité des hommes est le corollaire invincible de la solidarité des univers. Le lien démocratique est de même nature que le rayon solaire. »

Proses philosophiques, L'âme

Victor Hugo

Table of contents

List of Figures

Chapter 3

Chapter 4

Chapter 5

Appendix of chapter 3

Appendix of chapter 4

Appendix of chapter 5

List of Tables

Chapter 0. Résumé de la thèse

« Il est un agent puissant, obéissant, qui se plie à tous les usages: il m'éclaire, il m'échauffe, il est l'âme de mes appareils mécaniques. Cet agent, c'est l'électricité »

dans Vingt Mille Lieues sous les mers,
Jules Verne (8 février 1828 – 24 mars 1905) célèbre écrivain français de romans d'aventures.

0.1 Introduction

Depuis la fin du XVIIIe siècle, les ressources d'énergies fossiles telles que le charbon, le gaz et le pétrole sont massivement exploitées pour subvenir à nos besoins énergétiques. Pourtant, pour des raisons environnementales (épuisement des stocks, méthodes d'extraction parfois polluantes, émissions de gaz à effet de serre, etc.) et d'équité sociale (accès universel à l'énergie), il apparait que l'actuel système énergétique fortement centralisé pourrait être amélioré. En effet, de nouveaux modes de production décentralisés intégrant des sources renouvelables (solaire, éolien, hydraulique, biomasse, etc.) sont prometteurs et semblent proposer une alternative crédible permettant une électrification mondiale s'inscrivant dans une démarche de développement durable.

Dans cette thèse, nous nous sommes intéressés aux concepts de « smartgrid » et « microgrid » (MG) qui bénéficient d'un essor important dû aux progrès accomplis en électronique de puissance (notamment dans le domaine des alimentations à découpage à haut rendement) et en technologies de communication (internet, connectivité sans fil, etc.). Un MG est un réseau électrique de puissance moyenne (inférieure au mégawatt) constitué d'au moins une source d'énergie renouvelable, d'éléments de stockage, de systèmes permettant la bonne gestion des flux énergétiques, ainsi que d'une possible connexion au réseau conventionnel centralisé. L'association de plusieurs MGs communicants entre eux constitue un smartgrid.

Le recours à une distribution à courant continu (CC) au sein des MGs progresse du fait du nombre croissant de sources CC renouvelables (par exemple le solaire photovoltaïque) et des charges CC (comme les semi-conducteurs largement utilisés en informatique, les batteries, les nouveaux dispositifs lumineux à diodes électroluminescentes, etc.). Ainsi, de nombreux MGs hybrides alliant les distributions à courants alternatif (AC) et continu (CC) se développent. Ce type de MG sera le principal cas d'étude de ce manuscrit.

L'objectif de cette thèse est de modéliser un MG afin d'optimiser le dimensionnement et la gestion d'éléments de stockage. Pour ce faire, des données réelles provenant du système photovoltaïque (100 kilowatt-crête) et de la consommation du bâtiment ADREAM du LAAS-CNRS ont été utilisées. Plusieurs technologies de stockage (batteries plomb-acide, batteries lithium-ion et supercondensateurs) sont comparées et modélisées pour cette application. Ainsi, une méthodologie générique de dimensionnement optimal est proposée. Plusieurs niveaux de gestion sont présentés et un prototype de quelques kilowatts a été conçu pour valider une stratégie de commande.

0.2 Les sources d'énergie renouvelables et micro-réseaux

Ce chapitre traite le positionnement des sources d'énergie renouvelables au sein de notre système énergétique planétaire. De ce fait, la politique environnementale internationale est abordée et différentes sources d'électricité sont comparées d'après des aspects environnementaux, économiques et sociaux, trois piliers définissant le développement durable. Nous avons sélectionné plusieurs indicateurs pour quantifier la notion de développement durable comme par exemple le coût actualisé de l'électricité, le niveau d'émissions de gaz à effet de serre sur l'ensemble du cycle de vie, le temps de retour sur investissement énergétique et l'acceptation sociale.

Les propriétés des MGs AC et DC sont exposées afin de mettre en lumière l'émergence de topologies à architecture DC, qui permettent notamment une intégration aisée des énergies renouvelables. Ainsi, dans un contexte urbain, le solaire photovoltaïque (PV) fut la principale source renouvelable étudiée, notamment du fait des études antérieures de l'équipe sur les architectures reconfigurables. Par ailleurs, cette thèse est alimentée de nombreuses données acquises au cours des quatre dernières années en provenance du bâtiment PV ADREAM du LAAS-CNRS.

Enfin, le stockage est un élément majeur dans la constitution d'un MG car il permet d'absorber les fluctuations de production des sources renouvelables. Ce dernier peut être utilisé à la fois pour maintenir la stabilité d'un MG sur des temps très courts mais aussi pour assurer une certaine autonomie de fonctionnement en cas de panne sur le réseau électrique principal. Notre choix s'est porté sur le stockage électrochimique qui présente de bonnes caractéristiques en termes de maturité, sécurité et robustesse.

0.3 Les éléments de stockage

Différentes technologies de stockage (mécanique, chimique, électrique, électrochimique et thermique) sont présentées en début de chapitre. A partir de la littérature, une comparaison est menée en s'appuyant sur leurs principales caractéristiques (temps de réponse, coûts d'achat et d'opération, énergie et puissance spécifiques, durée de vie en cyclage et en calendaire, etc.).

En choisissant le stockage d'énergie adapté pour les bâtiments intelligents, nous nous sommes focalisés sur les batteries au plomb-acide, les batteries lithium-ion et les supercondensateurs (SCs). Le principe de fonctionnement de ces trois éléments est présenté afin de mieux expliquer leurs similitudes et différences en termes de rendement et durée de vie notamment.

Ensuite, les grandeurs utiles telles que la capacité nominale ou encore l'état de charge sont définies conjointement pour les technologies étudiées. Une attention particulière fut portée à l'estimation du vieillissement des éléments de stockage. Deux approches sont d'ailleurs mises en avant pour estimer l'état de santé, l'une basée sur le principe de suivi du nombre d'ampère heures échangés et l'autre basée sur un cumul d'évènements (rainflow counting).

Pour finir, différents outils de modélisation sont analysés afin de définir un modèle adapté pour le dimensionnement et à la planification d'éléments de stockage. La modélisation type circuit a été retenue pour son bon compromis entre complexité mathématique et bonne approximation du comportement du stockage dans les conditions de fonctionnement d'un MG PV. Quelques résultats expérimentaux effectués sur des batteries au plomb et SCs sont présentés.

0.4 Dimensionnement optimal d'éléments de stockage

Dans ce chapitre, le dimensionnement optimal d'un système de stockage est traité. Les principales méthodes d'optimisation mono et multiobjectif sont présentées, notamment la méthodologie de Pareto. Différents critères liés à la notion de développement durable sont développés pour évaluer l'optimalité du dimensionnement du stockage au sein d'un MG. Ainsi, une méthode générique d'optimisation multiobjectif basée sur l'optimalité de Pareto a été développée.

Un premier cas d'étude présente le dimensionnement à trois objectifs d'un stockage hybride constitué de batteries au plomb-acide et de SCs. Le profil de fonctionnement est basé sur les données historiques du bâtiment ADREAM. Le comportement électrique, le vieillissement et le coût du stockage sont modélisés afin de définir les combinaisons optimales qui satisfont au mieux les objectifs choisis. L'optimisation du dimensionnement prend en compte différentes contraintes, notamment les limitations (relatives à la capacité du stockage) des courants de charge et de décharge qui sont imposées afin de ne pas diminuer la durée de vie du stockage par une mauvaise utilisation.

Le dimensionnement d'une batterie lithium-ion, s'appuyant sur les données du réseau électrique Danois, est notre second cas d'étude. Ce travail fut réalisé lors de mon séjour de quatre mois à l'Université d'Aalborg dans l'équipe « Microgrid » dirigée par Josep M. Guerrero. Le profil de fonctionnement est traité différemment du cas précédent (étude probabiliste), ce qui permet notamment d'analyser plus simplement le vieillissement du stockage en se basant sur la notion de profondeur de décharge journalière.

Finalement, pour montrer l'adaptation de cette méthode d'optimisation à divers problèmes, celle-ci est appliquée au dimensionnement d'un éclairage à LED. Le but étant de trouver les valeurs de courant d'alimentation, de dissipation thermique et nombre de LEDs qui optimisent les caractéristiques d'efficacité lumineuse, de consommation électrique et de consommation tout au long du cycle de vie d'un luminaire. Cette étude a été menée en collaboration avec l'équipe « Lumière et Matière » dirigée par Georges Zissis du laboratoire LAPLACE à Toulouse.

0.5 Commande optimale d'un micro-réseau

Ce dernier chapitre est consacré au pilotage optimal des MGs. Parmi la multitude de techniques de commande adaptées aux MGs AC et DC, celle par niveaux hiérarchiques nous apparaît particulièrement intéressante pour optimiser, sur différentes échelles de temps, le fonctionnement des différents organes du MG (notamment le stockage) tout en assurant la stabilité de ce dernier.

Dans un premier temps, une méthode de planification optimale est présentée pour un pack de batterie lithium-ion intégré dans un MG fonctionnant avec les données du réseau électrique Danois. L'objectif est de diminuer les coûts de fonctionnement liés à la consommation électrique du réseau ainsi que ceux liés à l'usage du stockage. Comme pour le dimensionnement, des contraintes de fonctionnement sont imposées sur le stockage mais aussi sur l'utilisation du réseau (limitation de la puissance échangée).

Pour conclure ce manuscrit, la plateforme expérimentale de MG à échelle réduite mise en œuvre au LAAS-CNRS sous le nom d'Open Platform for the ADREAM building (OPA) est dévoilée. Cette plateforme multidisciplinaire nous a notamment permis de valider les couches bas niveaux de la commande hiérarchique, à savoir le DC bus signaling et la régulation cascade. Nous montrons comment cette commande peut être implémentée de manière décentralisée afin de s'affranchir des problèmes liés à des erreurs de communication.

0.6 Conclusion

« On ne fait jamais attention à ce qui a été fait ; on ne voit que ce qui reste à faire »
Marie Skłodowska-Curie (7 novembre 1867 – 4 juillet 1934) chimiste et physicienne polonaise
naturalisée française qui obtint deux prix Nobel dans des domaines scientifiques distincts
(physique en 1903 pour des travaux sur les radiations, et chimie en 1911
pour des travaux sur le polonium et le radium).

Notre système énergétique mondial a été présenté dans ce manuscrit de thèse. La production d'énergie renouvelable décentralisée et développée au sein des MGs semble une solution prometteuse pour un avenir s'inscrivant dans une démarche de développement durable.

Le défi majeur est de fournir une sécurité d'approvisionnement de l'électricité avec des sources intermittentes qui dépendent des conditions climatiques. C'est pourquoi nous avons étudié les principaux systèmes de stockage afin de mieux appréhender les avantages et inconvénients de chaque technologie. Dans le cadre du développement d'un MG urbain, nous avons sélectionné les batteries au plomb-acide, les batteries lithium-ion et SCs pour des raisons de coûts d'achat et d'opération, de rendement, de durée de vie, etc.

Ainsi, nous avons abordé trois thèmes que sont la modélisation, le dimensionnement et la planification des éléments de stockage. Nous avons ensuite défini des critères permettant d'évaluer l'optimalité de la solution de stockage envisagée. Une méthodologie générique d'optimisation multiobjectif a par ailleurs été développée.

Enfin, nous nous sommes concentrés sur la commande du MG en nous appuyant sur une technique de pilotage à trois niveaux hiérarchiques. Un démonstrateur de quelques kilowatts a été conçu pour valider les deux niveaux de commande les plus bas. L'intérêt de ce travail est de proposer une solution de pilotage ayant un mode de fonctionnement optimal avec supervision et planification, mais aussi un mode « dégradé » qui est décentralisé et autonome en cas de panne de communication.

Les perspectives sont multiples. Il faut envisager l'amélioration et la validation de la modélisation des éléments de stockage, notamment le modèle vieillissement « rainflow counting ». L'analyse du cycle de vie des éléments de stockage est également primordiale pour valider les choix technologiques. Enfin, il paraît intéressant de mener une analyse concernant l'influence de la stratégie de gestion du stockage sur le dimensionnement et vice versa.

Chapter 1.　Introduction

During the past years, the phasing out of fossil fuel resources (i.e. coal, gas, oil), which have been the main energy carriers since the first industrial revolution at the end of the 18th century, is accelerated towards the creation of a new energy system relying on renewable energy sources (e.g. solar photovoltaic energy, wind energy, marine energy, biomass, etc.) and distributed energy generation. This energy transition is supposed to ensure a more sustainable electrification, universally accessible and environment-friendly.

The shift to renewable sources can be explained by many reasons such as economic (decreased dependency to fossil fuels), environmental (e.g. reduction of greenhouse gases) and social (energy accessibility in remote areas). Despite the fact that the concept of 'smartgrid' was born some decades ago, the recent technological breakthrough advances in power electronics combined with information and communication technologies (ICT) opened up numerous possibilities in the optimization of energy management, production, and distribution. Similarly to the internet, a smartgrid can be seen as an interconnected network of many nodes named 'microgrids', which are small distributed architectures having their own hardware configuration (usually constituted of a renewable energy source, an energy storage system, some controllable loads, and at least a control unit with measurement points placed within different parts of the grid). The users of a microgrid are often called prosumers (i.e. producers and consumers of energy), they can choose to be connected or not to the main grid in order to increase the penetration of renewable energy sources and decrease the cost of electricity. In order to mitigate the variable nature of renewable energy sources, which endangers the stability of the electrical grid, energy storage seems to be a good solution that can also help achieve the goals of a microgrid that are to increase efficiency, reliability and resiliency of electricity generation and distribution.

Thus, it appears that the sizing and energy management of energy storage systems is difficult because of incertainties related to renewable energy sources production (that is difficult to forecast) and varying load requirements (which is affected by the meteorological conditions, user's behaviour, etc.). A large number of studies in academic and industrial fields are developing new energy storage systems that can be adapted to any type of applications. The challenge is to propose a good model that encompasses instantaneous performances and lifetime estimation under real-life conditions.

Beyond the concept of microgrid, the old debate about AC and DC current distributions has re-emerged because of the recent technological evolutions (especially in power converters that are now able to replace efficiently AC transformers), the development of renewable sources such as solar photovoltaic delivering a DC current, and a lot of new loads that need DC supplies (batteries, electronic devices, LEDs, etc.). New objectives will be investigated in the development of a sustainable energy system, which has to be universally accessible and environment-friendly.

In this context, this thesis addresses the modelling and energy management of a microgrid (MG) constituted of energy storage systems and renewable sources. A particular overview on multi-objective

optimization has been done with the selection of different criteria that enables to evaluate the cost of electricity, the self-consumption of the renewable source, etc. The analysis of distributed control and monitoring solutions have been important in order to propose our own DC microgrid. The modelling, simulation and multi-objective optimization of the sizing have been implemented in MATLAB and the scheduling optimization problem has been solved with General Algebraic Modeling System (GAMS). For the experimental validation, a low voltage DC prototype has been developed in the laboratory. This small microgrid is constituted of a string of solar photovoltaic (PV) panels (1 kWp), some energy storage systems (more than 10 kWh of installed capacity), and some controllable loads (servers from a datacenter, LED ligthtings, sensors and actuators for an internet of things network). Hence, this experimental platform will be used in the future to validate new smart management of MGs.

My supervisors, Professors Corinne ALONSO and Bruno JAMMES, started to work in the field of microgrids via the creation of the ADREAM building in the LAAS-CNRS, which is an experimental platform of 1700 m² with a solar PV source of 100 kWp (large PV façade and tens of PV panels are placed on the roof). With this building, inaugurated in 2012, an extensive research has been carried out in the fields of PV array reconfiguration under partial shading conditions and PV fault detection. Analysing production and consumption profiles, the research work naturally moved towards the integration of storage systems in this microgrid. The doctoral school 'Génie Electrique Electronique Télécommunications' (GEET) granted a doctoral contract of 3 years to pursue the sizing and energy management of energy storage systems in microgrids.

This thesis is organized as follows, **chapter 2** presents the context of this work defining the concept of energy system from primary to useful energy, and proposing a short overview of the world's situation (energy access, environmental issues, etc.). The electrification of our society is also explained and a comparison between all electricity sources has been made based on some selected criteria that promote sustainable development. New electrical architectures such as smartgrid and microgrid are introduced, as well as energy storage systems, which are seen as a possible evolution of our actual electrical grid. Thereafter, in **chapter 3**, the main technologies of energy storage systems are presented and their performances are investigated through a literature review (capital cost, operating cost, cycle efficiency, lifetime expectancy, etc.). A particular focus has been put on lead-acid batteries, lithium-ion batteries, and supercapacitors with the modelling of their electrical performances and ageing behaviour. Indeed, some definitions will be given such as available capacity, state of charge, and state of health, in order to propose a realistic model of energy storage systems. The steps for the elaboration of an equivalent-circuit model have been detailed. This model is seen as the best trade-off between electrochemical model and black-box model in our application (computation resources are limited and a reasonable number of experimental tests are necessary to investigate the different parameters of the storage system, depending on the desired accuracy, especially in applications with large variations of current rates). Then, the optimal sizing of an energy storage system is developed in **chapter 4**. Some mono and multi-objective optimization techniques are presented in order to select the most adapted methodology to our application. Several criteria have been defined to evaluate the sizing in terms of reliability, costs, environmental impact, and social political factors. Different study cases have been developed, firstly, the optimal sizing of a hybrid storage system (i.e. association of two storage systems) with a pre-defined strategy of storage and historical data that define the operating profile of the microgrid. The aim of this first study was to evaluate the possible benefits of the hybridization of storage systems in microgrid applications because several studies already demonstrated the benefits in the transportation sector for example. In a second step, a similar study has been conducted with a simple storage system in order to define the optimal capacity and cycle depth of the storage system. The proposed multi-objective methodology of sizing, based on Pareto optimality, has also been adapted to the sizing of LED lightings, finding the best current supply, number of LEDs, and heatsink in order to minimize the annual cost of the luminaire, the electrical consumption, and the primary energy consumed during its entire life (life cycle analysis). Afterwards in the **chapter 5**, the optimal scheduling and the distributed control of a microgrid are presented through two study cases. Indeed, the Danish grid data has been used to propose

an optimal scheduling of a lithium-ion battery pack managing the high penetration of renewable sources. Hence, a non-linear optimal problem has been set and solved in order to minimize the cost of electricity and the cost of the storage system. The distributed control has been experimentally validated through a small-scale microgrid based on 'DC bus signaling', which enables to define different modes corresponding to a specific use of energy storage systems, PV source, and energy exchanges with the main grid. Finally, the conclusion of this thesis is given, highlighting the main contributions of this work and the perspectives for further developments of the sizing methodology and operation of the microgrid.

Chapter 2. Renewable sources and Microgrids

"Earth provides enough to satisfy every man's needs, but not every man's greed."

Mohandas Karamchand 'Mahatma' Gandhi (2 October 1869 – 30 January 1948) Indian politician and philosopher who inspired a lot of movements for civil rights towards the world.

Energy is often seen as a driver of societal development and economic growth. In order to meet our energy needs and be always more convenient to use, different forms of energy have been mastered such as animal power, mechanical power and electrical power. Yet, our actual production, transportation and use of energy has to evolve because of (i) the depletion of fossil resources that are massively powering mechanical and electrical power, (ii) the greenhouse gas (GHG) emissions due to fossil fuel combustion which contributes to climate change, and (iii) the high world's population growth rate (inducing a higher energy demand in the future). The global context of energy will be presented with a particular focus on electrification of our society and the integration of new distributed resources. This chapter emphasizes the importance of developing efficient, environment-friendly and more accessible energy carriers such as renewable energy sources. Indeed, renewable energy has many potential benefits such as reduction in GHG emissions, diversification of energy supplies (improvement of reliability), reduced infrastructures for electricity transportation (in case of local consumption), and reduced dependency on fossil fuel resources.

This chapter is organized as follows:

First the concept of "energy system" is presented with a review on the global trends of energy production and consumption. Then, a historical overview is given over the past decades concerning the international "energy transition" which is supposed to turn our actual dependency from fossil fuels to renewable sources. Finally, the development of the electrical grid is described unveiling the latest architectures such as the microgrid that produces its own energy combining renewable energy sources and energy storage systems (ESSs).

Table of contents of chapter 2

2.1 Energy context

2.1.1 Energy system definition

The analysis of energy systems, from production to use of energy, is a key to assess environmental, economic and social impacts of our energy policy [1]-[2]. As presented in Fig. 2.1, energy can be classified into the four following categories:

- Primary energy (PE) concerns available energy in nature, which has not been transformed by human (e.g. fossil fuels, biomass, solar radiation, etc.). Usually, PE is not convenient for transportation and direct use.

- Secondary energy (SE) is the result of the transformation of PE (e.g. electricity, gasoline, etc.). This energy is often called energy carrier because it enables to use energy wherever and whenever the user wants.

- Final energy (FE) is the energy delivered to the end-user that is directly consumed (e.g. electricity at home, gasoline at the service station). This energy is exchanged through formal monetary transactions on which some taxes are levied.

- Useful energy (UE) reflects the effective energy that is transformed to provide services. It enables to take into account the efficiency of the end-use device (e.g. illumination is provided by a light bulb that convert only around 10% of the final energy into light).
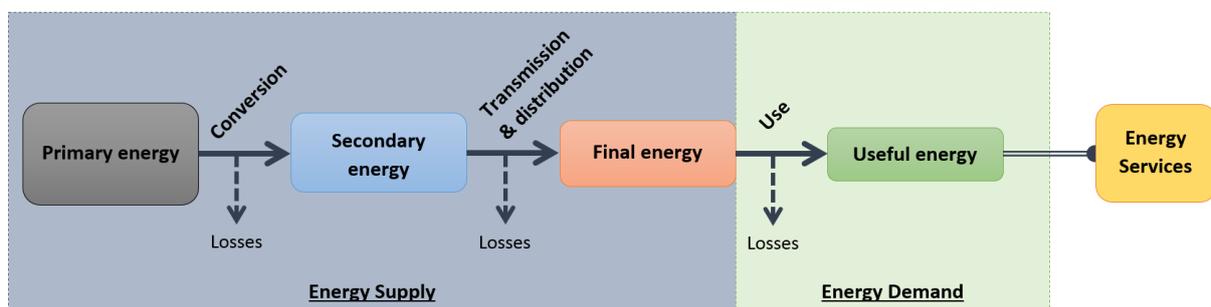
Figure 2.1 The energy system from primary energy to energy services

As illustrated in Fig. 2.1, energy losses occur when PE is transformed into SE, when the SE is delivered to the end-user as FE and when the FE is used through the end-use device. These losses are crucial because it proves that energy services can be fulfilled with less primary energy through more efficient conversion processes, delivering processes and devices.

For the past decades, the world total final consumption (also called end-use energy) has been continuously increasing, as presented in a report from the international energy agency (IEA) [3] and illustrated in Fig. 2.2. It can be seen that the energy demand has more than doubled since 1971, reaching 9 425 Mtoe (tonne of oil equivalent) in 2014 (according to the IEA, 1 Mtoe corresponds to 11.63 TWh). It is also noticeable that the use of electricity has substantially grown, from 9.4% in 1971 to 18.1% in 2014.

The following notes were initially added to the graph presented in Fig. 2.2: international aviation and international marine bunkers have been included. Peat and oil shale have been aggregated with coal. For some countries, biofuels and waste final consumption data have been estimated. Other includes geothermal, solar, wind, heat, etc.

(Mtoe)
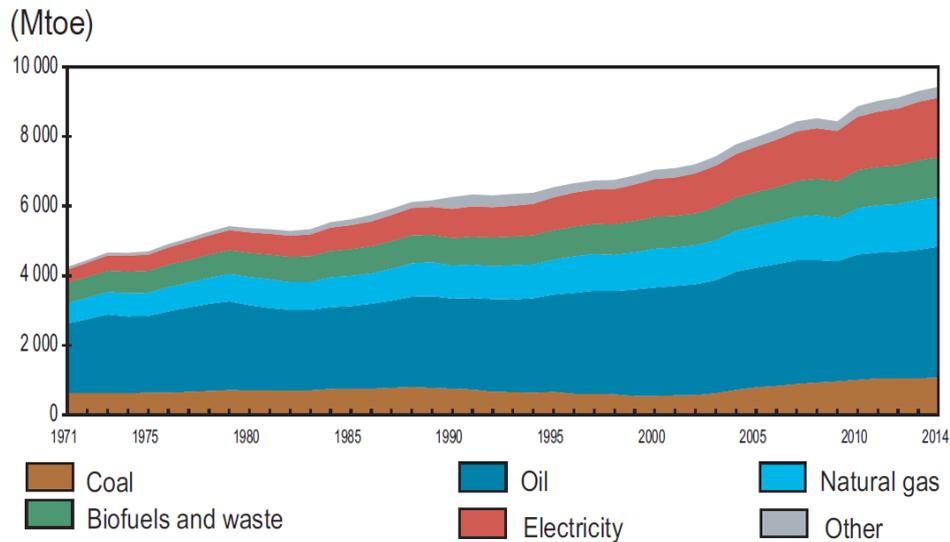
Figure 2.2 World total final consumption from 1971 to 2014

According to the statistics collected in the IEA website [4], industry, transport and buildings (residential and commercial) are the three main sectors in terms of energy demand, see Fig. 2.3. In this figure, IEA indicates that "non-energy use" deals with fuels that are used as raw materials in different sectors and are not consumed as a fuel or transformed into another fuel. "Non-specified" includes fuels that have not been classified elsewhere (e.g. military fuel use for mobile and stationary consumption).
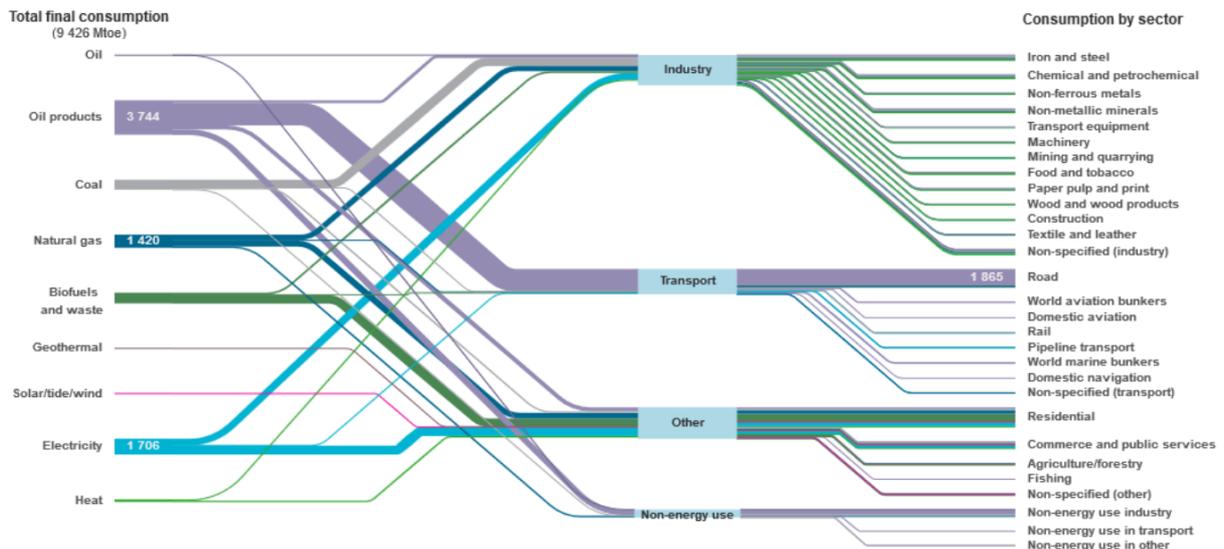
Figure 2.3 World final consumption in 2014

The following sub-sections briefly outlines the major concerns about our global energy system.

2.1.1 Access to energy and world's population growth

The energy supply is very different from a country to another, as illustrated in Fig. 2.4. Historically, countries that are member of the organisation for economic co-operation and development (OECD) are by far the countries that benefit from the largest share of the total energy supply.
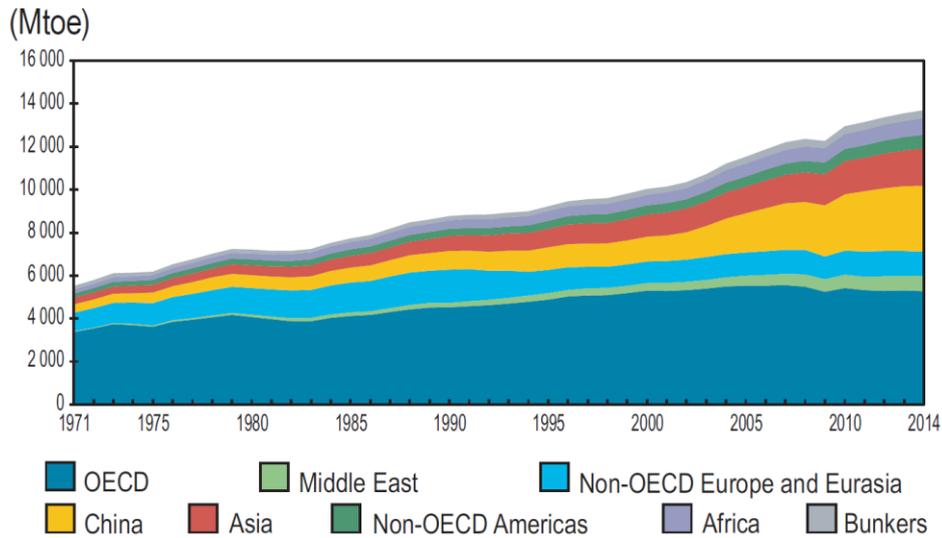
Figure 2.4 Primary energy supply by region [3]

Nowadays, it has been estimated that 1.2 billion people do not have access to electricity, most of them are from sub-Saharan Africa or developing Asia, as illustrated in Fig. 2.5. This lack of modern energy access increases inequalities because such households are suffering the deprivation of lighting, communication, healthcare, etc. An additional issue is related to cooking because traditional inefficient stoves are fuelled by solid biomass in poorly ventilated spaces. The consequences are numerous: deaths related to diseases contracted because of the air pollution (mainly children below 5 years old and adults over 30 years old), forest and soil degradation, greenhouse gas (GHG) emissions, etc. As presented in [5], millions of lives can be saved by investing in access to modern cooking fuels.
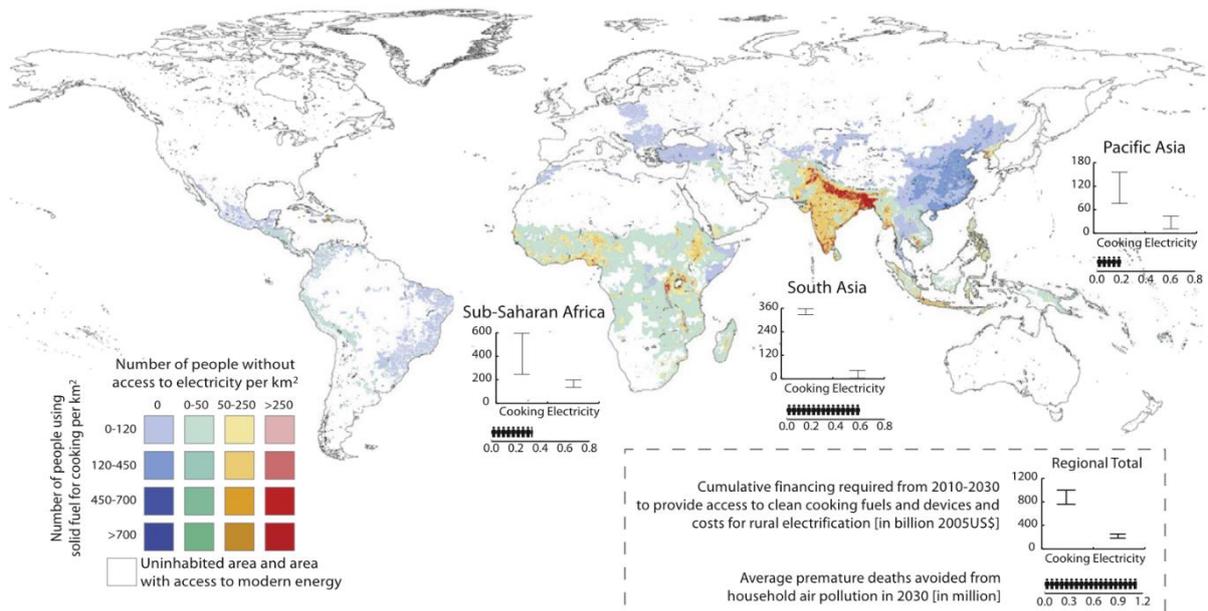
Figure 2.5 Cooking and electricity access – Global inequalities [5]

Last but not least, another major issue is the growth of the world's population. Indeed, a report from the Department of Economic and Social Affairs of the United Nations (UN) Secretariat [6], projected that the global population will increase by nearly one billion people over the next 13 years (reaching 8.6 billion in 2030), and will increase further to 9.8 billion in 2050 and 11.2 billion by 2100. A detailed report by regions is provided in table 2.1.

Region	Population (millions)			
	2017	2030	2050	2100
Africa	1 256	1 704	2 528	4 468
Asia	4 504	4 947	5 257	4 780
Europe	742	739	716	653
Latin America and the Caribbean	646	718	780	712
Northern America	361	395	435	499
Oceania	41	48	57	72
World	7 550	8 551	9 772	11 184

Table 2.1 United Nations world population projections [6]

As presented in Table 2.1, the main increase in world's population comes from Africa (expected to double by 2050, and then double again by 2100). Such projections on world's population implies to wisely design our new global energy system because the demand for energy services will massively rise.

2.1.2 Environmental issues

In 2014, the world total supply was getting close to 14 000 Mtoe, see Fig. 2.6. By comparing the global energy supply to the final consumption, the efficiency of the energy supply system is around 70%. Questions arise with respect to the nature of primary energies that constitutes our total primary energy supply. Indeed, what is the impact of our energy consumption on earth resources and on the environment knowing that around 75% of our global energy supply comes from non-renewable resources, such as fossil fuels (coal, oil and natural gas) and nuclear energy (rare earth minerals). These resources cannot be renewed in a human timescale (at least some thousands years for carbon based materials) and their combustion contribute to the rise of the average temperature observed of the Earth's climate system, as described in the fifth assessment report delivered by the Intergovernmental Panel on Climate Change (IPCC) [7]. In the global energy mix, oil, coal, natural gas, biofuels and waste, nuclear, hydro and renewable energy resources (solar, wind, geothermal, etc.) have a share of 31.3%, 28.6%, 21.2%, 10.3%, 4.8%, 2.4% and 1.4%, respectively [3].
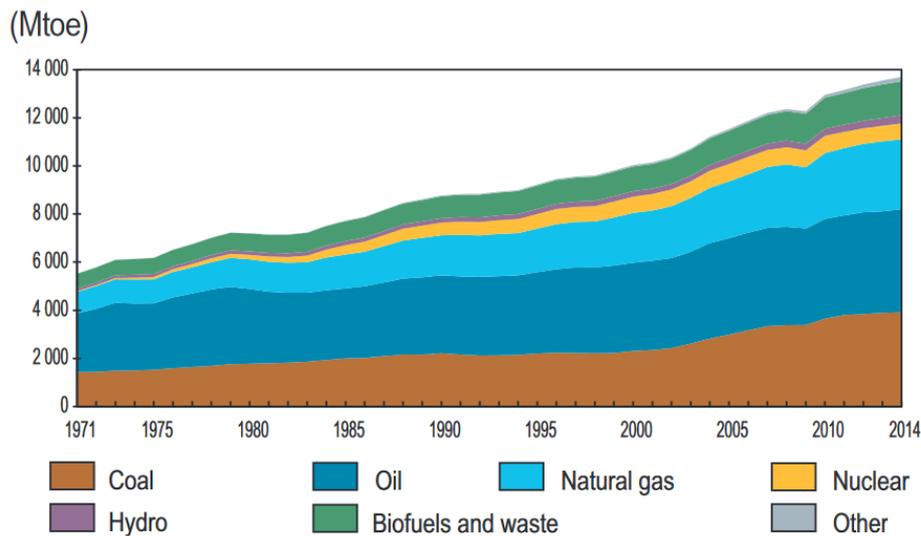
Figure 2.6 World primary energy supply by fuel type [3]

This way of consumption mainly relying on fossil fuels is not sustainable and has to be changed. An international non-profit organization, Global Footprint Network, advertises about our ecological footprint (i.e. the impact of human activities on Earth resources) and estimated that mankind's resources consumption is equivalent to 1.7 planets. This organization also warns every year about the "Earth overshoot day" which corresponds to the day when our global energy demand on nature exceeds what

Earth can sustainably yearly provide. In 2017, the Earth overshoot day was on the 2nd of august. It is to notice that these calculations based on estimates and relying on equivalent factors is not accepted by all the scientific community but it seems important to make people aware that our way to produce and consume energy is not sustainable.

Climate models and scenarios of emissions

Fossil fuel combustion and industrial processes contributes to GHG emissions such as carbon dioxide (CO_2), methane (CH_4) and nitrous oxide (N_2O). These gases remain in the atmosphere and are stored in soils and in the ocean causing warmer global surface temperature, ocean acidification, retreat of glaciers, etc. Climate models are essential to assess the Earth system's response to human activities and also our capacity to adapt to the predicted changes (ecosystems, economic activities, infrastructures, etc.). The main variables and parameters of climate models are illustrated in Fig. 2.7. Due to the complex interactions between several scientific disciplines (socioeconomic, environmental and technological trends), many parallel scenarios are studied in order to evaluate the uncertainties related to the potential consequences on the Earth's system. A timeline highlighting the major developments in such models is presented in [8].
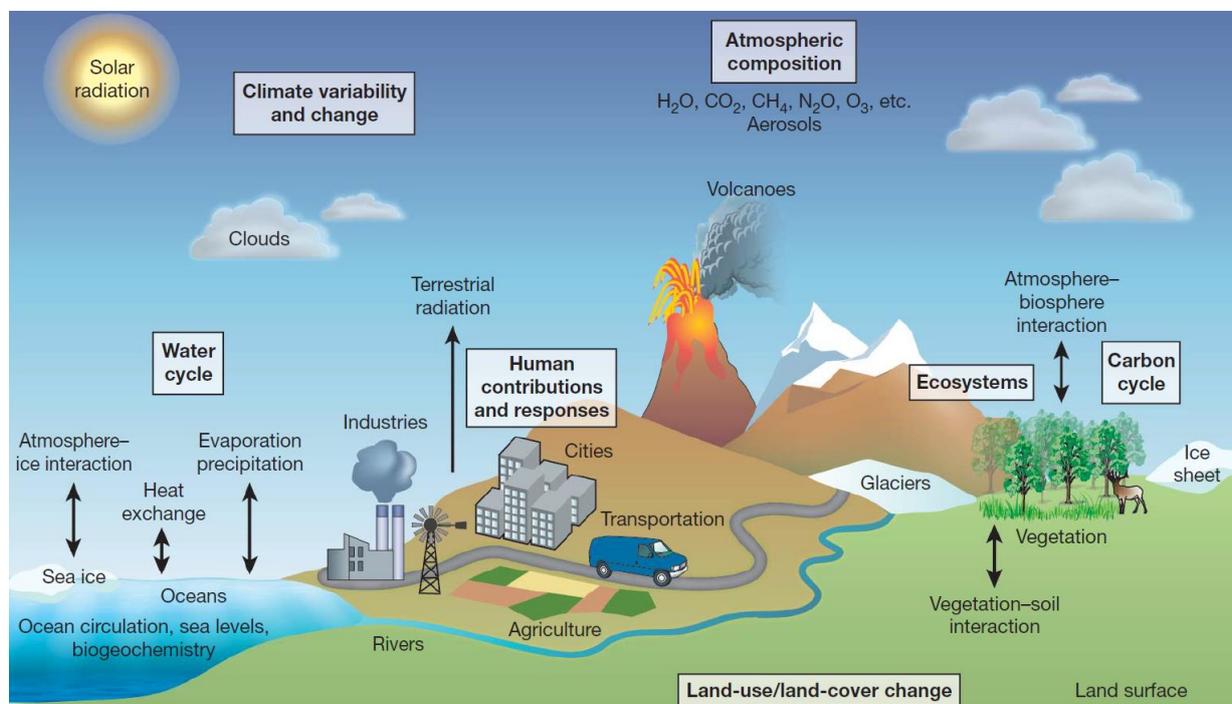
Figure 2.7 Main parameters involved in the climate system modelling [8]

According to the IPCC [7], around 50 Gt CO_2-eq were due to anthropogenic activities in 2010 and 65% of these global GHG emissions were related to fossil fuel combustion and industrial processes. The WWF [9] also warns to limit our GHG emissions in order to prevent a temperature rise above 2°C compared to the pre-industrial temperature level (mid-19th century). Indeed, such temperature can lead to massive reductions in biodiversity (animals and plants) and risks over vital resources (water, food, natural resources). From 1970 to 2012, the vertebrate population abundance has already decreases by 58% [9]: the business-as-usual (BAU) trajectory is unsafe. Some projections made by IPCC (called "representative concentration pathways" (RCPs)) predict the possible global rise of average temperatures by 2100 based on our annual anthropogenic CO_2 emission trends, see Fig. 2.8. In 2014, the concentration was around 400 ppm and it should not exceed 530 ppm to achieve the 2° C goal. By 2011, about 1900 Gt CO_2 have been emitted. Yet, the cumulative CO_2 emissions from anthropogenic

sources have to remain in a range of 2550 to 3150 Gt CO_2. This is why our annual emissions have to be reduced as presented in RCP 2.6 and RCP 4.5 in order to avoid irreversible changes.
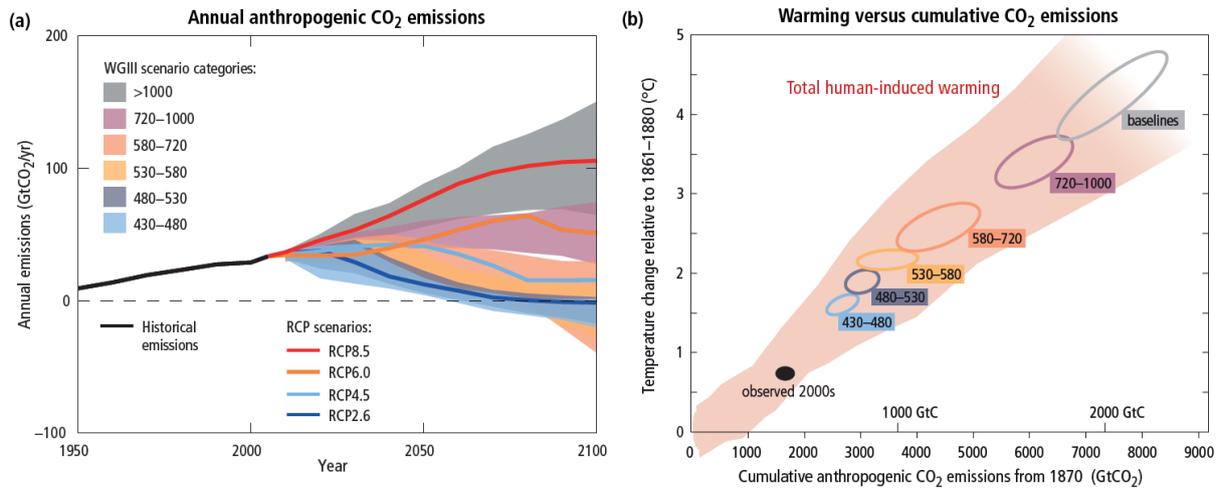
Figure 2.8 Global anthropogenic CO_2 emissions and possible temperature changes [7]

Several organizations propose scenarios of emissions assessing new global energy mix in order to guide policy makers for reducing carbon emissions. For example, the IEA [10] and the international renewable energy agency (IRENA) [11] have proposed scenarios that highlight the need of both improving energy efficiency and increasing the development rate of renewable sources in order to achieve universal and sustainable access to modern energy (for the IRENA, the global renewable share of the energy mix has to double by 2030). The négaWatt Association, a French non-profit organisation, also proposed a scenario for France involving a supplementary solution called the sufficiency [12]. Sufficiency is defined as a mean to "reduce the overall need for energy-using services through a better sizing, using, and sharing equipment, better organising land and society, etc.". Based on this scenario for 2050, the French final energy consumption is nearly halved (sufficiency and efficiency contribute to 60% and 40%, respectively) and the renewable sources nearly cover 100% of the primary energy demand (40% from the biomass and more than 50 % from wind, solar and marine energies).

In [13], another strategy is proposed, the idea is to stabilize the global annual carbon emissions for the next 50 years and then decrease of about two-thirds during the 50 following years. The stabilization of emissions can be achieved by choosing 7 from the 15 proposed options that are technically available. One option involves the replacement of some energy produced with coal fuel by PV sources. To validate this option, authors claim that 2000 GWp are needed, which correspond to about 50 times the capacity that has been installed in 2014 (see section 2.2.3, Fig. 2.15). This example shows how complex is the shifting to renewable sources.

2.2 World electrification

Brilliant researchers such as André-Marie Ampère, Charles-Augustin de Coulomb, Benjamin Franklin and Alessandro Volta laid the foundations for electricity theory. Hence, electrification and oil development during the end of the 18th century have been the drivers of the second industrial revolution. Thereafter, numerous inventions in the field of electrical science and technology enabled to make electricity be more convenient, more efficient and more accessible. The main milestones of this field have been listed by the Institute of Electrical and Electronics Engineers (IEEE) [available online at http://ethw.org/Milestones:List_of_IEEE_Milestones].

However, over the past 25 years, power generation and transport sectors have represented the main anthropogenic GHG emissions. In 2015 in the OECD countries, the power generation has been the

largest GHG emitting sector with a share of 39% in total emissions, followed by the transport (30%) and industry (11%) [14], as presented in Fig. 2.9.
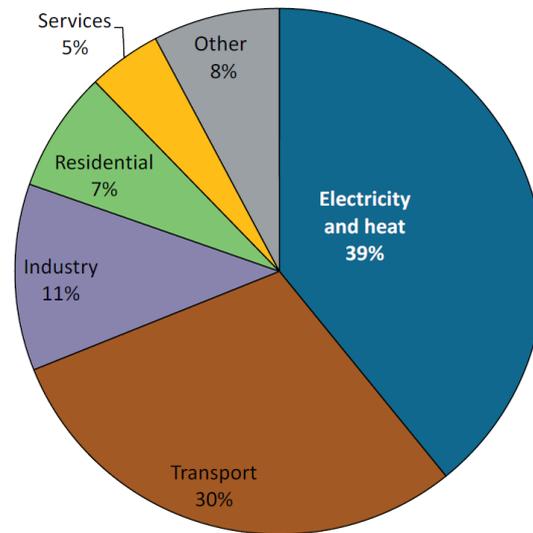
Figure 2.9 Breakdown of CO$_2$ emissions by sectors in OECD countries [14]

The expansion of electricity generation and evolution of supply sources in the global mix over the last four decades is presented in Fig. 2.10. It appears that electricity is mainly produced by non-renewable sources that are the most GHG emitting. This is why, a new energy policy called "energy transition" (or "green transition") aims at encouraging the development of renewable energies and the decarbonisation of the global energy system. Moreover, in some countries, renewable energy sources are seen as a chance to ensure energy sovereignty and do not rely anymore on the availability of natural resources from another country (e.g. in order to avoid an energy crisis such as oil crisis in the 1970s).
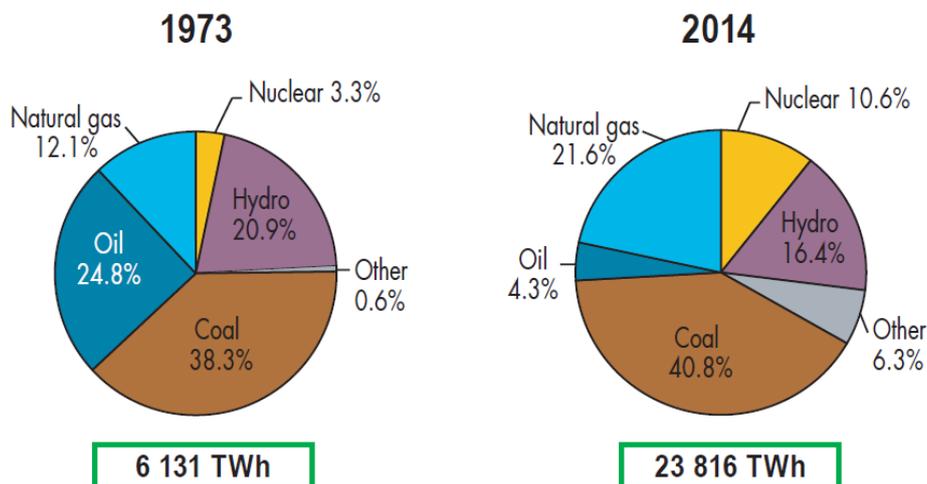
Figure 2.10 Historical evolution of global electricity generation by fuel type [3]

2.2.1 Actual energy sources for electricity generation

Since the industrial revolution in the middle of the 19th century, the demand for **non-renewable resources** such as **oil**, **coal** and **natural gas** have massively grown. In the 1950s, the American geologist Marion King Hubbert suggested the decline and depletion of these resources, in particular oil for which he predicted the so-famous "peak-oil" of world crude-oil production (i.e. time when the maximum rate

of extracted oil resources has been reached). Three terms aim to evaluate the quantity of fossil fuel resources depending on the demonstrated estimation of recoverable fossil fuel under current economic and operating conditions: proved resources correspond to a reasonable certainty (above 90%), probable resources denote chances above 50% and finally, possible resources are the least probable resources (i.e. lower than 50% chance). According to the global fossil fuel statistics presented in [15], based on our consumption rate actual and proved reserves, depletion dates for oil, gas and coal are estimated in 2066, 2068 and 2126, respectively. Of course recent discoveries such as shale gas or oil sands (also called unconventional oil) in many countries are delaying the end of fossil fuels. The point is that energy from fossil fuel will be harder to extract and thus less cost-effective. This depletion can lead to major issues concerning energy access, and thus threatening food and water supplies.

Uranium is another non-renewable resource that is used in nuclear power plants (and also as a military weapon). As fossil fuels, uranium is a vital resource for some countries such as France with 58 nuclear reactors providing 79% of the total electricity supply in 2012 [16]. The fission of uranium, nuclear chain reaction which generates large amounts of energy has a great advantage over the previously mentioned fossil fuels because the GHG emissions are very low. This is partly why in 2011 the GHG emissions per inhabitant in France were nearly 2 tCO_2eq lower than the mean of the European Union (EU) countries (9.1 tCO_2eq [16]). Two main issues comes with nuclear energy: the safety of nuclear waste which are harmful for thousands years and the nuclear risk in case of extreme weather conditions (e.g. Fukushima in 2011 which led some countries such as Germany to stop their nuclear production).

Concerning **renewable sources**, our planet offers thousands times more than our actual energy needs [17]. A diversified portfolio of energy technologies is available to harvest this renewable energy. The following sources of energy are listed by order of importance (from the actual greatest production to the lowest):

- **Bioenergy** corresponds to energy created from the biomass such as biofuels and electricity from organic waste. The production of bioenergy accounted for 10.3% in 2014, approximately 1413 Mtoe [3]. Ethanol is one of the most famous biofuels worldwide, mainly produced in Brazil. The main drawback is that biofuel production is sometimes replacing food production.

- **Hydropower** is a very mature and efficient way to produce electricity from a stream of water. Large hydroelectric dams have been constructed worldwide (e.g. the most powerful is the "three Gorges Dam" in China with an installed capacity of 22 500 MW). Such systems have a high capital cost and can have a large environmental impact (modified water streams, soil erosion, reshaped landscape to create large reservoirs, etc.), but this technology is low GHG emitting and the operating cost are low. Thus, the energy cost is relatively inexpensive [17] and numerous dams that benefit from reservoirs are often used as a very efficient storage system, called pumped hydroelectric energy storage (PHES).

- **Solar energy** can be used to produce either thermal energy (concentrated solar thermal and concentrated solar power) or electricity (photovoltaic cells). Due to the large availability of sunlight, these solar-based technologies are widely developed and their cost is fast decreasing. More explanation about its development will be given in the next section.

- **Wind energy** is producing electricity by converting mechanical power created by air flow through wind turbines. Onshore and offshore wind farms referring to a group of wind turbines that are installed in a land field and off the coast in large bodies of water, respectively. The latter ones are bigger because there are less constraints concerning the neighbourhood but the operation costs are higher. As for solar energy, the massive integration of such sources is an important challenge because the production of electricity is intermittent.

- **Geothermal energy** refers to heat energy collected from the Earth at different depths of the ground. Some projects also aim at providing seasonal storage by injecting heated fluids in some cavities and pumping it back later at the same temperature.

- **Marine energy** gathers technologies that use tidal stream, tidal range, waves, ocean temperature and salinity gradients. Nowadays the installed capacity is very small (around 0.5 GW in operation worldwide, 99% of them are from tidal range technology which is very similar to hydropower facilities) but the resources potential is huge [18]. One of the main challenges, except the reduction of both capital and operation cost, is to limit the impact on the ecosystem of marine animals (underwater noise, disruption of water streams, etc.).

Now that the main technologies of electricity supply have been defined, the following section aims at comparing them with sustainable indicators.

2.2.2 Indicators of sustainability

Since the creation of the United Nations Environment Programme at the Stockholm conference in 1972, international environmental conventions have been organized worldwide in order to promote an international policy dealing with environmental issues related to our energy system [19]. It is commonly accepted that the concept of sustainable development has been introduced worldwide in the Brundtland report (*Our Common Future*) in 1987: "Sustainable development is development that meets the needs of the present without compromising the ability of future generations to meet their own needs". Nowadays, the sustainable development is often illustrated with a Venn diagram (see Fig. 2.11) highlighting the three pillars of sustainable development that are economic growth, environmental protection and social equality.
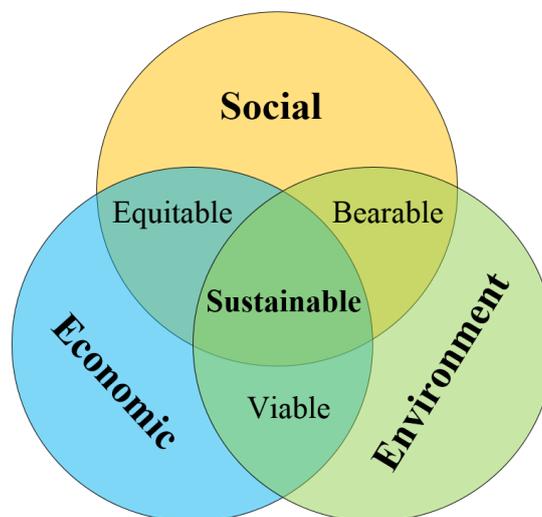
Figure 2.11 Venn diagram of sustainable development

In [20], the following list of sustainable indicators assessing power generating technologies has been presented: price of electricity generation, efficiency of energy generation, GHG emissions, land use, water use, social impacts, availability of resources and technological limitations. Given all these indicators, wind energy appears more sustainable than hydro energy (high social impacts and land use), then comes PV energy (that exhibits a poor efficiency, high generation cost and variable energy production), and finally geothermal (poor efficiency, high social impacts, GHG emissions and water consumption).

In order to evaluate the different sources of energy with the criteria of sustainable development described in Fig. 2.11, the following metrics can be used:

• **Levelized cost of electricity (LCOE)** is often employed to compare different technologies of energy supply [18], [21]. The LCOE assesses the total life-cycle costs of the power generating system (capital and operation costs) per unit of supplied electricity (in general, MWh). A mathematical definition of LCOE will be given in chapter 4. The main actual technologies have been assessed by Bloomberg New Energy Finance (BNEF) and presented in [18], see Fig. 2.12. For the central scenario in 2015, it has been estimated that the LCOE of large hydro (70 US$/MWh) is nearly the cheapest renewable source and is very competitive compared to non-renewable sources (between 50 US$/MWh and 280 US$/MWh). Wind technologies present a non-negligible gap (83 US$/MWh for onshore and 174 US$/MWh for offshore) whereas PV technologies are exhibiting similar performances (around 130 US$/MWh). Marine energy is currently the most costly technology (higher than 440 US$/MWh).

In [21], the LCOE is shown has an unfair criteria, especially when used for comparing variable renewable sources (such as wind and solar) with conventional technologies that are dispatchable (i.e. that can be controlled). Indeed, the authors introduce the concept of "System LCOE" which takes into account the uncertainties related to the power output of renewable sources, which have to be handled in order to ensure the grid stability (i.e. energy supply must be equal to demand at each moment). In this regard, an additional cost named "integrating costs" is modelling the adaptation of the actual energy mix (adjustments in terms of dispatchable capacity) in response to variable renewable sources integration. With a high share of variable renewable facilities, the system LCOE is very high because the matching between the supply and power demand is bad. This cost can be reduced by introducing some flexibility in the demand profile (e.g. demand side management (DSM) is a promising methodology currently developed) or increasing the electricity storage capacities (pumped hydro, chemical storage, thermal storage, etc.). This latter point is the solution that will be discussed in this thesis.

In [22], the authors also show that a high penetration scenario of variable renewable sources will induce a higher cost of electricity because of the limited flexibility of electrical systems. Different approaches to assess the cost of integrating variable renewable sources are presented in [23].
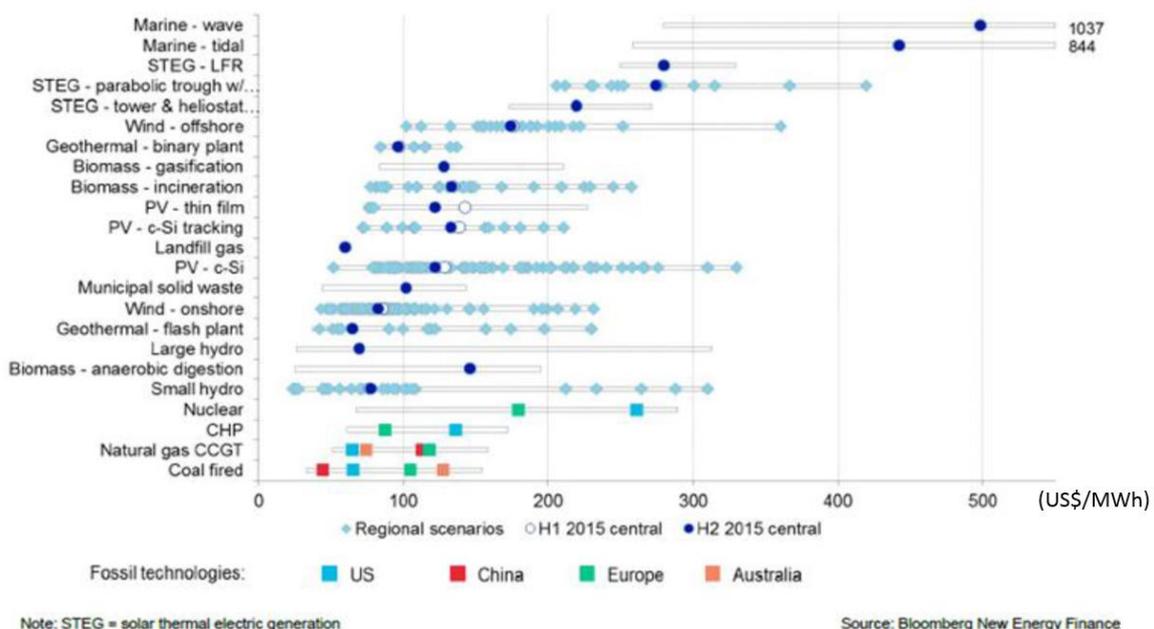
Figure 2.12 Levelized cost of energy for different technologies [18]

• **Life cycle GHG emissions** reflect the impacts on the environment. Based on 79 studies of life cycle analysis (LCA), the authors of [24] compared renewable and conventional fuel sources of electricity, as presented in Fig. 2.13. For renewable sources, the upstream stage (fuel extraction, processing and delivery) is the most GHG emitting, whereas for conventional sources it is the

downstream stage (use and end-of-life disposal). In Fig. 2.13, the **worst case scenario** (maximum emissions values) and the **average values** have been used for the **renewable energy sources** and the **conventional sources**, respectively. It appears that some renewable technologies (such as the waste treatment and the dedicated biomass) and conventional sources contributes to similar GHG emissions. On the whole, it is not surprising to find that the conventional sources (excepted for nuclear which exhibits others concerns such as the disposal of radioactive material) are more GHG emitting than renewable sources. Offshore wind turbine technology is the lowest GHG emitting (it seems that the maximum value has not been properly reported in the figure because it should have been 24 instead of 9 gCO_2eq/kWh (electricity)). There is a significant difference with onshore wind technology explained by economies of scale due to larger installations and because there is no forest felling to place wind turbines. The results for marine technologies are promising but the authors warn about the fact that this technology is not as mature as wind or solar sources (i.e. there is more uncertainties because less information is available). The mean value of photovoltaic (PV) GHG emissions is around 90 gCO_2eq/kWh (electricity) which corresponds to more than the double of mean GHG emissions of onshore wind turbines (increasing the efficiency of PV modules is a crucial issue).
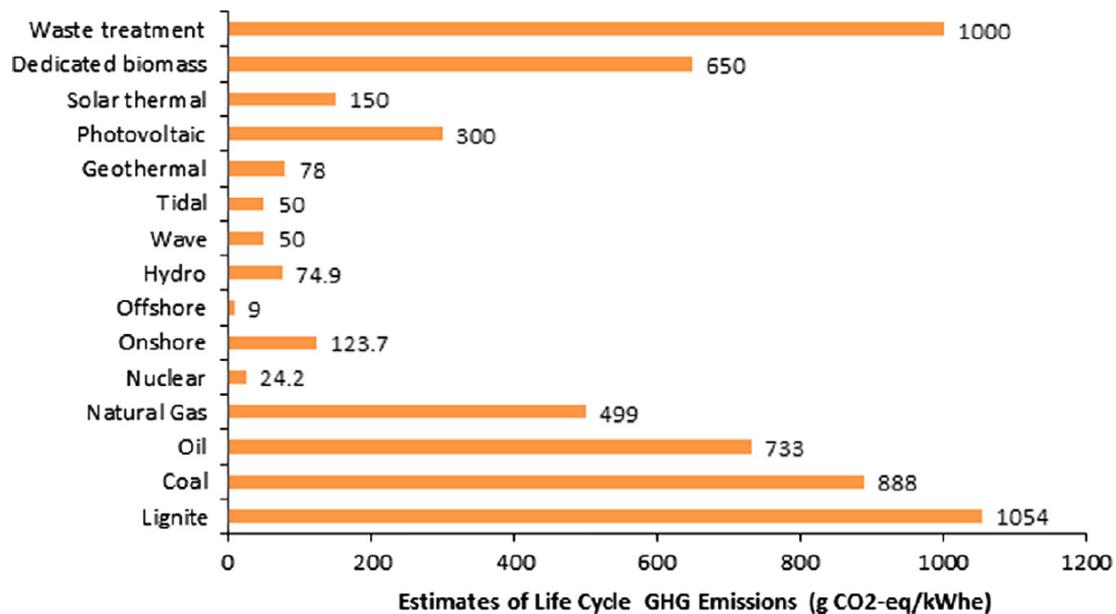
Figure 2.13 Estimated GHG emissions for different electricity generation technologies [24]

- **Energy pay-back time (EPBT)** is presented in [25]. It indicates the number of years to recover the primary energy of the entire life cycle of the energy generating system (based on LCA and on the estimated annual production of this system). Several studies have been reviewed in [25] in order to calculate the EPBT of different renewable sources, see Fig. 2.13 (a value of 15.5 years has been removed for solar PV source in order to properly display the small values of the other sources).

Therefore, solar PV source exhibit a longer EPBT than other renewable sources (ranging from 1 to 15.5 years). As shown in a more recent study [26], the EPBT of solar PV tends to decrease because of more efficient PV modules.

On a broader level, according to the expected lifetime of these renewable sources (between 20 and 30 years), the amount of produced energy during the whole life cycle will be twice to 30 times higher than the energy dedicated to the life cycle of the generating source. This measurement is called energy return on investment (EROI) (or energy returned on energy invested (EROEI)). This dimensionless indicator reflects the effectiveness of the energy production and delivery by evaluating the final energy obtained from a unit of energy spent in the process of harvesting energy. Our different energy sources shows an important gap between fossil fuel sources and renewable sources as presented in [27]-[28]. Historically,

oil, coal and gas were having an EROI between 50 to 1 and 100 to 1 which has now decreased to a range between 15 to 1 and 40 to 1 (because of depletion, more difficult to extract, as earlier explained). In comparison, wind energy is between 5 to 1 and 15 to 1, and solar energy is between 3 to 1 and 10 to 1. It is suggested in [28], that there is a correlation between EROI and our social and economic development. Indeed, reaching a high EROI (superior to 10 to 1) enable to satisfy vital needs and higher aspirations such as education and arts.
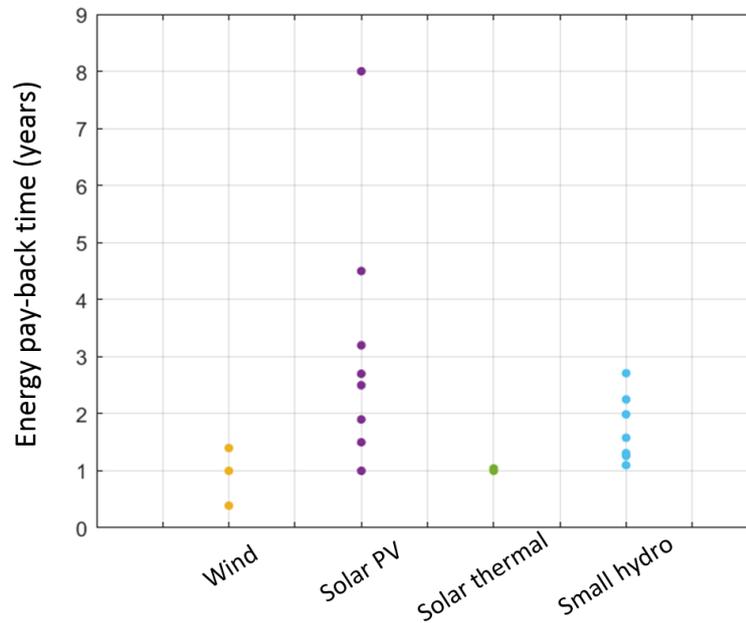
Figure 2.14 Energy pay-back time of different renewable sources.

• **Social acceptance (SA)** of renewable energy sources has been discussed in [29], [30]. According to [29], SA relies on three interconnected pillars that are socio-political acceptance (i.e. public support for a technology, national policy framework), community acceptance (i.e. local acceptance of a technology), and market acceptance (i.e. willingness of consumers and investors to develop a technology). A key issue in the deployment of renewable projects (such as wind power farms) is to involve local communities in the making process in order to avoid the 'not-in-my back-yard' (NIMBY) phenomenon (i.e. people that are favourable to a technology if it is not developed in their living area). The challenge is to translate national objectives that have a good public support into local policies accepted by local communities. The social acceptance of electricity production by renewable sources instead of fossil fuels has been studied in [30]. This study aims to outline the willingness to pay of local communities for renewable sources in order to prevent environmental damages. It appears that people with higher income and educational level are eager to pay more for renewable energy sources. A greater willingness to be pay has been also found with homeowners and urban people compared to tenants and rural populations, respectively. Renewable energy sources are seen as a technological advancement for people living in remote areas (such as islands) who are more favourable to such electricity production. However, authors warn that a positive attitude to renewable energy sources is not guaranteeing an action because of distrust in energy suppliers, switching inertia, etc.

In this thesis, the LCOE adapted to energy storage systems (ESSs) will be used in order to assess the cost of stored electricity by taking into account the lifetime of the storage system. Some key figures will be given at the end of this chapter about GHG emissions concerning batteries. The concept of EBPT cannot be used for storage systems but a life cycle analysis expressed in terms of primary energy consumption is sufficient to give an overview of environmental impacts (if it is combined with GHG emissions). The literature in social acceptance for microgrids with storage systems is scarce, this is why we will not be able to evaluate this criteria in our methodology.

2.2.3 International environmental policy

A significant step towards a global and strong environmental policy has been made in 1992 with the Earth Summit in Rio de Janeiro. Indeed, few months later, the international environmental treaty named United Nations Framework Convention on Climate Change (UNFCC) was adopted. It results in the organization of the annual conference of the parties (COP) in order to assess progress done in GHG emission reductions, set new objectives and conclude legally binding obligations for the future. We remind in this manuscript two major conferences that contributed to the adoption of global environmental policies:

- **Kyoto protocol** (COP 3 in 1997) commits 192 state parties to reduce GHG emissions. An average decrease of 5% below 1990 levels was the objective of the first commitment period (2008-2012) that entered into force in 2005. For the second period (2013-2020), a reduction of at least 18% has been set but this commitment is not entered into force due to the insufficient favourable number of parties. After the first commitment, the European Union has defined in 2008 a new energy policy for 2020 called "three 20 targets" (or 20-20-20). The objectives by 2020 are to reach 20% of renewable energy in the total consumption, reduce by 20% the GHG emissions and increase the energy efficiency by 20% taking 1990 emission levels as reference. In 2014, more ambitious objectives have been set for 2030 (47% of GHG emissions reduction, 27% of renewable sources, 27% of energy efficiency compared to 1990 levels).

- **Paris Agreement** (COP 21 in 2015) enhances the objectives of GHG emission reduction for the 195 signatories in order to hold the increase of the global average temperature below 2°C (even further to 1.5°C) above pre-industrial levels. As explained earlier, the risks and impacts of climate change would be reduced if this goal is achieved. By 2020, a climate finance of 100 billion USD have also been decided to support developing countries for climate adaption and mitigation.

As presented in Fig. 2.15, the share of additional renewable sources increasing every year and reached more than 45% of world power generation capacity additions in 2014 (wind power accounted for 37% of the total renewable capacity additions, solar power was nearly one third and hydropower was more than a quarter).
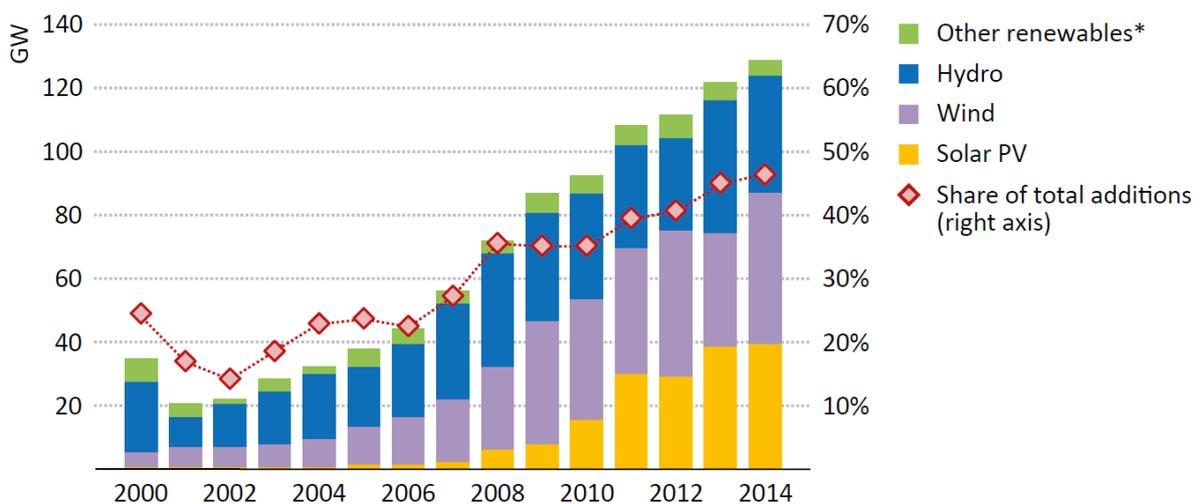
* Includes geothermal, marine, bioenergy and concentrating solar power.

Figure 2.15 Global capacity additions by type of renewable source [10]

In Europe, the official data from Eurostat (available online, last accessed: October 2017, http://ec.europa.eu/eurostat/statistics-explained/index.php/Renewable_energy_statistics) show the share of renewable energy in gross final energy consumption and the targets for 2020 (legally binding). As depicted in Fig. 2.16, individual targets have been set for each EU country.
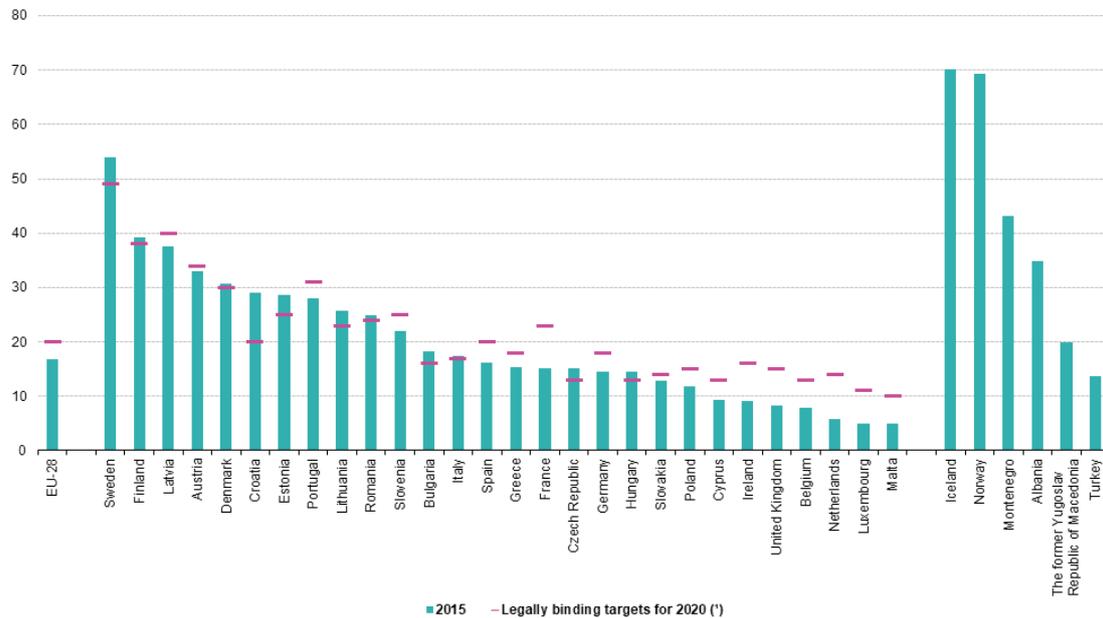
Figure 2.16 Share of renewables for EU countries in gross final energy consumption in 2015 and targets for 2020

The increasing proportion in electricity production from renewable energy sources in EU countries is illustrated in Fig. 2.17 (data from Eurostat). This growth of renewable production raises the issue of storage capacity because of the intermittent and non-dispatchable nature of these new sources. This point will be explained in more details in the next section.
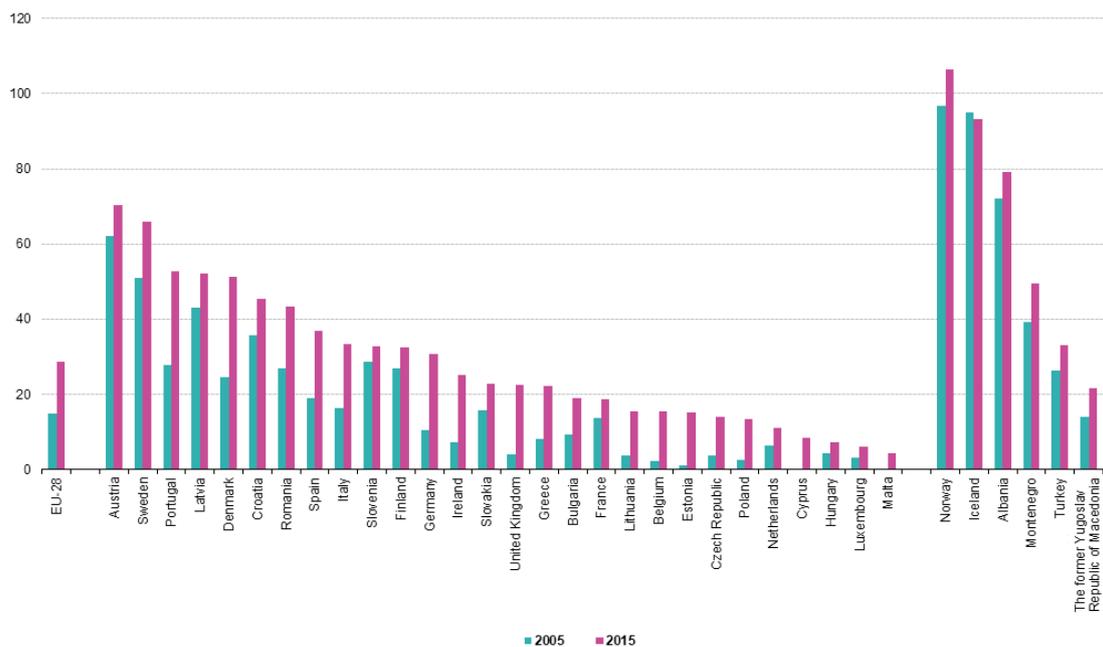
Figure 2.17 Proportion of electricity generated from renewable sources in EU countries in 2005 and 2015

2.3 Towards the next generation of electricity grid

2.3.1 Alternating current (AC) and direct current (DC) distributions

At their early stage of development in the 1880s, direct current (DC) and alternating current distributions were struggling to dominate the electricity market. In 1882, the DC based station of Pearl Street, designed by Thomas Edison, powered hundreds of incandescent light bulbs in lower Manhattan, New York. The main disadvantage was the high current transmission due to low voltage levels (110V at the beginning replaced by 200V) which generate high ohmic losses, high voltage drops for long distances between generation and load, and high cost due to large amount of copper. In the 1890s, driven by the efforts of Nikola Tesla and George Westinghouse, the alternating current (AC) made a final breakthrough with the illumination of the Chicago World's Fair (thousands of lamps and spotlights) and the long distance power transmission demonstrated by the Niagara hydroelectric power plant. Indeed, the AC distribution, relying on AC motors and transformers, is now the worldwide standard for electricity generation and supply. The main issue is to precisely control the voltage and the frequency of the transmitted energy at end user.

The existing AC utility grid has been structured as a centralized grid with a one-way power flow and long distance transmission lines. The frequency of the AC utility grid is 50Hz or 60Hz depending on the country and three levels of voltage have been defined in order to improve the efficiency of transportation and delivery. Electricity is transported through transmission lines at high voltage (HV) (voltage higher than 100 kV and capacity higher than 50 MW) whereas for safety reasons, distribution is done at medium voltage (MV) and low voltage (LV) (voltage lower than 1000 V) [31], [32].

Energy demand is met by using least-cost economic dispatch, based on available generation and transmission means. In this regard, large generation power plants (nuclear, coal-fired, hydroelectric, etc.) supply the base load demand (unvarying demand). Peaking power plants such as gas turbines (or more local combined heat and power (CHP) plants) are operating a few hours per day to meet the peaking demand.

The aging of power delivery infrastructures have some consequences such as a higher failure rate (more outages, more inspection maintenance costs, etc.), insufficient capacity due to increasing demand (so additional substations have to be build), difficulty to integrate these infrastructures in new network because the facility was not built to communicate and operate in a group.

The need of new less polluting generators such as renewable sources is limited because of the intermittent and not dispatchable nature of these sources. For example, based on the literature review done in [33], the maximum penetration of PV generators should be limited to levels between 10 and 50%.

Furthermore, it is estimated that the transmission process is responsible for around 8% of power losses over the power and 20% of the generation capacity has been built only to meet peak demand which occurs only 5% of the time [34]. A new scheme called smart grid, based on the principle of integrating distributed generation, involves a better integration of renewable sources and it is expected to ensure a better utilization of the distribution grid (the transmission lines will not have to be oversized for peak demand).

2.3.2 Smart grid and microgrid (MG) – The challenge of renewable sources

The concept of smart grid has been developed notably through the electricity market liberalisation, the development of power electronics (efficient power converters), and enhancement of information and communication technologies (ICT) [34].

Smart grids are supposed to handle bidirectional energy flows and integrate distributed generation plants. The advantages of developing a distributed topology are numerous: increasing the flexibility of the grid (better penetration of renewable sources), reduction of power losses, increasing the reliability of electricity supply, etc [35]-[36].

A smart grid can be seen as the aggregation of several cells called microgrids (MGs) that operate at MV and LV levels and can be either interconnected to the main grid or "islanded" (i.e. working autonomously) [37]. A MG is constituted of distributed energy resources (DERs) such as distributed generators (that can be renewable or not) and storage systems [38]. This new electrical scheme is possible because of the recent developments in the field of power electronics, which proposes various topologies of power converters to connect almost any type of feeder to any type of load with very good performances (efficiency and reliability) [39].

A good overview of the benefits (feeder losses reduction, local reliability and resiliency improvement, renewable energy sources integration, etc.) and the technical issues (modelling and control) related to the development of MGs is given in [40]–[43].

A lot of architectures of MGs can be found in the literature, either based on AC, DC or mixed distribution [44]. An example is given in Fig 2. 18 with multiple AC and DC devices connected to the same MG through two distribution buses. The DC distribution is becoming more popular because a lot of systems connected to the network are DC native (batteries, PV panels, LED lighting, electronic devices, etc.). Hence, some conversion stages could be removed. Moreover, the control is simpler because only the voltage has to be regulated (instead of voltage and frequency for the AC distribution) and there is no reactive power. The drawbacks of utilizing a DC distribution are related to its low maturity: a higher cost of protections (DC breakers does not benefit from the zero crossing current that is used in AC distribution). The following studies make some comparisons between the AC and DC distribution systems [45]–[47].
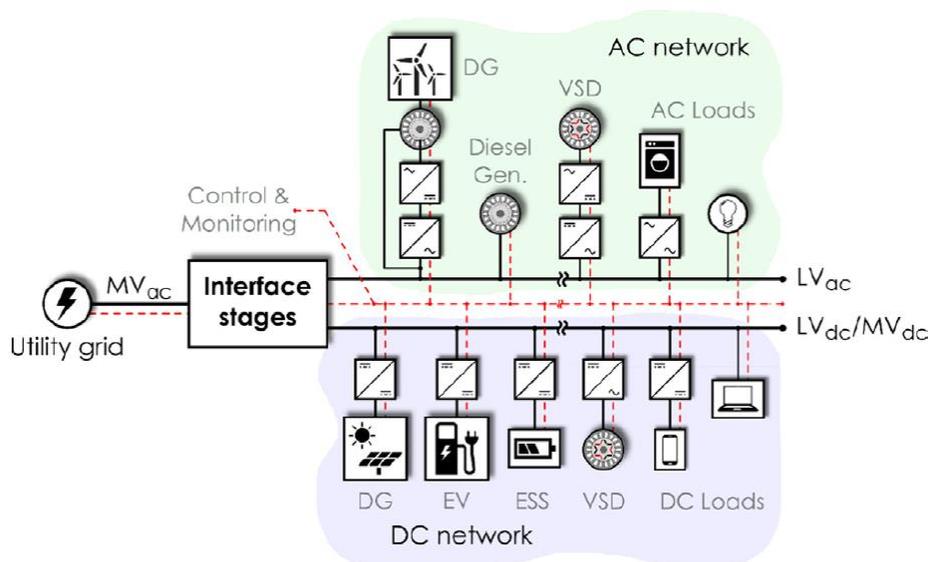
Figure 2.18 Typical hybrid microgrid configuration [44]

Concerning the possible topologies in DC distribution (monopolar, homopolar, bipolar), a study has been done in [48]. The standard voltage levels with their main applications in LVDC MG are presented in [49].

2.4 Case study: the solar (PV) source

"Nobody can embargo sunlight. No cartel controls the Sun. Its energy will not run out. It will not pollute the air; it will not poison our waters. It's free from stench and smog. The Sun's power needs to be collected, stored and used."

Jimmy Carter (born on the 1st October 1924), 39th President of the United States (1977-1981) who established the U.S. Department of Energy in 1977.

2.4.1 PV systems background

Solar photovoltaic (PV) technology is converting the abundant, universally available and free energy from sunlight into electricity. In 1839, Edmond Becquerel observed the photovoltaic effect, paving the way for the development of solar cells [50]. The first practical silicon solar cell has been developed in 1954 at Bell labs and the PV silicon technology benefited from the success and the recognized know-how of microelectronics (reproducible deposition techniques, long-term stability, etc.). PV technology has several benefits such as easy integration in buildings, very modular and adaptive current-voltage output (due to series-parallel association), no noise during power generation (contrary wind turbines), robust (service life between 25 and 30 years at a guaranteed minimum rated output of 80% and 70%, respectively [51]).

This source of energy has been studied since the creation of the LAAS-CNRS in the 1970s in the field of embedded applications such as satellites. The research team, 'Intégration de Systèmes de Gestion de l'Energie' (ISGE), in which this doctoral thesis has been done, has focused one of its interest on electrical architectures dedicated to PV arrays. These works were supervised by Prof. Corinne Alonso [52]. The last studies investigated the impact of shadows on PV systems, their modelling and the design of reconfigurable architectures [53]–[55]. Hence, the integration of this energy source in the grid is the actual challenge that must be carried out.

A PV system encompasses a PV array (association of PV modules, itself association of PV cells) and the balance of the system (BOS) components (such as a power converter, controller, wiring, protection, etc.) that enable to connect the PV array to a load (AC or DC appliances), see Fig. 2.19. The maximum power point tracking (MPPT) controller aims at extracting the largest amount power from the PV module under any conditions (solar irradiance, temperature, shading, etc.) and is also often ensuring the regulation of the load voltage (e.g. batteries have a maximum voltage to not exceed). Several MPPT methods have been developed with their specific hardware setup (sensed parameters, analog or digital control, etc.) and exhibit various performances (convergence speed, range of effectiveness, etc.) [56]. "Perturb and Observe" and "Hill climbing" are two very popular methods involving only PV current and voltage measurements and requiring a low complexity in calculations for a good effectiveness [56].
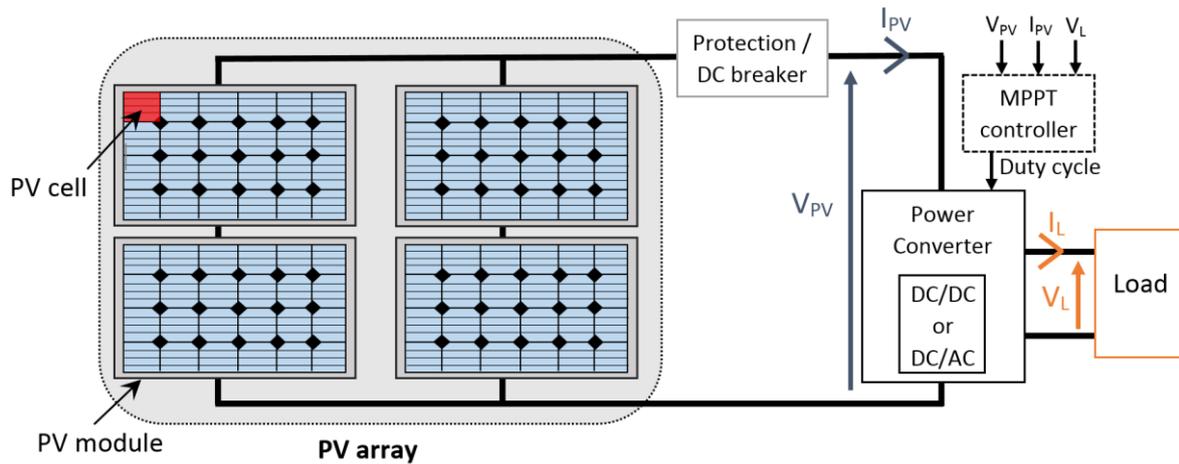
Figure 2.19 Typical PV system feeding a load (AC or DC)

The main characteristics of a PV module are:

- Installed capacity, expressed in "watt-peak" (W_p), refers to the rated power produced by a PV module under standard test conditions (STC). The STC used to evaluate PV modules are the following: vertical irradiance of 1000 W/m², average module temperature of 25°C, air mass of 1.5 (i.e. it models the atmosphere thickness during solar zenith for medium latitudes such as the United States) and a specific irradiance spectrum (similar to the solar irradiance) [51].

- Performance ratio (PR) evaluates the performances of the complete PV system such as the efficiency of the MPPT controller, the losses in the power converter, ohmic wiring losses, dirt on PV modules, etc. PR is the ratio between the PV system real power output and the calculated maximum output (based on the characteristics of the PV system, irradiance and temperature conditions, etc.). In [51] well designed PV systems are assumed to achieve a PR of 80% to 90% throughout the year. In the literature review done in [33], the effective PR is lower (between 55% and 76% for more than one hundred PV systems mounted in Europe) underlining that the operation conditions of PV systems can be improved.

- Capacity factor or capacity utilization factor (CUF) is the ratio, often calculated on a yearly basis, between the real output of the PV system compared to its theoretical output running every hours in a year (8766 hours) at the installed capacity. An example from India shows an average capacity factor of PV systems about 22% [57].

- Open circuit voltage (V_{OC}) is the maximum available voltage from a PV module (current is zero).

- Short circuit current (I_{SC}) is the maximum available current from a PV module (voltage is zero).

- Maximum power point (MPP) is the maximum power produced by the PV module at a given solar irradiance and temperature. Indeed, when the solar irradiance decreases, the current output is decreasing, and when the temperature deviates from 25 °C (standard temperature), the voltage is decreasing, thus in both case the power output is decreasing.

The typical I-V and power curves of a PV module with their main characteristics are illustrated in Fig. 2.20.
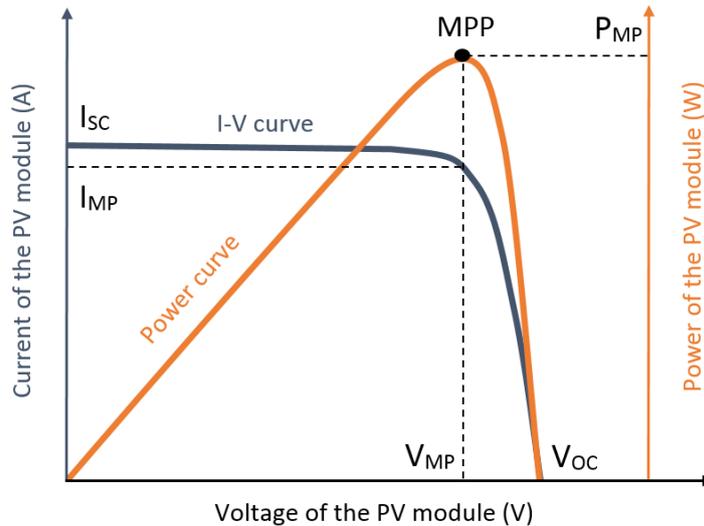
Figure 2.20 Typical I-V and power curves of a PV module

Numerous PV technologies have been developed and commercialized (Thin-Film, Crystalline Si, Single junction, Multijunction, organic, etc.). The National Renewable Energy Laboratory (NREL) has been compiling the efficiencies of the main advances of PV cells that have been measured with respect to STC since 1976. The plot presented in Fig. 2.21 is courtesy of the National Renewable Energy Laboratory, Golden, CO (available online, last accessed: October 2017, https://energy.gov/eere/sunshot/downloads/research-cell-efficiency-records).
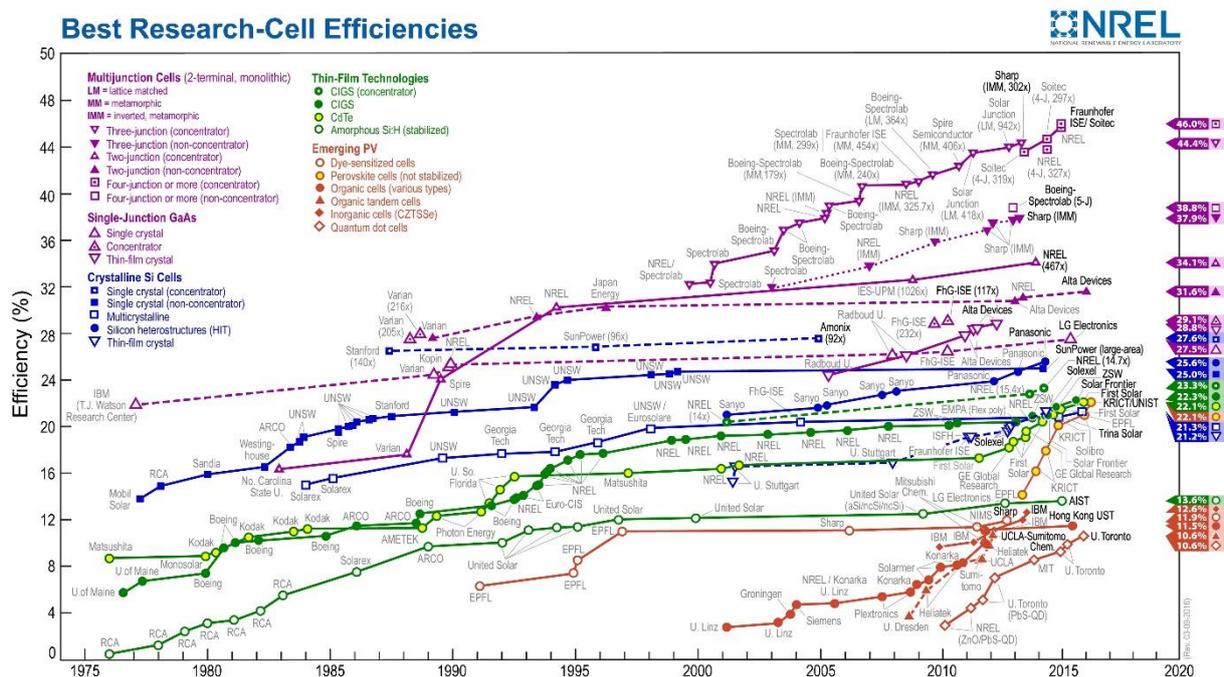
Figure 2.21 PV cell efficiency results involving different families of semiconductors

Due to the increasing efficiency of PV cells, the improvement of industrial processes and a continuous global high demand, the price of PV modules per unit of produced electricity is decreasing, as well as the GHG emissions and the EPBT (dropped to around 1 year in some cases for mono and poly-Si [58] and around 2 years in Germany [59]). In the last 40 years, the prices of PV modules decreased from

about 100 USD per Wp to 0.8 USD in 2012 (and it is expected to continue with a price of 0.4 USD per Wp by 2035), as illustrated in Fig. 2.22 [51].
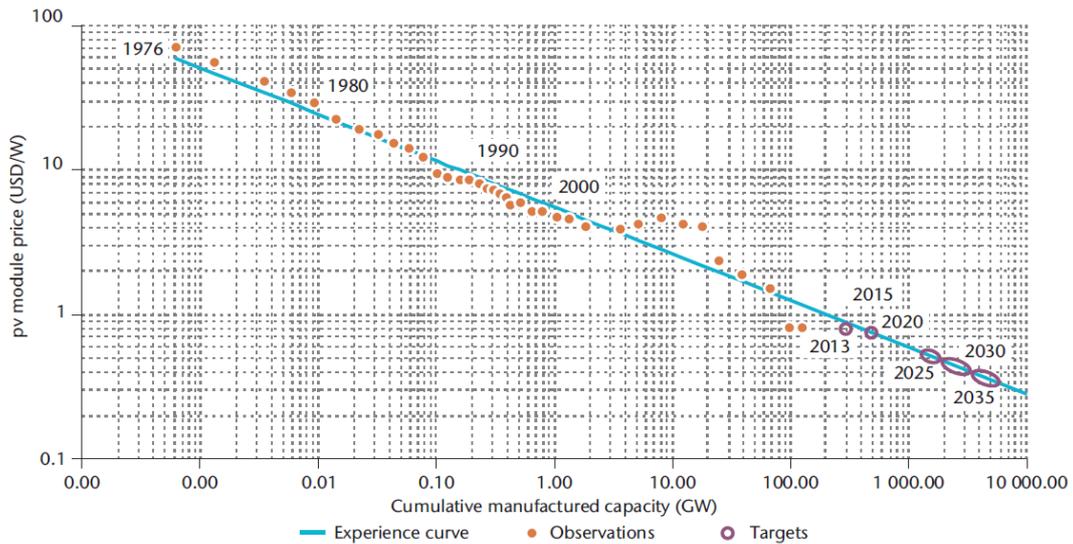
Figure 2.22 Evolution and projections of PV module price [51]

Relying on the technological advances and on world solar resource (global horizontal irradiation), the global EPBT of PV systems presented in the Fig. 2.23 reveals the countries that could benefit the most from solar energy such as Africa, Latin America, Australia and the Southern Asia [60].
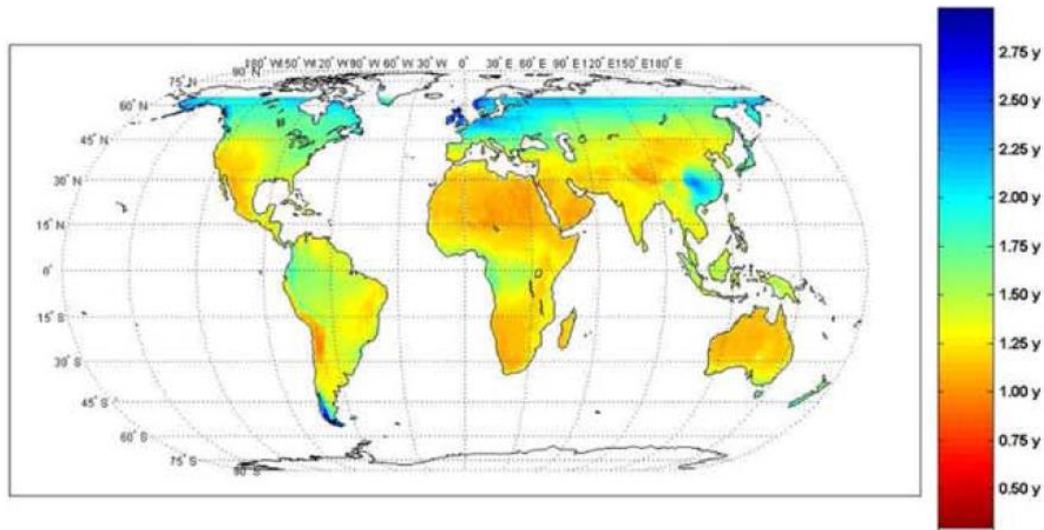
Figure 2.23 Worldwide EPBT of on-grid PV modules including all BOS components for the year 2010 [60]

Over the last few decades, many projects have brilliantly proven that PV energy may be used in numerous applications:

- Transport sector

The first demonstration of solar PV car have been done in 1982 by the car named the "Quiet Achiever" which travelled across Australia during 20 days (more than 4 000 km from Perth to Sydney). Since then, an international race called "World Solar Challenge" is held in Australia to promote research on solar-powered cars.

In 2016, the PV solar aircraft named "Solar Impulse 2" achieved the circumnavigation of the globe (around 42 000 km) in 16 months (the first test flight of "Solar Impulse 1" was on December 2009). This plane was flying during days and also nights thanks to a large battery pack (weighting more than a fourth of the total weight).

More recently, a vessel called "Energy Observer" started is journey in 2017. This project involves a mix of renewable energies (PV solar and wind turbines) and innovative storage system (hydrogen fuel cell). All these projects are illustrated in Fig. 2.24.

Figure 2.24 Projects of vehicles powered by PV solar systems – A) Quiet Achiever, B) Solar Impulse, C) Energy Observer

- Energy and building sectors

Rooftop solar PV and building integrated PV (BIPV) systems are widely used as a complementary "green" source of energy to the main grid [61]. Such systems are sometimes associated to batteries in order to provide auxiliary services.

Large PV systems are also designed to play the role of power plant. Main topologies are presented in [62] and new floating PV plants are developed in order to limit land use [63]. The environmental impacts of these systems has been analysed in [64].

PV technology enables the rural electrification, replace fossil fuels and poorly efficient solutions in standalone systems. Some examples of implementation in Argentina are given in [65]. Applications such as solar homes, pump irrigation and desalination systems are reviewed with the different PV technologies in [66].

In this thesis, historical data that have been obtained since 2012 from the ADREAM building of the LAAS-CNRS (available online, last accessed: October 2017, https://www.laas.fr/public/en/adream) helped us define the requirements of PV building (consumption and production are monitored on a minute basis). In this building presented in Fig. 2.25, 25 kWp out of 100 kWp of installed PV panels are dedicated to research work (PV panels modelling, enhancement of MPPT algorithms, PV array recombination in case of shadows, etc.). In order to work on PV production forecasting, a meteorological station has been installed (measurements of wind speed and direction, global and diffuse irradiance, temperature and humidity) [67]. In addition, three reversible heat pumps are used for cold/hot water and air cooling/heating. We have recently installed 59 kWh of lead-acid batteries and 56 kWh of lithium-ion batteries.

Figure 2.25 ADREAM building of the LAAS-CNRS

More than 7000 sensors have been installed outside and inside the ADREAM building. The main aim of this equipment is to increase our knowledge on PV systems in different configurations in order to increase the production of the building and also reduce the energy consumption by monitoring and supervising lighting and ambient temperature. The ultimate objective is to become a Plus-Energy Building (i.e. producing more energy than consumed over a year). An overview of the experimental benches is given in Fig. 2.26.
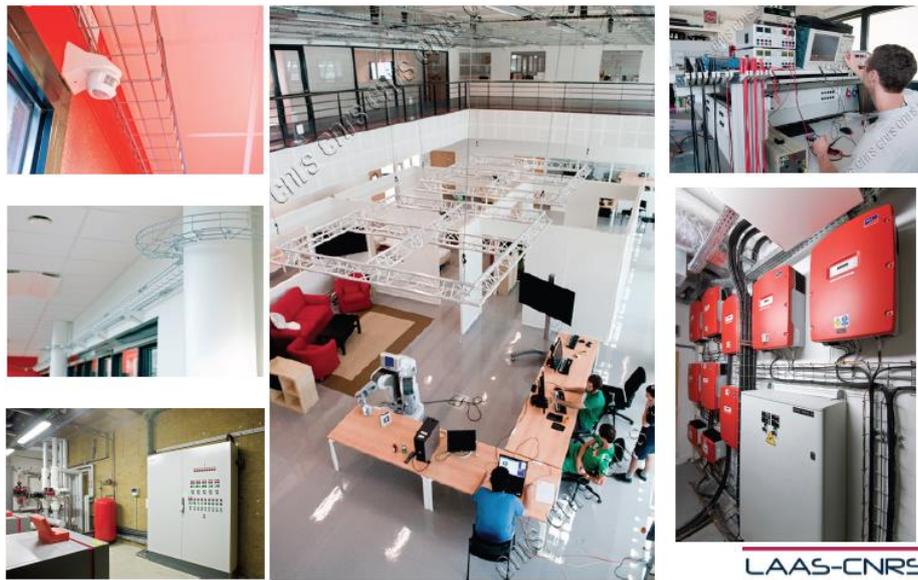
Figure 2.26 Different views inside the ADREAM building

An example of power balance (PV production minus energy consumption) of the ADREAM building is illustrated in Fig. 2.27. A complete description of three years of data will be given in chapter 4.
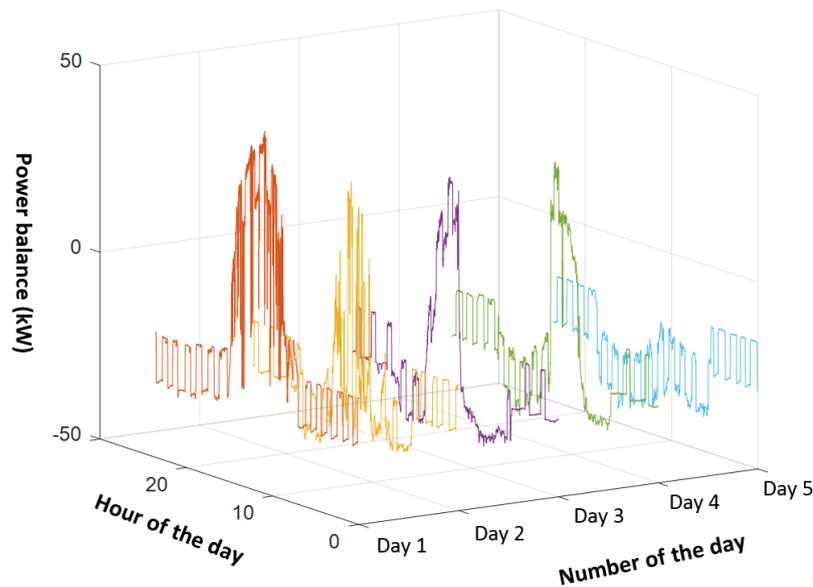
Figure 2.27 Example of power balance of the ADREAM building during 5 days of December 2016

An example of PV production injected in the local grid is presented in Fig 2.27 through 5 days of power balance of the ADREAM building. The effect of the weather on PV systems can be seen with a highly varying production from a day to another (the surplus power reaches 30 kW during day 1 and there is no surplus power during day 5). Hence, in order to make a PV source more dispatchable and enhance the autonomy of the building, an energy storage system (ESS) can be integrated in the building but the difficulty is to optimally size the capacity of the storage system. This is the point of the chapters 3 and 4.

2.4.2 Energy storage systems (ESSs)

As explained in a report from the National Renewable Energy Laboratory (NREL), the actual utility grid mainly operates without storage but the storage of electrical energy may increase the flexibility of the grid and thus integrate more renewable sources that are difficult to predict [68]. Indeed, forecasting is the key to achieve a high reliability and a low cost. Typical day-ahead forecast errors are from 1 to 3% for load, from 6 to 8% for wind and higher for PV solar.

As explained in [69]–[72], an ESS can provide numerous benefits such as:

- Environmental: integration of renewable sources (the variability of these sources threatens the grid stability), replacement of diesel generators (in off-grid sites), pollution reduction (by reducing peak demand often met with harmful and costly plants), etc.

- Societal: electricity supply in remote areas, reliability improvement (possibility to maintain the grid stability or operate separately from the utility in a so-called islanded mode), duration of outages decreased (ESS can perform a black-start), etc.

- Economic: energy cost decrease (due to electric energy time shift that enables to buy cheap energy and then sell and/or use it when it is expensive), use of expensive thermal power plants diminution (with advanced energy management strategies), electric peak demand flattening, power factor correction, transmission and distribution (T&D) investment deferral, etc.

Every actor of electricity from the end-user to the utility operator may find one or more benefits to install an ESS facility. Indeed, potential synergies might be achieved, for example by charging batteries during off-peak demand and discharging during on-peak, energy cost will be reduced (because energy is bought

cheap and sold expensive), energy losses (I^2R) will be reduced (because on-peak demand will be reduced, especially if the location of the ESS is close to the demand point), pollution may be reduced (because in general cleaner power plants are used for baseload demand), T&D deferral or life extension of the utility can be fulfilled because it mainly depends on the peak-demand. Two typical use cases are illustrated in Fig 2.28. In Fig 2.28-A, the ESS helps reduce the peak-demand. Hence, the production of the power plant responsible for the baseload increases to charge the ESS (in general this plant is cheaper and less pollutant than the plants used to meet the peak-demand). During peak-demand, the ESS replaces peaking power plants. The penetration of renewable sources facilitated by an ESS is illustrated in Fig 2.28-B. The ESS stores the surplus energy and ensures the grid stability. When the cost of electricity is high, the ESS supplies and can enable both peak shaving and energy cost reduction.
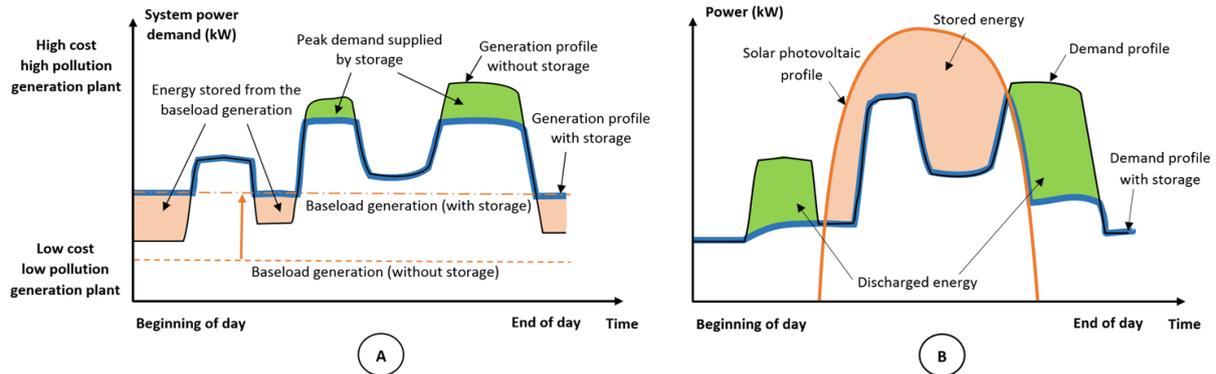
Figure 2.28 Typical use cases of ESS, A) Peak shaving and load levelling, B) Integration of renewable sources

Grid-scale storage facilities through the world have been gathered in a large database from the U.S. DOE [73] as depicted in Fig. 2.29. A full description is given for most of them such as the date of creation, the location, the technology, the rated capacity, the rated power, the use cases, a picture of the project, etc. Some energy policies (incentives, legislature, commissions, etc.) are also available. The conclusion that can be drawn from this database is that:

- The global storage resource is small: the operational maximum power storage is around 170-180 GW. It corresponds to less than one percent of our energy production (14 TW, see section 2.1).

- The main storage technology (in terms of rated power) is by far pumped hydro (~96%) followed by thermal (> 2%), electrochemical (>2%), electro-mechanical (>1%) and chemical (close to 0%).

- Electrochemical projects are the most numerous (nearly one thousand) followed by pumped hydro (352), thermal (206) and electro-mechanical (70).

- The main use cases of these ESSs are electric energy time shift, electric supply capacity, renewable capacity firming, frequency regulation and electric bill management (in figure II. 2 each project can have more than one use case).

(note: in this website, electro-mechanical designates flywheel and compressed air energy storage)

Due to a good scalability (from mW to MW and from mWh to MWh), fast response time (ms), flexibility of operation (power output can be easily changed), easy transportation and installation, battery energy storage system (BESS) facilities have spread out since the 1980s [74].
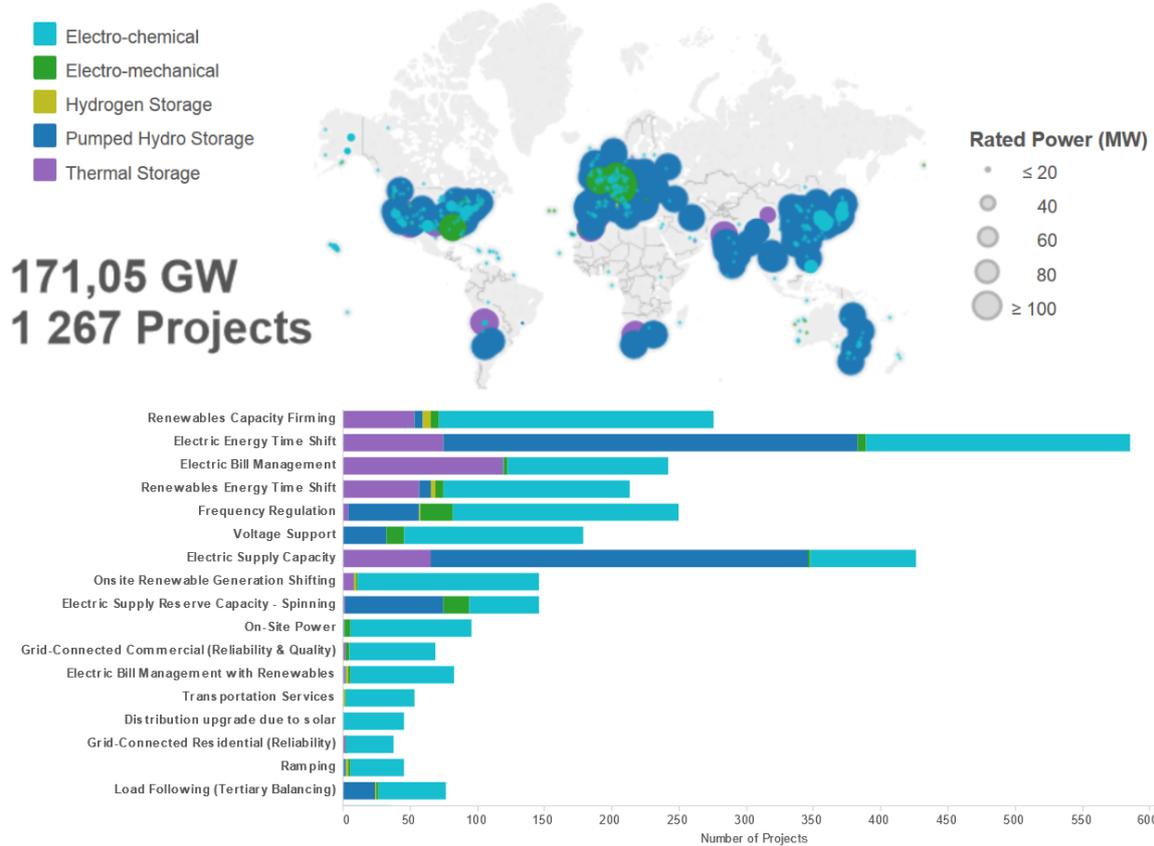
Figure 2.29 Storage facilities through the world [73]

Maturity of ESSs

In the case of electrochemical cells, they are suited to a very wide range of applications such as powering portable electronic devices, starting the engine of fossil fuel vehicles, powering electric vehicles, storing surplus of energy from photovoltaic systems, etc. Since 1990, the average growth rate of battery pack market is 5% per year [75]. The battery pack is defined as the association of electrochemical cells, cells assembly, battery management system and connectors. Power electronics (DC/DC converters, invertors) is not included under this term of battery pack. Lead-acid batteries are very successful worldwide, especially SLI batteries for vehicles, ideal for Starting (the engine), Lighting and Ignition (of the engine). Due to the low cost and the robustness of this battery, lead-acid batteries are the most sold batteries in the world, as presented in Fig. 2. 30. Lithium batteries are the second most sold batteries because of their high performances (capacity, power capability, lifetime) which are mainly used in cell phones, robots and electric vehicles. However, their cost is still a hurdle for some applications. As presented in [76], lithium-ion batteries for battery electric vehicles (BEVs) will be cost-competitive with internal combustion engine vehicles (ICVs) at 150 $ per kWh (it is nearly three times higher today).
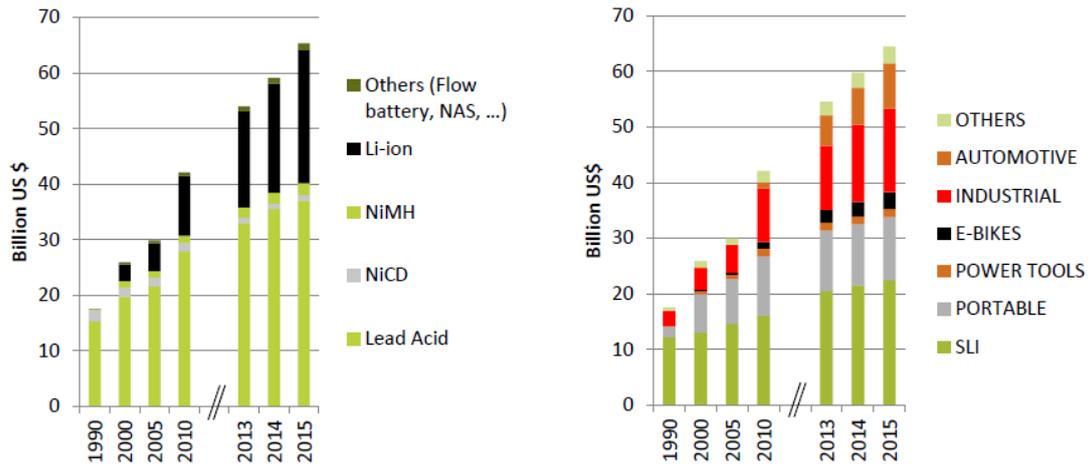
Figure 2.30 Worldwide battery market from 1990 to 2015 [75]

This market analysis is very important when choosing an ESS. For example, due to the increasing global sales of BEVs, the research and development (R&D) improvements in cell designs and cost of input materials, the cost of lithium-ion batteries for BEVs has been decreasing from 2007 to 2014 and it is expected to pursue this trend. The cost of competiveness of batteries (150 $ per kWh) could be reached in 2025, Fig. 2. 31. These forecasts are based on economies of scale relying on the success of large-scale battery production facilities (e.g. Tesla battery gigafactory) and assuming that public incentives to buy BEVs will continue.
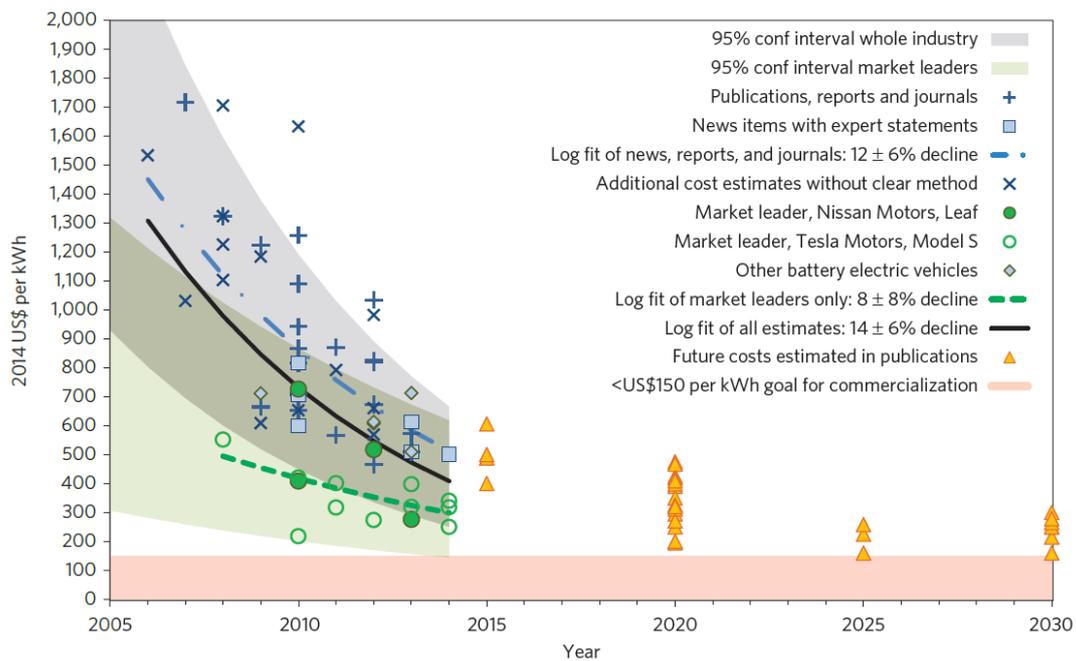
Figure 2.31 Cost reduction of lithium batteries [76]

Safety and robustness

The safety of ESS is very important and may sometimes need extra protections such as the underbody shields that were installed in 2013 on Tesla S model cars to protect the battery pack from debris on the road. More recently in 2016, Samsung made 3 million of recalls of the Galaxy Note 7 because of thermal runaway due to the design of the battery (short circuits between cells because of either a pinching that can occur on the top corner, or welding burrs on the positive electrode). Other safety issues concerning the thermal runaway of lithium batteries have been illustrated in **Fig. 2. 32** (In 2006, SONY recalled

about 9.6 million notebook batteries worldwide due to explosions. In 2013, all the Boeing 787 fleet was grounded for some months because of an internal short-circuit between two cells which was cascaded to other cells creating a massive thermal runaway).

Hence, a malfunction of an ESS can lead to the death of the user. This is why some protections have to be added to the ESS such as a battery management system (BMS), a solid casing, a cooling system, etc. These protections implies a higher cost and also a more important weight and volume that may make the ESS not suitable for the desired application.

Figure 2.32 Safety issues with lithium batteries, a) Sony notebook batteries, b) Yuasa battery in Boeing 787 Dreamliner, c) Tesla S model, d) Samsung galaxy note 7

A lead-acid battery also need a solid casing because it contains lead and sulfuric acid that are very harmful for human health and environment. Moreover, for most of lead-acid technologies, a ventilated environment because when the battery is overcharging, some hydrogen gassing occurs which is highly explosive (especially when its concentration goes higher than 4%).

Environmental impacts - Life cycle analysis (LCA)

The end-of-life of an ESS is a major issue in order to propose more sustainable devices. Indeed, for batteries some materials are toxic and need some treatments before disposal. Moreover, when materials are not abundant, the recycling option seems interesting. In this purpose, the LCA aims at assessing the environmental impact of a device by taking into account four stages that are manufacturing, transportation, use and end-of-life.

In [77] a comparison between the main battery types (lead-acid, Ni-Cd, Ni-MH, NaS and lithium-ion) has been performed based on a life-cycle inventory (LCI) analysis from cradle to gate (i.e. production, manufacturing and assembly of battery materials). The conclusion is that, per kilogram of battery, lead-acid batteries are the lowest energy demanding and the fewest CO_2 and GHG emitting. This performance is enhanced by the fact that 95% of lead-acid batteries are recycled and new batteries are made of recycled content from 60 to 80%. However, this method has some uncertainties because it depends on the availability of data concerning manufacturing processes that are not often published. Thus, it is difficult to accurately assess fast evolving technologies such as lithium-ion batteries.

More recently, main lithium-ion battery technologies have been analysed [78]. The purpose of this study was to compare energy consumption and GHG emissions of internal combustion engine vehicles (ICVs) and electric vehicles (EVs), and also to determine if recycling batteries is worth. First, the fuel cycle is analysed from well-to-pump (i.e. how electricity is generated), from pump-to-wheels (consumption of energy during the use) and from manufacturing/assembly of batteries. Depending on the efficiency of the battery assembly plant, EVs are more energy intensive than ICVs (from 10% to 250%). However, on a per km basis, an EV consumes from 1.6 to 3.4 times less than an ICV (depending on the energy mix of the grid). Thus, in total EVs are less energy demanding and less GHG emitting than ICVs. In addition, it appears that some substantial savings can be done by recycling batteries (50% of the GHG emissions for a whole recycled battery). Indeed, the manufacturing and assembly of a cathode electrode is high energy intensive and high GHG emitting, especially when it contains cobalt and nickel (their mining has a very harmful local impacts such as acid rains, heavy metal soil contamination, wetland acidification, etc.). Moreover, an additional reason to recycle old batteries is that cobalt and nickel

resources are not extensible. The authors are confident about the lithium supplies (available from natural brines, ore and seawater) even considering a high EV penetration scenario. There is still some environmental concerns with lithium production, such as in South America's "lithium triangle" (Chile, Argentina and Bolivia), worldwide main producer of lithium, with the intensively pumping brines from salt deserts.

2.5 Summary

It has been shown in this chapter that energy consumption has been continuously growing worldwide during the past decades. Even if energy can be supplied by several sources, most of the global energy production comes from non-renewable sources that exhibit a finite stock and are considered harmful for the environment (due to GHG emissions). The desired energy system must be universally accessible, low cost, secure (reliable and resilient), and environmental friendly.

In this sense, a new decentralized architecture named microgrid aims at using the advancements in power electronics in order to reduce the power losses due to energy transportation on long distances and enable the massive integration of renewable sources. However the energy production of renewable sources is very varying and may endanger the stability of the grid. Numerous studies explain that the power fluctuations can be compensated by the installation of ESSs but it seems that some work can be done to develop a method enabling to find the optimal sizing and operation of storage systems.

This is why we have chosen to study the behaviour of ESSs and propose a model combining electrical and ageing behaviours. This latter will be useful to determine the most appropriate ESS for microgrid application and to define suitable operating conditions by taking into account cycle efficiency, costs, ageing, etc. Hence, a careful work has been conducted in the next chapter on the study of the main technologies of ESSs and the criteria that enable to compare these systems.

Chapter 3.   Energy Storage Systems

"Essentially all models are wrong but some are useful"

George E. P. Box (18 October 1919 – 28 March 2013) British statistician who contributed in the fields of statistics in experiments, time series analysis and Bayesian statistics.

Electricity has become an essential good in almost every aspect of daily life (lighting, cooking, communication, mobility, etc.). The storage of electricity is a major issue because it is far more expensive compared to other conventional energy forms such as fossil fuels. Moreover, the massive integration of variable renewable sources in our conventional grid endangers the equilibrium between supply and demand that must be satisfied at every moment. This is why new energy storage systems (ESSs) are growing rapidly to handle the further development of renewable sources in the global energy mix. Earlier, large ESSs have already been employed for decades (e.g. pumped hydro facilities based on the potential energy of water streams) in order to provide cheaper electricity during peak hours (large scale power plants are continuously producing electricity and ESSs are charging or discharging according to the load demand). Today, several technologies of ESS are commercialized, scaled for any power and energy requirements, and thus exhibiting very different behaviours concerning the safety, cost, performances and sustainability. For example, since the beginning of off-grid PV systems, new lead-acid batteries adapted to PV solar profiles have been massively developed and used to ensure the stability and the autonomy of these stand-alone power systems. The goal of this chapter is to present a model of ESS (such as lead-acid battery, lithium-ion battery and supercapacitor) that takes into account different criteria (e.g. lifetime cost, energy and power limitations, etc.) in order to help their sizing in microgrid applications (i.e. involving variable operating profiles due to intermittent renewable sources).

This chapter is organized as follows:

First, the main energy storage technologies are presented with their specific performances (efficiency, cost, lifetime, maturity, etc.). Then, lead-acid batteries, lithium-ion batteries and supercapacitors are described in more detail. Later, the main characteristics that assess the efficiency of an ESS in a microgrid application are defined. Finally, models enabling the monitoring of the previously presented ESSs are presented.

Table of contents of chapter 3

3.1 Overview of ESSs and their performances

3.1.1 Major technologies of ESSs at a glance

Electricity can be stored in many different ways such as chemical, electrochemical, mechanical, thermal and electrical, as listed in Fig. 3.1 (the list is not comprehensive).
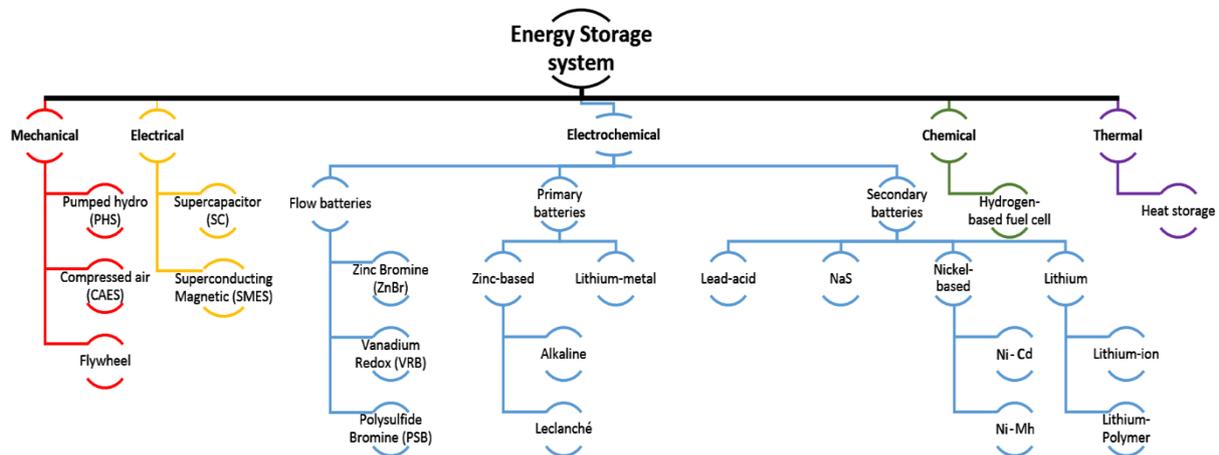
Figure 3.1 List of main available energy storage systems

In the literature, a lot of studies propose to compare the different technologies in order to determine the most adapted to a given application. Based on some reviews [72], [79]–[82], the main properties of the technologies listed in Fig. 3.1 are given below:

- **Mechanical storage** presents a lot of assets such as relatively high cycle efficiency, low operation cost and long lifetime, but the capital cost is high, a large footprint is needed (partly due to safety requirements) with appropriate geographical topologies such as mountains and caverns for hydroelectric and compressed air plants, respectively. The three main technologies related to mechanical storage are defined below. **Pumped hydro energy storage (also referred as pumped hydroelectric storage, PHS)** is a very mature technology (worldwide commercial applications began in 1930's) based on potential energy. When electricity is affordable, water is pumped in a reservoir located at a high height area whereas, when the electrical demand is high (expensive cost), water from the higher reservoir is released through turbines generating electricity. The rated power of such facility is about hundreds of MW with a moderate cycle efficiency (70-85%) which makes this storage technology well adapted to large stationary storage [79]. In addition, this technology involves a long lead time (about 10 years), a high capital cost (several millions of euros) and non-negligible environmental impacts (land flooded, water ecosystem disturbances, etc.) [79]. For **compressed air energy storage (CAES)**, the air is compressed under high pressure in large tanks or underground caverns and turbines produce energy when air is released. Some recent developments enabled to improve the energy efficiency of the system to 70% [72], [81]. **Flywheel storage** uses the principle of kinetic energy. Through an electrical motor/generator, the speed of the flywheel increases when electricity is stored and it decreases during discharge. In order to minimize the energy losses, the flywheel is kept in a vacuum environment which enables to reach up to 95% of cycle efficiency [79]. However, due to the relatively high self-discharge rate (about 20% per hour), the flywheel is more adapted to short-term storage (seconds to tens of minutes) [80].

- **Electrochemical storage** is an interesting solution because of its high scalability and ease of use even in embedded systems. A lot of different designs have been developed involving different efficiency, lifetime, maturity, capital and operating costs. **Primary batteries** are based on quasi

irreversible redox systems (i.e. cannot be easily recharged) so they are only employed as a single use electricity generator whereas **secondary batteries** are rechargeable and can perform a large number of cycles charge/discharge (several hundreds to thousands). More explanations about the principle of batteries and electrochemical cells are given in section 3.2. **Flow batteries** (or redox flow batteries) are based on two electrolytes stored in external tanks. The electrolytes are pumped to an electrochemical cell in order to produce electricity. The energy density depends on the size of the tanks and the power density depends on the rate of chemical reactions occurring in the electrochemical cell. These batteries can be fast to recharge by changing the electrolytes. In general, the chemical reactions are reversible conversely to fuel cells. This technology has been demonstrated for large scale storage (some hundreds of kW to few MW) but is not commercially available as other more mature storage systems (such as secondary batteries) [82].

- **Electrical storage** involves electrostatics and electromagnetism. Capacitors and inductors are well known and widely used in power electronics to store electricity on very short periods (some milliseconds). **Supercapacitor storage (SC)** is a promising fast evolving technology that has already been successfully commercialized in numerous sectors (a full description is provided in section 3.3). For **superconducting magnetic energy storage (SMES)**, a cryogenically cooled superconducting coil stores electricity as a magnetic field. Indeed, this technology benefits from the zero electrical resistance due to the superconducting state reached when the coil is at a very low temperature (around some tens of kelvin, depending on the material). SMES is very efficient (up to 98%) but presents a prohibitive cost to be used in major applications and has a negative environmental impact related to strong magnetic fields [72], [82].

- **Chemical storage** is employed to convert chemical energy into electricity. **Hydrogen based fuel cell** is the most developed technology, relying on the chemical reactions between hydrogen and oxygen. Several types of fuel cells exist such as alkaline (AFC), polymer electrolyte membrane (PEMFC), phosphoric acid (PAFC), etc. Fuel cells for stationary storage application are relatively mature but the cycle efficiency is low (between 20% and 66%) and the recycling of such technology is still under investigation [82].

- **Thermal storage** uses the thermal properties of some solids and liquids. When materials are cooled and heated to produce electricity, the **heat storage** is called **sensible**. When the energy comes from a phase change of the material, the **heat storage** is called **latent**. These technologies are based on tanks, pipes, pumps, heat exchangers and chiller units. Hence, the storage density is very low and the losses can be important (depending on the level of insulation) [81].

Beyond the outline given for the different energy storage technologies, the next section is focused on the criteria that enable to understand the important characteristics of an ESS.

3.1.2 Comparison between ESSs

Taking into account the application requirements (power and energy profiles, available volume, operating temperature, costs, etc.), an ESS technology may be more suitable than another. The main criteria for choosing the most adapted ESS to a specific application are listed below:

- **Response time:** the ESS has to charge/discharge in a given period. Fast response time (s-min) are needed to remove power fluctuations inherited from PV source generation.

- **Capital cost:** different costs have to be considered such as the cost of rated power (€/kW), the cost of rated capacity (€/kWh) and the cost on the long run also called life cycle costs (€/(cycle.kWh)).

- **Operation and maintenance (O&M) cost:** every ESS has its proper O&M requirements. It is difficult to find a clear trend in the literature because it is highly dependent on the location (labour costs) and on the age of the facility.

- **Specific energy (Wh/kg) and specific power (W/kg):** enables to know the weight of ESS to achieve power and energy requirements of the application. Energy and power densities, respectively in Wh/l and W/l, are other metrics representative of the volume aspect.

- **Cycling lifetime (number of cycles):** maximum number of cycles that the ESS can perform.

- **Calendar lifetime (years):** maximum shelf life of the ESS.

- **Cycle efficiency (%):** Also named round-trip efficiency, the energy discharged by the ESS is lower than the energy initially charged into the ESS. It can be measured by calculating the ratio between energy discharged to the energy charged E_{out}/E_{in}. This calculation should not take into account self-discharge.

- **Self-discharge:** due to friction, parasitic chemical reactions or other physical phenomenon, the charges stored in the ESS decreases. This process can be accelerated or slowed by external conditions (e.g. temperature, humidity) but also by operating conditions (e.g. state of charge of the battery, previous rate of charge, etc.).

- **Operating temperature (°C):** an ESS is efficient in a given operating temperature range.

- **Environmental impacts and safety:** reflects the drawbacks of using the ESS because it may use toxic materials (e.g. some batteries), it may jeopardize the biodiversity (e.g. installation of a new PHES), etc.

- **Maturity:** a technology is said mature when there is a strong scientific background and numerous users have improved its reliability, production process and/or performances. For mature technologies only few incremental improvements are expected whereas a new technology is evolving fast thanks to breakthrough advances.

In order to distinguish the differences between the major available ESS technologies, their main characteristics have been gathered in table 3.1, from the literature review of [72], [79]–[82]. The purpose of this table is to propose some trends and not an in-depth analysis, especially for the energy and power costs which sometimes exhibit a large difference between the low and high boundaries. For further details, a list of the main manufacturers of the different technologies is proposed in [80].

Concerning the volume and the weight of an ESS (that are characterized by power and energy densities, and specific power and energy, respectively), different ESSs are compared in pseudo Ragone plots in Fig. 3.2. These parameters may be crucial for applications that have strong constraints on volume and/or weight (such as electric vehicles, satellites, cell phones, laptops, etc.).

ESS Technology	Response time	Rated energy (MWh)	Energy capital cost (€/kWh)	Power capital cost (€/kW)	Specific energy (Wh/kg)	Specific power (W/kg)	Cycling lifetime (nb. cycles)	Calendar lifetime (years)	Cycle efficiency (%)	Self-discharge per day	Maturity
PHES	s	Up to 8000	5 - 100	2000 - 4000	0.5 - 1.5	N/A	10000 - 30000	> 40	70-85	Very small	M
CAES	s - min	Up to 2860	2 - 120	400 - 1000	30 - 60	N/A	8000 - 12000	> 30	70-80	Small	C
Flywheel	ms	Up to 5	1000 - 14000	200 - 350	5 - 100	400 - 1500	$> 10^5$	15-20	90-95	100%	EC
SMES	ms	Up to 0.015	500 - 72000	200 - 489	0.5 - 5	500 - 2000	$> 10^5$	20 - 30	>95	10 - 15%	D
SC	ms	Up to 0.0005	300 - 2000	100 - 450	0.05 - 5	10^4	$> 10^5$	10 - 30	> 95	20 – 40%	D/ EC
Lead-acid	ms	Up to 40	50 - 400	200 - 600	30 - 50	75 - 300	200 - 2500	5 - 15	70-80	0.1 – 0.3 %	M
Lithium-ion	ms	Up to 10	600 - 3800	900 - 4000	75 - 200	150 - 1000	1000 - 10000	10 - 20	85 - 95	0.1 – 0.3 %	EC
NaS	ms	Up to 244.8	300 - 500	1000 - 3000	150 - 240	150 - 230	2500 - 4500	10 - 15	65 - 85	20%	C
Ni-Cd	ms	Up to 6.75	400 - 2400	500 - 1500	50 - 75	150 - 300	1500 - 3000	10 - 15	60-70	0.2 – 0.6%	C
Flow batteries	ms	Up to 120	150 - 400	400 - 2500	10 - 50	45 - 150	2000 - 10000	5 - 15	60 - 85	Small	D/ EC
Fuel cell	s	Up to 39	2 - 15	500 - 3000	800 - 10000	> 500	> 1000	5 - 15	25 - 45	Almost 0	D
Heat storage	s - min	N/A	20 - 60	100 - 400	80 - 250	10 - 30	N/A	5 - 30	30 - 60	0.05- 1%	Dev /D

Table 3.1 Comparison between the main technologies of ESSs

Note: NaS and Ni-Cd refer to sodium-sulfur and nickel-cadmium batteries, respectively.
The levels of maturity (ranked by increasing value) are Dev: development / D: demonstration / EC: early commercialized / C: commercialized / M: mature.

As shown in Fig. 3.2-A, the batteries offer medium performances and a good compromise between power and energy per unit of volume. PHES, CAES and flow batteries exhibit low performances and thus, require large volumes typically adapted to stationary storage for utility grid support. Similar results are given in Fig. 3.2-B which explain why highly compact technologies are powered by batteries, especially lithium-ion batteries. Fuel cells and thermal storage have good performances in terms of energy but have a limited power capability.
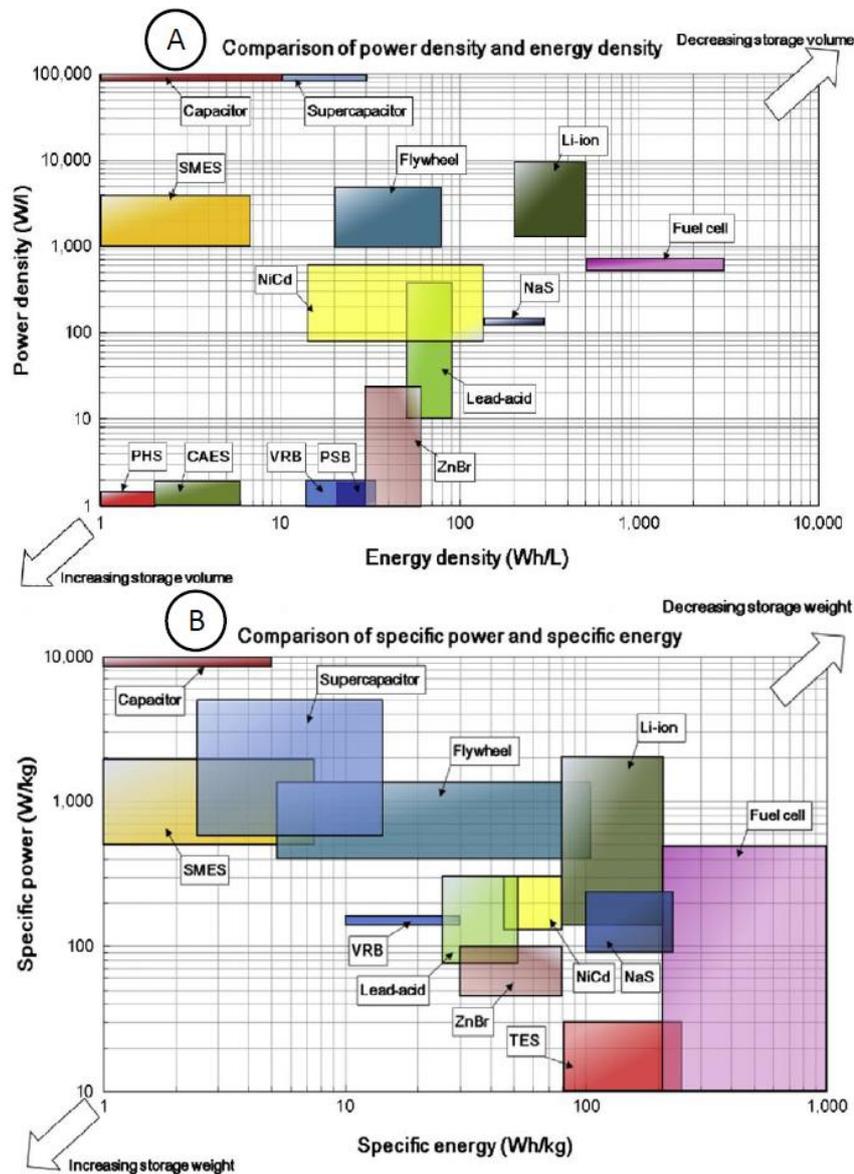
Figure 3.2 Weight and volume characteristics of different ESSs [82]

3.2 Electrochemical and electrical storage systems for smart buildings

Nowadays, the use of storage systems in buildings that are connected to the main grid and that produce their own electricity is very scarce. During the past decades, lead-acid batteries have been widely used in isolated power systems for remote areas, uninterruptible power supply for critical equipment, etc. [72]. This mature technology exhibits a low capital cost but the cycling lifetime is relatively low compared to newer technologies such as lithium-ion batteries. Indeed, lithium-ion batteries, which have

been dramatically developed in the field of transportation with electric vehicles, are also becoming attractive for stationary storage because of their falling costs (the trend will continue because of the development of large factories such as Tesla battery gigafactory) [76].

Whatever the technology of battery, pulsed current operation should be avoided in order to prevent a lower efficiency and accelerated ageing. In PV systems, the production is highly varying, and among the technologies that are suitable for high power applications (i.e. flywheel, SMES, SC), we found that SC technology is the best solution, taking into account its costs (capital cost and O&M costs), safety, and high scalability (easy association of several packs).

Hence, we have chosen to study these three technologies in more details in this chapter.

3.2.1 Lead-acid batteries

An electrochemical cell converts chemical energy into electric energy, and vice versa for rechargeable cells [83], [84], [85]. A cell consists of a set of two electrodes (oxidizer and reducer) and an electrolyte, as illustrated in Fig. 3.3. Each set leads to a given voltage output and a capacity. These cells can be connected in series, parallel, or both in order to adapt the output voltage and current. The aggregated system is called a battery.
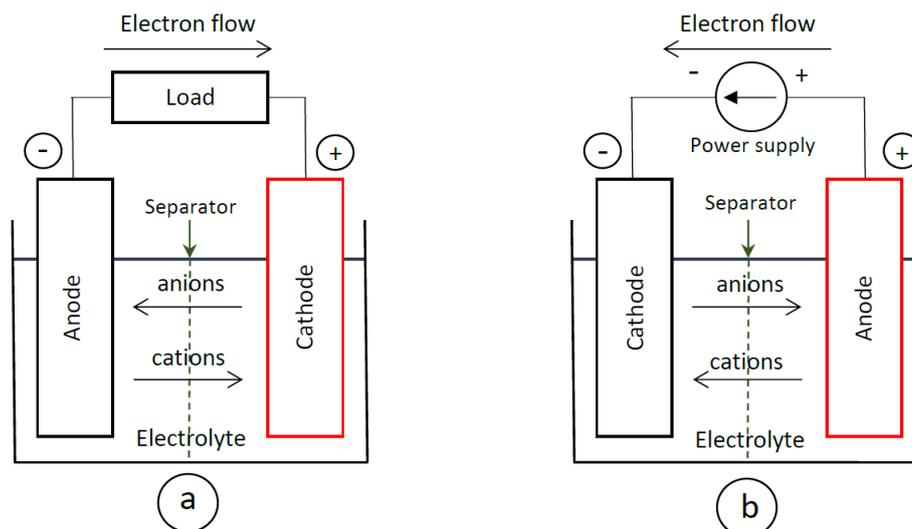
Figure 3.3 Operation of a cell during a) charge and b) discharge.

Since the end of the 18th century with the development of the Volta pile, "voltaic pile", numerous designs of batteries have been invented, the first ones are presented in Fig. 3.4. Based on always new applications with specific needs (power and energy requirements), new associations have been tested and manufactured with different electrode materials, electrolytes, casings, separators, management systems, etc. Hundreds of systems have been created but almost 2 dozens of them are currently commercialized [85].
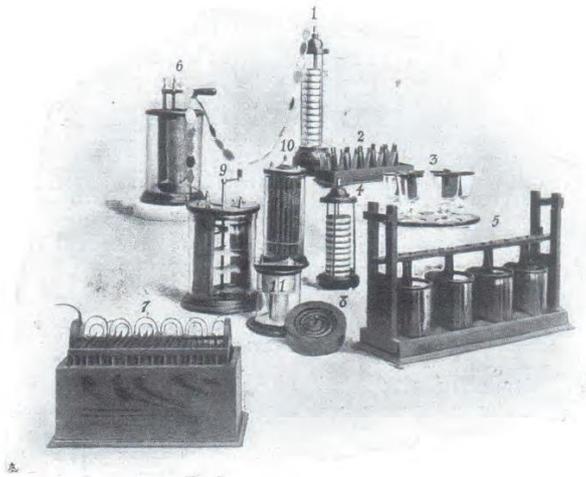
Figure 3.4 First cells/piles/batteries of the history [86]

The historical development of the main battery chemistries is presented in Fig. 3.5. Scientists are always looking for chemistries enabling higher energy and power densities and if possible, this design should be affordable with environmental friendly and widely available materials. The voltage potential of a cell is typically around 2.3 V for lead-acid batteries and around 3.6 V for lithium batteries. Gaston Planté developed the first practical lead-acid battery in 1859 and Sony commercialized the first lithium battery in 1991.
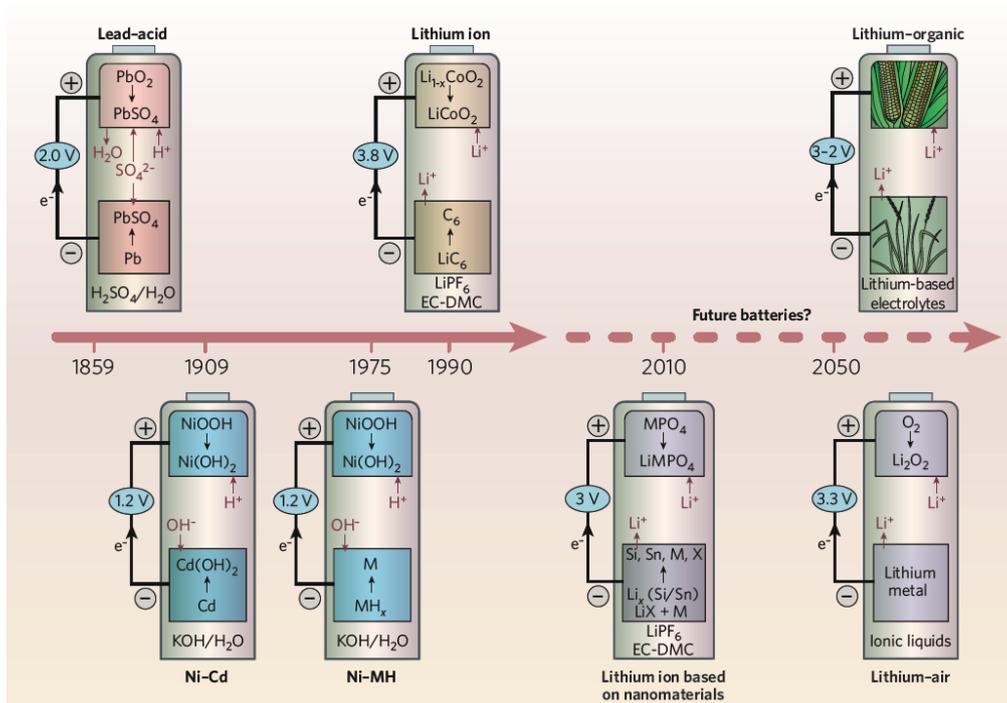
Figure 3.5 Different Battery chemistries through history [87]

Lead-acid batteries, the most mature technology, have an aqueous electrolyte made of water and sulfuric acid (H_2SO_4). During the discharge, the battery consumes the electrolyte leading to a concentration of sulfuric acid from 30-40% to 12-24% [85]. Aqueous electrolyte offers a better conductivity but a lower potential compared to non-aqueous electrolyte. Flooded (or vented) battery is the initial design of lead-acid technology. It is a cheap technology with a moderate lifetime (5-15 years, hundreds of cycles) which needs some water refills and to be disposed in a ventilated room (because of gassing due to

electrolysis of water during the overcharging process, more explanations below). The performances of lead-acid batteries are limited by the active material utilization which is about 50% at low currents and drops to about 10% at high currents [85]. Depending on the application, the components of the battery can be slightly different, for example some batteries have thicker plates in order to improve the cyclability at the expense of peak current capability reduction. Some improvements have been made with new sealed battery designs such as valve regulated lead-acid (VRLA) and absorbent glass mat (AGM) which are nearly free of maintenance thanks to gas recombination.

The following equations give an overview of the lead-acid batteries charge-discharge operation principle. Concerning lead-acid batteries, during the discharge both electrodes are converted to lead sulfates (reversible reaction), this is why the reaction is commonly called double sulfation [83]. For more explanations about thermodynamics of electrochemical processes and kinetics of electrode processes, the reader is invited to refer to [83].

On the positive electrode, lead dioxide (PbO_2):

$$PbO_2 + 4H^+ + 2e^- \rightleftharpoons Pb^{2+} + 2H_2O$$ eq. 3.1

$$Pb^{2+} + SO_4{}^{2-} \rightleftharpoons PbSO_4$$ eq. 3.2
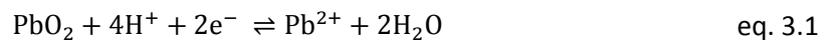
On the negative electrode, sponge lead (Pb):

$$Pb \rightleftharpoons Pb^{2+} + 2e^-$$ eq. 3.3

$$Pb^{2+} + SO_4{}^{2-} \rightleftharpoons PbSO_4$$ eq. 3.4

Overall reaction:

$$
\begin{array}{c}
\text{Discharge} \\
Pb + PbO_2 + 2H_2SO_4 \quad \rightleftharpoons \quad 2PbSO_4 + 2H_2O \\
\text{Charge}
\end{array}
$$ eq. 3.5
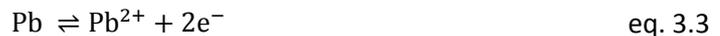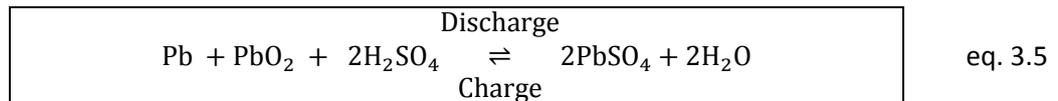
Self-discharge and ageing of lead-acid batteries are due to some secondary (parasitic) reactions such as the electrolysis of water (eq. 3.6) and the grid corrosion (eq. 3.7) [88]. These latter occur because of the potential of the electrodes (compared with the hydrogen's standard electrode potential).

$$2H_2O \rightarrow O_2 + 2H_2$$ eq. 3.6

$$Pb + 2H_2O \rightarrow PbO_2 + 4H^+ + 4e^-$$ eq. 3.7
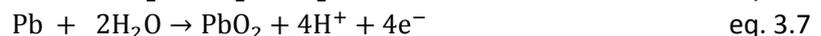
One major ageing mechanism of lead-acid batteries is irreversible sulfation. Indeed, after some cycles of charge and discharge, some lead sulfates are not recombined into electrolyte and become a crystalline form that no longer react. Thus, the active material decreases so the capacity of the battery decreases. Moreover, due to corrosion and sulfation, the plates are expanding and cracking leading to premature fatal failures. Another mechanism called acid stratification is limiting the performances of the battery. Indeed, it denotes a gradient in acid concentration on the vertical axis (acid stays at the bottom of the battery). In this case, overcharging the battery is a good way to stir the acid thanks to gassing. More details about ageing mechanisms can be found in [89]. A lifetime model, based on battery operations will be given in section 3.4.

The rates of all reactions involved in lead-acid batteries, depending on the potential of the electrodes, are presented in Fig. 3.6. As lithium-ion batteries, the recommended charging method is constant current – constant voltage (for more information, see Appendix 3.A).
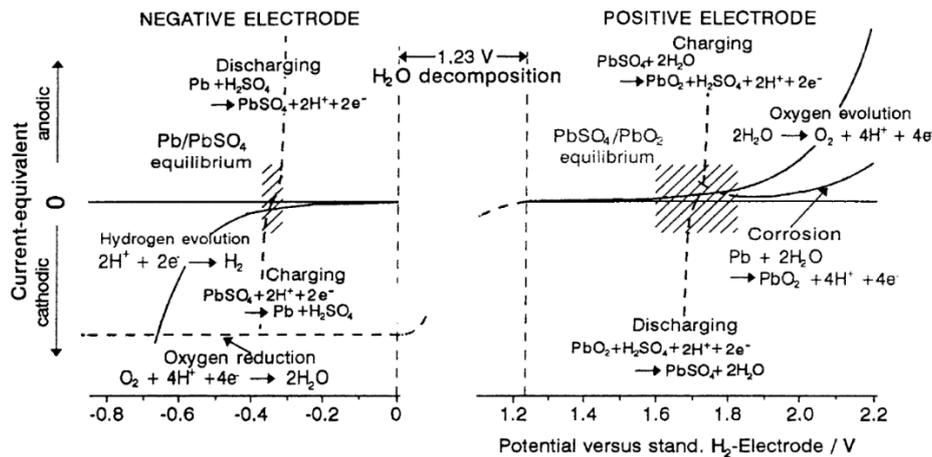
Figure 3.6 Reactions occurring in lead-acid batteries for different electrode potentials [88]

Recently, new designs of lead-acid batteries appeared: OPzV batteries (German abbreviation for 'Ortsfest Panzerplatten Verschlossen', which means stationary tubular batteries sealed, i.e. valve regulated) and OPzS batteries (German abbreviation, S stands for 'Standard', i.e. flooded battery). These batteries are interesting because they are characterized by an enhanced lifetime compared to AGM and gel lead-acid batteries. Based on data found in datasheets, the latest lead-acid battery technologies used in PV applications are compared in table 3.2.

Battery type	Cycle efficiency	Max C-rate	Lifetime	Capital cost
AGM	+	++	--	++
Gel	+	-	-	+
OPzV	+	-	++	--
OPzS	+	+	++	-

Table 3.2 Comparison of lead-acid battery technologies

Even if the capital cost of OPz batteries is higher than older technologies, the cost on the long run is supposed to be lower because of a lifetime expectancy defined by manufacturers between 2000 and 3000 cycles. The performances in terms of cycle efficiency are very similar but it seems that the C-rate is more limited for OPzV than other technologies. We will see in chapter 4 that the limitation of C-rate is usually not a problem because the operating profile in microgrid application requires a large capacity (energy is more restrictive than power).

3.2.2 Lithium-ion batteries

The development of high energy density lithium batteries is based on the properties of lithium (Li) metal: it is the most electropositive and the lightest metal [90]. Conversely to lead-acid batteries, a non-aqueous electrolyte (polymer electrolyte for lithium ion and lithium polymer batteries) is used because of the reactivity of lithium with aqueous electrolyte. Indeed, first developed lithium metal batteries experienced some failures because of short-circuits due to the growth of dendrites. The positive electrode (cathode during discharge) has been initially based on metal oxide components $LiMO_2$ (M

designates Co, Ni, Ti, V, Cu, Al, Mn) and the negative electrode (anode during discharge) is based on graphitic carbon layers (new designs such as lithium titanate oxide are also developed).

Lithium-ion cells are designed with different sizes and shapes, as illustrated in Fig. 3.7 (for lithium-ion batteries, the 18650 cell is a very popular cylindrical cell which is used in laptops, LED flashlights and even associated in large packs for electric vehicles).

Lithium-ion batteries are storing charges differently from lead-acid batteries. Indeed, as presented in Fig. 3.8-a, some lithium ions will be inserted reversibly (at the charge and the discharge) into the electrodes, in a so-called intercalation process. The electrolyte, made of lithium salt, transports lithium ions from an electrode to another during the charge and the discharge. The use of metal oxides in cathodes and graphitic carbon in anodes enables to create layered compounds in which lithium ions can intercalate.
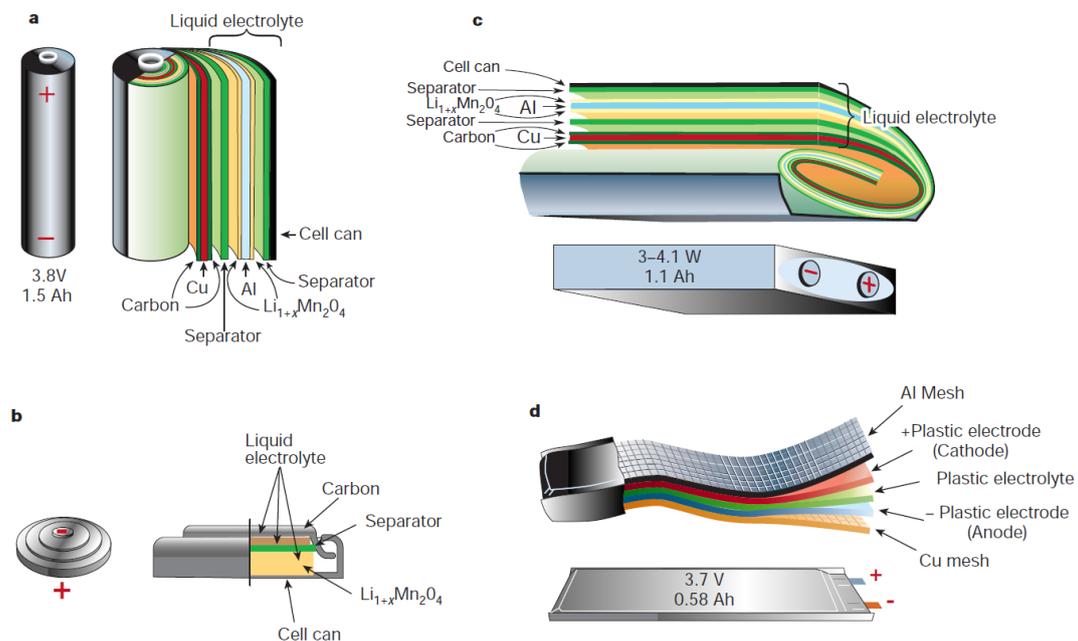
Figure 3.7 Lithium-ion battery packaging a) Cylindrical, b) coin, c) prismatic, and d) thin and flat [90]

A lot of efforts have been put in finding mechanically stable structures of layered compounds (to ensure a good lifetime) while developing nanomaterials (e.g. carbon-based materials) to improve the quantity and the speed of lithium ions intercalation (higher energy and power densities can be obtained). The study of the interactions between electrodes and the electrolyte are crucial to improve the performances of lithium-ion batteries. Thus, a protective layer, named solid electrolyte interface (SEI), is developed at the anode during the first cycles, Fig. 3.8-b. The SEI is permeable for lithium ions and impermeable for other electrolyte components so it contributes to the mechanical stability and the corrosion protection of the electrode [91]. However, lithium ions from the electrolyte are irreversibly consumed which leads to a loss of capacity. Moreover, the growth of this layer reduces the power capability of the battery due to a rise of the electrode impedance. This growth has to be limited by controlling the operating conditions of the battery (i.e. high SOC, high temperature and high current rate have to be avoided). More explanations will be given in section 3.4.

The first successful cathode (still commercialized) has been layered $LiCoO_2$. This technology has a relatively high energy and power densities (due to high cell voltage) but a quite expensive cost (cobalt-based) and some serious safety issues due to thermal runaway (due to cobalt no overcharge of the cell is allowed and the operating temperature must be controlled). Then, other elements have been studied to replace the cobalt (toxic and more expensive than other metals). Hence the use of cobalt has been

reduced in some mixed-metal layered oxides designs such as NMC (lithium nickel manganese cobalt oxide, $LiNi_{0.33}Co_{0.33}Mn_{0.33}O_2$) batteries and NCA (lithium nickel cobalt aluminium oxide $LiNi_{0.8}Co_{0.15}Al_{0.05}O_2$) batteries. Cobalt has also been replaced by another metal oxide in LMO (lithium manganese oxide) batteries or by polyanion materials (lithium iron phosphate (LFP), $LiFePO_4$). These materials have different crystal structures presented in [92]. In 2014, the cobalt was still well represented in the global market of cathode materials of lithium-ion batteries with LCO (40%), NMC (22%), LMO (19%), LFP (10%) and NCA (9%) [75].
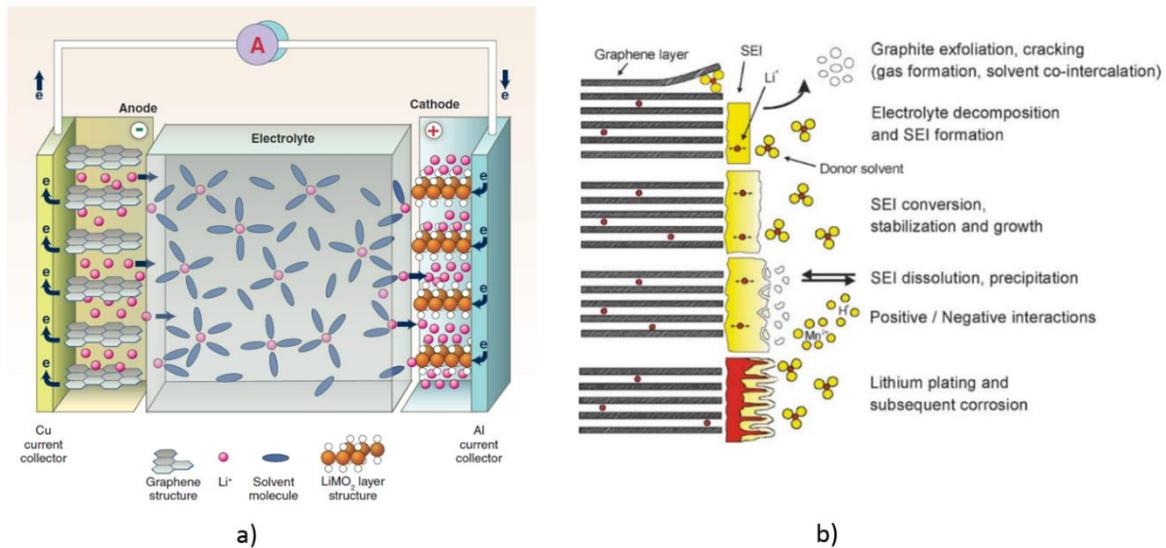
Figure 3.8 Lithium ion battery a) whole cell principle [93] and b) SEI at the anode [91]

Other research work deal with anode materials such as graphitic carbon (very popular material which is relatively cheap, abundant and presents a good cyclability), lithium titanium oxide (LTO batteries, $Li_4Ti_5O_{12}$ good cyclability, suitable for high power applications) or silicon (under development, mainly limited by the volume changes at the charge and discharge which affects negatively the lifetime of the structure, which is not mechanically stable) [94].

Fig. 3.9 presents a summary of lithium-ion batteries characteristics. In this chart, "Performance" refers to the ability of a battery to keep a good behaviour in a wide range of operating temperatures [95].
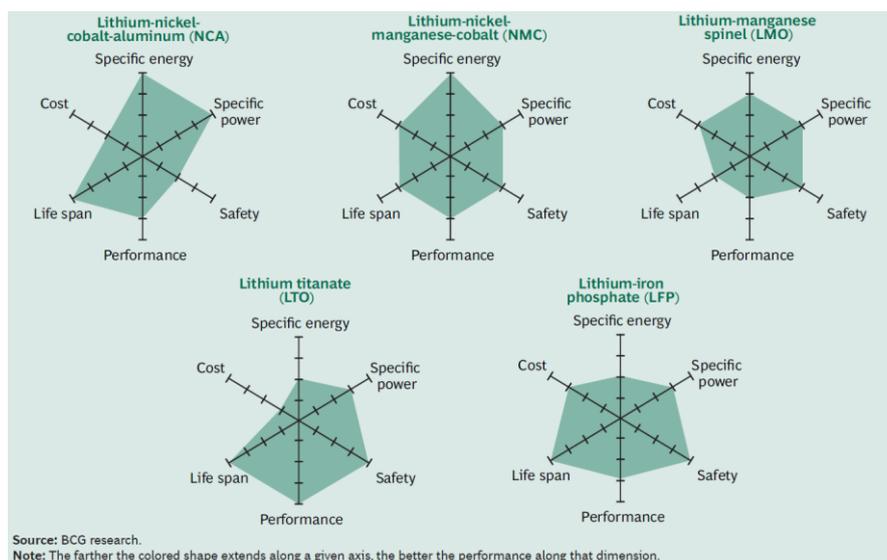
Figure 3.9 Characteristics of the main lithium battery technologies [95]

3.2.3 Supercapacitors

The family of supercapacitors (SCs) is constituted of two main technologies involving different charge storage mechanisms [96]. Indeed, electrostatic storage is used in SCs called **electric double-layer capacitors (EDLCs)**. Electrostatic storage has many advantages over batteries (redox chemical reactions) such as a higher rate of charge/discharge and a higher lifetime (because the volume of electrodes is not changing at the charge/discharge, so the mechanical stability of the structure is enhanced). The main disadvantages are the poor energy density (1-10 kWh/kg) which is about 10 times lower than batteries (30-110 kWh/kg) and the high cost of the device (mainly due to the activated carbon to coat the electrodes). Wider range of operating temperature can also be obtained compared to batteries because the choice of electrolyte is not limited by the charge mechanism (conversely to batteries) [97]. The other main SC technology is **pseudo-capacitor** based on a Faradaic charge storage. This storage mechanism is close to batteries because redox reactions are involved but only close to the surface of electrodes. Thus, a pseudo-capacitor has a better energy density than EDLC but a poorer power density and cycle lifetime (electrode swelling and cracking as batteries). Many researchers are developing hybrid SCs, such as lithium-ion capacitors (LICs) that involve one SC electrode and one lithium-ion battery electrode, in order to take advantage of both capacitive and electrochemical properties.

Due to their properties, SCs are used in high power applications (i.e. fast charge/discharge cycle applications such as regenerative braking of EVs, quick charge buses, etc.). SCs are also used in energy harvesting applications (due to higher lifetime compared to batteries). Aircraft auxiliaries and secondary power systems are using SCs instead of lithium-ion batteries because of the safety issues due to thermal runaway discussed earlier. Some packages of SC modules from Maxwell technologies are presented in Fig. 3.10.

Figure 3.10 Example of Maxwell SC packages

As presented in Fig. 3.11, a SC is made of two electrodes, a separator and an electrolyte. EDLCs have generally a symmetric design with two identical electrodes made of metal foils coated with activated carbon, whereas pseudo-capacitors are asymmetrical with an electrode material similar to lithium-ion batteries (polymers or transition metal oxides such as ruthenium oxide RuO_2 and manganese oxide MnO_2). As noted earlier, aqueous electrolytes have a better conductivity than organic electrolyte and also have a lower cost. But due to the redox reaction of water, the cell voltage window is limited to 1 V compared to 2.7 V (organic electrolyte). This limitation is a major drawback because the energy stored in the SC is proportional to the square of the cell voltage.
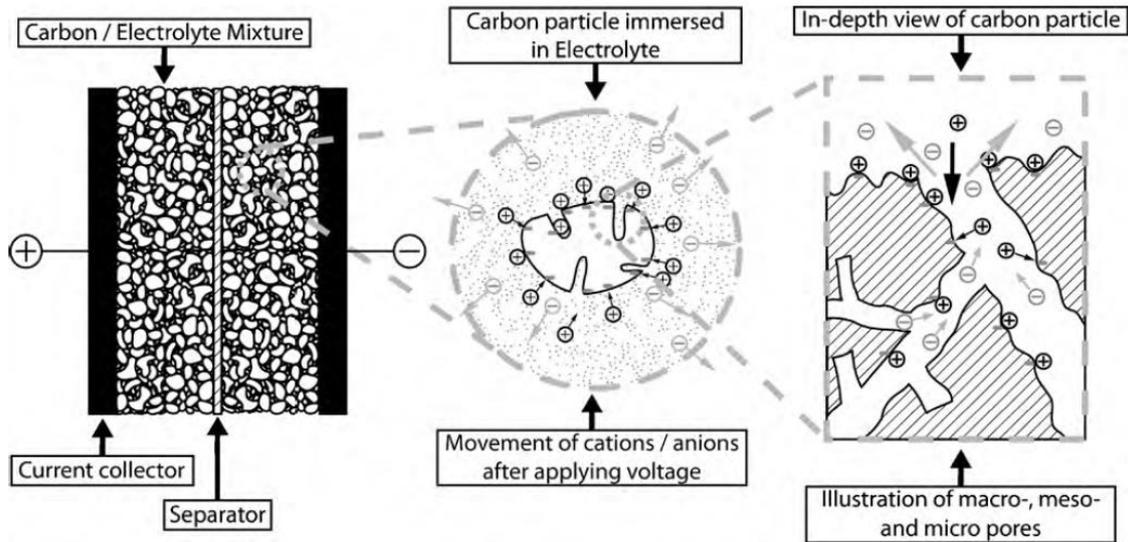
Figure 3.11 Design of an EDLC and movements of ions in the electrolyte [98]

The double layer capacitance described by Helmoltz in 1853 is calculated as follows:

$$C = \frac{\varepsilon_r\,\varepsilon_0\,A}{d}$$

eq. 3.8

where ε_r and ε_0 are the electrolyte and the vacuum dielectric constants, respectively. A is the electrode surface area and d is the thickness of the double layer.

Three popular models are commonly used to explain the electric double layer formed at the interface of the solid electrode and the liquid electrolyte, see Fig. 3.12 (Helmoltz model is the simplest and Stern model is the most accurate). Ψ_0 refers to the electrode potential, Ψ is the potential in the cell, IHP and OHP designate the inner and the outer Helmoltz planes, respectively. There is still a lot of research work aiming to describe more accurately the behaviour of ions in nanoporous carbon electrodes [97].
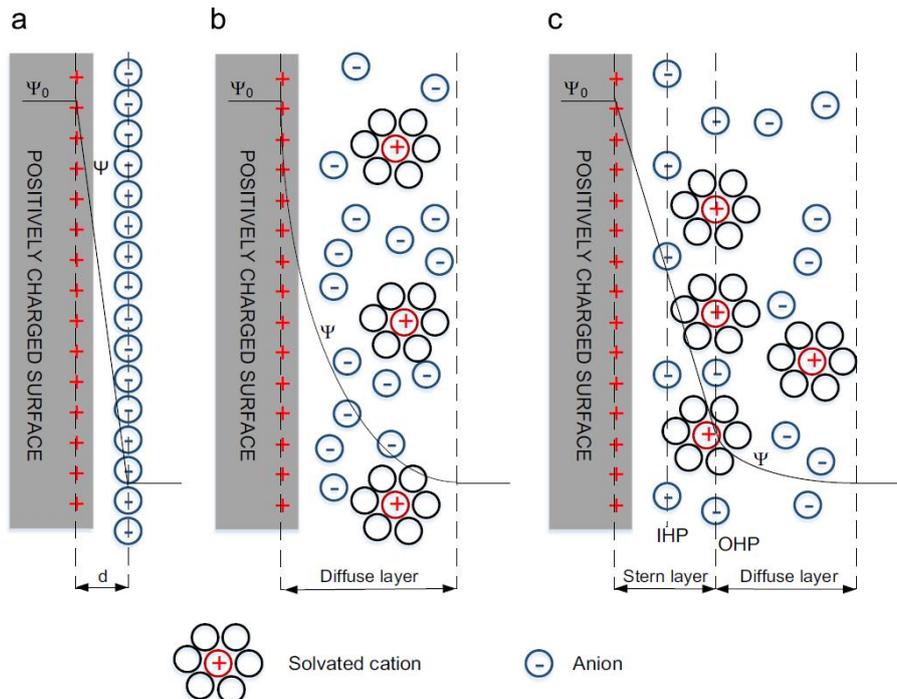
Figure 3.12 Electric double layer models, a) Helmholtz, b) Gouy–Chapman and c) Stern [96]

Thus, based on eq. 3.8, the use of materials with high specific surface area improves the capacitance of the EDLC, this is why activated carbons are widely used (nanotubes and onions are also studied [97]).

3.3 Definitions describing electrochemical and electrical ESSs

3.3.1 Nominal and rated capacity

Nominal capacity and rated capacity designate the same physical quantity which is the maximum energy that can be stored in the ESS. Indeed, for a battery, the rated capacity C_n at charge (or discharge), expressed in ampere-hours (Ah), depends on the level of current (constant) and the duration n of the charge (or discharge), expressed in hours. For example, if a battery is charged during 20 hours at a current noted I_{20} of 2 A, the rated capacity is $C_{20} = 40\ Ah$.

$$C_n = I_n \times n \qquad \text{eq. 3.9}$$

Complementary to the term rated capacity, the charge (or discharge) current is often referred to a charge (or discharge) rate named C-rate and expressed in h^{-1}. For example, a C-rate of 0.25 corresponds to a charge (or discharge) during 4 hours at a current $I_4 = 1.25\ A$ for a rated capacity of 5 Ah.

$$C_{rate} = \frac{I_n}{C_n} = \frac{1}{n} \qquad \text{eq. 3.10}$$

3.3.2 Available capacity

The available capacity, noted $Cap(t)$, reveals the quantity of charges that are stored in the battery (generally expressed in Ah).

$$Cap(t) = \int_0^t i(t)\ dt \qquad \text{eq. 3.11}$$

The stored energy can also be expressed in watt-hour by multiplying the available capacity (Ah) by the voltage of the battery (the potential of a battery varies depending on the number of charges that have already been stored). For a precise evaluation of the available capacity, some weighting coefficients are often added to eq. 3.11 in order to take into account the operating conditions affecting the value of available capacity such as the C-rate and the temperature (see section 3.3.6 related to the state of charge).

In comparison, the energy stored in a SC (similarly to a capacitor), expressed in Joule (J), can be calculated as follows:

$$E_{SC} = \frac{1}{2}\ C_{SC}\ (V_{SC\_max}{}^2 - V_{SC\_min}{}^2) \qquad \text{eq. 3.12}$$

where C_{SC} (in F) is the capacitance of the SC, V_{SC_max} and V_{SC_min} (in V) are the maximum and minimum voltages of the cell, respectively. The stored energy can be expressed in Wh by dividing E_{SC} by 3600 (since 1 J = 1 W.s).

Thus, the 500 F / 16 V SC module that we have experimented (see in Appendix 3. B) exhibits a rated capacity of nearly 18 Wh. In order to give an idea about the cost per unit of energy, the price of such module is about 600 €. In comparison, the same capacity is obtained with a 6 V lead-acid battery of 3 Ah which costs around 10 €. Hence for the same rated capacity, a SC is about 60 times more expensive

than a lead-acid battery, and its volume and weight are also about 10 times higher. This could become an overwhelming obstacle for some applications.

3.3.3 Peukert's law

The available capacity non-linearly decreases when C-rate increases because of a less efficient use of active material (chemical reactions at the surface of electrodes), especially for lead-acid batteries. In 1897, Peukert introduced an empirical relationship based on the current level and the duration of the discharge.

$$C_P = \text{T}_{Dis} \times \text{I}_{Dis}{}^k \qquad \text{eq. 3.13}$$

where C_P is the Peukert capacity (in Ah), T_{Dis} is the duration of discharge (in h), I_{Dis} is the current level of discharge (in A), and k is the Peukert coefficient which depends on the temperature, the ageing and the technology of battery (between 1.1 and 1.5 for lead-acid batteries at 25 °C [99], between 1 and 1.2 for NiMH batteries and between 1 and 1.1 for lithium-ion batteries [100]).

According to the datasheet of the lead acid battery YUASA YUCEL Y7-12 (see Appendix 3. B), the variation of nominal capacity depending on the C-rate has been reported in Fig. 3.13 (based on eq. 3.13, $C_P = 5.913$ Ah and k = 1.164 (R^2 error=0.9995 and RMSE=0.2332)).
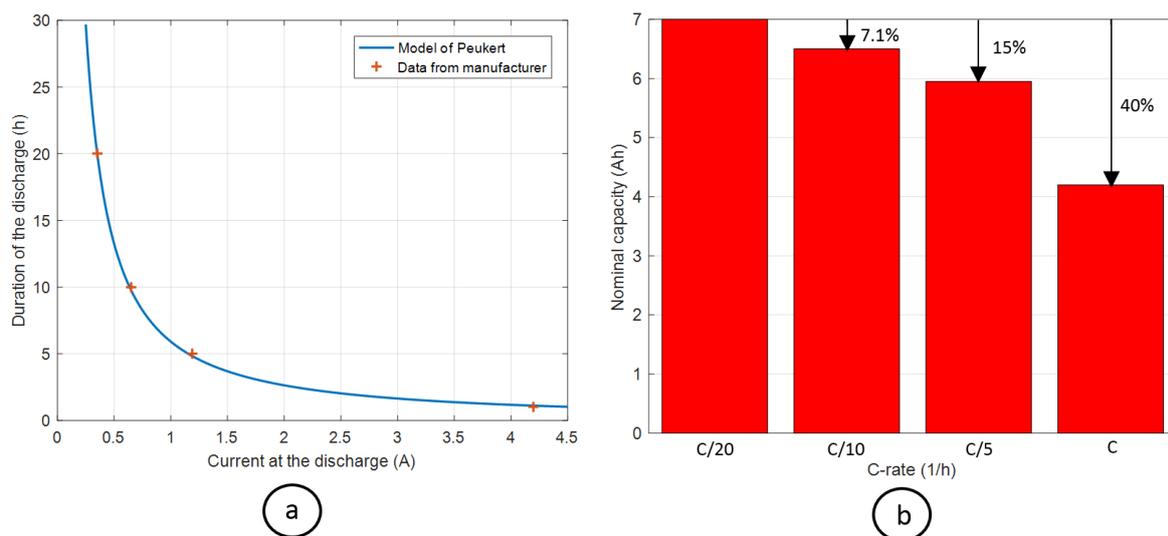
Figure 3.13 Lead-acid battery capacity for different C-rates - A) Peukert's model, B) Absolute and relative decrease of capacity

Three technologies of batteries have been tested in [101] exhibiting both the effect of C-rate and temperature on the discharged capacity. Even if the temperature strongly affects the discharged capacity of lead-acid and lithium-ion batteries (higher capacities are obtained at higher temperatures), this parameter will not be discussed in this thesis, assuming that the battery is installed in a controlled room-temperature and the operating conditions (mainly C-rate) are limited to avoid self-heating. The results of this study concerning the influence of the C-rate on the discharged capacity are presented in Fig. 3.14. The nominal capacity has been normalized, based on the capacity obtained with a C-rate of 1C at 25°C. It appears that VRLA batteries are the most affected by the C-rate with a large drop of capacity for high C-rates (nearly 4 times lower at 4C than C/4). Lihium-ion batteries such as LFP and LTO are also experiencing a decrease of capacity for high C-rates but the variation is smaller (almost 0 for LFP and lower than 20 % for LTO).

An issue with the Peukert model is that the relation presented in eq 3.13 is given for a constant level of current at the discharge. Hence, this model is not able to predict the discharged capacity when different currents are applied during the same discharge [99], [100] and [102]. We have done some experiments in this way on lead-acid batteries and lithium-ion batteries. It appears that, for lead-acid batteries that are more affected by the C-rate (as presented in Fig. 3.14), even with only two level of currents (one low C-rate and one high C-rate), the estimation of the discharged capacity is not accurately predicted by Peukert's law. For now, we are not able to propose a general and easy formulation that can be adapted to any type of battery. In this regard, the limitation of C-rate to 1C enables to keep a good estimation of available capacity.

For SCs, we have tested some products from Powerstor (10 F, 2.7 V) and Maxwell (150 F, 16 V). It appeared that there is no effect of C-rate on the discharged capacity.
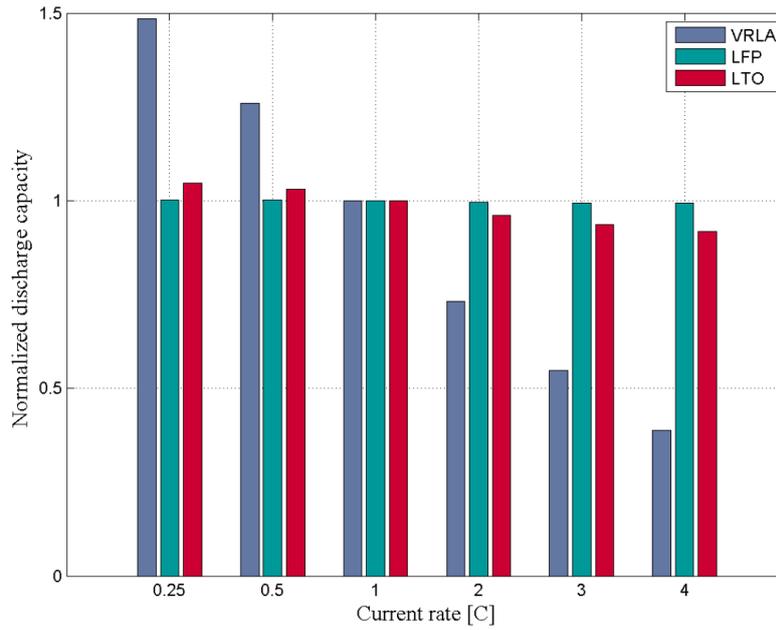
Figure 3.14 Normalized discharged capacity of three types of batteries evaluated for different C-rates at a working temperature of 25°C [101]

3.3.4 Efficiency

Two different definitions of efficiency are used in our work to describe the performance of an ESS.

➢ Mainly used in electrical and electrochemical ESSs, the coulombic efficiency describes the ampere-hour efficiency for one cycle.

$$\eta_C(t) = \frac{\int_{cycle} I_{Dis}\, dt}{\int_{cycle} I_{Ch}\, dt} \qquad \text{eq. 3.14}$$

where I_{Ch} and I_{Dis} are the level of current at the charge and at the discharge, respectively.

➢ A more complete picture is given by the energy efficiency (also referred as round-trip efficiency) which describes the watt-hour efficiency of the ESS during one cycle.

$$\eta_E(t) = \frac{\int_{cycle} P_{Dis}\, dt}{\int_{cycle} P_{Ch}\, dt} \qquad \text{eq. 3.15}$$

where P_{Ch} and P_{Dis} are the exchanged power at the charge and at the discharge, respectively.

The coulombic efficiency is always higher than the energy efficiency due to the hysteresis of the charge/discharge potential curve (i.e. voltage during the charge is higher than during the discharge, see section 3.3). Indeed, coulombic efficiencies of lithium-ion batteries and lead-acid batteries are respectively estimated to 99% and 80-90% compared to 95% and 70-75% for energy efficiency [83].

These concepts can be measured by plotting the voltage of cell for different exchanged quantities of milli Ampere-hour during complete cycles of charge-discharge. In Fig. 3.15, some experimental results are presented for a lead-acid battery Yuasa Y7-12 (datasheet is given in Appendix 3-B). Hence, the coulombic efficiency is between 84.8 and 85.1%, and the energy efficiency is between 70.9 and 73.4% for the presented cycles.
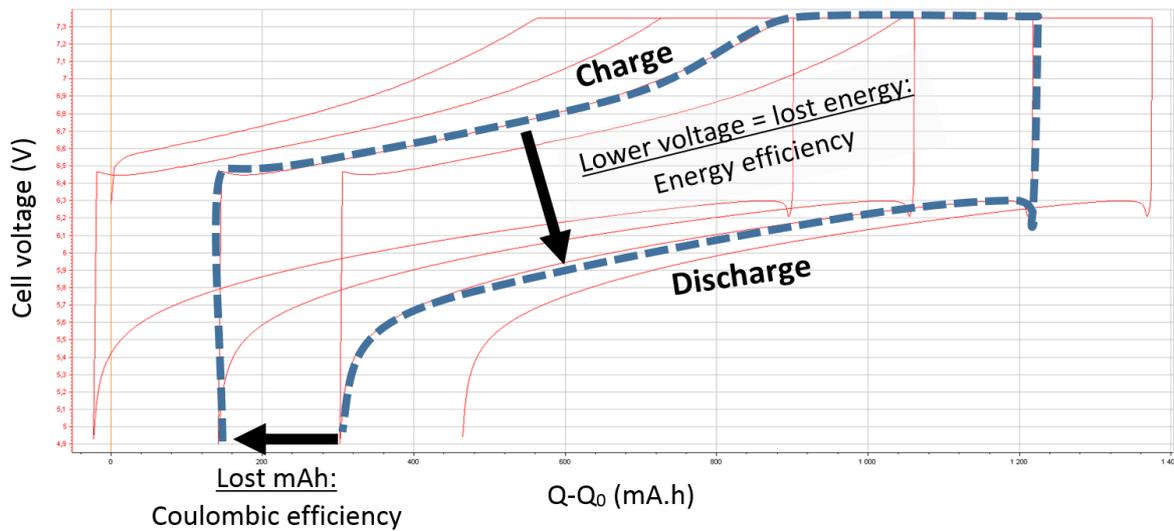
Figure 3.15 Energy and coulombic efficiencies of a Yuasa lead-acid battery

It is important to notice that the efficiency of an ESS is affected by the operating C-rate and the temperature (this latter will not be discussed in this work, considering that the temperature of the environment is kept constant). Broadly speaking, the energy efficiency is decreasing at higher C-rates, as described in Fig. 3.16 with experimental data of valve regulated lead-acid (VRLA), lithium iron phosphate LiFePO4 (LFP) and lithium titanate (LTO) batteries [101].
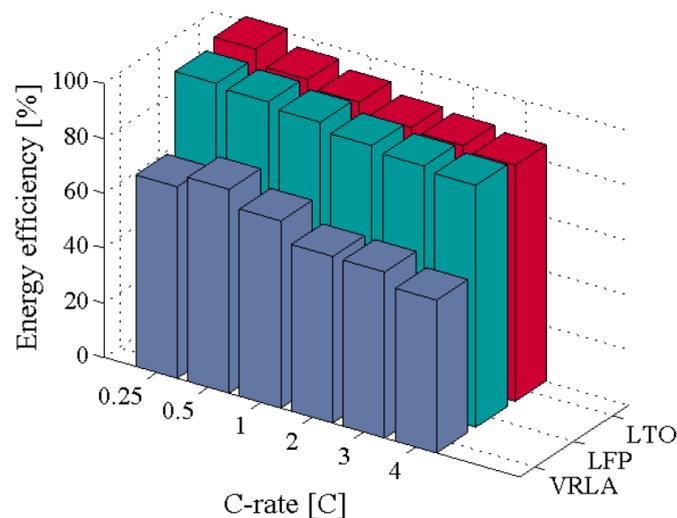
Figure 3.16 Energy efficiency at 25°C under various C-rates [101]

3.3.5 Self-discharge

During rests, the available capacity of an ESS is decreasing because of the loss of stored charges. This phenomenon is called self-discharge. The self-discharge rate of batteries and SCs depends on the number of charges already stored and the ambient temperature. Hence, fully charged and/or high temperature induce a higher self-discharge rate [83]. In [98], the self-discharge mechanism of a SC is modelled and explained: during the first 15 minutes, a recombination of charges occurs (exponential decrease of the voltage across the SC) and then the main process is the self-discharge (linear decrease of the voltage).

We have done some experiments on SCs, lead-acid batteries and lithium batteries and we found that the self-discharge rates are 1%/day, 2%/month and 1.5%/month, respectively (the self-discharge rates of batteries have been extrapolated from the slope of a one week experiment).

3.3.6 State of charge (SOC)

The state of charge (SOC) of an ESS is a critical variable to supervise. As presented earlier, an overcharge of a battery or a SC can lead to severe damages. The SOC of a battery is defined as the ratio between the available capacity and the nominal capacity:

$$SOC(t) = \frac{Cap(t)}{C_n(t)}$$
<div align="right">eq. 3.16</div>

In [103], [104] and [105], the estimation of SOC is enhanced by including some relationships such as the coulombic efficiency previously mentioned. The online calculation of SOC based on current measurement (sometimes called ampere-hour counting) is done as follows:

$$SOC(t) = SOC(t-1) + \eta_{Ch}\frac{I_{Ch}(t) \cdot \Delta t}{C_n(t)} - \frac{I_{Dis}(t) \cdot \Delta t}{\eta_{Dis} \cdot C_n(t)}$$
<div align="right">eq. 3.17</div>

where η_{Ch} and η_{Dis} are respectively the charge and discharge coulombic efficiencies of the ESS (in [103], the coulombic efficiency is considered equal to 1 during the discharge and smaller than 1 during the charge, due to unwanted side reactions). $I_{Ch}(t)$ and $I_{Dis}(t)$ are the current-level of charge and discharge, respectively.

As explained earlier, the available capacity at the discharge is affected by the C-rate. Hence, some methods propose improvements of this ampere-hour counting method by using correcting factors on the current at the discharge, based on the Peukert's law but also on the past operating conditions such as the C-rate of the last half cycle [102].

The SOC of a SC, which is defined as the ratio between the remaining energy and the maximum stored energy, can be calculated as follows, using eq. 3.12:

$$SOC_{SC}(t) = \frac{V_{SC}(t)^2}{V_{SC\_max}^2}$$
<div align="right">eq. 3.18</div>

where $V_{SC}(t)$ and V_{SC_max} are respectively the actual voltage and the maximum voltage of the SC, respectively. Based on this definition, it can be noticed that 75% of the energy stored in a SC is contained in the upper half of the cell voltage. This is why the SCs are often used only from 50% to 100% of their maximum voltage in order to be the most effective [106].

Another variable widely used in the literature is the depth of discharge (DOD) which describes the emptiness of battery (conversely to the SOC).

$$DOD(t) = 1 - SOC(t)$$ <div align="right">eq. 3.19</div>

As presented in [105], several methods are used to evaluate the SOC by sensing other variables such as the open-circuit voltage (OCV) (also called electromotive force (EMF) which reflects the ESS SOC, see next section), the impedance of the ESS or the concentration of sulfuric acid in the electrolyte (for lead-acid batteries [102]). But these measurements implies to stop the ESS for several hours in order to reach the electrochemical equilibrium (voltage relaxation and electrolyte homogenization). In [83] for VRLA batteries, the rest time is supposed to be 24 h or 5 days to have an accuracy within 20% and 5%, respectively. In our experiments, we found that the minimum rest time to limit the error to 5 % is around 24 hours for lead-acid batteries, 10 hours for lithium batteries and it is nearly instantaneous for SCs (mainly because of a very low internal resistance around 1 mΩ).

Other methods called "adaptive" (e.g. fuzzy logic, neural network, Kalman filter) are based on direct voltage measurement in order to estimate the OCV of the ESS (and then, deduce the SOC). In this case, the measure is easy and fast (no need to stop the system) but it requires high computational resources and a good dynamic model of the ESS (a lot of tests under several conditions have to be done). In [107] a fast characterization of a lithium-ion battery is proposed (based on a single full voltage relaxation measurement of 24 hours and extrapolation with 5-hour measurements for other SOCs). The voltage relaxation is modelled with a 5th order parallel RC network and enables to estimate the SOC without waiting the end of the voltage relaxation. The voltage relaxation of an ESS and possible SOC estimation error are presented in Fig. 3.17.
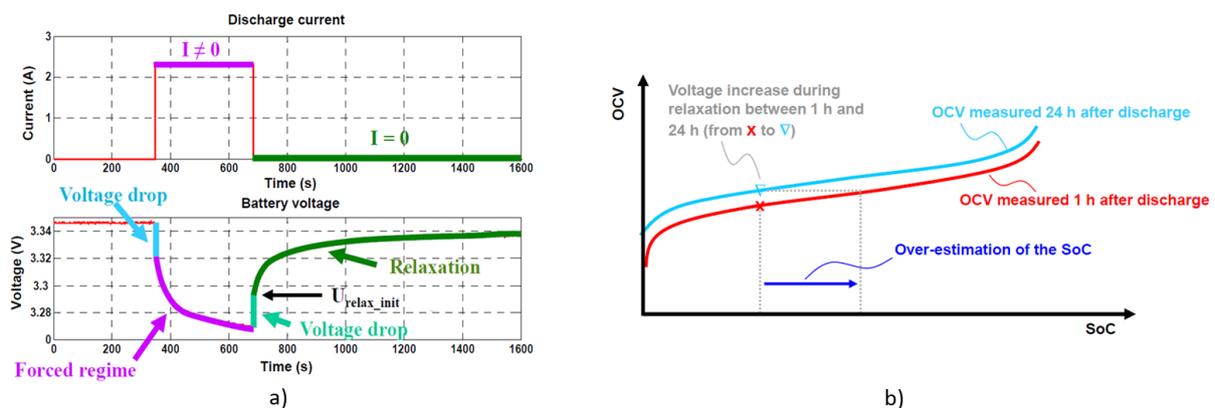
Figure 3.17 a) Voltage relaxation of a lithium-ion battery after a discharge,
b) SOC estimation after different relaxation times [107]

Finally, some hybrid methods are used to improve the accuracy and the confidence in the SOC estimation. In our case, we use an enhanced ampere-hour counting method (in order to take into account the efficiency of the ESS, capacity loss due to ageing and self-discharge) and voltage measurements (i.e. voltage limitations have been set on the operating window of the ESS).

3.3.7 State of health (SOH)

The nominal capacity of an ESS depends on ageing. Indeed, due to irreversible reactions, the active material is decreasing and the electrode interfaces are deteriorated. In this case, the capacity is irreversibly fading and the internal resistance is increasing (power capability fade). In order to know when to change an old ESS with decreasing performances to a fresh one, a common criteria is to consider the end-of-life (EOL) of a battery and SC when its initial capacity decreases by 20% [108]. This limit

of 20% has been initially set because of the behaviour of lead-acid batteries: the capacity fade is quite linear until 20% and then there was a sudden drop of capacity. Of course all the batteries do not exhibit the same behaviour, this is why some projects such as the second life of batteries have been created (old batteries that do not fulfil the automotive requirements are replaced and used in new stationary projects).

Usually the ageing of batteries and SC is monitored by measuring the nominal capacity. In this case, the battery reaches its EOL when the state of health (SOH) comes to 80%.

$$SOH(t) = \frac{C_n(t)}{C_n(t_0)}$$
eq. 3.20

The other way of tracking the ageing of an ESS is to measure the internal resistance (an increase of 100% is often used as the EOL criterion).

In [109] and [110] different approaches are presented to model the lifetime of lead-acid batteries such as physico-chemical (involves a deep knowledge of the overall chemical composition and design of the battery), weighted watt-hour throughput (assumption that the battery is able to exchange a given amount of energy whatever the operating conditions) and event-oriented (e.g. each cycle performed by the battery involves an incremental lifetime decrease). In our approach of building a generic model of ESS based on a few parameters mainly available from datasheets, the physico-chemical model is discarded because it needs a large number of parameters that are obtained through a lot of experimental tests. In [111], a model close to physico-chemical approach describes some ageing processes in lead-acid batteries such as the effect of cycle depth and current rate on grid corrosion and degradation of the active material due to acid stratification, gassing and sulfation (sulfate crystal growth). The two other models will be presented in more details in the following subsections.

The lifetime of any ESS is affected by two ageing mechanisms: calendar and cycling. Calendar lifetime represents the shelf-life of the ESS (the ESS is stored in a room and does not exchange energy with a load or a generator). In this case, the ESS suffer from self-discharge, increase of internal resistance and decrease of nominal capacity (due to calendar ageing). In [112] and [113] calendar and cycle lifetime have been investigated on Li(NiMnCo)O$_2$/C and LiFePO$_4$/C batteries, respectively. In Fig. 3.18, the results obtained by an accelerated calendar lifetime (due to the high temperature of 50°C) of a lithium-ion battery are presented [112]. It can be noticed that the ageing is more important (both increase of internal resistance and decrease of nominal capacity) when the battery is stored at high SOC.
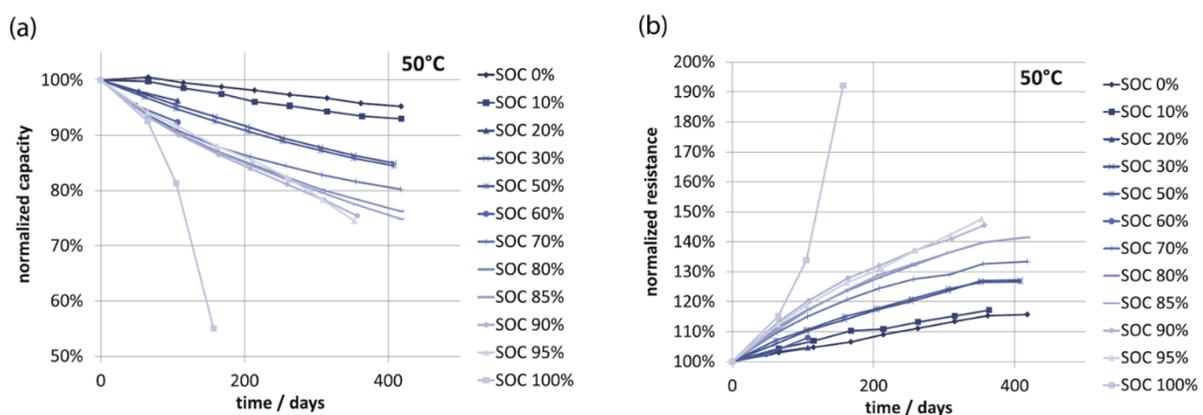
Figure 3.18 Calendar lifetime of lithium-ion batteries at 50°C, a) effect on nominal capacity, b) effect on internal resistance [112]

Concerning the cycle lifetime, it mainly depends on the cycle depth and SOC-level (effect of temperature is out of the scope in this work). The cycle depth is defined as the difference between the maximum and minimum value of SOC reached by the ESS during one cycle. The SOC-level is the mean value of SOC during one cycle. In [112] and [113], it has been experimentally shown that cycling a battery creates

additional degradations in comparison with shelf-life. As presented in Fig. 3.19, the cycle lifetime of a lithium battery is maximized for low cycle depths and mid-range SOC (50%). Assuming that the ESS has a calendar lifetime of 25 years and will perform one cycle per day (due to PV application), a maximum lifetime value slightly above 9000 cycles can be fixed.
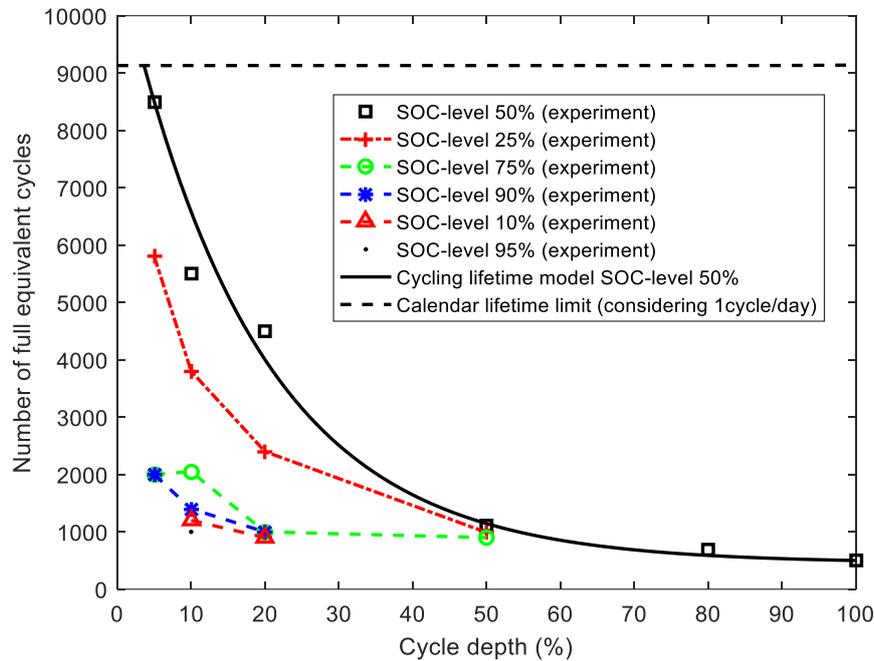
Figure 3.19 Cycle lifetime vs. cycle depth of lithium-ion batteries (modified from [112])

According to Fig. 3.19, the maximum number of cycles can be calculated based on the cycle depth that has been performed by the battery.

$$N_{Cycle} = a \exp^{(-b\Delta\text{DOD})} + c \qquad \text{eq. 3.21}$$

where the fitting coefficients $a = 1.057e4$, $b = 0.05459$, and $c = 455$ for the curve related to the SOC-level of 50% (with $\Delta\text{DOD} \in [0,100]$, R²=0.9729, and RMSE=689.1).

The curve presented in Fig. 3.19, which indicates the number of cycles that a battery can withstand for a given cycle depth and SOC-level is the more exhaustive than usual. Indeed, manufacturers are often presenting the maximum number of cycles for only 3 or 4 values of DOD. In this case, the problem is that these data based on DOD are far from the operating conditions of a battery installed in a renewable microgrid (the batteries are cycling around different SOC-level due to the volatility of PV and wind sources, they are not fully charged after every cycle, etc.). Obviously, if no other curve is available this information is valuable because is indicates at least a rough idea of the maximum number of cycles. This way to represent the lifetime of a component is derived from the study of material mechanical fatigue (Wöhler curves also referred as S-N curves, S and N designate the magnitude of the cyclic loading stress and the cycles to failure, respectively).

Weighted watt-hour throughput

As presented in [109] and [114], this method is based on the assumption that the exchangeable energy of a battery is nearly the same for any DOD. For example, in Fig. 3.20, the total watt-hour throughput is close to 1100 kWh, especially for DOD that are higher than 40%.

The watt-hour throughput can be calculated as follows:

$$E_{max} = 2 \, N_{max}(\Delta DOD) \times \Delta DOD \times C_n(t_0) \qquad \text{eq. 3.22}$$

where the factor 2 reminds that a cycle is composed of a charge and a discharge (it has been added in [114] from the initial formula of [109]), $N_{max}(\Delta DOD)$ is the maximum number of cycles performed for a given cycle depth and $C_n(t_0)$ is the initial nominal capacity of the battery expressed in watt-hour (the capacity expressed in ampere-hour can also be used if it is multiplied by the average voltage of the ESS).
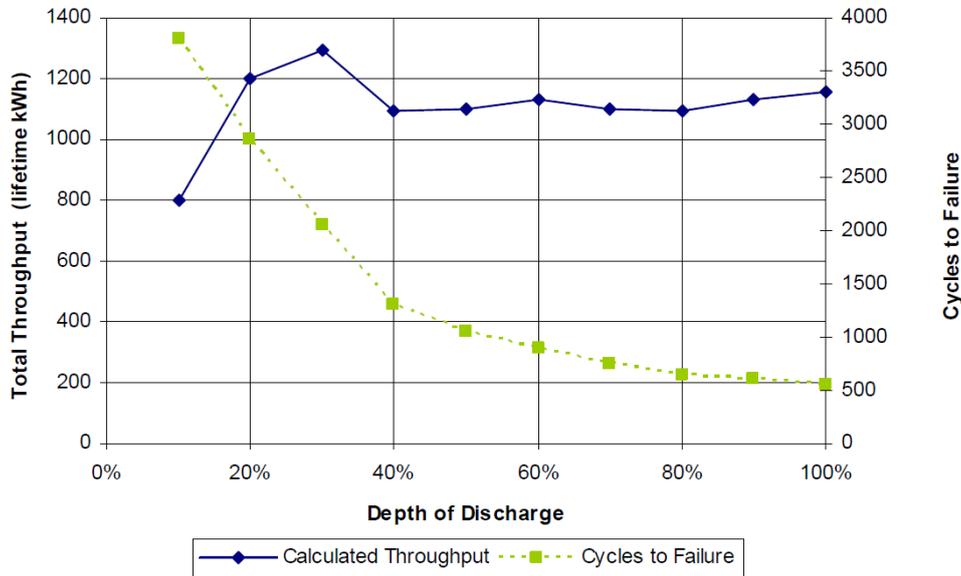
Figure 3.20 Lifetime model of a 2.1 kWh flooded flat plate battery [109]

The EOL can be written as in eq. 3.21. The ESS has to be replaced when $EOL(t)$ is equal to 1.

$$EOL(t) = \frac{\int_{t_0}^{t} |E_{exch}(t)| \, dt}{E_{max}} \qquad \text{eq. 3.23}$$

where $E_{exch}(t)$ is the energy exchanged by the battery at the charge or discharge.

This model can be more accurate if additional information are known on the degradation behaviour of the battery (effect of the C-rate, SOC-level, temperature, etc.). In this case, some weighting factors can be used to improve the lifetime estimation. In [115], some stress factors are presented and studied in order to give some clues on ageing degradation under various operating conditions.

Event-oriented ageing model - Rainflow counting

Assuming that the degradation caused by cycling is linear, the relation depicted in Fig. 3.19 can be more efficiently used by using the rainflow counting method. In this case the event is a cycle performed with a given cycle depth and SOC-level. A very popular algorithm of rainflow counting has been presented by Downing and Socie [116]. Initially developed to estimate the mechanical stress in automotive and building industries, the rainflow counting is often employed to describe the ageing of batteries, as in [117]. Given a battery SOC time series, it is possible to extract the number of cycles with their associated cycle depth and SOC-level. An example of the use of rainflow counting method is presented in Fig. 3.21. This method is usually used offline but can be implemented on-line by storing in a buffer the local extrema that have not been used to define a cycle. A complete example is explained in Appendix 3-C based on the rainflow algorithm I presented in [116].
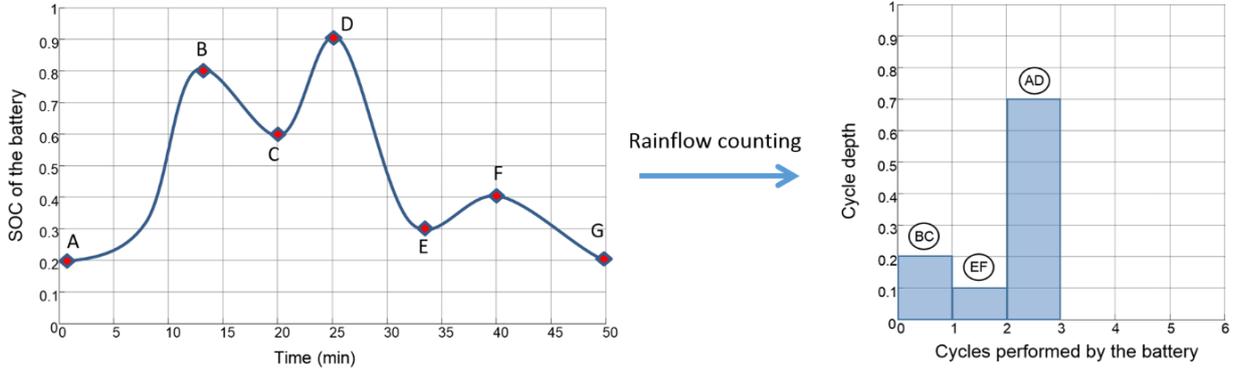
Figure 3.21 Rainflow counting example on an arbitrary SOC time series

The EOL criterion can be calculated as follows. As previously, the EOL is reached when $EOL(t)$ is equal to 1.

$$EOL(t) = \sum_i \frac{1}{N_{max}(\Delta DOD_i)}$$

eq. 3.24

The operating conditions of the ESS are better tracked with this method, which enables to take into account the very different cycling conditions in renewable MGs. For SCs, it seems that the cycle depth has no effect on the lifetime (mainly affected by temperature and C-rate [106]). In this case, the weighted watt-hour throughput is well adapted to estimate the ageing.

3.4 ESS modelling and monitoring

Monitoring is crucial to ensure good performances of an ESS. A battery management system (BMS) is always associated to any type of battery pack or SCs in order to protect them for over-(dis)charge, short circuit, high temperature, unbalance quantity of charges between cells, etc. [118]. This implies to employ an accurate model of ESS. Electrochemical, electrical and black box are the three main families of models that can be used to describe batteries and SCs. An electrochemical model is very accurate but needs a lot of information concerning the chemical composition of the ESS and high computational resources due to the large number of non-linear equations. In [119], such model describes a lithium battery on both microscopic scale (e.g. transport of lithium ions in the electrolyte and in the solid phase, concentration and potential inside the battery, etc.) and macroscopic scale (e.g. voltage and current of the battery). In the case of electrical modelling, an equivalent electrical circuit is created based on either i) DC current steps and measurement of the voltage response of the cell, or ii) electrochemical impedance spectroscopy (EIS) measurements [120] (see more explanations in Appendix 3-D). An example of black box modelling is given in [121], underlining that no *a priori* knowledge is needed on the ESS but a lot of experiments are necessary to achieve an accurate and robust model. Finally, electrical modelling has been chosen in this thesis because it is a good compromise between *a priori* knowledge of the ESS and number of experiments (for different C-rates, cycle depths, temperatures, etc.).

3.4.1 Experimental setup

In order to characterize the behaviour of batteries and supercapacitors and to ensure the reproducibility of measurements, we have used a battery cycler (BioLogic BCS-815, on the desk in Fig. 3.22) and a temperature chamber (ESPEC SU-221, placed below the desk). Two types of lead-acid batteries have been cycled: Yuasa 6 V 1.2 Ah and Yuasa 12 V 7.0 Ah (the corresponding datasheets can be found in Appendix 3.B). We have chosen to experiment and model batteries with a small capacity and a low

voltage, considering that this model is valid when these batteries are associated together (i.e. large battery pack of series-parallel association of battery cells). Some lithium batteries (Samsung INR18650-30Q) and a 16V SC module Maxwell have also been characterized (datasheets are available in Appendix 3.B).

Figure 3.22 Experimental setup for cycling batteries

3.4.2 Electrical equivalent circuit modelling

In the literature, many studies have investigated the equivalent circuit modelling based on the voltage response of a battery to current steps [122], [123], [124]. Indeed, as presented in [118] and illustrated in Fig. 3.23, a battery can be modelled by a variable voltage source which reflects the SOC (this source is often called OCV or EMF) with a series resistance (reflecting the ESS internal resistance related to electrolyte resistance, the electrode material, etc.) and one or more parallel RC networks (added in series, that take into account the different kinetics such as the short and long-term relaxation effects of the transient response).

In [123], different models of batteries are compared and it appears that the model called dual polarization (also called Thevenin model in other articles), constituted of two parallel RC pairs, is well adapted to describe the transient behaviour of a battery.

As investigated in [122], the issue in finding the right values of the parameters is that they exhibit some dependency to the operating conditions such as the C-rate (hysteresis behaviour at the charge and at the discharge), the SOC and the temperature. In [124] a network of two parallel RC has been chosen to model the step responses of a polymer lithium-ion battery. This model is presented as the best trade-off between accuracy, computational and parametrization complexity. As explained earlier, all parameters (series resistance and transient RCs) depend on C-rate (amplitude and direction), SOC, temperature and also ageing (calendar and cycling). In this model, good results have been obtained by taking into account only the SOC dependency. In [125], an adaptive approach is proposed to estimate the SOC and the parameters of the model. The originality of this work is to update the parameters based on the battery operating conditions.
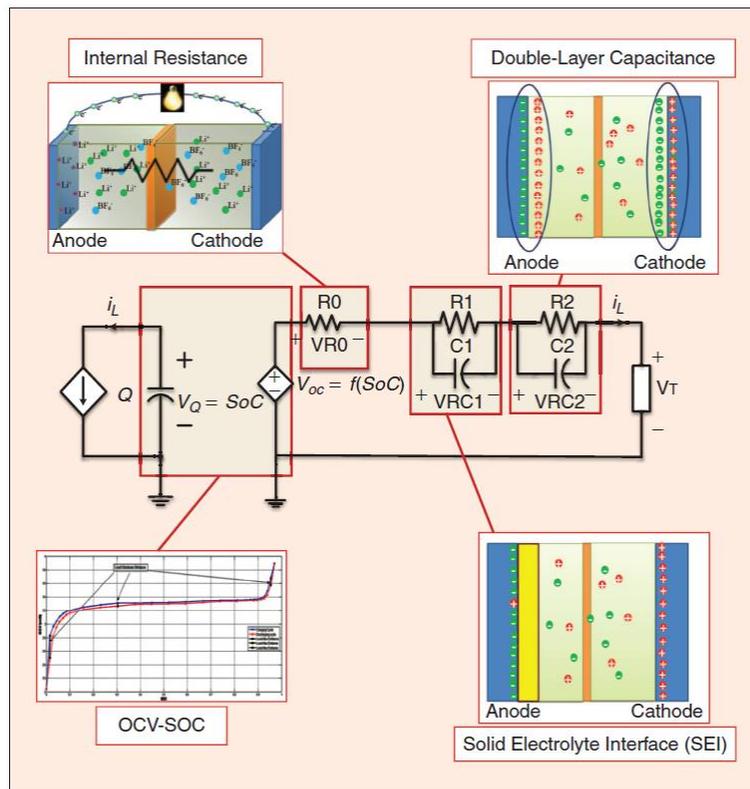
Figure 3.23 Thevenin model of a lithium-ion battery with two parallel RC [118]

In PV applications, the ESS will be confronted to varying currents (and even varying temperatures, depending on the installation). We have tried to propose a simple realistic model based on a few parameters that can be found in datasheets in order to assess the behaviour of different ESSs and then choose the most adapted to our application. In this approach of modelling the voltage of the ESS for different C-rates, no kinetic process will be modelled because some of them are faster than the simulation time step (1-minute for the sizing and usually 1-hour for the scheduling) and the longer ones are difficult to manage if the current is varying too much (see Peukert's law for varying current). In the model described by eq. 3.24 and illustrated in Fig. 3.24-a, the SOC dependency of the internal resistance has been neglected in order to limit the number of cycles to perform. Indeed, some cycles are already necessary to identify the C-rate dependency of the internal resistance (the temperature dependency is not in the scope of this study).

$$V_{ESS}(t) = V_{OC}(t) + R_S(i_{ESS}) \times i_{ESS}(t) \qquad \text{eq. 3.25}$$

As we described in [126] and in Fig. 3.24-b, we investigated the relation between the OCV and the SOC of a lead-acid battery (Yuasa 6V 1.2Ah). This relation is linear for a lead-acid battery (conversely to lithium-ion batteries that can be highly non-linear, depending on the technology). As explained earlier, experimental data have been obtained after long rests (at least a day to have a good accuracy) in order to reach the end of the voltage relaxation (around 1 mV per hour).

a)   b)
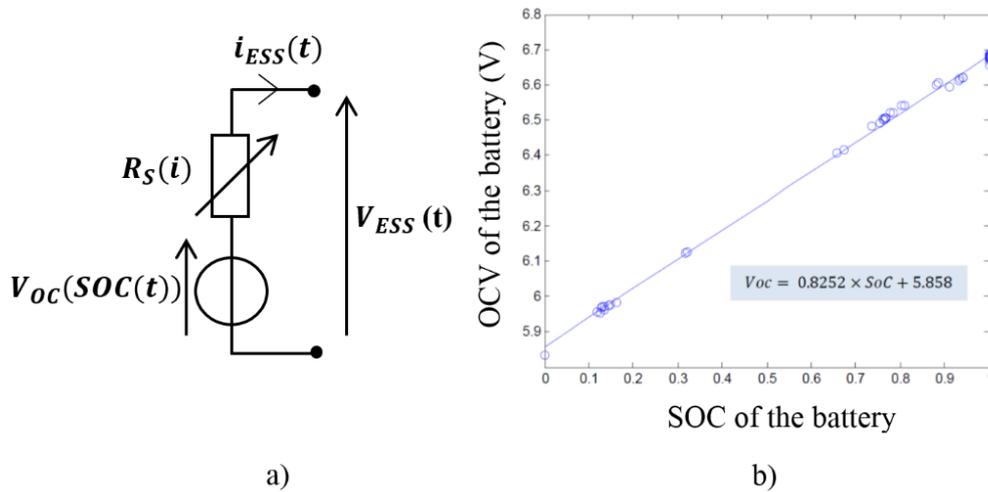
Figure 3.24 a) Simplified model describing an ESS, b) OCV vs. SOC of a lead-acid battery

Hence, the open circuit voltage of a lead-acid battery can be expressed as follows:

$$V_{OC}(t) = A_{Batt} \times SOC(t) + B_{Batt}$$

eq. 3.26

where A_{Batt} and B_{Batt} are two coefficients that are specific to the studied battery (for the Yuasa battery, we respectively found $A_{Batt} = 0.8252\ V$ and $B_{Batt} = 5.858$ V).

We have also made some experiments on 16 V 500 F SC modules (some characterization tests are presented in Appendix 3.B) and we found a very low internal resistance (about 1 mΩ). So the voltage response is very close to the OCV. We have noticed a high dependency with temperature but this is out of the scope of this study. In Fig. 3.25-a, a large window of C-rates (from C/10 to 3C) at the discharge have been tested in order to find a relation between the value of internal resistance and C-rate (the tests at the charge have not been presented because the ESS will operate on a narrower C-rate window, limited to 0.4 C. In this case, the internal resistance can be considered constant). Considering a SOC range of interest from 20% to 100%, the relative error between the model and experimental data presented in Fig. 3.25-a is lower than 10% for the lead acid batteries. For SCs, the current at the charge has been experimented from 1 to 10 A. It appeared that the internal resistance is very low (voltage responses are overlapped). The static model presents a relative error lower than 15% on the full range of SOC.
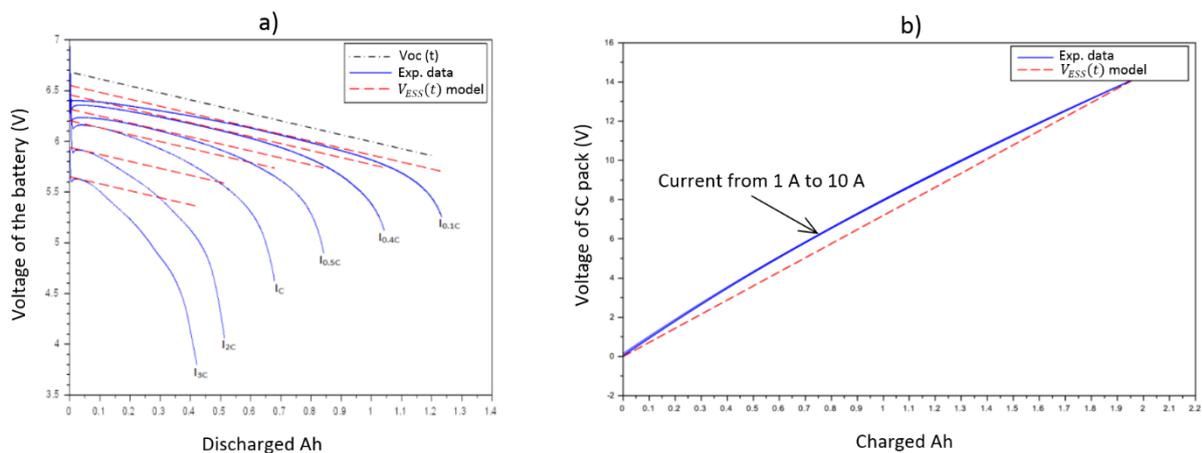
Figure 3.25 Comparison between experimental data and model of an ESS a) discharge of a lead-acid battery, b) Charge of a SC module [126]

The experimental non-linear relation between the internal resistance and the C-rate of the 1.2 Ah 6V Yuasa lead-acid battery is presented in Appendix 3.E.

3.5 Summary

The main technologies of ESSs with their major characteristics have been presented in this chapter. Different criteria (e.g. cost, lifetime, efficiency, level of maturity, etc.) have been presented to wisely choose an ESS for a given application.

Lead-acid batteries, lithium-ion batteries, and SCs have been studied in more details because they have been selected to be integrated in the ADREAM PV building and to be experimentally tested in a small-scale MG application. Some definitions have been given to model some crucial states of ESSs such as SOC and SOH.

Moreover, the study of these three technologies enabled to define some optimal operating conditions such as the limitation of cycle depth in order to increase the maximum number of cycles performed by batteries. Indeed, a special attention has been paid to the literature review in the field of lifetime modelling with the search of the main stress factors (such as cycle depth, SOC level, C-rate, and obviously temperature but this latter is not in the scope of this study).

An equivalent circuit modelling has been done with some experimental tests in order to verify the basic relationships defining electrochemical and electrical storage systems.

The presented model and criteria developed in this chapter will be used in the next chapters for the sizing and the scheduling of ESSs in MGs.

In order to study all aspects of the MG operation (i.e. optimal sizing and control), we had not enough time to perform all experimentations related to ESS modelling, in particular the evaluation of internal resistance and ESS efficiency for different SOCs. In addition, the adapted equipment (temperature chamber and precise battery cycler) arrived at the end of my second year of doctoral thesis so the verification of lifetime models, which necessitate several months of tests (depending on the technology of ESS and C-rates), has not been performed.

Chapter 4. Optimal sizing of energy storage systems

"If you want to find the secrets of the universe, think in terms of energy, frequency and vibration."

Nikola Tesla (10 July 1856 – 7 January 1943) Serbian-American electrical engineer and physicist who developed major inventions such as AC induction motors and electrical transmission equipment.

The optimal sizing of an energy storage system (ESS) relies on the appropriate choice of criteria assessing the performances of the storage system in the microgrid (MG). The use of multiple criteria (which are sometimes conflicting) enables to broadly evaluate with a generic methodology different configurations of MG (i.e. autonomous grid, connected to the utility grid, connected but limited in peak-power, etc.). Because of the complexity of the problem, which gathers many fields, a multi-objective optimization technique has been chosen among different approaches. Indeed, Pareto optimality seems a very convenient tool, because it avoids to make assumptions on the valuation of some criteria (e.g. it is possible to find a trade-off between GHG emissions and annual cost of the storage system without putting a cost on GHG emissions). Hence, we have developed an optimal sizing methodology taking into account the model of ESS (presented in the previous chapter) and the operating profile of the MG (which can be either based on historical data such as the ADREAM building, or generated scenario via Monte Carlo approach).

This chapter is organized as follows:

First, mono and multi-objective optimization methods are discussed. Then, several criteria that aim to evaluate the optimality of the ESS sizing are discussed for MG applications. Two study cases are developed based on the ADREAM PV building and two storage systems have been optimally sized based on different criteria. The first study case has been done to propose a hybrid energy storage system, which associates two storage technologies, with a pre-defined strategy of storage. The second study case propose to find the optimal capacity and cycle depth of a lithium battery pack. Finally, the multi-objective optimization is applied to design appliances such as a light emitting diode (LED) lighting.

Table of contents of chapter 4

4.1 -   Optimization techniques for ESS sizing

Several optimization techniques have been developed to solve real-world problems in many fields such as transportation (e.g. the travelling salesman problem), engineering (e.g. structural design subject to static and dynamic loading), finance (e.g. resource allocation and scheduling), etc. The optimization process consists of three main steps:

- Definition of an objective function $f(x)$,

- Identification of the decision variables x,

- Formulation of a mathematical model.

A general formulation of an optimization problem is given in eq. 4.1 [127].

$$\begin{cases} minimize \; f(x) \; (or \; maximize \; f(x)) \\ \qquad subject \; to \\ x = (x_1, x_2, \ldots, x_n) \in \mathbb{R}^n \end{cases} \qquad \text{eq. 4.1}$$

In many cases, a set of constraints and inequalities is added in the formulation of the optimization problem. The exhaustive search technique (i.e. enumerating and checking all possible candidates for solution) is often intractable when a large number of combinations have to be calculated (combinatorial explosion). This is why, specific optimization methods have been developed to solve such problems. The main methods can be classified as below:

- **Linear programming (LP)** refers to problems in which the objective function, equalities, and inequalities are linear and the variables are continuous (real value).
- **Non-Linear programming (NLP)** refers to problems in which the objective function or the constraints (or both) are non-linear and the variables are continuous.
- **Mixed integer linear programming (MILP)** refers to linear problems in which at least one variable is assigned to a discrete value (integer value). When the problem involves nonlinearities in the objective function or constraints, the optimization technique is called **mixed integer non-linear programming (MINLP)**.
- **Quadratic programming** refers to problems in which the objective function has quadratic terms with linear constraints.
- **Stochastic programming** refers to problems in which the deterministic mathematical model is enhanced by the inclusion of uncertainties with random variables.

For the sizing of energy systems, [128] presents a review on optimization techniques, objective functions and constraints. It appears that heuristic and metaheuristic methods have been well developed during the past decades to handle complex problems in order to minimize the computational resources and find a satisfactory solution (i.e. which is not always optimal). Some examples of optimization techniques are presented such as genetic algorithms (GAs), simulated annealing, particle swarm, ant colony, etc.

Often, the minimization of the system's life cycle cost is the only objective that is used in the sizing of small autonomous electrical grids with renewable sources and ESSs: an iterative method has been proposed in [129], [130], and a robust MILP has been developed in [131].

Recently, a large number of studies have proposed some multi-objective optimization techniques, optimizing simultaneously different criteria such as life cycle costs, reliability, environmental impacts, etc. The concept of multi-objective optimization is well explained in [132], [133] and has been reviewed in the field of MG in [134], [135].

A multiobjective optimization problem consists of minimizing or maximizing k conflicting objective functions f_i by finding the appropriate input values (decision vector $\boldsymbol{x}$) belonging to a feasible set $S \subset \mathbb{R}^n$. Such problem can be mathematically formulated as follows:

$$minimize \ (or \ maximize) \ \{f_1(\boldsymbol{x}), \dots, f_k(\boldsymbol{x})\}$$

$$subject \ to \ \boldsymbol{x} \in S$$

<div align="right">eq. 4.2</div>

It can be noticed that in multiobjective optimization, the optimal solution is not unique. By using the Pareto technique, a set of non-dominated solutions forms the so-called Pareto front as described in [136], [137]. In Fig. 4.1, a bi-objective problem is presented, showing the Pareto front and the dominated solutions. If we consider two solutions belonging to the Pareto set, one solution is better than the other on some objectives, but also worse on at least one objective. Indeed, a solution $\boldsymbol{x_p} \in S$ is said Pareto-optimal if there does not exist another solution $\boldsymbol{x} \in S$ such that $f_i(\boldsymbol{x}) \leq f_i(\boldsymbol{x_p})$ for all $i = 1, \dots, k$ and $f_j(\boldsymbol{x_p}) < f_j(\boldsymbol{x})$ for at least one index j.

In order to help the decision maker to choose one optimal solution amongst others, an ideal point, noted utopia point (Fig. 4.1), can be set for each Pareto front. The coordinates of this ideal point correspond to the global minimum of the Pareto front on each objective. After normalization of the objectives, the optimal point of the Pareto set is the nearest point to the ideal point, according to its Euclidean distance [137], [138].
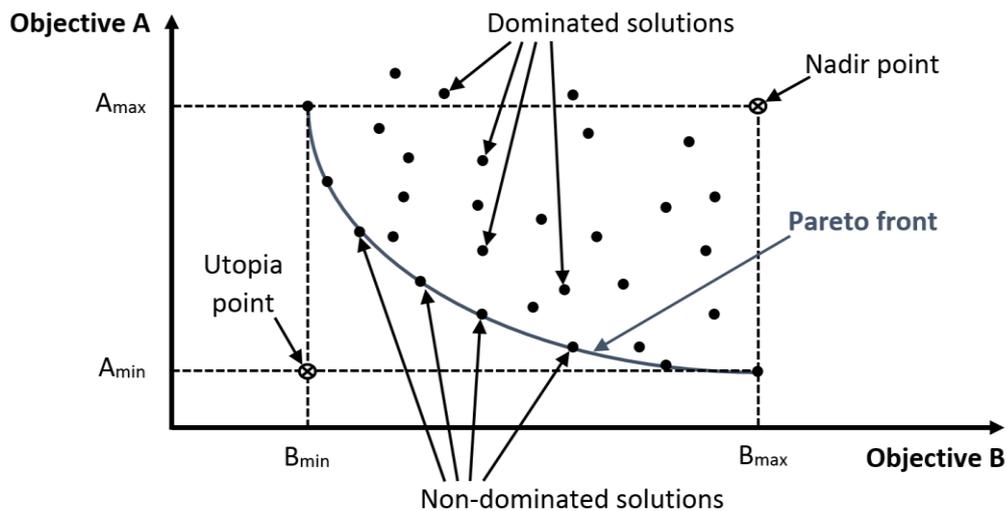
Figure 4.1 Bi-objective minimization problem – Pareto front and dominated solutions

Many studies in the literature describe step by step how to build a multi-objective method for the optimization of a MG:

[139] presents a bi-objective optimization based on the cost of energy and GHG emissions of a small autonomous hybrid power system constituted of a diesel generator, renewable sources and ESSs. A Pareto optimization technique has been developed and a good explanation is given concerning the parametrization of the non-dominated sorting GA (NSGA-II) technique (i.e. population, crossover and mutation rate, etc.) that has been used in order to find the best Pareto front in a reduced computational time. In this study, a comparison has been made between lead-acid battery technology and hydrogen tank combined with fuel cell and it appears that lead-acid batteries are a better ESS on both economic and environmental objectives.

A similar system (stand-alone PV-wind-diesel source with battery storage) and criteria (costs and pollutant emissions) have been studied in [140]. In this study, the authors developed a new complete MG sizing tool named hybrid optimization by genetic algorithms (HOGA). The reliability of the system is also introduced by taking into account the unmet load (a solution of sizing is considered valid if at least 99.5% of the load demand is satisfied).

Three objectives (i.e. life cycle cost, embodied energy, and loss of power supply) have been used in [141] to optimally size a hybrid PV-wind-battery system. As in previous studies, a GA has been used to handle the large number of combinations and ensure the rapid convergence to an optimal Pareto front.

Different software tools for MG simulation and sizing have been reviewed in [142]–[144]. The most popular have been developed by the NREL: Hybrid Optimization Model for Electric Renewables (HOMER) and Hybrid Power System Simulation Model (HYBRID2). Despite the fast implementation of a good MG model, a higher flexibility in terms of modelling and optimization method is obtained with other more classical tools such as MATLAB and General Algebraic Modeling System (GAMS). We have chosen to work with the two latter tools in order to develop our own simulation and optimal sizing methodology.

Before presenting our work, we define in the next section several sizing criteria and the selection we made for our sizing methodology.

4.2 - Definition of criteria for ESS optimal sizing

Several criteria classified into categories such as economic, environmental, socio-political, and/or technological factors can be formulated in order to evaluate the performances of the ESS sizing in the MG. Hence, the result of the sizing methodology is entirely based on the choice of a combination of some of the following objectives.

4.2.1 - Reliability

The reliability of the electrical grid is a crucial issue. As presented in [145], the Sendai MG in Japan was able to supply critical consumers (such as an hospital) during an outage due to a natural disaster. It is important when sizing an ESS to evaluate the potential reachable autonomy and also analyse the trade-off that can be made between the cost of the capacity and the availability of the ESS (in case of non-critical loads). In this regard, the two following criteria are well describing the reliability of the MG.

- **Loss of power supply probability (LPSP)** defines the energy that has not been supplied to load. It is calculated as the ratio of energy deficit to the load demand for a given period [146], [147].

$$\text{LPSP}(t) = \frac{\int_{t_0}^{t} E_{deficit}(t)\, dt}{\int_{t_0}^{t} E_{load}(t)\, dt} \qquad \text{eq. 4.3}$$

- **Level of autonomy (LA)** indicates the availability of the power distribution. It is defined as the ratio of the hours that exhibit a loss of load (HLOL) to the total hours of operation (HTOT) [146].

$$\text{LA} = 1 - \frac{\text{H}_{\text{LOL}}}{\text{H}_{\text{TOT}}} \qquad \text{eq. 4.4}$$

For the application of storage in PV buildings, the two previous criteria are enough to have a good evaluation of the system's reliability. To have a complete overview of the existing criteria, other ones

also aim at assessing the reliability of the MG (i.e. equivalent loss factor [142], loss of load expected [142], expected energy not supplied [3], etc.).

4.2.2 - Cost analysis

The costs associated to the generation of electricity are often the first objective to minimize. Two main costs have to be considered in the sizing of ESSs, the initial capital cost C_{cap} (usually expressed in €/kWh), and the annual costs of operation and maintenance $C_{O\&M}$ (also expressed in €/kWh).

- **Annualized cost of system (ACS)** reflects the annual cost of the ESS on the long-run, as calculated in eq. 4.5 and illustrated in Fig. 4.2, by taking into account the C_{cap}, $C_{O\&M}$, and the lifetime expectancy (included in the calculation of the capital recovery factor (CRF), described in eq. 4.4) [147].
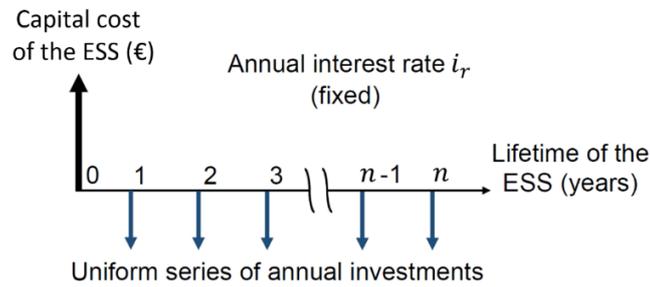
Figure 4.2 Annualized cost of an ESS

In [148], [149], the ACS of a MG was evaluated and a replacement cost of the ESS was added in the calculation because the duration of the project was based on the lifetime expectancy of renewable sources which is longer than batteries lifetime.

$$\text{ACS} = C_{cap} \times CRF + C_{O\&M} \qquad \text{eq. 4.5}$$

CRF enables to calculate annual equal payments over the lifetime of the ESS, based on the initial capital cost, as explained in [150], [151]. The calculation of CRF (see eq. 4.6) is based on the ESS lifetime expressed in number of years n, and the interest rate i_r (typically between 5 and 10% [152], depending on the duration of the project. 7.7% has been considered in [148] for an ESS project).

$$\text{CRF} = \frac{i_r(1 + i_r)^n}{(1 + i_r)^n - 1} \qquad \text{eq. 4.6}$$

- **Levelized cost of energy (LCOE)** assesses the total cost of energy (generally expressed in euros per kilowatt-hour) by taking into account the cost of all equipment involved in energy production over their entire lifetime, as presented in Chapter 2. It can be adapted to ESS by using the annualized discharged energy E_{dis}, as proposed in eq. 4.7.

$$\text{LCOE} = \frac{\text{ACS}}{E_{dis}} \qquad \text{eq. 4.7}$$

The LCOE of different types of batteries has been calculated in [153], with a supplementary analysis concerning the applications of ESSs (i.e. the LCOE of each application is analysed separately because an ESS involved in utility time-shift service will deliver far more energy than another ESS used for frequency regulation). This discussion is very interesting because it addresses issues such as the business model and policy of ESS integrated in the electrical grid, but it is out of the scope of this thesis.

Other formula can assess the economic aspect of the ESS such as the net present value (NPV) [142]. Indeed, this calculation takes into account the capital and operation costs, the revenues generated by the system and the residual value of the system at the end of the project. It has been chosen to not use this criteria because it implies a supplementary hypothesis compared to ACS concerning the residual value of the system. When the ACS is used, the system is used until its end-of-life (i.e. no residual value because the ESS will not be re-used in another project).

4.2.3 - Environmental impacts

Considering a grid-tied MG with a renewable source and an ESS, the use of the renewable source can be enhanced by the ESS. The criteria described in eq. 4.8 and 4.9 reflect the good integration of renewable sources at a local scale, close to the consumption. The self-consumption presents several benefits such as a possible mitigation of the peak-demand on the grid which may avoid investments in transmission and distribution infrastructures (because of the energy demand growth), and the transmission losses could decrease if the electrical system is properly sized.

- **Self-consumption of renewable sources (s_{cons})**, defined in [154], describes the level of use of the generated renewable energy. For a MG with a PV source and an ESS, the total energy generated by the PV source is noted E_{PV}, the energy directly used from the PV system to the load is noted E_{DU}, and the PV energy charging the ESS is noted E_{BC}. The self-consumption is calculated as follows:

$$s_{cons} = \frac{\int_{t_0}^{t} (E_{DU} + E_{BC})\, dt}{\int_{t_0}^{t} E_{PV}\, dt} \qquad \text{eq. 4.8}$$

- **Self-sufficiency (s_{suf})**, also defined in [154], reveals the share of locally generated energy in the total energy demand E_{Demand}.

$$s_{suf} = \frac{\int_{t_0}^{t} (E_{DU} + E_{BC})\, dt}{\int_{t_0}^{t} E_{Demand}\, dt} \qquad \text{eq. 4.9}$$

- **Total energy lost (TEL)** shows the energy that is neither used to feed the load nor to charge the ESS (i.e. wasted energy). Derived from [142], TEL can be described by using E_{gen} (generated energy in the MG) and E_{use} (sum of energy going to the load and to the ESS):

$$\text{TEL} = \sum_t E_{gen} - E_{use} \qquad \text{eq. 4.10}$$

- **Life-cycle analysis (LCA)** describes environmental impacts of a device by taking into account all four life stages that are manufacturing, transportation, use and end-of-life. In these studies, some data are difficult to obtain and are often estimated (especially those concerning the manufacturing processes which are fast evolving due to improvements of technologies). The result of a LCA analysis is often expressed in terms of CO_2 emissions or primary energy consumption [77]. In [141], the term **embodied energy (EE)** is used to describe the total primary energy used to produce a system such as a PV panel, a wind turbine, or a battery.

Additional criteria can expand the evaluation of environmental impacts such as the analysis of power losses or the fuel consumption (in non-renewable plants) that should be minimized [142].

4.2.4 - Socio-political factors of the MG

Due to the globalization of the energy market, energy resources come from foreign countries and are transported on long distances, which increases the risk of non-delivery and possible shortage. Nearly all countries are in a situation of energy dependency (e.g. according to the IEA, France mainly imports uranium from Niger, Canada and Kazakhstan, natural gas from Norway, Russia, and Netherlands through cross border pipelines, and oil from Middle Eastern countries).

- **Portfolio of risks** has been defined in [142] as an objective related to the dependency of fossil fuels (i.e. the penetration of renewable sources is limiting the fossil consumption so the price variations of fossil fuels will have a lower impact on the energy system). This criteria can be extended in our case to the constituting materials of ESSs in order to prevent the use of a unique solution that may create a too high pressure on a few resources.

- **Social acceptance (SA)** of a technology such as renewable sources has been discussed in [30]. This criterion defines the possible barriers that can make a population reluctant to use and/or to pay a product or a service. In this study, the purpose was to assess the willingness of local communities to invest in green energy that are more expensive than conventional fuels but less harmful for the environment. In the case of ESSs, the SA can be extended because a successful use of ESSs in a MG also relies on the training of the users [145].

Even if it seems obvious to take into account these socio-political criteria in the sizing of ESSs, these latter will not be developed in this work because of a lack of literature reviews on the deployment of ESSs in the electrical grid.

The following sizing method is based on the study of Pareto optimality of a hybrid ESS combining batteries and SCs. In order to evaluate the different configurations, a modular scheme has been developed. It takes into account a model of the ESS (performances and ageing, as defined in Chapter 3), an operating profile of the MG based on historical data of the ADREAM building, an energy flow management between load demand and ESSs, and the definition of criteria to evaluate the sizing.

4.3 - Multi-objective optimal sizing of a hybrid ESS

Because of the very different performances of each ESS (power and energy densities, cycle efficiency, lifetime, etc.) and their costs, we have selected three commercialized technologies that are SCs, lead-acid and lithium-ion batteries, in order to make a hybrid ESS that contains at least two storage systems and benefits from their complementarities. In the literature, different associations of ESSs already exist such as the passive hybrid association of a battery and a SC, which has been analytically studied for pulsed loads in [155]. Hence, it appears that the hybrid system enables to increase the peak power, to decrease the internal losses, and to enhance the lifetime, compared to a battery system without a SC. As analysed in [156] and illustrated in Fig. 4. 3, the first step is to choose the electrical association of the two storage systems. The different topologies of hybridization with classical power converters (such as buck, boost, or buck-boost) are globally well adapted to connect several ESSs to a DC bus. The advantages and drawbacks of each hybrid topology are summarized in Table 4.1.

Other different hybrid associations of ESS technologies through DC/DC converters have been widely studied, especially in the field of transportation [157]–[159]. A hybrid topology with proper management applied to a PV source with a DC bus has also been developed in [160]. Another topology adapted to AC MGs has been presented in [161], in which a three-level neutral point clamped inverter is shown as the best topology for the association of a vanadium redox battery with SCs. This power converter enables to decreases power losses and total harmonic distortion but the control algorithm is more complex.

In our case, we have chosen to consider the parallel active hybrid topology that enables the full and independent controllability of ESSs with a good efficiency of power converters (because they will run nearly always at their nominal power, one adapted to high power and the other to low power).
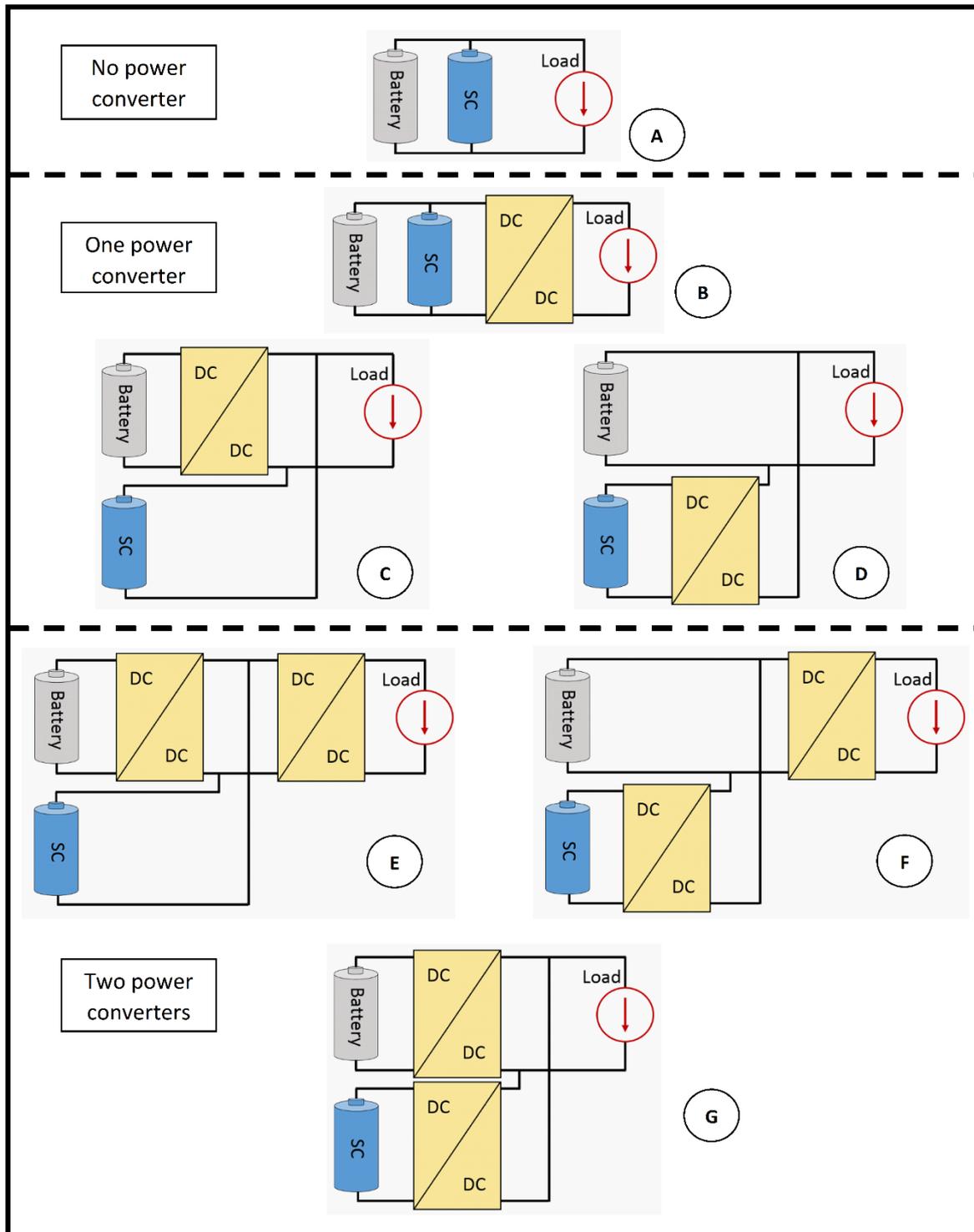
Figure 4.3 Some hybrid topologies of ESSs adapted to DC MGs

Topology	Advantages	Drawbacks
A – Passive	• Very easy to implement (no control and power electronic) • Low cost	• ESSs are not controllable (current is shared depending on internal resistances of ESSs) • ESSs are used on a limited voltage window • ESSs are not protected from bad operations (voltage and current) • Load voltage is not regulated • Voltage matching between load and ESSs is necessary
B – Parallel semi-active	• Easy to implement (only one power converter with a simple control) • Load voltage can be regulated • Load and ESSs voltages are decoupled	• ESSs are not controllable separately • Use of a small voltage window of SC (compared to battery) • DC–DC converter will not run efficiently in case of pulsed load (because designed for the maximum power load demand, so low efficiency at low power)
C – Battery semi-active	• Easy to implement • Load voltage can be regulated • Battery is controllable • Load and battery voltages are decoupled • Efficient use of the power converter (because it has been sized for the nominal power)	• SC is not controllable • Use of a small voltage window of SC • Voltage matching between load and SC is necessary which implies a large capacitance value of SC
D – SC semi-active	• Easy to implement • Load voltage can be regulated • SC is controllable • Load and SC voltages are decoupled • Full use of SC (on a large voltage window)	• Battery is not controllable • Voltage matching between load and battery is necessary
E – Battery series active	• Load voltage can be regulated • Load and ESSs voltages are decoupled • ESSs are independently controllable (fully usable)	• Reduced efficiency compared to previous topologies (because two DC/DC conversion stages are used) • Higher control complexity
F – SC series active	• Load voltage can be regulated • Load and ESSs voltages are decoupled • ESSs are independently controllable (fully usable)	• Reduced efficiency compared to battery series active topology (because both power converters are designed for the maximum load power) • Higher control complexity
G – Parallel active	• Load voltage can be regulated • Load and ESSs voltages are decoupled • ESSs are independently controllable (fully usable) • Power converters can be efficiently designed (average load demand for battery and peak demand for SC)	• Higher control complexity (a control scheme is proposed in chapter 5)

Table 4.1 Comparison of different hybrid topologies of ESSs

Concerning the sizing of ESSs, the objective is to determine if the hybrid topology leads to better electrical performances (high energy and power densities) and enhances life cycle costs. The next section aims at providing a methodology that evaluates the sizing with such criteria.

4.3.1 - Hybrid strategy of energy storage:

This study has been the first step in the development of a new experimental platform placed inside the ADREAM building, named 'Open Platform for the ADREAM building' (OPA). This project has been launched by Marise Bafleur and Thierry Monteil in order to propose an innovative common platform that will be used by different teams of the LAAS-CNRS. Hence, this platform enables to validate some energy management strategies and develop a new Internet of Things (IoT) network (with sensors and actuators placed in an experimental living apartment). This small scale MG of some kilowatts will be presented in more details in chapter 5.

The following generic DC MG connected to the main grid with a PV solar source and two ESSs has been considered for the explanation of this method, as depicted in Fig. 4.4.
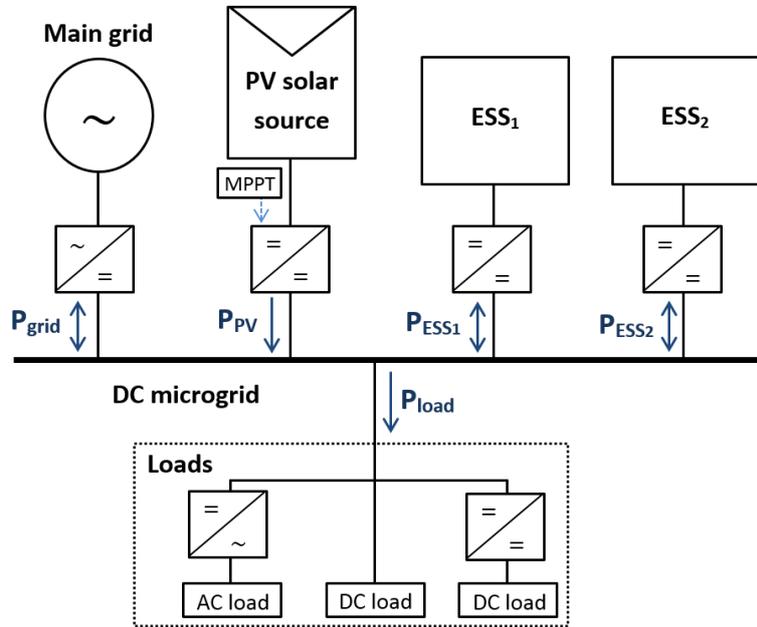
Figure 4.4 Topology of the PV microgrid with two ESSs

It is to notice that the following sizing method can also be used for AC MG. In this case, all sources and loads are directly connected on an AC node instead of a DC bus.

The strategy of storage consists of supplying the load demand by renewable power supplies in priority. In our study, the difference between the PV source and the load demand power is named power balance, noted $P_{balance}(t)$, as described in eq. 4.11. Surplus of power from the PV system and residual demand within the MG that cannot be met by the PV system (i.e. deficit of power) are denoted by a positive and a negative value, respectively.

$$P_{Balance}(t) = P_{PV}(t) - P_{Load}(t)$$

eq. 4.11

where $P_{PV}(t)$ is the PV power production and $P_{Load}(t)$ is the load consumption of the MG.

The strategy of hybrid ESS is supposed to take advantage of the complementary characteristics in terms of power and energy of both technologies. The algorithm describing the storage strategy is presented in Fig. 4.5. Hence, if the renewable source does not meet the load demand, the remaining load demand has

to be supplied by the first ESS, and then by the second ESS if there is a residual demand. If both ESSs are not capable of storing all the PV surplus, or cannot deliver all the power asked by the load, the value of the mismatching quantity of energy is stored in a criterion for the final evaluation of the sizing. Hence, both ESS are working with the same inner strategy but they have different SOC and power limitations, which impose their operating conditions.

In this study, two ESSs are assessed: a lead-acid battery pack (based on the parameters found in chapter 3 of Yuasa 6V) and a SC pack (based on the Maxwell pack presented in chapter 3). We have chosen to simulate the OPA platform that is a small-scale MG of the ADREAM building (1/100). Hence, the voltage of the battery pack and the SC pack are considered to be around 36 V and 48 V, respectively (because it is well adapted, for power conversion reasons, to the DC bus voltage of the experimental platform fluctuating around 55V, which is within the limit of touch voltage that is acceptable according to the European legislation EN 50 122-1). The voltage parameters of the lead-acid battery and the SC pack that have been obtained in chapter 3 have been adapted to this higher voltage (1:6 and 1:3, respectively).The complete algorithm of the strategy of storage of the hybrid ESS is presented in Fig. 4.5.
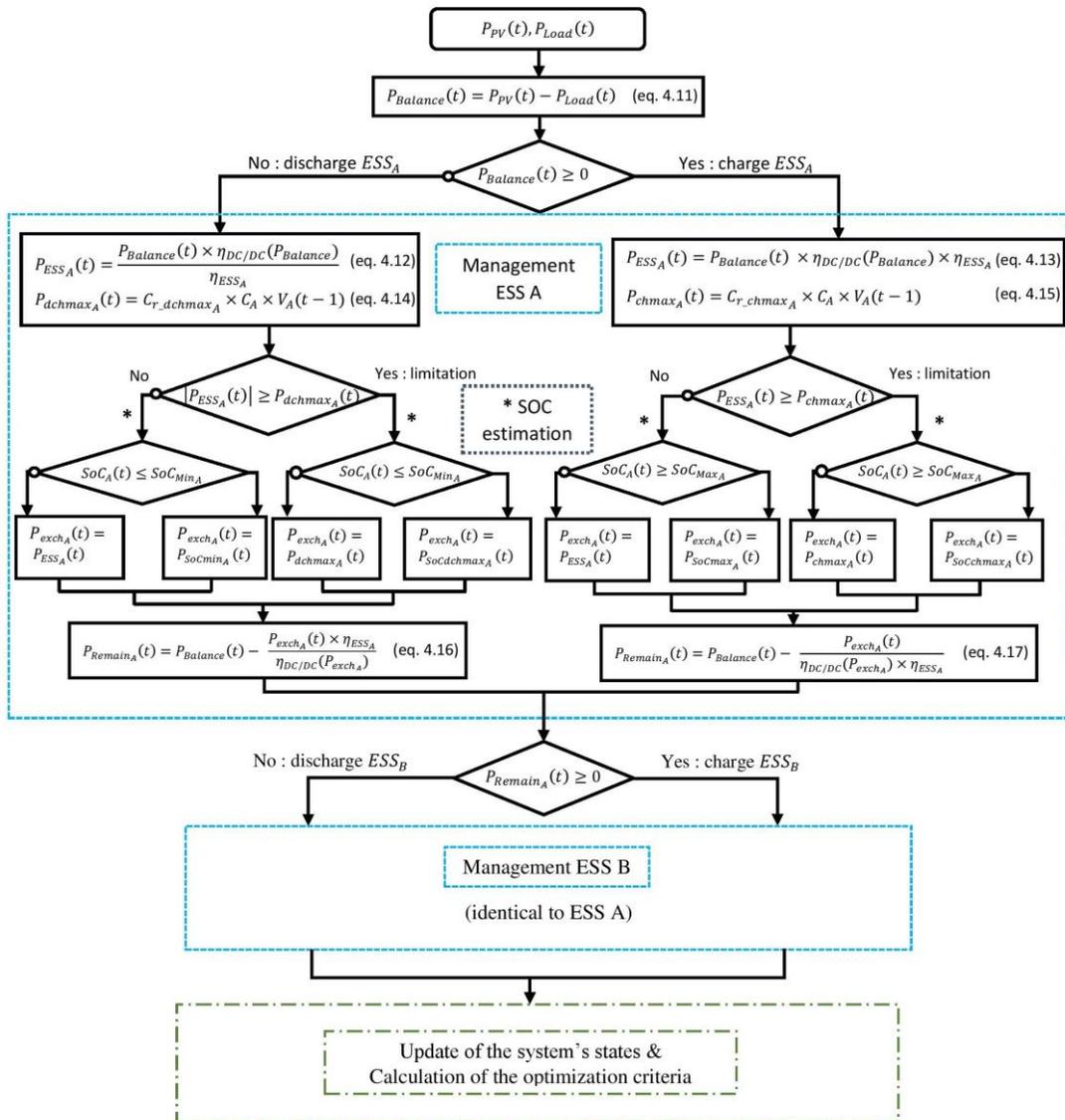
Figure 4.5 Algorithm of ESS management

Concerning the formula used in the algorithm depicted in Fig. 4.5, eq. 4.12 and eq. 4.13 take into account the cycle efficiency of the ESS η_{ESS} (80% and 95% have been considered for lead-acid batteries and SCs, respectively) and the power converter efficiency $\eta_{DC/DC}$ (see below) in order to estimate the power that need to be delivered or absorbed by the ESS without taking into account its SOC and power limitations. The power limitations at the charge $P_{chmax}(t)$ and the discharge $P_{dchmax}(t)$ are described by eq. 4.14 and eq. 4.15. These limitations take into account the maximum C-rate at the charge $C_{r\_chmax}(t)$ (1/3 has been considered for lead-acid batteries) and at the discharge $C_{r\_dchmax}(t)$ (1.5 for lead-acid batteries), but also the nominal capacity of the ESS (expressed in Ah), and the voltage of the ESS (evaluated from the previous time step, assuming that the voltage is not varying during the time step of 1 minute, because of the large capacity of the storage system). For SCs, no power limitation has been considered. Finally, the remaining power that has not been either delivered or absorbed by the ESS is calculated by eq. 4.16 and 4.17. This formula takes into account the ESS efficiency and the power converter efficiency based on the power that has been exchanged by the ESS $P_{exch}(t)$ in order to accurately evaluate the remaining power.

In this study, a simple model of the efficiency of DC/DC power converters has been developed. Indeed, a single efficiency curve has been considered, corresponding to the average operation voltage of the lead-acid battery pack and the desired voltage of the DC bus (Vin=36V and Vout=55V). The efficiency of our self-designed bidirectional DC/DC boost converter has been measured and modelled in Fig 4.6. According to the input power P_{in}, the efficiency of the power converter can be modelled as follows:

$$\eta_{DC/DC} = A \exp(B \times P_{in}) + C \exp(D \times P_{in}) \qquad \text{eq. 4.18}$$

where $A, B, C,$ and D are fitting coefficients (equal to 98.65, -6.741e-05, -18.61, -0.02833, respectively. R-square=0.9915 and RMSE=0.1835).
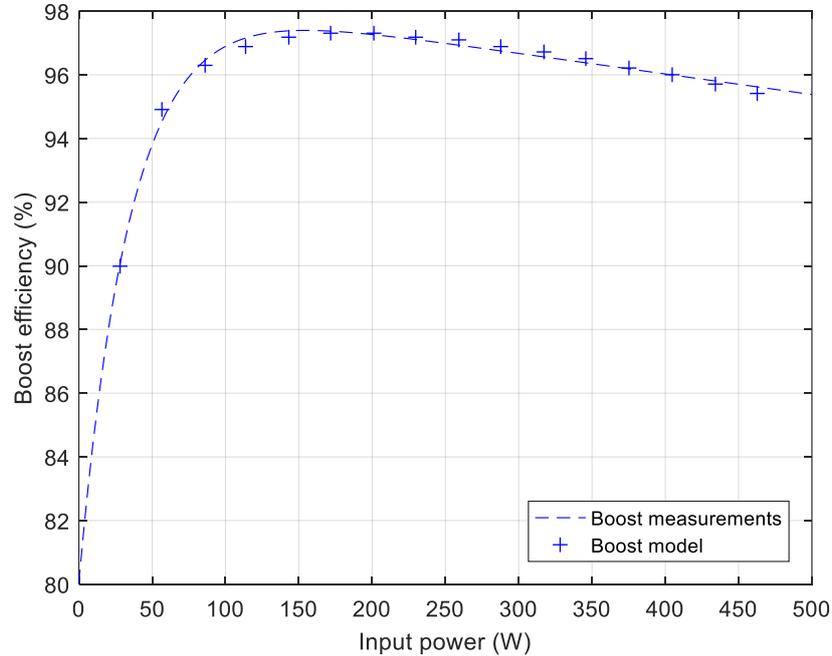
Figure 4.6 Efficiency of a bidirectional DC/DC boost converter for different input power

In Fig. 4.5, the power exchanges performed by the ESS that lead to a limit on SOC (i.e. $P_{SoCmin_A}(t)$, $P_{SoCdchmax_A}(t)$, $P_{SoCmax_A}(t)$, and $P_{SoCchmax_A}(t)$) are calculated as follows:

$$P_{exch_A}(t) = \frac{SoC_{\max(or\ min)_A} - SoC_A(t)}{\Delta T} \times C_{ref_A} \times V_A(t-1) \qquad \text{eq. 4.19}$$

Calculation of the system's states:

For the estimation of SOC, the following equations have been implemented:

$$\begin{cases} SoC_{Batt}(t) = SoC_{Batt}(t-1) + \dfrac{P_{Batt}(t) \times \Delta T}{C_{ref_{Batt}} \times V_{Batt}(t-1)} & \text{eq. 4.20} \\[4mm] SoC_{SC}(t) = \dfrac{V_{SC}(t)^2}{V_{SC\_max}^2} & \text{eq. 4.21} \end{cases}$$

where $P_{Batt}(t)$ is the power exchanged by the battery, ΔT is the time step (1 minute in this study), $C_{ref_{Batt}}$ is the nominal capacity (Ah), $V_{Batt}(t-1)$ is the voltage of the battery at the previous time step, $V_{SC}(t)$ is the actual voltage of the SC, and V_{SC_max} is the maximum voltage of the SCs.

The calculation of the voltage of ESSs, which is a linear relationship for lead-acid batteries (as described in chapter 3, Fig. 3.24-b) and that is derived from the definition of a capacitor (I=C.dV/dt):

$$\begin{cases} V_{Batt}(t) = SoC_{Batt}(t) \times A_{Batt} + B_{Batt} + R_{Batt}(P_{Batt}) \times \dfrac{P_{exch_{Batt}}(t)}{V_{Batt}(t-1)} & \text{eq. 4.22} \\[4mm] V_{SC}(t) = V_{SC}(t-1) + \dfrac{P_{exch_{SC}}(t) \times \Delta T}{C_{SC} \times V_{SC}(t-1)} & \text{eq. 4.23} \end{cases}$$

where A_{Batt} and B_{Batt} are the fitting coefficient that have been found in chapter 3 (eq. 3.26), R_{Batt} is the internal resistance of the lead-acid battery, and C_{SC} is the capacitance of SC (F).

Ageing is calculated by throughput method, considering that a given energy can be exchanged during the entire lifetime of an ESS (expressed in Watt-hour, see chapter 3). Hence, eq. 3.21 and 3.22 enable to determine the maximum energy that can be exchanged.

$$\text{E}_{max} = 2\,(a\exp^{(-b\Delta DOD)} + c) \times \Delta DOD \times C_{ref_{Batt}} \times \langle V_{batt} \rangle \qquad \text{eq. 4.24}$$

where a, b, and c are fitting coefficient of the curve of lifetime (number of cycles vs. cycle depth). According to the datasheet of Yuasa batteries, $a = 7618$, $b = 6.605$, $c = 169.7$. $\langle V_{batt} \rangle$ is the average voltage of the battery during all the simulation.

For SCs, we have assumed that the cycle depth has no effect on the maximum number of cycles, N_{max} (1 million of cycles has been considered). Hence, the maximum exchangeable energy (in Watt-hour) is:

$$\text{E}_{max_{SC}} = \dfrac{C_{SC}}{3600} \times V_{SC\_max}^2 \times N_{max} \qquad \text{eq. 4.25}$$

For every ESS, the exchanged energy is calculated as follows:

$$E_{exch_{ESS}}(t) = E_{exch_{ESS}}(t-1) + \left| P_{exch_{ESS}}(t) \right| \times \Delta T \qquad \text{eq. 4.26}$$

Finally, the lifetime, expressed in years, is calculated according to the maximum energy that can be exchanged.

$$n = \dfrac{\text{E}_{max}}{E_{exch_{ESS}}(end)} \times T_{Simu} \qquad \text{eq. 4.27}$$

where T_{Simu} is the total duration of the simulation horizon (expressed in years).

Calculation of the sizing criteria:

We have chosen to evaluate three criteria that are the LCOE, the self-consumption rate and the LPSP. For the LCOE, the eq. 4.7 has been used. The capital cost for lead-acid batteries and SCs are 150 €/kWh

and 2000 €/kWh, respectively. For the CRF, an interest rate of 7.7% has been considered [148]. If the power balance is the only available variable (i.e. production and consumption cannot be obtained separately), the following formula can be used to evaluate the self-consumption rate (eq. 4.28) and the LPSP (eq.4. 29).

$$s_{cons}(t) = \frac{\sum_{P_{Balance}>0}^{t}(P_{ESS_A}(t) + P_{ESS_B}(t))}{\sum_{P_{Balance}>0}^{t} P_{Balance}(t)}$$ eq. 4.28

$$LPSP(t) = \frac{\sum_{P_{Balance}<0}^{t} P_{remain_B}(t)}{\sum_{P_{Balance}<0}^{t} P_{Balance}(t)}$$ eq. 4.29

4.3.2 - Optimal multi-objective sizing methodology

The complete methodology is illustrated in Fig. 4.7. In an iterative way, different configurations of hybrid ESSs will be evaluated (several nominal capacities will be tested and both ESSs will be tested as ESS$_A$ and ESS$_B$, i.e. priority to charge and discharge). The hybrid strategy refers to the algorithm presented in Fig. 4.5 and the ESS model corresponds to all equations that have been written for the evaluation of SOC, evaluation of voltage, power limitation, etc.
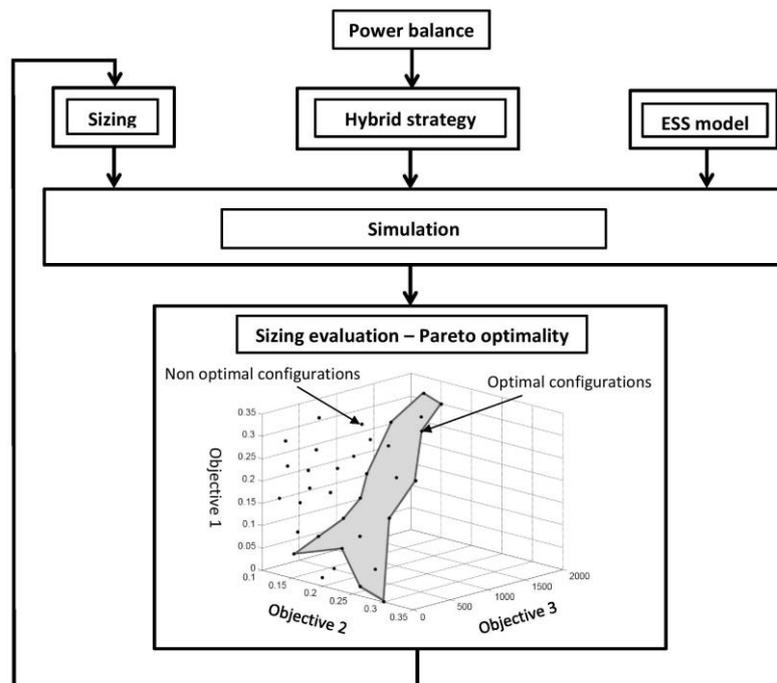
Figure 4.7 Multi-objective sizing methodology of a hybrid ESS

4.3.3 - Results

A three year operating profile (1-min resolution) has been used to optimally size the hybrid storage system. Fig. 4.8 illustrates one day of operation of the simulation (ESS$_A$ is a 10 Ah 36 V lead-acid battery pack, and ESS$_B$ is a 500 F 48 V SC module. In Fig. 4.8-A, the power limitation at the charge of the battery can be noticed (around 150W) with a remaining power supplied by the supercapacitor pack between 9.20 am and 10.30 am. At 10.30 and 11.30, the SCs and batteries are respectively full, no additional power can be absorbed until the discharge of ESSs, as illustrated with the SOC evolution in Fig. 4.8-B. At the end of the day, the batteries are discharging without power limitation (because higher power capability than at the charge, as described earlier) until their low SOC limitation (fixed at 0.3), then the SCs are totally discharged.
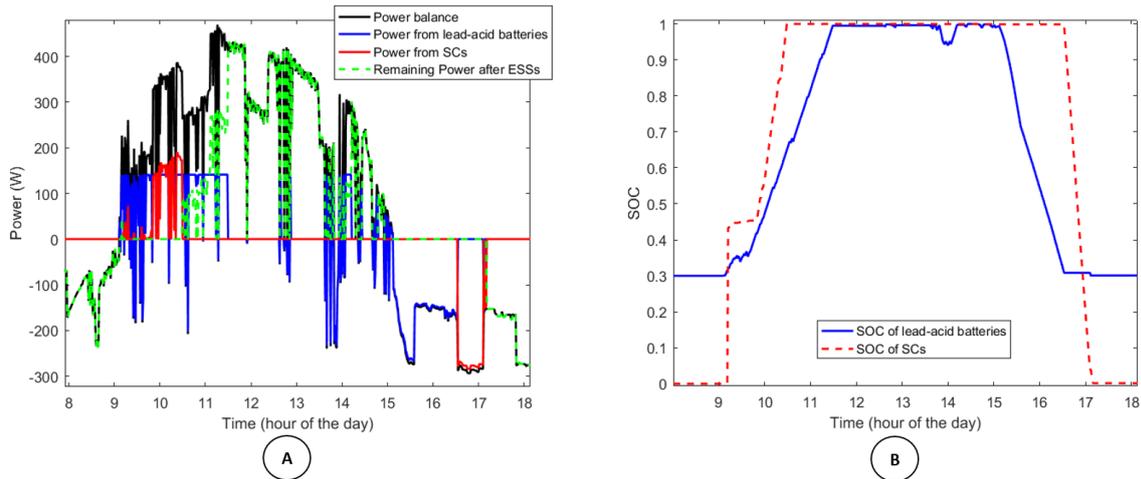
Figure 4. 8 One day of simulation – A) Power profiles, B) SOC profiles

Different configurations of ESSs have been assessed based on the 3 selected criteria, as illustrated in Fig. 4.9. Three different groups of sizing are to take into account: battery pack alone; SC pack alone; and finally, SCs as ESS_A and batteries as ESS_B.
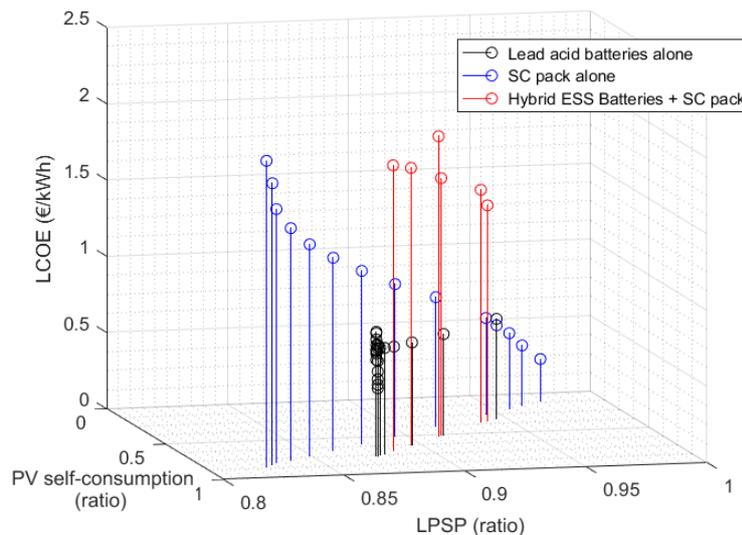
Figure 4. 9 Optimal hybrid ESS configurations

Concerning the sizing of only battery packs, we analysed capacities from 10 Ah to 300 Ah. It appears that 140 Ah is the optimal capacity because for higher capacities the LPSP and PV self-consumption are improved by only less than 1 % while the LCOE is dramatically increasing. For the sizing of only SC packs, capacities from 100 F to 5000 F have been tested. It can be noticed that the LCOE to achieve similar performances compared to batteries in terms of LPSP and PV self-consumption is prohibitive. Nevertheless, due to a higher cycle efficiency, the SCs are able to reach higher LPSP and PV self-consumption compared to batteries (i.e. if the cost does not matter, SCs are intrinsically better than batteries). Finally, in the case of hybridization, it appears that the configurations with low battery capacity (as a consequence strong power limitation) are the most favourable for hybridization. But the LCOE is very high due to the SCs. Finally it seems that this operating profile with such power limitation (1/3 at the charge, it is not very stringent in this application which highly requires energy), is not favourable to the hybridization of ESSs. In a future work, the analysis of the strategy of storage with the sizing should be addressed because it may enable to use more efficiently SCs. Moreover, a more precise

model of losses in power converters can be developed, as it has been previously done in our team for a 3 phases DC/DC boost converter [162]. Hence, another criteria based on power converters losses can be implemented. In the next section, a sizing methodology for a single ESS, lithium-ion batteries, has been proposed. This study adds some constraints on the storage strategy and propose a probabilistic analysis of the power balance in order to reduce computation time.

4.4 -   Optimal sizing of a single ESS

Main results of this optimal methodology were presented in [163]. Our goal is to find the optimal capacity and cycle depth of a lithium battery pack in order to minimize the annual cost of the ESS and improve the PV self-consumption by storing all the energy surplus. Indeed, this energy management is supposed to flatten the peak demand and decrease both transmission and distribution losses of the utility grid [164]. In order to estimate the annual cost of the system, a model of ESS has been developed to describe performances and lifetime subject to C-rate, cycle depth and SOC-level. Real energy and power requirements of the ADREAM PV building from the LAAS-CNRS have been used to determine the operating profile of the ESS. The topology of the MG is similar to the previous configuration depicted in Fig. 4. 4, excepted that only one ESS is considered in this study case.

4.4.1 - Operating profile and management of energy flows

The power balance analysis of the ADREAM building (previously presented in chapter 2) is depicted in Fig. 4.10. In Fig. 4.10-A, the maximum and minimum power balance over the three-year data set are represented in bold black line while some days (coloured lines) illustrate the very different possible daily production profiles in PV buildings. The power capability of the ESS must satisfy two constraints that are the maximum power at the charge (70.2 kW) and at the discharge (74.5 kW).

For the ESS, the maximum energy to store per day is obtained during a sunny day (worst case scenario). So, it has been decided that the ESS will perform only one cycle per day (the discharge during the day is not allowed and the discharge during the night will be only at low C-rate in order to maximize the lifetime). According to this, the lifetime of the ESS can be estimated based on the probability distribution of surplus energy per day, which is illustrated in Fig. 4.10-B (surplus energy per day of the ith bin, also called 'class interval', is noted E_{Charge_i}).
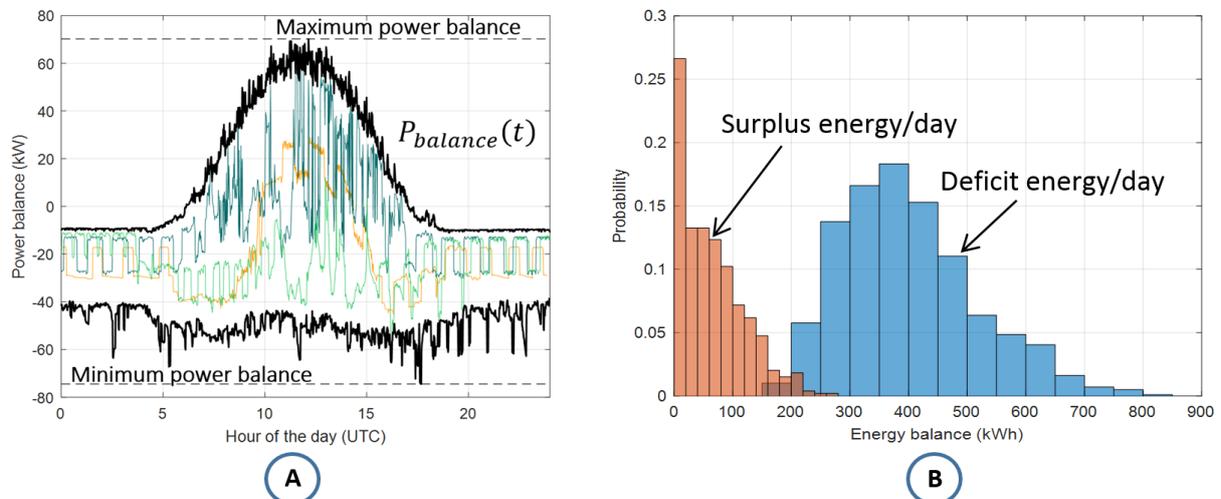
Figure 4.10 ADREAM PV building, A) Minimum and maximum power balance based on a 3-year data set, B) Probabilistic analysis of surplus and deficit energy per day

A complete representation of the ADREAM building power balance is depicted in Fig. 4.11. On this plot x-axis and y-axis represent the surplus energy per day (energy to store in the ESS) and the surplus power (enabling to evaluate the possible C-rates), respectively. Finally, the z-axis shows the number of occurrences in the 3-year data set of power surplus.
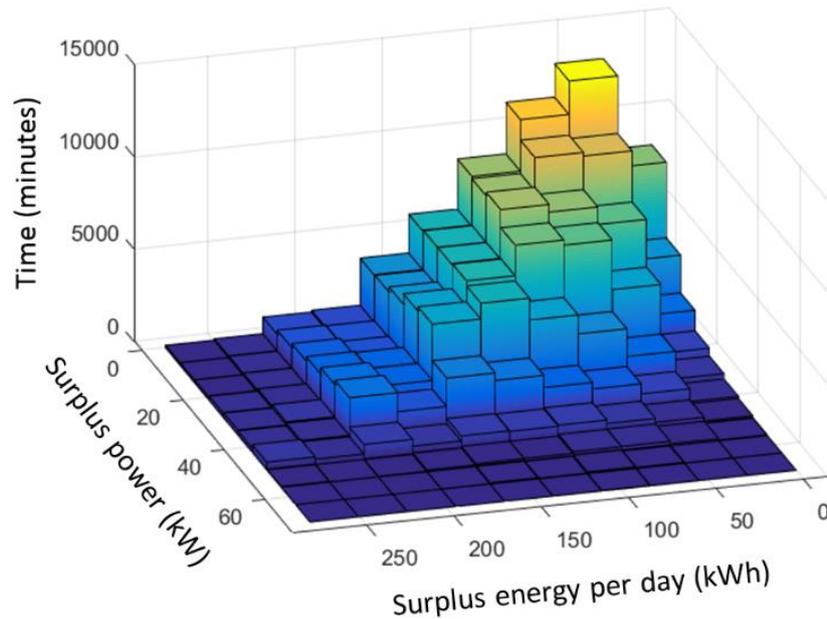
Figure 4.11 PV surplus power and energy per day of the ADREAM building over the 3 last years

It appears that the energy per day around 70 kWh is very probable and power balance is rarely higher than 50 kW.

4.4.2 - Model of the ESS

In order to minimize the annual cost of the battery energy storage system (BESS), a trade-off has to be made between a high nominal capacity (i.e. high capital cost) and a long lifetime (i.e. setting some limitations on the power capability and the available capacity). Indeed, as presented in Chapter 3, C-rate, cycle depth, SOC-level and temperature are the main stress factors acting on lithium batteries performances and lifetime [109], [112], [113], [117]. In this study, the following limitations have been set:

- Limiting the C-rate ensures a minimum available capacity (see Peukert's law in Chapter 3) and a minimum cycle-efficiency (ranged from 86% to 99% with a C-rate of 4 and 0.25, respectively [101]). Thus, at the charge and the discharge, the C-rate will be limited to 0.5 and 2, respectively.

- Limiting the cycle depth (ΔDOD) in order to improve the maximum number of cycles [112]. Different cycle depths will be tested in this study, in order to define the cycle depth that optimize the objective.

- The battery has to cycle in a medium SOC-level around 50% to ensure the highest cycling lifetime [112].

As explained in chapter 3, the major consequence of BESS ageing is the decrease of the nominal capacity, as depicted in Fig. 4.10. Obviously, this implies that the available capacity also decreases so the cycle depth tends to increase for the same operating profile.
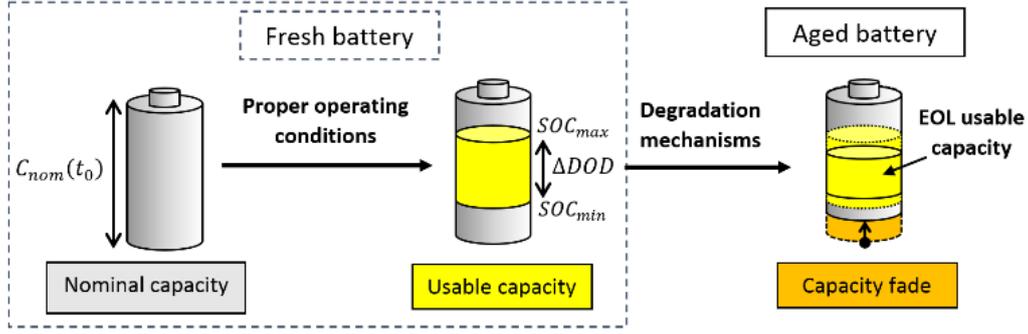
Figure 4.12 Capacity fading of a battery due to ageing

In an iterative way, we have evaluated the possible cycle depths, ΔDOD_i (comprised between 0 and 1), obtained for different nominal capacity of ESS (expressed in kWh) and based on the energy per day E_{Charge_i} described in Fig. 4.10-B.

$$\Delta DOD_i = min\left(\frac{E_{Charge_i}}{C_{nom}}, 1\right)$$ eq. 4.30

The cycling lifetime, which expresses the maximum equivalent number of full cycles for a given cycle depth (as described in [112] and illustrated in chapter 3 (Fig. 3. 19)), has been modelled by:

$$N_{cyc} = a\, exp^{(-b \times \Delta DOD)} + c$$ eq. 4.31

where the following parameters have been used to fit the 50% SOC-level curve described in Fig. 3. 19: a=1.057e4, b=0.05459, c=455 ($\Delta DOD \in [0,100]$ (expressed in %), R²=0.9729 and RMSE=689.1).

Considering both calendar (N_{cyc}) and cycling (N_{cal}) lifetimes, the number of days of operation is calculated as follows:

$$N_{cyc\_life} = \sum_{nbin=1}^{n}\left(p_{nbin} \times min\left(N_{cyc}, N_{cal}\right)\right)$$ eq. 4.32

where p_{nbin} is the probability of the ith bin of energy surplus per day (see Fig. 4. 10-B).

Assuming that the ESS will perform one cycle per day, the number of years of operation of the ESS is:

$$n = \frac{N_{cyc\_life}}{365.25}$$ eq. 4.33

The annual energy stored by the ESS, noted E_{Ch_year}, is calculated based on the probability distribution of surplus energy per day (Fig. 4. 10-B) and on the usable capacity of the ESS (which can limit the amount of energy stored when the battery is full):

$$E_{Ch\_year} = 365.25 \sum_{nbin=1}^{n}\left(p_{nbin} \times min\left(E_{nbin}, C_{nom\_BOL} \times \Delta DOD\right)\right)$$ eq. 4.34

Finally, the annual energy delivered by the ESS takes into account the cycle energy efficiency η_{BESS} (typically about 92% for a lithium battery).

$$E_{Disch\_year} = \eta_{BESS} \times E_{Ch\_year}$$ eq. 4.35

4.4.3 -Cost minimization

The first requirement of the minimization problem is to store all the PV surplus energy. Considering the capacity fade due to the ageing of the ESS, the nominal capacity must satisfy the following constraint:

$$C_{nom\_BOL} \times \Delta DOD \geq 1.25 \, E_{Charge_{max}}$$ eq. 4.36

where C_{nom_BOL} is the nominal capacity of the ESS (in kWh) at its beginning of life (BOL), and $E_{Charge_{max}}$ is the maximum energy to store per day (around 280 kWh in this study case). The coefficient 1.25 reflects that the BESS is considered at its end-of-life (EOL) for a capacity fade of 20% (usual criterion often considered).

Fig. 4.13 represents the evolution of the minimum value of the BOL nominal capacity that fulfil energy, power and lifetime requirements for every possible cycle depth. The energy and power constraints are based on the maximum PV surplus energy per day and power (280 kWh and 70.2kW have been considered, as presented in Fig. 4.10). The power capability fade due to ageing of batteries has been neglected, according to results found in [113]. In this application, the power constraint does not affect the minimum nominal capacity because the maximum C-rate (considered to be $C_{nom}/2$) is always higher than 70.2 kW (maximum surplus power delivered by the PV system described in Fig 4.10-A).
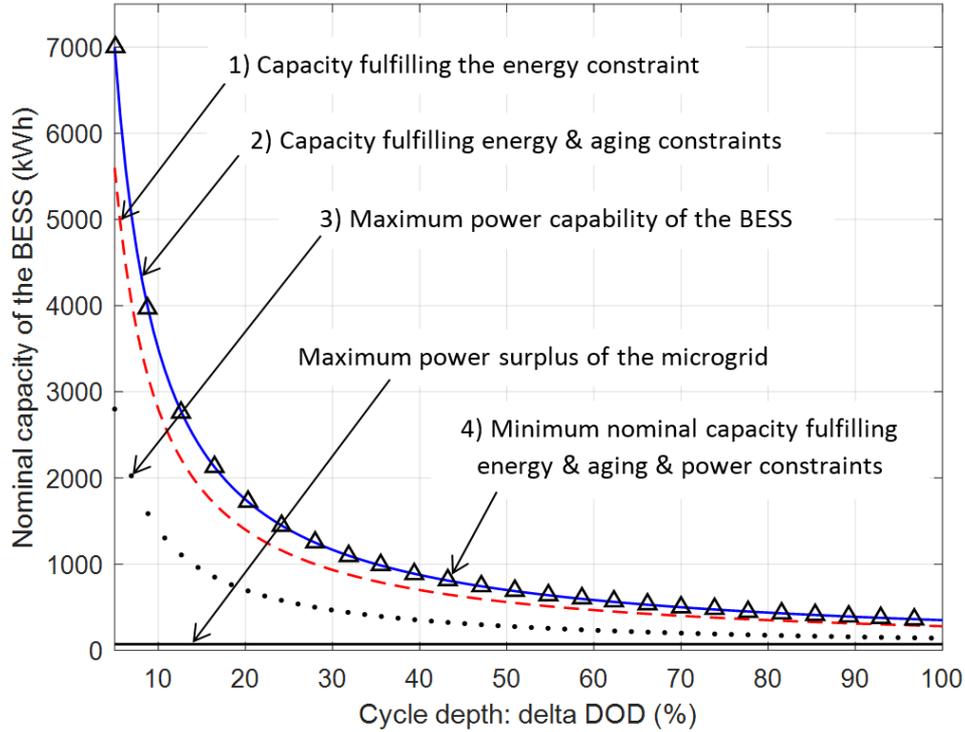
Figure 4.13 Minimum nominal capacity of the ESS satisfying power, energy and lifetime constraints

Given these constraints, the minimization of the cost of stored energy can be done by selecting the best combination of nominal capacity and cycle depth. The minimization of the cost of electricity delivered by the ESS (expressed in €/kWh) is:

$$Min \left\{ C_{StoredEnergy} = \frac{C_{1kWh} \times C_{nom\_BOL} \times CRF}{E_{Disch\_year}} \right\}$$ eq. 4.37

where C_{1kWh} is the cost of one kilowatt-hour (euro/kWh) of a lithium-ion battery (350€/kWh [11]), and E_{Disch_year} is the annual energy delivered by the BESS.

4.4.4 - Results and sensitivity analysis

Considering an energy to store per day of 280 kWh, the cost of electricity delivered by the ESS is presented in Fig. 4.14. It appears that this cost is minimized for a cycle depth about 30% (the solid line depicts the result obtained from the lithium-ion battery lifetime model [112]). In order to analyse the importance of the lifetime model, the lifetime model of lead acid batteries [109] has been computed (in this case, the minimum value is obtained for a cycle depth around 40%). Hence, the lifetime model has a strong influence on the life cycle cost of the ESS. Unfortunately, a precise lifetime model of a random battery is not available because information delivered by manufacturers is often poor (only 3 to 5 points indicating the number of cycles for a given SOC). Moreover, as explained earlier, the validity of this model is questionable because the C-rate in real applications is often varying which is not the case for batteries that are tested (for reproducibility reasons). In our case, we consider that the worst case scenario is obtained at high C-rate, so if the maximum C-rate of the battery is limited to the C-rate defined in the lifetime tests of datasheets then the lifetime model is the worst case scenario.
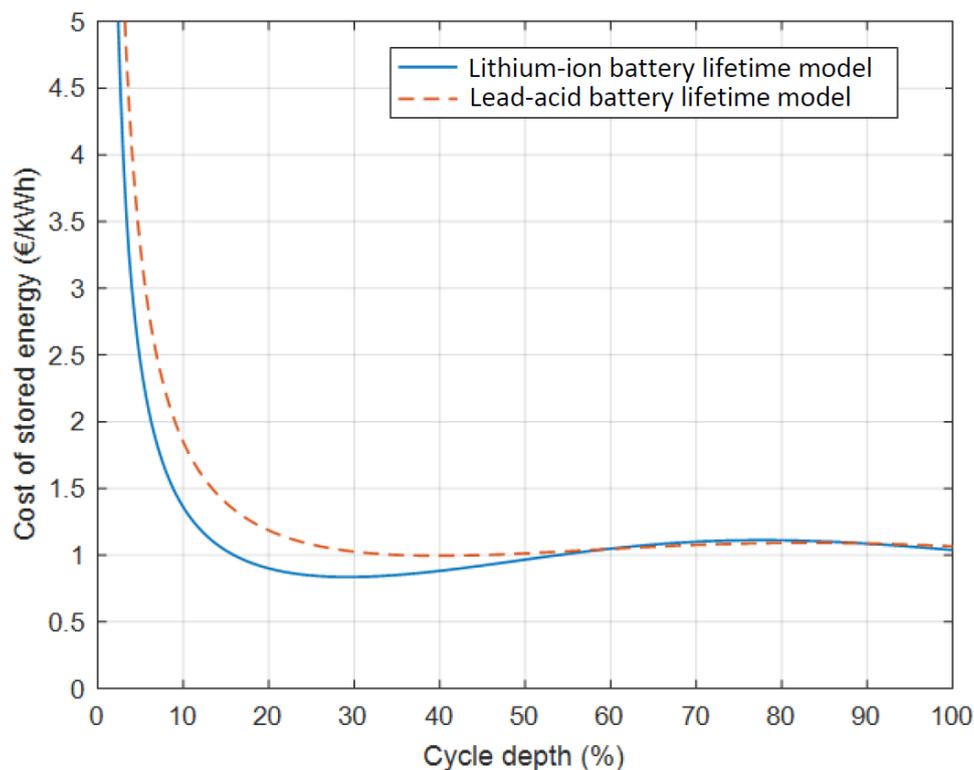
Figure 4.14 Cost of stored energy for different cycle depths and lifetime models

Now, if the constraint of storing all the PV surplus is relaxed, a lower energy per day to store can be considered. According to the probabilities depicted in Fig. 4. 10-B, if the limit of daily energy to store is set at 100 kWh, 140 kWh, 180 kWh, and 220 kWh, it accounts respectively for 75.7%, 89%, 95.9% and 99.2% of the cumulative distribution of surplus energy per day. After the rearrangement of the probability distribution (i.e. when the highest energy bin is removed, its probability is added to the immediate lower bin, so only 20 kWh (width of the bin) at the probability of the highest bin is lost). The cost of stored energy (€/kWh) for different energy per day is presented in Fig. 4.15. The best trade-off is to store a maximum energy per day of 180 kWh because the cost of stored energy is about 0,48 €/kWh for a BESS BOL nominal capacity of 225 kWh. In this case, less than 5% of the PV energy surplus is wasted and the cost of stored energy decreases for more than 26% (compared to solution leading to 100% energy surplus stored in the BESS).
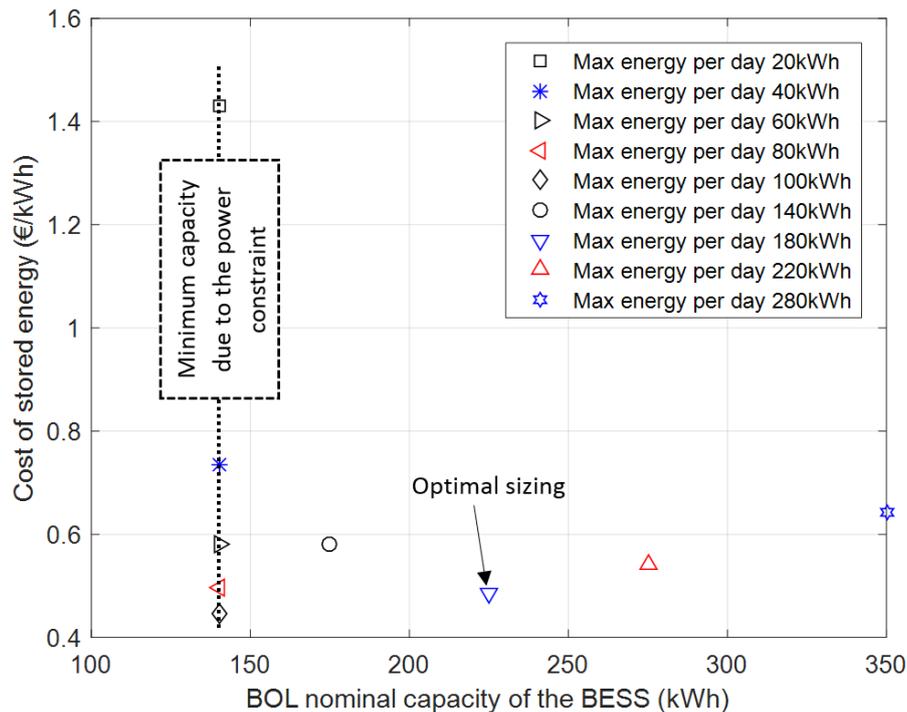
Figure 4.15 Cost of stored energy for different BESS nominal capacities

Low BESS capacities (that could be used to store less than 100 kWh per day) have also been analysed in Fig. 4.15 in order to show the effect of the constraint related to the C-rate. As the maximum surplus power is 70.2 kW and the maximum C-rate is 0.5, the minimum nominal capacity should be higher than 140.4 kWh (neglecting the effect power fade due to ageing). Similarly to the energy per day to store, a trade-off can be made again concerning the maximum surplus power to store. Indeed, according to Fig. 4.9, it appears that there is a low probability to have a surplus power higher than 55 kW (it implies a capacity reduction of about 20% in the case of low BESS capacities). Hence, an important work has to be done in the analysis of the operating profile in order to define the power and energy requirements that may be the most suitable in order to find the best compromise between the full utilization of renewable sources and the cost of ESS. In this study, we used three years of a 1-minute resolution dataset which gives a good overview of the system's behaviour and its boundaries. If less data are available, the generation of Monte-Carlo scenarios is a good technique to determine the worst case scenario or to simulate the behaviour of the system by taking into account future changes (increasing load demand profile, increasing efficiency of solar cells, warmer temperatures, etc.).

This method can be adapted to any type of ESS and can be used to study more complex cycling conditions (provided that the rainflow counting method is implemented). The next section is an example of adaptation of the multi-objective optimization based on Pareto optimality to a promising load device, the light emitting diode (LED).

4.5 -   Multi-objective optimization of LED lightings

The energy transition needs to go also through the improvement of energy efficiency from electrical load. As the multi-objective optimal methodology presented in the last section is generic, we wanted to apply it for another system of the microgrid. In our team, another PhD student already worked on the design of LED lightings [165], so we decided to adapt this methodology for LED lightings. A good example is the lighting sector and the development of light emitting diode (LED) solid-state lighting (SSL). Indeed, the average electricity to light conversion efficiency of an LED is around 35%, compared to 5% for incandescent light bulbs and 20% for fluorescent lamps [166]. According to the U.S.

Department of Energy (DOE), in 2013 lighting accounted for 18% of the total U.S. electricity use, and the potential energy savings can be very important: at the U.S. scale, a good penetration of LED lighting could represent 60 % of energy annual savings that are equivalent to the consumption of 36 million homes [167], [168]. In the same way, it seems that environmental impacts of LED lighting compared to other technologies is minimized [169], [170].

This is why, we have worked on such load, which will be integrated in our LVDC MG, [171], [172]. We have developed a Pareto multiobjective optimization to design a new 3600 lm LED luminaire (which corresponds to a standard lamp constituted by 3 fluorescent – 1200 lm tubes of 14 W), in order to find the best trade-off between ACS, annual energy consumption and environmental impacts.

The decision variables of the optimization problem are the level of forward current that supplies the LED device, the number of LEDs and the value of thermal dissipation of the heatsink associated to the luminaire. Indeed, a LED is supplied by a power converter named LED driver, which usually operates in continuous conduction mode (CCM) and regulates the current of the luminaire with a single current control loop [173], [174]. It is important to wisely choose the level of forward current because it affects the LED junction temperature, which defines the light output (spectral composition and luminous flux) and the ageing behaviours [175].

Three types of white LEDs with similar properties have been tested, their main characteristics have been gathered in Table 4-2.

	Cree XTEAWT GE5	**Lumileds** LUXEON Rebel plus LX18-P140-3	**OSRAM** OSLON square 5L7N-1
Viewing angle (°)	115	120	120
Luminous flux (lm) at 85°C junction temp.	130 @350mA	103 @350mA	194 @700mA
Forward voltage (V)	3.4	2.85	2.85
Max. junction temp. (°C)	150	150	150
Max. thermal resistance junction/solder point (°C/W)	5	9	3.9
Purchase price (€)	1.36	1.36	2.38

Table 4.2 Main performances of white LEDs (data from manufacturers)

4.5.1 - Optimization methodology

In this study, a luminaire is constituted of a series-parallel association of LEDs, which ensures a good reliability, luminous efficacy and uniformity [165]. In an iterative and incremental way, the effect of different forward currents (from 0.1 mA up to 700 mA per LED) on different luminaire configurations (number of LEDs and heatsink) will be simulated. Hence, as presented in Fig. 4.16, this optimal methodology enables to calculate the annual cost, annual consumption and environmental impact of each configuration. Finally, all configurations are compared based on Pareto optimality, as defined in the first section of this chapter.

In order to evaluate all luminaires on the same basis, we have arbitrary chosen a common operating profile that can be encountered in a shopping center (i.e. 12 hours a day, 6 days per week and 52 weeks per year). Hence, the luminaire will operate 3744 hours per year.
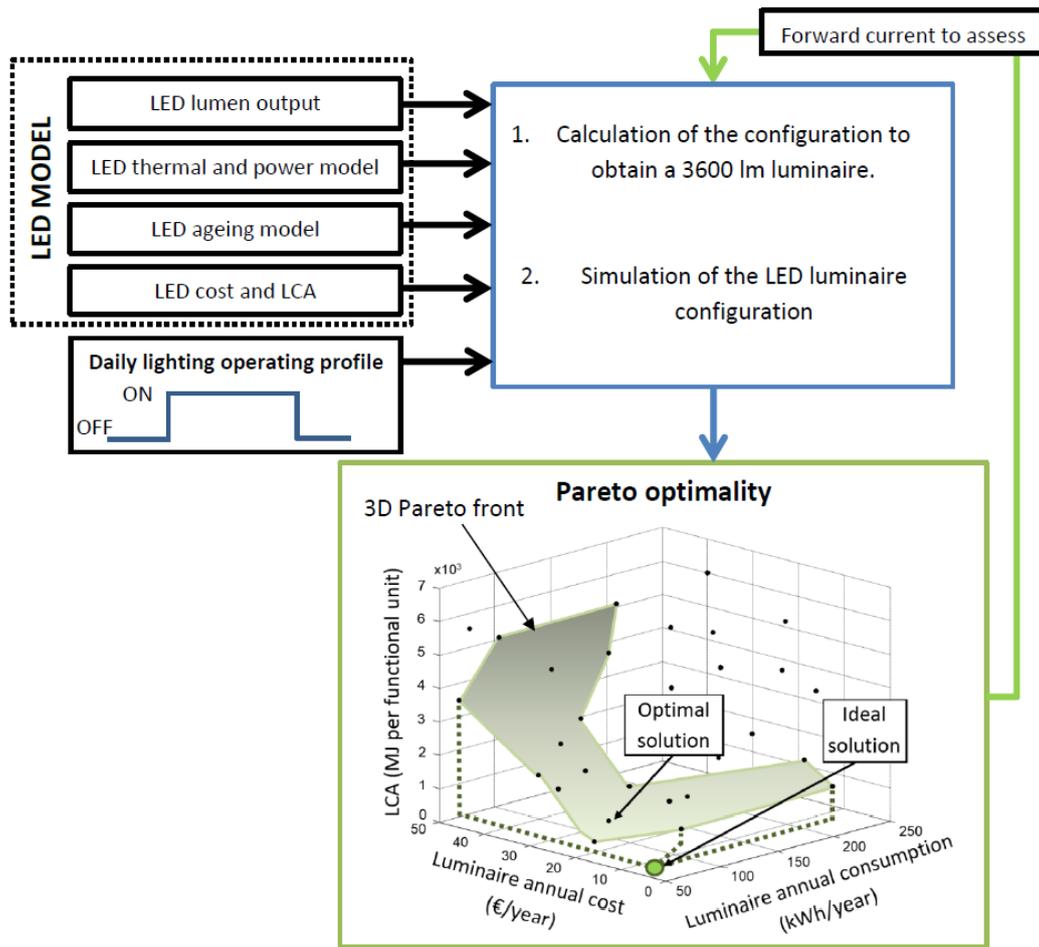
Figure 4.16 Multi-objective methodology developed for LED sizing

A complete LED model depending on the forward current and thermal dissipation is proposed in the next section in order to evaluate ageing, life cycle costs, etc. Three LEDs of each type have been associated in series and soldered on an insulated metal substrate printed circuit board (PCB) for the experimental tests.

4.5.2 - LED model

- **LED light output**

The luminous flux has been evaluated in a controlled temperature environment (22°C) with an integrating sphere, a spectrometer and a precise current source. The results for each type of LED is presented in Appendix 4.A. The number of LEDs, noted N_{LED}, required to achieve a 3600 lm luminous flux, can be calculated as follows:

$$N_{LED} = \frac{F_d}{F_{LED}} = \frac{F_d}{\varepsilon_{LED}(P_{LED}) \times P_{LED}}$$

eq. 4.38

where F_d and F_{LED} are respectively the desired luminous flux of the luminaire and the luminous flux of a LED, $\varepsilon_{LED}(P_{LED})$ is the luminous efficacy of an LED for a given electrical power noted P_{LED}.

The different configurations of LED luminaires (number of LEDs and power consumption) are presented in Fig 4.17 (forward current of 0.1 mA per LED is not presented because hundreds of thousands of LEDs are necessary to obtain the desired luminous flux). It can be seen that some

configurations (i.e. low forward current per LED below 10 mA for Cree, 20 mA for Lumileds, and 30 mA for Osram) are not optimal because they lead to both higher number of LEDs and higher power consumption. Moreover, it can be considered that a high number of LEDs is not suitable. In this case, if we consider a limit of 250 LEDs, a forward current per LED lower than 50 mA should be withdrawn.
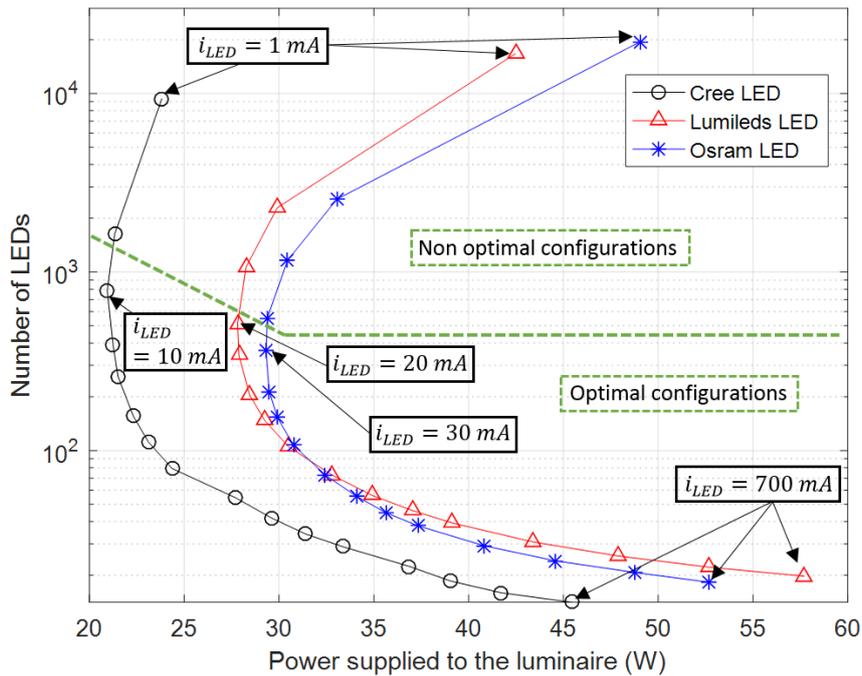
Figure 4.17 Number of LEDs vs. power supplied to the luminaire

- **Thermal modelling**

In this study, a steady state thermal model has been developed, derived from [175] (See appendix 4-B for the modelling). The LED junction temperature has been estimated by a thermocouple soldered as close as possible to the LED (this measurement is called "solder point temperature").

If the junction temperature remains below 80°C, the luminous flux of the different tested LEDs will drop from less than 10%. This drop can be neglected because it is not visible for the common human eye [176].

- **LED ageing model**

The study of LED aging, also called lumen maintenance, is determined by the lumen depreciation. The lifetime of an LED is defined by the number of operating hours before the luminous flux decreases below 70% of its initial value. This lifetime is often noted L70. According to the Illuminating Engineering Society of North America (IESNA), the standard TM 21 provides a method to assess the lumen maintenance of LEDs. The LED lifetime model is based on [176] (see Appendix 4-C).

- **Annual cost of the LED luminaire**

As this method compares different LED luminaire configurations which roughly need the same supplied power, the cost of LED drivers is assumed to be identical, and consequently will not be considered in this analysis. No cost of maintenance is needed, the LED luminaire will be replaced according to the L70 lifetime. The annual cost (€/year) of the luminaire can be defined as:

$$C_{year\_lighting} = C_{purchase} \times CRF$$

<div align="right">eq. 4.39</div>

where CRF is defined in section 4.2 (5% have been considered in this study), and $C_{purchase}$ (€) is the initial capital cost (purchase price) of the luminaire corresponding to the cost of LEDs and heatsink:

$$C_{purchase} = \mathrm{N}_{LED} \times (C_{LED} + C_{Heatsink}) \qquad \text{eq. 4.40}$$

where C_{LED} is the price (€) of a single LED (cf. table 4-2) and $C_{Heatsink}$ is the additional cost per LED of 0.6 €, 0.35 € and 0.2 € respectively corresponding to 0.4 K/W, 1.2 K/W and 2 K/W heatsinks.

Obviously, the annual energy consumption of the lamp is:

$$E_{year\_lighting} = T_{op\_year} \, \mathrm{P}_{Lum} \qquad \text{eq. 4.41}$$

As illustrated in Fig. 4. 18, one Pareto front per type of LED is obtained (solid line). For Cree and Osram components, each heatsink leads to an optimal configuration for a given range of power. When the power supplied to the luminaire increases, more expensive and high dissipative heatsinks are optimal. For Lumileds LEDs, the lowest dissipative heatsink does not lead to an optimal configuration because of its high junction to solder point thermal resistance. All the configurations leading to a junction temperature higher than 80°C have been removed from the Fig. 4.18.
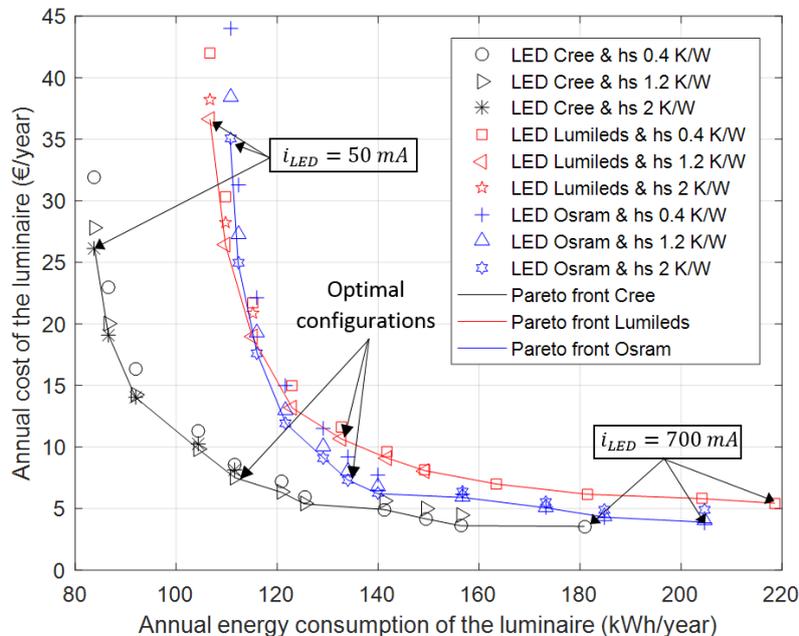
Figure 4.18 Annual cost vs. energy consumption of the LED luminaire

The optimal configurations (i.e. solution that minimizes its distance to the ideal point, as explained in the first section) are 42 Cree LEDs at 200 mA, 57 Lumileds at 200 mA, and 45 Osram LEDs at 250 mA. A 2K/W heatsink is sufficient for Osram devices whereas a 1.2 K/W is needed for Cree and Lumileds.

- **LCA of the LED luminaire**

Life cycle assessment (LCA), which enables to quantify the environmental impact of industrial devices, is the last objective of this study. A functional unit based on the quantity of luminous flux for a given time, expressed in Mlm.hrs [169], [170], [177], has been chosen in order to fairly compare lighting devices. The considered functional unit is defined as the annual lighting service of a 3600 lm luminaire that is assumed to operate 3744 hours per year (so the functional unit is close to 13.5 Mlm.hrs). The results of the LCA will be given in terms of primary energy consumption and expressed in MJ per functional unit.

Four main life stages are studied to calculate the energy consumed over the entire life of the product, see Appendix 4. D.

The results of the LCA are presented in Fig. 4.19 (similar to the predictions presented in [170] about LED technology from 2015). The minimum primary energy consumption is obtained for a current per LED around 200 mA. By taking into account the manufacturing stage, the energy consumption of the configurations that need a large number of LEDs increases significantly. It is to notice that LCA for LED devices is quite difficult to manage because of the fast development of this technology in comparison with conventional lamps.
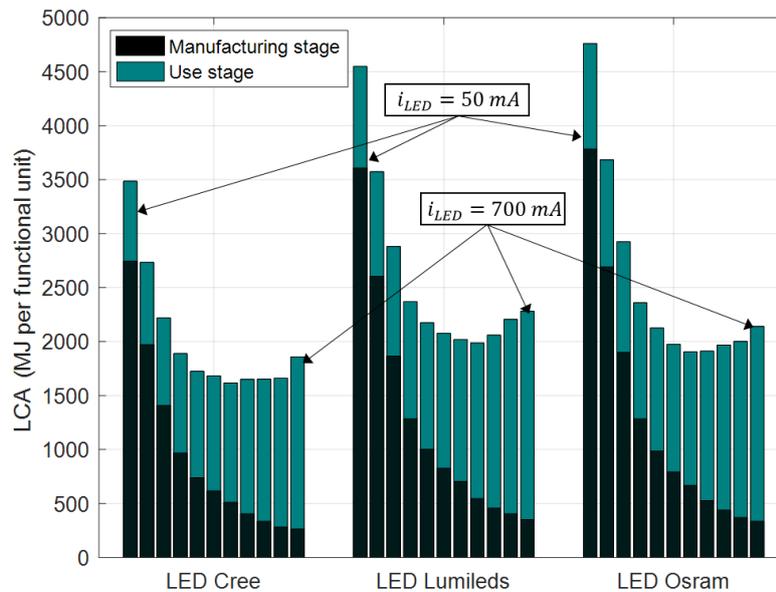
Figure 4.19 Manufacturing and use stages LCA for different LED configurations

4.5.1 - Results and comparison with conventional lamp technologies

In Fig. 4.20, the Pareto fronts for the different LEDs have been represented, which are the optimal configurations subject to the annual cost, annual energy consumption, and LCA. The heatsink does not influence neither the energy consumption of the luminaire (assuming that the power does not change when the junction temperature increases until 80°C) nor the LCA (it has been assumed that the LCA is the same for the three heatsinks). In this case, for each LED, the Pareto front is not a surface but a line. Thus, the non-dominated solutions are the one previously described in Fig. 4.18. When LCA is taken into account (especially the manufacturing stage), the configurations involving a high number of LEDs and a low annual energy consumption are very far from the ideal point.

According to Fig. 4.20, the optimal configurations for Cree and Osram LEDs are those presented in Fig. 4.17. But for Lumileds LEDs, the LCA shifts the optimal configuration to a higher forward current (250 mA instead of 200 mA) and a lower number of LEDs (47 instead of 57).

A comparative study with conventional lighting devices (halogen lamp, incandescent lamp and compact fluorescent lamp) has been done based on data presented in Table 4-3 (from a report of the U.S. DOE [168] corresponding to A19 light bulbs of conventional lighting).
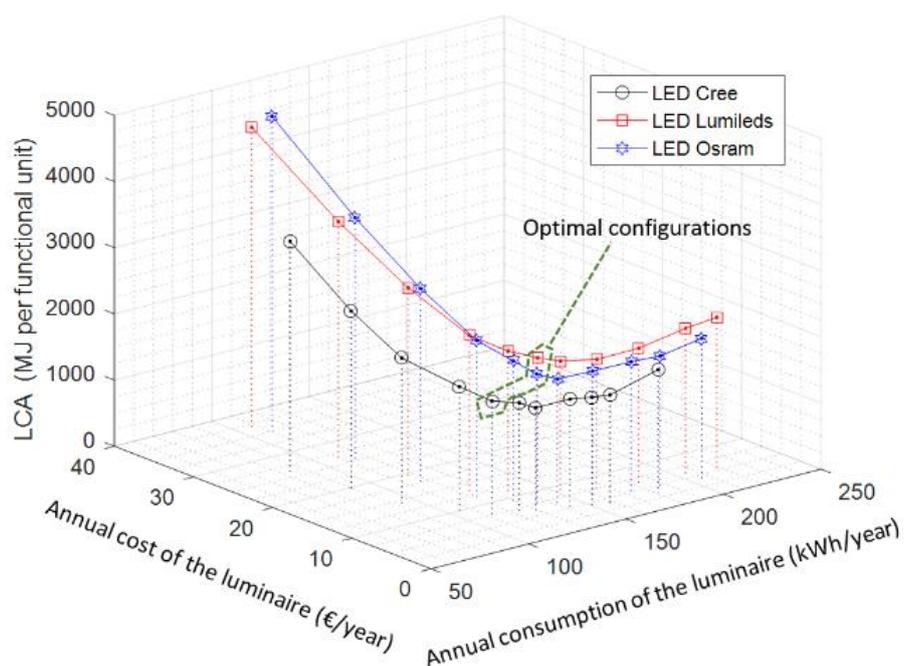
Figure 4.20 Optimization of three objectives

As in the previous section, no ballast cost will be considered, assuming that the different ballasts and LED drivers have the same price. In Fig. 4.21, the optimal configurations obtained in the previous section are compared to the commercialized lamps described in table 4.3. It is to remind that the results are given for a luminaire operating 3744 hours per year (12 hours a day, 312 days per year).

	Halogen	Incandescent	CFL
Luminous efficacy (lm/W)	20	15	70
Operational lifetime (h)	8400	1000	12000
Price (€/klm)	2.33*	0.59*	1.86*

Table 4.3 Main characteristics of different commercialized lamps

* Conversion EURO/Dollar: 1$=0.93€

Due to a high luminous efficacy, LED lamps and CFL have both a low annual energy consumption and low energy needs on their entire life (LCA). CFL is today the cheapest device but if we consider a cost of 0.1 € per kWh, the energy consumption gap between LED and CFL is sufficient to make LED lamps the cheapest lighting technology (considering both purchase and energy consumption costs). The same remark can be done on halogen lamps which are nearly three times less expensive than LED lamps but consume more than three times more. Incandescent lamps are by far less effective than any other lighting technology.

As for batteries, the lifetime modelling of LEDs is assessed in standardized conditions that are not always illustrative of real-life conditions.
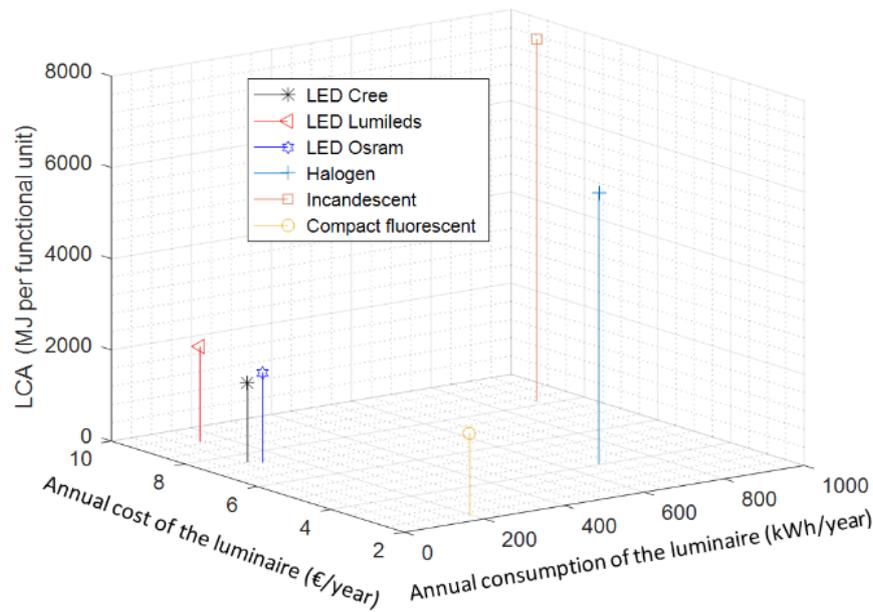
Figure 4.21 Comparison all lighting technologies

Finally, it appears that the optimal current is between 200 mA and 250 mA per LED. The use of LCA enables to point out the significant energy consumption related to the manufacturing stage. A comparison with other lighting technologies shows that LED lightings have better performances than CFL, halogen and incandescent lamps in terms of energy consumption and LCA. The overall cost based on purchase price and cost of annual energy consumption is also optimal for LED devices.

4.6 - Summary

The main mono and multi-objective methods of optimization have been presented. In our case, the multi-objective approach based on Pareto optimality has been chosen in order to fairly optimize different criteria that can be conflicting (e.g. life cycle costs and environmental impact).

Hence, several criteria have been presented to evaluate the ESS sizing (and also the MG scheduling, which will be presented in the next chapter).

Finally, a multi-objective methodology has been developed and applied on different study cases. First, a generic sizing method has been proposed for the hybridization of two ESSs. Beyond the results of the sizing that have been found, which depend on the chosen technologies, models, and strategy of storage, the conduct of the method is the most important. Then, another method has been employed to find the optimal capacity and cycle depth that optimize the annual cost of a battery pack in a MG. Historical data have been studied with a probabilistic approach in order to reduce the computation time. Finally, the multi-objective optimization that was used for the sizing of hybrid ESSs, has been employed for the sizing of LED lightings.

Chapter 5.   Optimal control of microgrids

"An experiment is a question which science poses to Nature,
and a measurement is the recording of Nature's answer."

Max Planck (23 April 1858 – 4 October 1947) German scientist who brought many contributions
to theoretical physics (Nobel Prize in Physics in 1918).

This chapter presents the work done on the control of a microgrid (MG) that is constituted by at least one renewable energy source and energy storage systems (ESSs). Before presenting our method, a review is performed on the control techniques that are employed to ensure a reliable energy management of MGs, especially those related to the DC distribution, case study of this thesis. According to the literature, it appears that the hierarchical control is a widespread control technique enabling to optimize some criteria such as the cost for large and medium timescales, and ensures the stability of the MG for short timescales. As the number of feeders and controllable loads connected to the MG can be large, the use of a centralized control with a supervisor should be avoided. Numerous ways are available to design a decentralized control, which prevents some faults that can be due to a loss of communication in the MG and avoid the use of a central controller that needs large computation resources. In this sense, a method based on 'DC bus signaling' will be presented.

This chapter is organized as follows:

First, different control techniques are presented with a particular focus on the definition of hierarchical control that is used in AC and DC MGs. Then, a scheduling study has been performed based on power grid data from Denmark. Finally, the DC bus signaling is explained and validated on an experimental platform, small-scale MG that has been built in the LAAS-CNRS.

Table of contents of chapter 5

5.1 Hierarchical control of a microgrid

The control of large AC power systems has already been widely studied and experimented by different laboratories and companies from all over the world. In Europe, guidelines and recommendations have been done by the UCTE (Union for the Coordination of Transmission of Electricity) during the last 50 years [178].

Hence, according to [42], the good operation of a MG involves a multi-scale control that coordinates all the subsystems connected to the MG through power converters such as distributed energy resources (DERs), loads (controllable or not), and ESSs. Several objectives can be achieved by the optimization of this control (i.e. cost reduction, enhancement of renewable source self-consumption, increased reliability, etc.). As defined in [179]–[181], a control architecture named hierarchical control is well adapted to microgrid operation. This latter is divided into the following three levels:

- **Primary control** (local controllers, short timescales from microseconds to milliseconds): ensures the stability and the connection of several sources and loads (e.g. droop control can be used to make an efficient current sharing between different sources and loads by controlling each system with a virtual impedance, which decreases the initial voltage reference). The inner control loops such as cascade regulation, which directly acts on power converters, can also be considered in this level. The operation of the MG is either grid following (for connected MGs, the main grid establishes the voltage and frequency) or grid forming (for islanded MGs, the voltage and frequency have to be established by a distributed energy resource or an ESS).

- **Secondary control** (energy management on medium timescales from second to minutes): ensures the stability of the entire MG. Some exchanges with the main grid can be done in order to regulate the voltage in case of DC MG, and frequency and/or reactive power in case of AC MG. In [178], a cascade control (voltage, reactive power) of power converters in MGs connected to the AC grid is presented with some strategies for harmonic compensation and operation with grid faults. Hence, it appears that some troubles are related to the process of connection/disconnection with the main grid (this point is out of the scope of our study). In this control level, several droop methods have also been proposed with some adaptive behaviour in order to be more flexible (i.e. more than one droop curve can be used for an element, depending on the state of the system). [182]–[184]

- **Tertiary control** (energy management on long timescales from hours to days): import/export of energy with the main grid in order to optimize operation costs of the MG, power quality, etc. According to [184], similar optimization techniques to the one presented for the sizing are applied to MG planning problems.

An illustrative scheme of the MG hierarchical control has been proposed in [179], as shown in Fig. 5.1. The decentralized control that can be obtained with for example droop control and DC bus signaling [185]. It enables to be more reliable (because independent from communication faults) and facilitates the integration of new sources and/or loads (i.e. 'plug and play' architecture) [186].
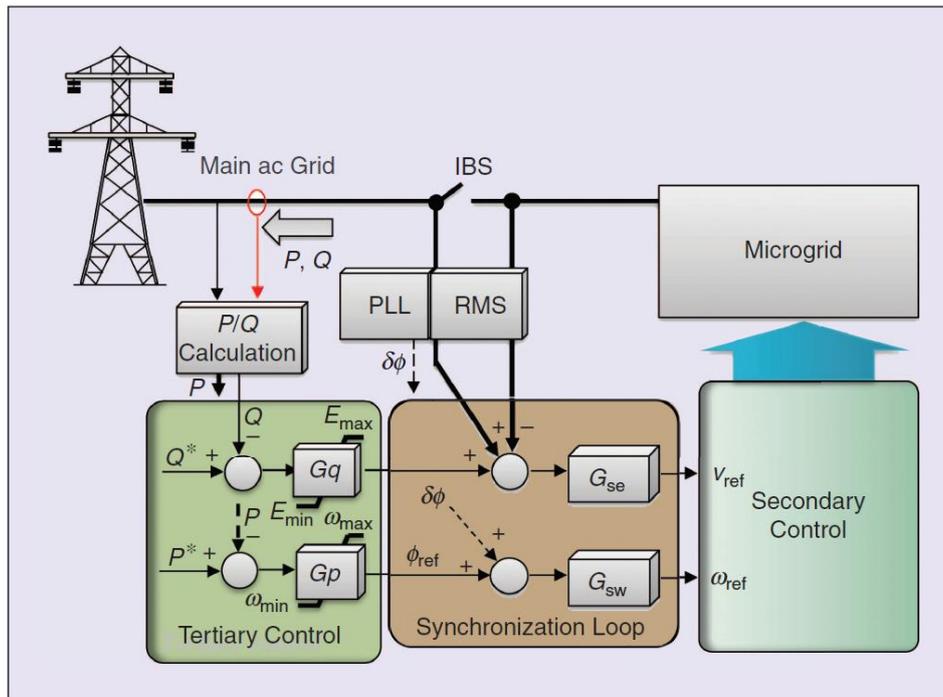
Figure 5.1 Three-level hierarchical control with synchronization control loop [179]

As explained in chapter 4 (section 4.3), an experimental platform, called 'Open Platform for the ADREAM building' (OPA), has been developed inside the ADREAM building. In this context, we developed a hierarchical control based on DC bus signaling as secondary control, followed by classical inner cascade regulation loops. As described in Fig. 5.2, a tertiary control can be performed by a scheduling method, which will send the optimal power output reference to the secondary control. A scheduling method, applied to another MG, will be presented in the next section.
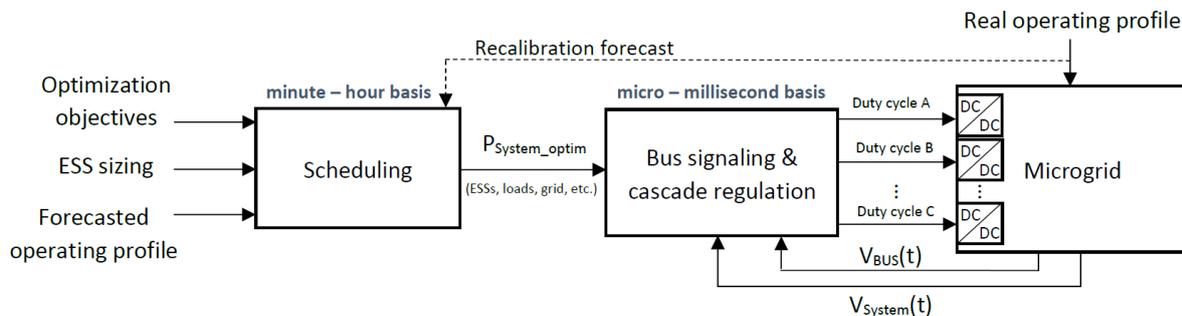
Figure 5.2 Hierarchical control of a MG based on scheduling and DC bus signaling.

5.2 Optimal scheduling of a microgrid

During the third year of my doctoral thesis, thanks to an ATUPS scholarship from the University of Toulouse III, I had the opportunity to work during 4 months in Aalborg University in the microgrid team supervised by Prof. Josep M. Guerrero. Hence, I have developed an optimal scheduling method for a connected MG with a lithium-ion battery pack, based on the data from the Danish grid.

In scheduling optimization, several goals can be achieved such as reliability improvement, cost of operation reduction, etc. [188]. In our study that has been published in [189], the main objective is to provide a scheduling approach that is generic in order to be implemented as a tertiary control in the MG hierarchical strategy. This scheduling method aims at providing the optimal power output of a battery

pack of lithium-ion batteries in order to minimize the cost of electricity and the cost of the ESS (both have been evaluated annually).

The architecture of the MG with the main variables involved in the scheduling problem are presented in Fig. 5.3.
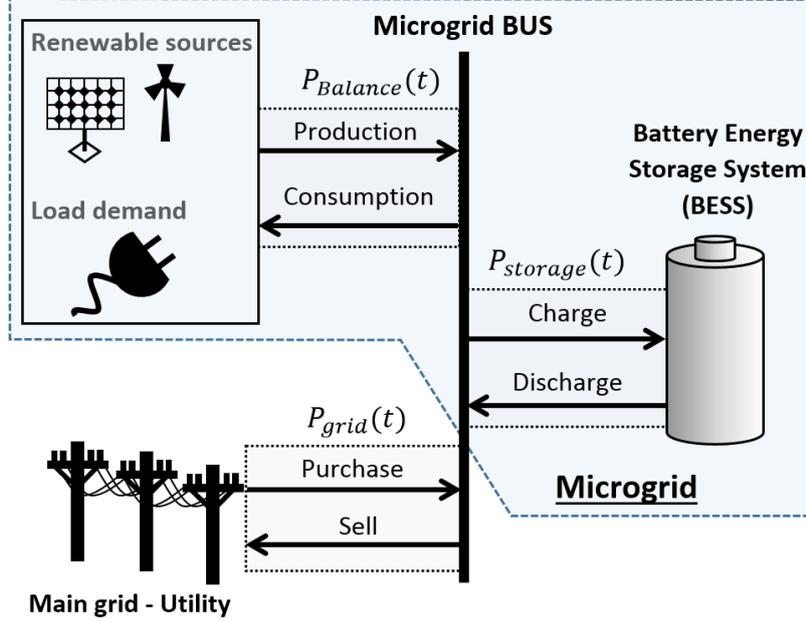
Figure 5.3 Microgrid architecture with the main variables

The variables defining the power exchanges within the MG are:
- $P_{Balance}(t)$, which is defined as the difference between the production from renewable sources and the consumption of the MG (eq. 5.1),
- $P_{storage}(t)$, which is defined as the difference between the power delivered and the power absorbed by the BESS (eq. 5.2),
- $P_{grid}(t)$, which is defined as the difference between the power that is purchased and sold from the main utility grid (eq. 5.4).

Hence, power that is injected into the MG has a positive value whereas the power taken out of the MG has a negative value.

$$P_{Balance}(t) = P_{Production}(t) - P_{Consumption}(t) \qquad \text{eq. 5.1}$$

$$P_{storage}(t) = P_{Discharge}(t) - P_{Charge}(t) \qquad \text{eq. 5.2}$$

$$P_{grid}(t) = P_{purchase}(t) - P_{sell}(t) \qquad \text{eq. 5.3}$$

Concerning the definition of power balance, we have used the three last years of hourly renewable generation and load demand profiles of the West Denmark electric market grid [190]. Two operating profiles have been defined by taking into account all the production of wind turbines and PV systems and half of the energy gross consumption of West Denmark, as depicted in Fig. 5.4. These two operating profiles (average and median) have been chosen in order to present a profile that produce more energy than consumed over a day (mean profile), and conversely (median profile).
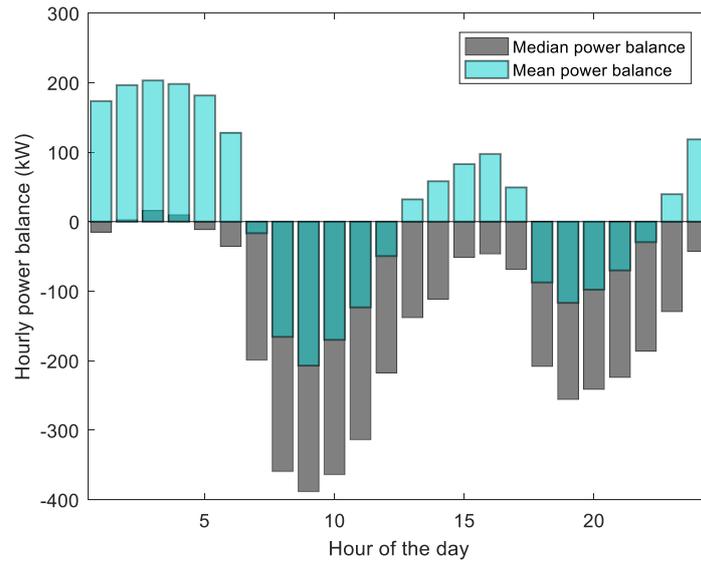
Figure 5.4 Examples of Danish operating profiles

The same analysis has been done with the cost of electricity, $C_{grid}(t)$, from the Nord Pool Elbas intraday market [190], as presented in Fig. 5.5. In this study, the hourly average value over the three last years (circle markers) is considered as the hourly price of electricity from the main grid.
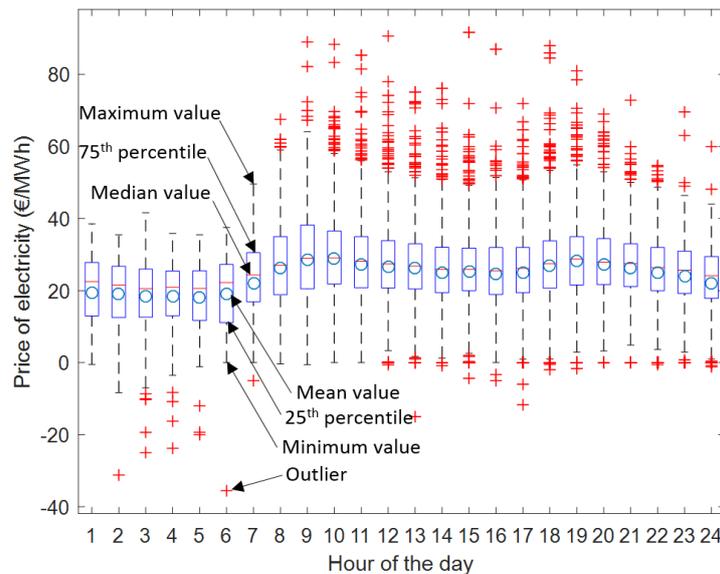
Figure 5.5 Cost of electricity during the last 3 years in West Denmark intraday market

Several constraints have to be respected in order to have a reliable operation of the MG. Firstly, the power exchanges within the MG must satisfy eq. 5.4 in order to ensure the stability of the MG. The SOC of the BESS has to be limited, as shown in eq. 5.5. Indeed, it has been shown in chapter 4 that a low cycle depth and a mid-range SOC level enhance the lifetime of lithium-ion batteries. So, the following values have been fixed: $SOC_{ini} = 50\%$, $SOC_{min} = 35\%$, and $SOC_{max} = 65\%$. The power capability of the BESS is limited at charge and discharge, as defined in eq. 5.7 and eq. 5.8 (i.e. as advised by manufacturers, for lifetime and energy efficiency reasons). By operating in such SOC range, the BESS will not operate under constant voltage (CV) charge, so no further constraint on the power limitation has to be considered. A power limitation on the exchanges with the main grid has also been considered in eq. 5.9.

$$P_{Balance}(t) + P_{storage}(t) + P_{grid}(t) = 0 \qquad \text{eq. 5.4}$$

$$SOC_{min} \leq SOC(t) \leq SOC_{max} \qquad \text{eq. 5.5}$$

$$SOC_{ini} = SOC_{end} \qquad \text{eq. 5.6}$$

$$0 \leq P_{dis}(t) \leq C_{rateDis}\, Cap_{nom} \qquad \text{eq. 5.7}$$

$$0 \leq P_{ch}(t) \leq C_{rateCh}\, Cap_{nom} \qquad \text{eq. 5.8}$$

$$P_{gridMin} \leq P_{grid}(t) \leq P_{gridMax} \qquad \text{eq. 5.9}$$

The SOC definition of the BESS is similar to the one presented in chapter 3, but in this case Cap_{nom} is expressed in kWh, considering that the voltage of the lithium battery is constant on the selected SOC range.

$$SOC(t) = SOC(t-1) + \eta_{Ch} \frac{P_{Ch}(t) \cdot \Delta t}{Cap_{nom}} - \frac{P_{Dis}(t) \cdot \Delta t}{\eta_{Dis} \cdot Cap_{nom}} \qquad \text{eq. 5.10}$$

A cycle efficiency of 92% has been considered for lithium batteries ($\eta_{Ch} = 0.92$ and $\eta_{Dis} = 1$).

In this study, the cycle depth, ΔDOD, has been fixed to 30%, which is the optimal value that has been determined in chapter 4 (section 4.4) for the lithium-ion battery presented in [112]. In order to calculate the maximum energy that the BESS is able to exchange during its lifetime, $E_{ExchMax}$, two relationships that have been described in chapter 3 are needed. Thus, eq. 3.21 is used to obtain the maximum number of cycles based on the cycle depth, and eq. 3.22 calculates the maximum energy that can be exchanged during the battery lifetime, based on Watt-hour throughput method. Finally, $E_{ExchMax}$ is given by:

$$E_{max} = 2\,(a \exp^{(-b\Delta DOD)} + c) \times \Delta DOD \times Cap_{nom} \qquad \text{eq. 5.11}$$

where the fitting coefficients that have been calculated in chapter 3 are $a = 1.057e4$, $b = 0.05459$, and $c = 455$ for the curve related to the SOC-level of 50% in [112] (with $\Delta DOD \in [0,100]$, R²=0.9729, and RMSE=689.1).

The exchanged energy per day by the ESS is calculated as follows:

$$E_{ExchDay} = \sum_t \left(P_{Dis}(t) + P_{Ch}(t) \right) \times \Delta t \qquad \text{eq. 5.12}$$

Finally, BESS lifetime (in years) is given by:

$$n = \frac{E_{ExchMax}}{365.25\, E_{ExchDay}} \qquad \text{eq. 5.13}$$

In this study, the objective function described by eq. 5.14 is a trade-off between the need to use intensively the BESS to decrease the annual cost of the electricity (eq. 5.15) and the need to improve the BESS lifetime (i.e. to reduce its annual cost) (eq. 5.16).

$$\text{Min}\,\{C_{Total} = C_{Elec} + C_{BESS}\} \qquad \text{eq. 5.14}$$

$$C_{Elec} = 365.25 \sum C_{grid}(t) \times P_{purchase}(t) \times \Delta t \qquad \text{eq. 5.15}$$

$$C_{BESS} = C_{1kWh} \times Cap_{nom} \times \text{CRF} \qquad \text{eq. 5.16}$$

A cost of 350€/kWh has been considered for C_{1kWh} of lithium-ion batteries [76]. For the CRF, an interest rate of 7.7% has been considered [148].

The proposed non-linear optimization problem has been solved with the General Algebraic Modeling System (GAMS) software. For this simulation, a 1.5 MWh BESS has been used and the maximum power that can be exchanged with the utility grid (eq. 5.9) has been arbitrary fixed to 200 kW in order to show the effect of limitations.

The results of the scheduling method are presented in Fig. 5.6. Due to the power exchanges limitations with the main grid that have been set, the BESS enables to reduce peak demand from 8:00 to 12:00 and from 19:00 to 22:00 for the median profile (Fig. 5.6-A). It can be also noticed that due to the price of electricity, the BESS is charging most of all when the tariffs are relatively low. As expected, the BESS satisfies the constraints of SOC, cycle depth and C-rate. Regarding the profile described in Fig. 5.6-B, the minimization of the BESS annual cost implies to minimize the energy exchanges between the MG and the BESS.
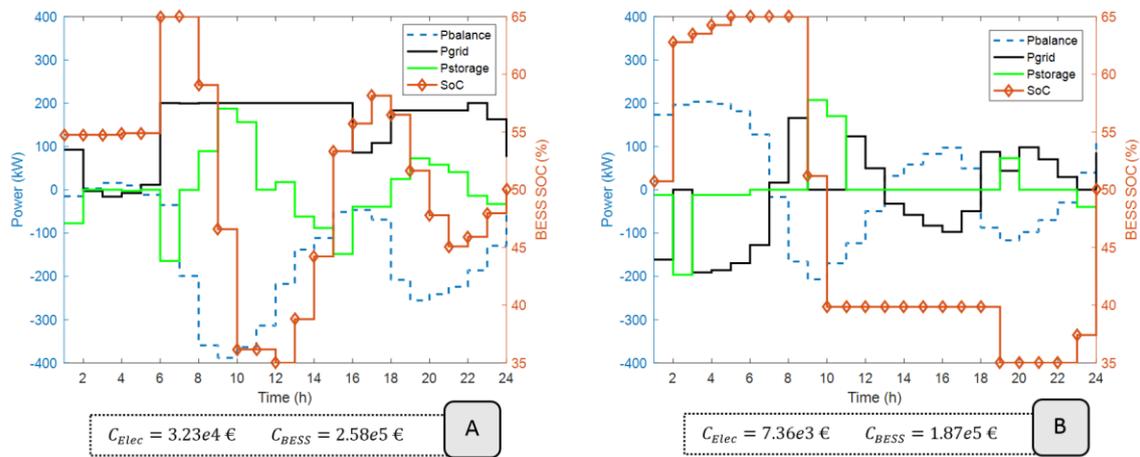
Figure 5.6 MG scheduling for a 1.5 MWh BESS A) Median profile, B) Mean profile

For both profiles, the annual cost of electricity is by far lower than the annual cost of the BESS. This is mainly due to the capacity and the cycle depth chosen in this example, based on a previous work on optimal sizing of a lithium battery pack, presented in chapter 4. Obviously, when the capacity of the BESS and the maximum daily cycle depth are changing, the optimal charge/discharge profile will be modified. This highlights the necessity to analyse together the sizing and scheduling problems in order to get the best from the BESS. Indeed, in this case, it seems that the actual sizing does not lead to the best scheduling that can be achieved.

5.3 DC bus signaling

5.3.1 Presentation of the OPA project

In the small-scale MG of OPA, a string of PV panels (1 kWp) from the roof of the ADREAM building (Fig. 5.7) is feeding a 48-60 V DC bus, which is powering some DC loads such as servers, sensors, USB chargers, etc. Some ESSs have also been connected to the DC bus through DC/DC converters, a 300 Ah – 36 V OPzV lead-acid battery pack (six VRLA 'power.bloc' batteries in series from Hoppecke, see Appendix 5-A), and a 330 F – 48 V supercapacitor pack (two modules in parallel from Maxwell, see Appendix 5-B). We have already published a document to present the development of this small-scale MG and its control [191].

The objective of OPA is to develop different projects such as experimental validation of energy management strategies, evaluation of scheduling algorithms, assessment of the DC distribution efficiency, etc. Hence, the use of controllable loads such as servers is very interesting regarding the implementation of scheduling and demand-side management algorithms. Furthermore, the use of DC distribution for the supply of datacenters is very competitive compared to AC distribution and seems more sustainable (especially at 380 V) [192].

Figure 5.7 ADREAM building – Rooftop PV panels

The list of the commercial systems that have been connected to the MG is presented in Table 5.1.

System	Reference	Ratings	Quantity	Total cost
Supercapacitor pack (bus)	BMOD0500 P016 B01	16.2V, 500F	4	2240€
Supercapacitor pack (ESS 1)	BMOD0165 P048 C01	48V, 165F	2	2726€
Lead-acid batteries (ESS 2)	Hoppecke OPzV bloc solar.power	6V, 300 Ah	12	5796€
WEB-BOX DATA LOGGER	ELOG	Non applicable	1	1250€
Indicators and RS485 communication	CA2150E	Non applicable	10	3850€
MPPT controller	Blue Solar charger, Victron	30 A, 100 V	1	310€

Table 5.1 Commercial systems that have been installed in the OPA MG

The power ratings of subsystems and the overall architecture of OPA connected to ADREAM building are illustrated in Fig. 5.8. Due to the connection with the utility grid, the OPA MG is able to operate in a 'connected mode' that can be used for feeding the DC bus, powering the data servers and charging the ESSs, in case of exceptional bad weather conditions. Under regular conditions, the MG is isolated from the main grid ('islanded mode').
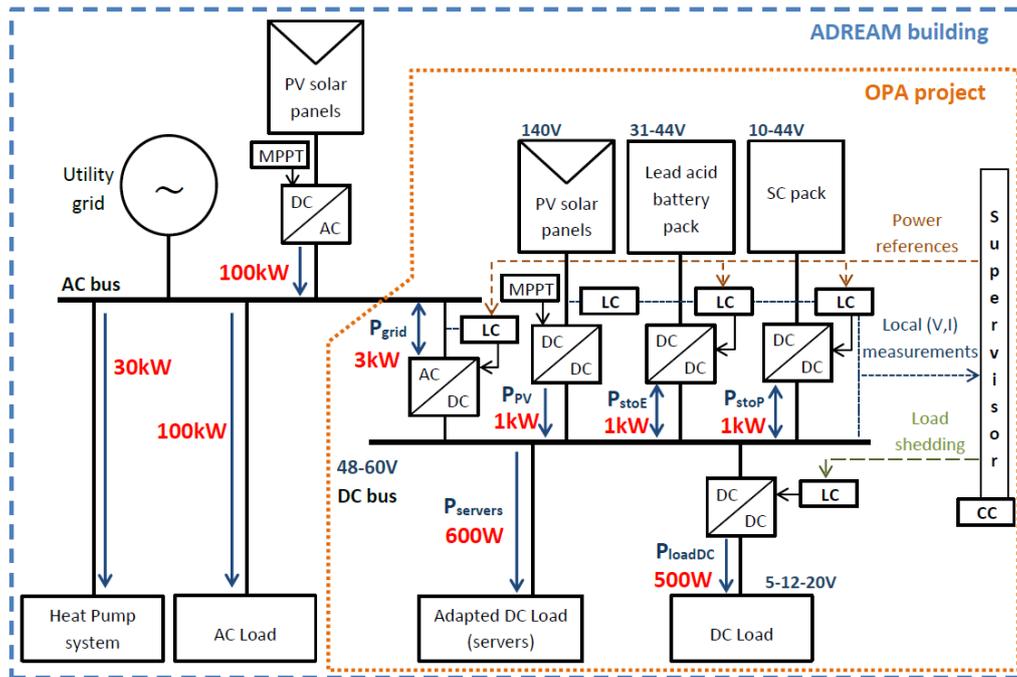
Figure 5.8 Architectures of the developed OPA microgrid and the ADREAM building of the LAAS-CNRS

As described in Fig. 5.8, every storage system is controlled independently by a local controller (LC), which evaluates the SOC of each ESS and is able to modify the current reference of this element (decentralized emergency mode). In centralized control, the LC sends local measurements of voltage and current to the central Controller (CC) that is responsible for the optimal energy management of the MG. This latter defines the operating mode of the MG and sends references to the LCs. The communication between LCs and CC is ensured by I²C protocol. A complete electrical scheme of the OPA MG is given in Appendix 5.C.

Bidirectional DC/DC boost converters and their associated control boards have been designed by Lionel Séguier, electrical engineer in LAAS-CNRS (Fig. 5.9). We have chosen to develop our own DC/DC converters because non-isolated converters with such power and voltage ratings were not commercially available. Moreover, self-designed power converters enable to implement our own control loops and communication with the CC.

Figure 5.9 Power electronics developed in the LAAS
On the left - 1kW bidirectional DC/DC converter, On the right – Control board of the power converter

5.3.2 Control methodology

Some papers have already proposed a control based on DC bus signaling [185], [193]. Hence, this method is well adapted to achieve a decentralized control. In this project, we want to implement this method as a control technique that ensures the operation of the MG while, for example, a communication fault occurs in the centralized control between a LC and the CC.

All systems connected to MG are operating with a control based on 'bus signaling'. Thus, the voltage of the bus is the signal that is defining the mode in which the MG is operating. Four levels of voltage, corresponding to different modes of operation, have been defined in our MG (presented from the highest to the lowest value of voltage), as illustrated in Fig. 5.10:

- **Mode I:** the MPPT solar charge controller is set in a constant voltage mode and the inverter injects power out of the MG in order to avoid any further increase of the DC bus voltage. In this case, both ESSs are in a full SOC.

- **Mode II:** lead-acid batteries are allowed to be charged. The battery pack is allowed to be discharged during the night only.

- **Mode III:** usual operating mode, the SCs are regulating the voltage of the DC bus (both charge and discharge).

- **Mode IV:** the AC/DC converter injects some power to the MG in order to ensure the bus voltage to be within the fixed limits. In this case, both ESSs are in an empty SOC.
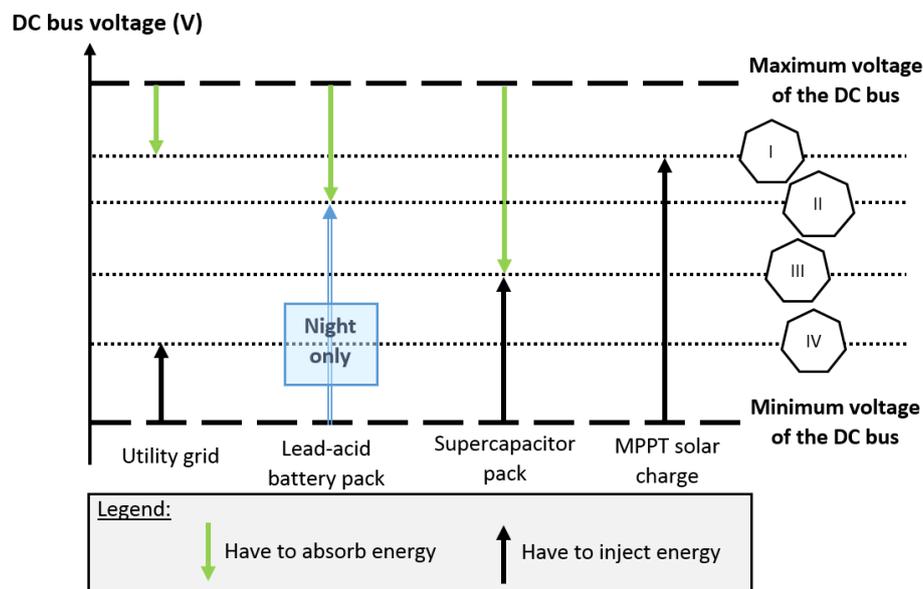
Figure 5.10 Voltage levels and operating modes of the ESSs in the MG

For now, the DC bus is operating between 48 and 60 V in order to feed the servers without additional power converters (direct connection). The modes II and III have been fixed to 54V and 53V, respectively. This enables to limit the number of cycles per day that the lead-acid batteries have to do.

During steady states operations (dotted lines in the Fig. 5.10), only one power converter controls the voltage level of the DC bus, the other ones operate as current sources. The voltage source that corresponds to modes I, II, III, and IV of the MG are the main grid (DC/AC converter), the lead-acid batteries, the SCs and the main grid (AC/DC converter), respectively.

Each ESS connected to the MG has its own cascade regulation (i.e. fast internal current loop and in this case two external voltage loops but only one is active at a time) that is implemented in its associated LC (corresponding to its specific characteristics related to power capability, SOC calculation, etc.). Hence, based on the voltage of the DC bus and the SOC of the storage system (provided measurements of current and voltage of the ESS), the current reference of the ESS is established, as illustrated in Fig. 5.11.

Thus, based on the SOC loop, the ESSs are not allowed to charge/discharge when their SOC is full/empty. Moreover, if the communication between systems is enabled, the batteries cannot be discharged until the SCs are empty, and can only be charged if the SCs are full. These rules aim at avoiding some bad operations (from a lifetime point of view) because the energy from the battery pack can go to the SC pack, and conversely. The design of our PI controllers and the transfer functions of our power converters have been explained in our previous paper [194] that was dealing with a simple current sharing method between a buck converter and a boost converter connected to the same DC bus (the modelling of power converters is presented in Appendix 5.D).
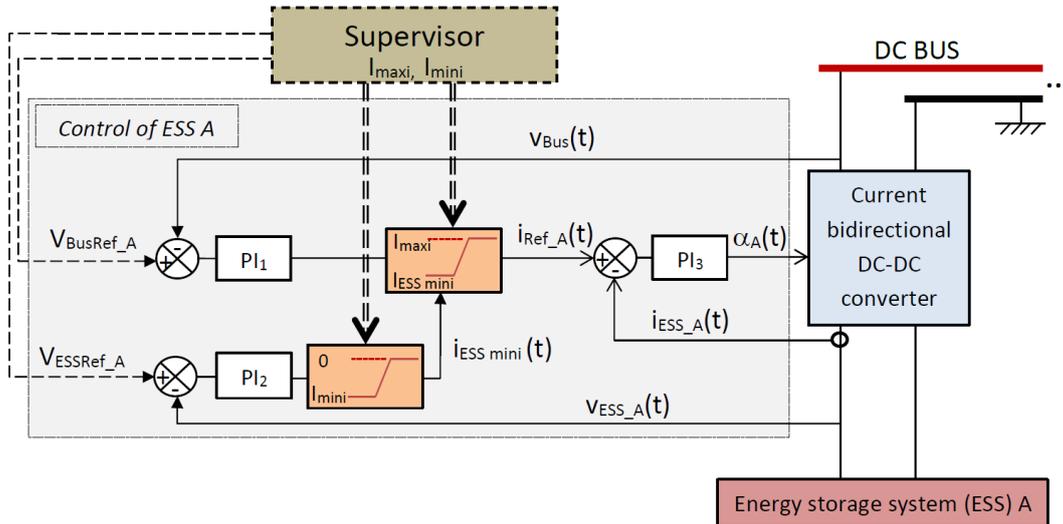
Figure 5.11 Cascade regulation implemented in every power converter of the MG

5.3.3 Experimental validation

The experimental setup of the OPA MG is presented in Fig. 5.12.
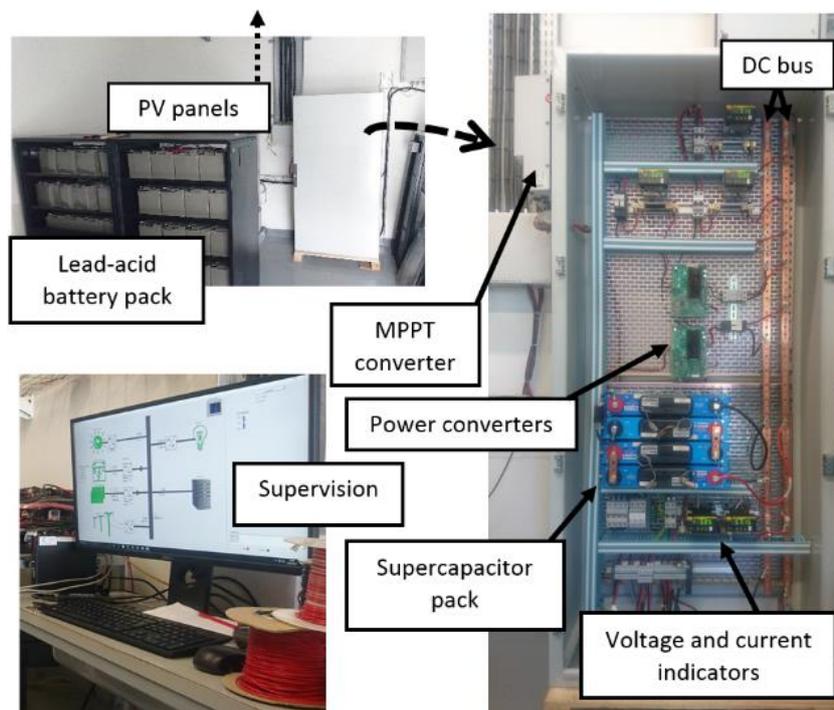
Figure 5.12 OPA experimental setup

The monitoring and supervision software of the MG has been developed by Lionel Séguier under LabWindows/CVI, as illustrated in Fig. 5.13. The voltages, currents, and SOC (if applicable) of every systems connected to the DC bus are sensed and saved in a database.
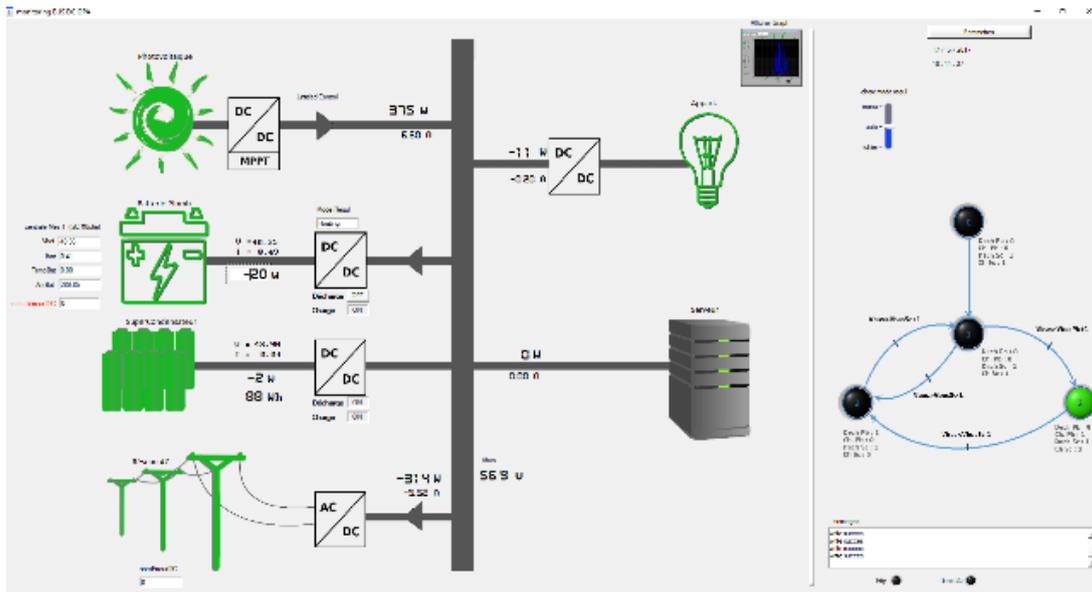
Figure 5.13 Monitoring interface of the OPA project

The energy management of ESSs that has been presented in Fig. 5.10, has been implemented with a state diagram, as illustrated in Fig. 5.14 (in this figure '0' means disabled and '1' means enabled). This state diagram has to be implemented in every LC in order to enable a cascade regulation that takes into account the voltage of the bus (additionally to the SOC of the ESS), as depicted in Fig 5.11.
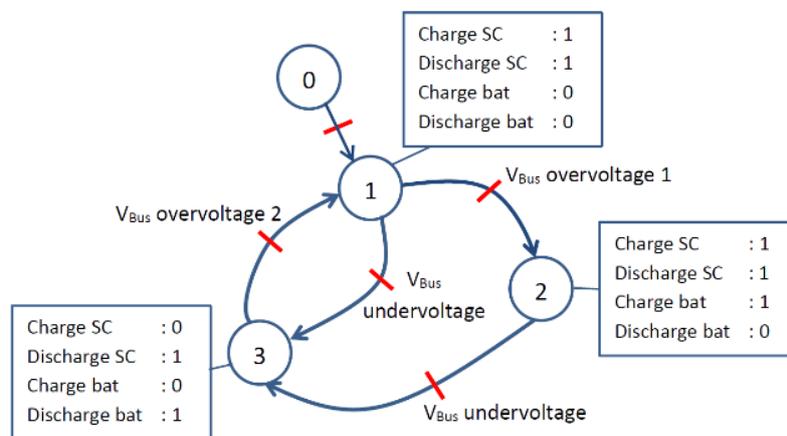
Figure 5. 14 State diagram describing the energy management of ESSs in the MG

A day of operation of the OPA MG is illustrated in Fig. 5.15 (the current going to the bus has a positive value). Hence, the different states of the energy management presented in Fig. 5.14 can be explained as follows.

- **State 1:** the battery is not allowed to be charged or discharged (Imaxi=Imini=0 in Fig. 5.11). According to the power balance of the MG, the pack of SCs may be charging ($P_{Load}<P_{PV}$) or discharging ($P_{Load}>P_{PV}$) to regulate the voltage of the DC bus at 52 V.

  When the SCs are fully charged (44 V), the voltage of the DC bus is increasing if the power balance remains positive. Once the voltage of the DC bus becomes higher than 53.5 V, the

supervisor allows to charge the batteries (Imaxi =18 A) and the MG mode changes to state 2. The voltage of the bus is regulated at 53 V, as illustrated in Fig. 5.15-B, t=9717 min.

Conversely, when the SCs are empty and the power balance is negative, the voltage of the bus decreases. Once it goes below 51.5 V, the supervisor allows batteries to be only discharged (Imini =-18 A and Imaxi =0 A) and prohibits SCs for charging, see. Fig. 5.15-C, t= 12 224 min. In this case the MG mode goes to state 3. The same state can be obtained from state 2, when the SCs are no longer able to meet the load demand.

- **State 2:** It is the "normal mode" during the day. Batteries are only allowed to charge and SCs can either charge or discharge. The advantage of this mode can be clearly observed in Fig. 5.15-D. Indeed, the SCs are regulating the DC bus voltage during partly cloudy days, avoiding micro-cycles from the batteries.

- **State 3:** All ESSs are allowed to only be discharged. If the PV production is higher than the load demand, the voltage of the DC bus increases. When it reaches 53 V, the supervisor allows the SCs to be charged and the MG goes to state 1, as depicted in Fig 5.14-E, t=4739 min.

Finally, if the DC bus signaling approach with its different modes of operation (Fig. 5.10) is coupled with the cascade regulation that takes into account the SOC of ESS (Fig.5. 11), the good operation of the MG is ensured even if the communication between LC and CC is lost.

Concerning the determination of the voltage levels that are used in the DC bus signaling method, which define the different modes of operation, we have for now arbitrary chosen these levels. In the future, we want to go further and propose a method to find the best values of voltage depending on the dynamics and the capacity of the ESSs connected to the DC bus. We expect that this new definition of voltage levels will have a direct impact on the sizing because a trade-off has to be made between the costs and the capacity in every control mode.
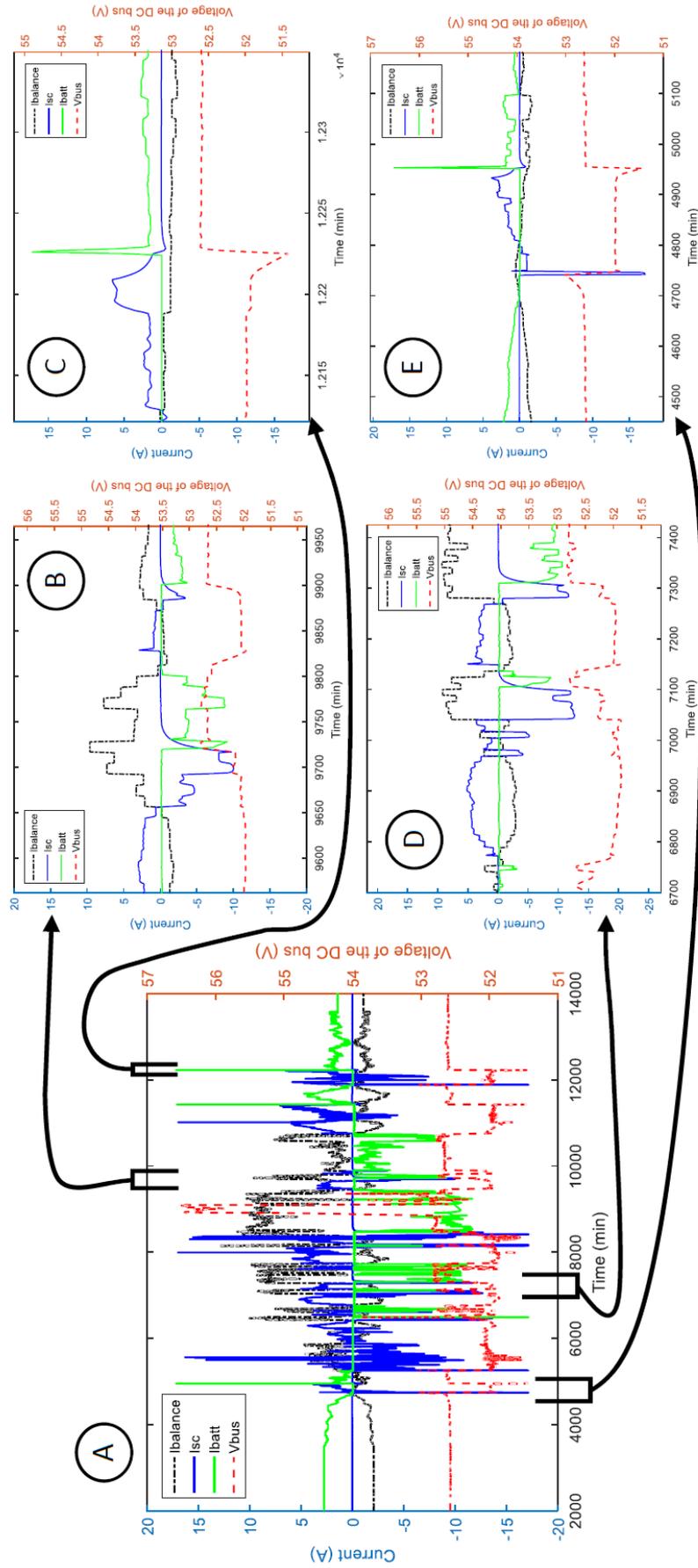
Figure 5. 15 OPA MG experimental profiles. A) complete day operation, B) to E) different operating modes

5.4 Summary

Different control techniques applied to MGs have been presented. Among them, the hierarchical control seems to be a good methodology that ensures good performances of the MG and enable to integrate a high level optimization planning for enhancing the economic dispatch.

Hence, we have decided to develop a scheduling approach in order to minimize the costs of operation of the MG (annual cost of the BESS and electricity). The formulation of this problem relies on the model of ESS presented on chapter 3, and on some of the criteria presented in chapter 4.

Moreover, a DC bus signaling control has been presented and experimented on a new MG in our laboratory. A decentralized control architecture has been proposed with the use of local controllers connected to power converters, in which a cascade regulation has been implemented. A voltage reference defined by the DC bus signaling method is also enhancing this control level and allows the use of several sources and ESSs without the need of a communication protocol.

In the future, the objective is to work on a complete hierarchical control that combines both scheduling and DC bus signaling (with cascade regulation) in order to optimize the operation of the MG at high large timescales and benefit of a safe and reliable control at low timescales. This control necessitates the integration of PV forecast models, a first work have already been done in our team few years ago [67], but some simulations will be necessary to evaluate the operation of such control structure (impacts of time step, accuracy, etc.).

Chapter 6.   Conclusion

"The universe doesn't allow perfection."

Stephen Hawking (born 8 January 1942) English theoretical physicist and cosmologist, he wrote several best-seller books dealing with popular science such as "A Brief History of Time"

This thesis investigated the use of energy storage systems in microgrids, highlighting the difficulty to propose an optimal technological choice, sizing and energy management. In chapter 3, several energy storage systems have been presented. Among them, three technologies have been studied in more details because of their good behaviour well adapted to their integration in buildings (i.e. lead-acid batteries, lithium-ion batteries, supercapacitors). A simple and generic electrical model, which is a trade-off between complex electrochemical models and experiment-based black box models, has been developed in order to be integrated in a MG simulation. This model can be partly parametrized by data from manufacturers and takes into account lifetime concerns, which are crucial for the sizing and control optimization. Our approach has been published in [163], [189].

For the sizing of an energy storage system, it appears that a lot of external parameters, going further than power and energy considerations, have to be integrated in the optimization process (i.e. self-consumption of renewable sources, levelized cost of electricity, greenhouse gases emissions, loss of power supply probability, etc.). Hence, we developed a multi-objective optimization methodology based on Pareto optimality that enables to find the best combinations of hybrid storage systems. In this way, a new publication is under preparation, taking into account the last results obtained with the OPA MG. The presented method of sizing and control is very generic. Thus, it can be adapted to any type of storage, source, and/or load. Hence, through a collaboration with the Laplace laboratory from Toulouse, especially Angel Barroso (PhD student), we have proposed a sizing method for LED lightings [171], [172] inspired by the first approach presented in chapter 4. It resulted in a best paper award from the IEEE IAS Industrial Lighting and Display committee. In each study case, the difficulty is to select the most relevant criteria well adapted to the application and then choose an optimal solution amongst others. This method will be soon applied to AC MGs in order to size the ESS that will be connected to an AC node in the ADREAM building.

The hierarchical control has been presented with an example of scheduling implementation and a decentralized control architecture combining DC bus signaling and cascade regulation have been developed. The control of a microgrid has been validated in real condition on a small-scale system of some kilowatts, as presented in [191]. Indeed, the experimental setup has been developed in the smart building ADREAM, in which some energy storage systems have been installed based on the analysis of production and consumption of the building.

During my doctoral thesis, thanks to the University Paul Sabatier – Toulouse III and the COMUE (Toulouse universities), I have been able to work abroad in Aalborg University. In this context, I joined between September 2016 and December 2016 a well-known Danish team working on microgrids and supervised by Prof. Josep M. Guerrero to develop my research work on the optimal sizing and scheduling of ESSs. This stay has been very fruitful for me, analysing the operation of other renewable sources (such as wind turbines), discovering other applications of microgrids (i.e. integration in vessels),

and publishing two conference papers and one book chapter. Since then, the two teams want to continue to collaborate in this field.

To our knowledge, no research work covers all the fields that have been presented (modelling of ESSs, multi-objective optimal sizing of ESSs in MG applications, MG control with scheduling, DC bus signaling and cascade regulation). One of the difficulty was to make the state of the art in all these fields and choose the appropriate models or methods that were the most suitable to be validated in the ADREAM building. During the past three years, a lot of advances have been done in our team in the fields of energy storage systems, control, and optimization.

Thus, several perspectives of this work can be expected. First, it is possible to go deeper in the modelling of energy storage systems and propose an experimental lifetime models of batteries for varying cycle depths and level of currents. Then, other energy management strategies for ESSs can be explored in order to find a better sizing and try to determine a relationship between energy management strategy and optimal sizing. A literature review can be done again on the life cycle analysis of batteries in order to propose an optimal sizing with a clear vision of environmental impacts based on recent data. In this sense, Margot Gaetani Liseo started her PhD thesis in October 2017. Two other PhD students, Kolja Neuhaus and Ilias Papas, who are exploring the supply of electrolysers by a DC bus powered with a concentrated solar PV source, will apply the multi-objective methodology to design a new DC microgrid.

On a broader level, the microgrid protection (fault detection and discrimination) is a real challenge for the successful development of microgrids and smartgrids. Moreover, cyber-attack opportunities are numerous because of the inherent communicating nature of such grids (sensors, actuators, software systems, etc.). Nevertheless, even if the lack of standards is slowing down the deployment of DC microgrids, this new power architecture is very promising and we can expect that this will be one solution to achieve a sustainable future.

Selected publications

Publications in Magazine:

- **Jérémy Dulout**, Bruno Jammes, Lionel Séguier, Angel Barroso, Pascal Dupuis, Georges Zissis, Corinne Alonso, *"Multiobjective optimal design of Light Emitting Diode (LED) lightings"*, (Accepted, to be published) IEEE Magazine Industry Applications Society, July-August 2018 , 9 pages.

Book chapter:

- Amjad Anvari-Moghaddam, **Jérémy Dulout**, Corinne Alonso, Bruno Jammes, Josep. M. Guerrero, *"Optimal Design and Operation Management of Battery-Based Energy Storage Systems (BESS) in Microgrids"*, (Accepted, to be published) Intech book chapter 'Advancements in Energy Storage Technologies' (ISBN 978-953-51-5713-7), 2017, 20 pages.

Publications in Proceedings with Peer Review:

- **Jérémy Dulout**, Adriana Luna, Amjad Anvari-Moghaddam, Corinne Alonso, Josep M. Guerrero, Bruno Jammes, "Optimal scheduling of a battery-based energy storage system for a microgrid with high penetration of renewable sources", ELECTRIMACS, Toulouse, 4-6 July 2017, pp. 1-6.

- **Jérémy Dulout**, Corinne Alonso, Lionel Séguier, Bruno Jammes. "Development of a photovoltaic low voltage dc microgrid for buildings with energy storage systems", ELECTRIMACS, Toulouse, 4-6 July 2017, pp. 1-6.

- **Jérémy Dulout**, Amjad Anvari-Moghaddam, Adriana Luna, Bruno Jammes, Corinne Alonso, Josep Guerrero, "Optimal sizing of a lithium battery energy storage system for grid-connected photovoltaic systems", International Conference on DC Microgrids (ICDCM), Nurnberg, 27-29 June 2017, pp. 582 - 587.

- **Jérémy Dulout**, Angel Barroso, Lionel Séguier, Bruno Jammes, Pascal Dupuis, Georges Zissis, Corinne Alonso, "Multi-objective methodology to find the optimal forward current to supply Light Emitting Diode (LED) lightings", Industry Applications Society (IAS) Annual Meeting, Portland, 2-6 Oct. 2016, pp. 1-7.

- Kolja Neuhaus, **Jérémy Dulout**, Corinne Alonso, "LVDC Grid Based on PV Energy Sources and Multiple Electrochemical Storage Technologies", International Conference on Ubiquitous Intelligence and Computing (UIC), 18-21 July 2016, pp. 990 – 997.

- **Jérémy Dulout**, Bruno Jammes, Lionel Séguier, Corinne Alonso, "Dimensionnement multi-objectif d'une association batterie supercondensateur pour une application photovoltaïque", JNRDM, Toulouse, 11-13 May 2016, pp. 1-6.

- **Jérémy Dulout**, Bruno Jammes, Lionel Séguier, Corinne Alonso, "Control and design of a hybrid energy storage system", EPE ECCE-Europe, Geneva, 8-10 Sept. 2015, pp. 1-9.

For most of these publications, they are available at https://hal.archives-ouvertes.fr/, an open archive from all academic fields.

Bibliography

"Our ignorance is not so vast as our failure to use what we know"
Marion King Hubbert (5 October 1903 – 11 October 1989) American geologist who notably modelled the production and discovery rates of oil and gas resources (see chapter 2).

[1] Arnulf Grubler *et al.*, 'Global Energy Assessment - Toward a Sustainable Future, Chapter 1: Energy primer', *Cambridge University Press*, 2012.

[2] Lina I. Brand-Correa and Julia K. Steinberger, 'A Framework for Decoupling Human Need Satisfaction From Energy Use', *Ecological Economics*, vol. 141, pp. 43–52, Nov. 2017.

[3] International Energy Agency (IEA), 'Key world energy statistics 2016', 2016.

[4] International Energy Agency (IEA), 'World final consumption by sector, https://www.iea.org/Sankey/#?c=World&s=Final%20consumption, [last access: 2017-08-29]'. .

[5] Shonali Pachauri *et al.*, 'Pathways to achieve universal household access to modern energy by 2030', *Environmental Research Letters*, vol. 8, no. 2, p. 024015, Jun. 2013.

[6] United Nations, Department of Economic and Social Affairs, and Population Division, 'World Population Prospects: The 2017 Revision', 2017.

[7] Rajendra K. Pachauri *et al.*, *Climate change 2014: synthesis report. Contribution of Working Groups I, II and III to the fifth assessment report of the Intergovernmental Panel on Climate Change*. IPCC, 2014.

[8] Richard H. Moss *et al.*, 'The next generation of scenarios for climate change research and assessment', *Nature*, vol. 463, no. 7282, pp. 747–756, Feb. 2010.

[9] WWF International, *Living Planet Report 2016. Risk and resilience in a new era*. Switzerland, 2016.

[10] International Energy Agency (IEA), 'Energy and Climate Change - World Energy Outlook Special Report', Mar. 2015.

[11] International Renewable Energy Agency (IRENA), 'Roadmap for a renewable energy future - 2016 edition'.

[12] Association négaWatt, 'The 2017-2050 négaWatt Scenario - Executive summary', 2017.

[13] Stephen Pacala and Robert Socolow, 'Stabilization wedges: solving the climate problem for the next 50 years with current technologies', *science*, vol. 305, no. 5686, pp. 968–972, 2004.

[14] International Energy Agency (IEA), 'Energy and CO2 emissions in the OECD', 2017.

[15] N. Abas, A. Kalair, and N. Khan, 'Review of fossil fuels and future energy technologies', *Futures*, vol. 69, pp. 31–49, May 2015.

[16] Jean-Paul Albertini, Anne Bottin, Irénée Joassard, and Valéry Morard, 'L'environnement en France - Édition 2014', *ISBN : 978-2-11-138802-4*, 2014.

[17] Omar Ellabban, Haitham Abu-Rub, and Frede Blaabjerg, 'Renewable energy resources: Current status, future prospects and their enabling technology', *Renewable and Sustainable Energy Reviews*, vol. 39, pp. 748–764, Nov. 2014.

[18] World Energy Council, 'World Energy Resources - Marine Energy 2016', 2016.

[19] Michael Zürn, 'The rise of international environmental politics: A review of current research', *World Politics*, vol. 50, no. 4, pp. 617–649, 1998.

[20] Annette Evans, Vladimir Strezov, and Tim J. Evans, 'Assessment of sustainability indicators for renewable energy technologies', *Renewable and Sustainable Energy Reviews*, vol. 13, no. 5, pp. 1082–1088, Jun. 2009.

[21] Falko Ueckerdt, Lion Hirth, Gunnar Luderer, and Ottmar Edenhofer, 'System LCOE: What are the costs of variable renewables?', *Energy*, vol. 63, pp. 61–75, Dec. 2013.

[22] Lion Hirth, 'The market value of variable renewables', *Energy Economics*, vol. 38, pp. 218–236, Jul. 2013.

[23] Ottmar Edenhofer *et al.*, 'On the economics of renewable energy sources', *Energy Economics*, vol. 40, pp. S12–S23, Dec. 2013.

[24] Nana Yaw Amponsah, Mads Troldborg, Bethany Kington, Inge Aalders, and Rupert Lloyd Hough, 'Greenhouse gas emissions from renewable energy sources: A review of lifecycle considerations', *Renewable and Sustainable Energy Reviews*, vol. 39, pp. 461–475, Nov. 2014.

[25] Varun, Ravi Prakash, and Inder Krishnan Bhat, 'Energy, economics and environmental impacts of renewable energy systems', *Renewable and Sustainable Energy Reviews*, vol. 13, no. 9, pp. 2716–2721, Dec. 2009.

[26] Khagendra P. Bhandari, Jennifer M. Collier, Randy J. Ellingson, and Defne S. Apul, 'Energy payback time (EPBT) and energy return on energy invested (EROI) of solar photovoltaic systems: A systematic review and meta-analysis', *Renewable and Sustainable Energy Reviews*, vol. 47, pp. 133–141, Jul. 2015.

[27] Charles A. S. Hall, Stephen Balogh, and David J.R. Murphy, 'What is the Minimum EROI that a Sustainable Society Must Have?', *Energies*, vol. 2, no. 1, pp. 25–47, Jan. 2009.

[28] Jessica G. Lambert, Charles A.S. Hall, Stephen Balogh, Ajay Gupta, and Michelle Arnold, 'Energy, EROI and quality of life', *Energy Policy*, vol. 64, pp. 153–167, Jan. 2014.

[29] Rolf Wüstenhagen, Maarten Wolsink, and Mary Jean Bürer, 'Social acceptance of renewable energy innovation: An introduction to the concept', *Energy Policy*, vol. 35, no. 5, pp. 2683–2691, May 2007.

[30] Eleni K. Stigka, John A. Paravantis, and Giouli K. Mihalakakou, 'Social acceptance of renewable energy sources: A review of contingent valuation applications', *Renewable and Sustainable Energy Reviews*, vol. 32, pp. 100–106, Apr. 2014.

[31] H. Lee Willis and Walter G. Scott, *Distributed power generation: planning and evaluation*. New York: Marcel Dekker, 2000.

[32] Rik W. De Doncker, 'Power Electronic Technologies for Flexible DC Distribution Grids', *International Power Electronics Conference (IPEC-Hiroshima 2014 - ECCE-ASIA)*, pp. 736–743, 2014.

[33] Mohamed A. Eltawil and Zhengming Zhao, 'Grid-connected photovoltaic power systems: Technical and potential problems—A review', *Renewable and Sustainable Energy Reviews*, vol. 14, no. 1, pp. 112–129, Jan. 2010.

[34] H. Farhangi, 'The path of the smart grid', *IEEE Power and Energy Magazine*, vol. 8, no. 1, pp. 18–28, Jan. 2010.

[35] G. Pepermans, J. Driesen, D. Haeseldonckx, R. Belmans, and W. D'haeseleer, 'Distributed generation: definition, benefits and issues', *Energy Policy*, vol. 33, no. 6, pp. 787–798, Apr. 2005.

[36] Grant Allan, Igor Eromenko, Michelle Gilmartin, Ivana Kockar, and Peter McGregor, 'The economics of distributed energy generation: A literature review', *Renewable and Sustainable Energy Reviews*, vol. 42, pp. 543–556, Feb. 2015.

[37] Nikos Hatziargyriou, Hiroshi Asano, Reza Iravani, and Chris Marnay, 'Microgrids', *IEEE power and energy magazine*, vol. 5, no. 4, pp. 78–94, 2007.

[38] Estefanía Planas, Jon Andreu, José Ignacio Gárate, Iñigo Martínez de Alegría, and Edorta Ibarra, 'AC and DC technology in microgrids: A review', *Renewable and Sustainable Energy Reviews*, vol. 43, pp. 726–749, Mar. 2015.

[39] Xiongfei Wang, Josep M. Guerrero, Frede Blaabjerg, and Zhe Chen, 'A Review of Power Electronics Based Microgrids', *Journal of Power Electronics*, vol. 12, no. 1, pp. 181–192, Jan. 2012.

[40] Huang Jiayi, Jiang Chuanwen, and Xu Rong, 'A review on distributed energy resources and MicroGrid', *Renewable and Sustainable Energy Reviews*, vol. 12, no. 9, pp. 2472–2483, Dec. 2008.

[41] Scott N. Backhaus *et al.*, 'DC Microgrids Scoping Study. Estimate of Technical and Economic Benefits', Los Alamos National Lab.(LANL), Los Alamos, NM (United States), 2015.

[42] Sina Parhizi, Hossein Lotfi, Amin Khodaei, and Shay Bahramirad, 'State of the Art in Research on Microgrids: A Review', *IEEE Access*, vol. 3, pp. 890–925, 2015.

[43] Ahmed T. Elsayed, Ahmed A. Mohamed, and Osama A. Mohammed, 'DC microgrids and distribution systems: An overview', *Electric Power Systems Research*, vol. 119, pp. 407–417, Feb. 2015.

[44] Eneko Unamuno and Jon Andoni Barrena, 'Hybrid ac/dc microgrids—Part I: Review and classification of topologies', *Renewable and Sustainable Energy Reviews*, vol. 52, pp. 1251–1259, Dec. 2015.

[45] Donald J. Hammerstrom, 'AC versus DC distribution systemsdid we get it right?', in *Power Engineering Society General Meeting, 2007. IEEE*, 2007, pp. 1–5.

[46] Peng Wang, L. Goel, Xiong Liu, and Fook Hoong Choo, 'Harmonizing AC and DC: A Hybrid AC/DC Future Grid Solution', *IEEE Power and Energy Magazine*, vol. 11, no. 3, pp. 76–83, May 2013.

[47] Kristopher Jones, 'AC versus DC Power Distribution in the Data Center', Nov. 2013.

[48] Jackson John Justo, Francis Mwasilu, Ju Lee, and Jin-Woo Jung, 'AC-microgrids versus DC-microgrids with distributed energy resources: A review', *Renewable and Sustainable Energy Reviews*, vol. 24, pp. 387–405, Aug. 2013.

[49] Enrique Rodriguez-Diaz, Fang Chen, Juan C. Vasquez, Josep M. Guerrero, Rolando Burgos, and Dushan Boroyevich, 'Voltage-Level Selection of Future Two-Level LVdc Distribution Grids: A Compromise Between Grid Compatibiliy, Safety, and Efficiency', *IEEE Electrification Magazine*, vol. 4, no. 2, pp. 20–28, Jun. 2016.

[50] Adolf Goetzberger, Joachim Luther, and Gerhard Willeke, 'Solar cells: past, present, future', *Solar energy materials and solar cells*, vol. 74, no. 1, pp. 1–11, 2002.

[51] International Energy Agency (IEA), 'Technology Roadmap - Solar Photovoltaic Energy, 2014 edition', 2014.

[52] Corinne Alonso, 'Contribution à l'optimisation, la gestion et le traitement de l'énergie', *Habilitation à diriger les recherches, Université Paul Sabatier-Toulouse III*, 2003.

[53] Youssef El Basri, 'Architecture de puissance distribuée reconfigurable dédiée à l'optimisation de l'énergie photovoltaïque', *PhD dissertation, Université Paul Sabatier - Toulouse III*, 2013.

[54] Alona BERASATEGI, 'Nouvelles Architectures Electriques Optimisées de Générateurs Photovoltaïques à Haut Rendement', *PhD dissertation, Université Paul Sabatier - Toulouse III*, 2013.

[55] Alonso GUTIERREZ GALEANO, 'Study of photovoltaic system integration in microgrids through real-time modeling and emulation of its components using HiLeS', *PhD dissertation, Université Paul Sabatier - Toulouse III*, 2017.

[56] Trishan Esram and Patrick L. Chapman, 'Comparison of Photovoltaic Array Maximum Power Point Tracking Techniques', *IEEE Transactions on Energy Conversion*, vol. 22, no. 2, pp. 439–449, Jun. 2007.

[57] B. Shiva Kumar and K. Sudhakar, 'Performance evaluation of 10 MW grid connected solar photovoltaic power plant in India', *Energy Reports*, vol. 1, pp. 184–192, Nov. 2015.

[58] Atse Louwen, Wilfried G. J. H. M. van Sark, André P. C. Faaij, and Ruud E. I. Schropp, 'Re-assessment of net energy production and greenhouse gas emissions avoidance after 40 years of photovoltaics development', *Nature Communications*, vol. 7, p. 13728, Dec. 2016.

[59] Harry Wirth, 'Recent Facts about Photovoltaics in Germany', *Fraunhofer ISE*, Oct. 2016.

[60] Marzella Görig and Christian Breyer, 'Energy learning curves of PV systems', *Environmental Progress & Sustainable Energy*, vol. 35, no. 3, pp. 914–923, May 2016.

[61] Emrah Biyik *et al.*, 'A key review of building integrated photovoltaic (BIPV) systems', *Engineering Science and Technology, an International Journal*, vol. 20, no. 3, pp. 833–858, Jun. 2017.

[62] Ana Cabrera-Tobar, Eduard Bullich-Massagué, Mònica Aragüés-Peñalba, and Oriol Gomis-Bellmunt, 'Topologies for large scale photovoltaic power plants', *Renewable and Sustainable Energy Reviews*, vol. 59, pp. 309–319, Jun. 2016.

[63] Alok Sahu, Neha Yadav, and K. Sudhakar, 'Floating photovoltaic power plant: A review', *Renewable and Sustainable Energy Reviews*, vol. 66, pp. 815–824, Dec. 2016.

[64] Damon Turney and Vasilis Fthenakis, 'Environmental impacts from the installation and operation of large-scale solar power plants', *Renewable and Sustainable Energy Reviews*, vol. 15, no. 6, pp. 3261–3270, Aug. 2011.

[65] P. Díaz, R. Peña, J. Muñoz, C.A. Arias, and D. Sandoval, 'Field analysis of solar PV-based collective systems for rural electrification', *Energy*, vol. 36, no. 5, pp. 2509–2516, May 2011.

[66] Bhubaneswari Parida, S. Iniyan, and Ranko Goic, 'A review of solar photovoltaic technologies', *Renewable and Sustainable Energy Reviews*, vol. 15, no. 3, pp. 1625–1636, Apr. 2011.

[67] Michaël Bressan, 'Développement d'un outil de supervision et de contrôle pour une installation solaire photovoltaïque', *PhD dissertation, Université de Perpignan*, 2014.

[68] Lori Bird, Michael Milligan, and Debra Lew, 'Integrating variable renewable energy: Challenges and solutions', National Renewable Energy Laboratory (NREL), Golden, CO., 2013.

[69] Marc Beaudin, Hamidreza Zareipour, Anthony Schellenberglabe, and William Rosehart, 'Energy storage for mitigating the variability of renewable electricity sources: An updated review', *Energy for Sustainable Development*, vol. 14, no. 4, pp. 302–314, Dec. 2010.

[70] Electric Power Research Institute (EPRI), 'Electricity Energy Storage Technology Options - White Paper Primer on Applications, Costs, and Benefits, Palo Alto, CA, 1020676.' Dec-2010.

[71] Jim Eyer and Garth Corey, 'Energy Storage for the Electricity Grid: Benefits and Market Potential Assessment Guide - A Study for the DOE Energy Storage Systems Program, Sandia report, SAND2010-0815'. 2010.

[72] Behnam Zakeri and Sanna Syri, 'Electrical energy storage systems: A comparative life cycle cost analysis', *Renewable and Sustainable Energy Reviews*, vol. 42, pp. 569–596, Feb. 2015.

[73] Sandia Corporation, 'DOE global energy storage database, energystorageexchange.org, [accessed: 06/06/2017]', 2017. .

[74] Carl D. Parker, 'Lead–acid battery energy-storage systems for electricity supply networks', *Journal of Power Sources*, vol. 100, no. 1, pp. 18–28, 2001.

[75] Christophe Pillot, 'The rechargeable battery market and main trends 2014–2025', in *32th Annual International Battery Seminar & Exhibit*, 2015.

[76] Björn Nykvist and Måns Nilsson, 'Rapidly falling costs of battery packs for electric vehicles', *Nature Climate Change*, vol. 5, no. 4, pp. 329–332, Mar. 2015.

[77] J.L. Sullivan and L. Gaines, 'Status of life cycle inventories for batteries', *Energy Conversion and Management*, vol. 58, pp. 134–148, Jun. 2012.

[78] J. B. Dunn, L. Gaines, J. C. Kelly, C. James, and K. G. Gallagher, 'The significance of Li-ion batteries in electric vehicle life-cycle energy and emissions and recycling's role in its reduction', *Energy Environ. Sci.*, vol. 8, no. 1, pp. 158–168, 2015.

[79] Haisheng Chen, Thang Ngoc Cong, Wei Yang, Chunqing Tan, Yongliang Li, and Yulong Ding, 'Progress in electrical energy storage system: A critical review', *Progress in Natural Science*, vol. 19, no. 3, pp. 291–312, Mar. 2009.

[80] Francisco Díaz-González, Andreas Sumper, Oriol Gomis-Bellmunt, and Roberto Villafáfila-Robles, 'A review of energy storage technologies for wind power applications', *Renewable and Sustainable Energy Reviews*, vol. 16, no. 4, pp. 2154–2171, May 2012.

[81] T. Kousksou, P. Bruel, A. Jamil, T. El Rhafiki, and Y. Zeraouli, 'Energy storage: Applications and challenges', *Solar Energy Materials and Solar Cells*, vol. 120, pp. 59–80, Jan. 2014.

[82] Xing Luo, Jihong Wang, Mark Dooner, and Jonathan Clarke, 'Overview of current development in electrical energy storage technologies and the application potential in power system operation', *Applied Energy*, vol. 137, pp. 511–536, Jan. 2015.

[83] David Linden and Thomas B. Reddy, Eds., *Handbook of batteries. ISBN: 978-0-07-135978-8*, 3rd ed. New York: McGraw-Hill, 2002.

[84] M. Broussely and G. Pistoia, *Industrial Applications of Batteries - From Cars to Aerospace and Energy Storage. ISBN: 978-0-444-52160-6*, Elsevier. 2007.

[85] Vladimir S. Bagotsky, Alexander M. Skundin, and Yury M. Volfkovich, *Electrochemical power sources - Batteries, Fuel Cells, and Supercapacitors. ISBN: 978-1-118-46023-8*, Wiley. 2015.

[86] Franco Maloberti and Anthony C Davies, *A Short History of Circuits and Systems. ISBN: 978-87-93379-69-5*. Aalborg: River Publishers, 2016.

[87] Michel Armand and J.-M. Tarascon, 'Building better batteries', *Nature*, vol. 451, no. 7179, pp. 652–657, 2008.

[88] D. Berndt, 'Valve-regulated lead-acid batteries', *Journal of power sources*, vol. 100, no. 1, pp. 29–46, 2001.

[89] Paul Ruetschi, 'Aging mechanisms and service life of lead-acid batteries', *Journal of Power Sources*, vol. 127, no. 1–2, pp. 33–44, Mar. 2004.

[90] J.-M. Tarascon and Michel Armand, 'Issues and challenges facing rechargeable lithium batteries', *Nature*, vol. 414, no. 6861, pp. 359–367, 2001.

[91] J. Vetter *et al.*, 'Ageing mechanisms in lithium-ion batteries', *Journal of Power Sources*, vol. 147, no. 1–2, pp. 269–281, Sep. 2005.

[92] M. Saiful Islam and Craig A. J. Fisher, 'Lithium and sodium battery cathode materials: computational insights into voltage, diffusion and nanostructural properties', *Chem. Soc. Rev.*, vol. 43, no. 1, pp. 185–204, 2014.

[93] Bruce Dunn, Haresh Kamath, and Jean-Marie Tarascon, 'Electrical energy storage for the grid: a battery of choices', *Science*, vol. 334, no. 6058, pp. 928–935, 2011.

[94] Naoki Nitta, Feixiang Wu, Jung Tae Lee, and Gleb Yushin, 'Li-ion battery materials: present and future', *Materials today*, vol. 18, no. 5, pp. 252–264, 2015.

[95] Andreas Dinger *et al.*, 'Batteries for Electric Cars - Challenges, Opportunities, and the Outlook to 2020, The Boston Consulting Group, BCG Focus', pp. 1–14, 2010.

[96] Ander González, Eider Goikolea, Jon Andoni Barrena, and Roman Mysyk, 'Review on supercapacitors: Technologies and materials', *Renewable and Sustainable Energy Reviews*, vol. 58, pp. 1189–1206, May 2016.

[97] Patrice Simon and Yury Gogotsi, 'Materials for electrochemical capacitors', *Nature materials*, vol. 7, no. 11, pp. 845–854, 2008.

[98] Maximilian Kaus, Julia Kowal, and Dirk Uwe Sauer, 'Modelling the effects of charge redistribution during self-discharge of supercapacitors', *Electrochimica Acta*, vol. 55, no. 25, pp. 7516–7523, Oct. 2010.

[99] Dennis Doerffel and Suleiman Abu Sharkh, 'A critical review of using the Peukert equation for determining the remaining capacity of lead-acid and lithium-ion batteries', *Journal of Power Sources*, vol. 155, no. 2, pp. 395–400, Apr. 2006.

[100] Noshin Omar, Peter Bossche, Thierry Coosemans, and Joeri Mierlo, 'Peukert Revisited-Critical Appraisal and Need for Modification for Lithium-Ion Batteries', *Energies*, vol. 6, no. 11, pp. 5625–5641, Oct. 2013.

[101] Ana-Irina Stan, Maciej Swierczynski, Daniel-Ioan Stroe, Remus Teodorescu, Søren Juhl Andreasen, and Klaus Moth, 'A comparative study of lithium ion to lead acid batteries for use in UPS applications', in *Telecommunications Energy Conference (INTELEC), 2014 IEEE 36th International*, 2014, pp. 1–8.

[102] A. Delaille, 'Développement de méthodes d'évaluation de l'état de charge et de l'état de santé des batteries utilisées dans les systèmes photovoltaïques.', PhD dissertation, Université Paris VI, 2006.

[103] Languang Lu, Xuebing Han, Jianqiu Li, Jianfeng Hua, and Minggao Ouyang, 'A review on the key issues for lithium-ion battery management in electric vehicles', *Journal of Power Sources*, vol. 226, pp. 272–288, Mar. 2013.

[104] Amin Gholami, Tohid Shekari, Farrokh Aminifar, and Mohammad Shahidehpour, 'Microgrid Scheduling With Uncertainty: The Quest for Resilience', *IEEE Transactions on Smart Grid*, vol. 7, no. 6, pp. 2849–2858, Nov. 2016.

[105] Wen-Yeau Chang, 'The State of Charge Estimating Methods for Battery: A Review', *ISRN Applied Mathematics*, vol. 2013, pp. 1–7, 2013.

[106] Noshin Omar *et al.*, 'Electrical double-layer capacitors: evaluation of ageing phenomena during cycle life testing', *Journal of Applied Electrochemistry*, vol. 44, no. 4, pp. 509–522, Apr. 2014.

[107] An Li, Serge Pelissier, Pascal Venet, and Philippe Gyan, 'Fast Characterization Method for Modeling Battery Relaxation Voltage', *Batteries*, vol. 2, no. 2, p. 7, Apr. 2016.

[108] IEEE Power & Energy Society and Stationary Batteries Committee, *IEEE Recommended Practice for Sizing Lead-Acid Batteries for Stationary Applications - IEEE Std 485^{TM}-2010*. New York: Institute of Electrical and Electronics Engineers, 2011.

[109] H Bindner, T Cronin, P Lundsager, Risø National Lab, and Roskilde (DK). Wind Energy Department, *Lifetime modelling of lead acid batteries. ISBN: 978-87-550-3441-9*. 2005.

[110] Dirk Uwe Sauer and Heinz Wenzl, 'Comparison of different approaches for lifetime prediction of electrochemical systems - Using lead-acid batteries as example', *Journal of Power Sources*, vol. 176, no. 2, pp. 534–546, Feb. 2008.

[111] Julia Schiffer, Dirk Uwe Sauer, Henrik Bindner, Tom Cronin, Per Lundsager, and Rudi Kaiser, 'Model prediction for ranking lead-acid batteries according to expected lifetime in renewable energy systems and autonomous power-supply systems', *Journal of Power Sources*, vol. 168, no. 1, pp. 66–78, May 2007.

[112] Madeleine Ecker *et al.*, 'Calendar and cycle life study of Li(NiMnCo)O2-based 18650 lithium-ion batteries', *Journal of Power Sources*, vol. 248, pp. 839–851, Feb. 2014.

[113] Daniel-Ioan Stroe, Maciej Swierczynski, Ana-Irina Stroe, Remus Teodorescu, Rasmus Laerke, and Philip Carne Kjaer, 'Degradation behaviour of Lithium-ion batteries based on field measured frequency regulation mission profile', 2015, pp. 14–21.

[114] Yaël Thiaux, 'Optimisation des profils de consommation pour minimiser les coûts économique et énergétique sur cycle de vie des systèmes photovoltaïques autonomes et hybrides- Evaluation de la technologie Li-ion', PhD dissertation, École normale supérieure de Cachan-ENS Cachan, 2010.

[115] Vojtech Svoboda *et al.*, 'Operating conditions of batteries in off-grid renewable energy systems', *Solar Energy*, vol. 81, no. 11, pp. 1409–1425, Nov. 2007.

[116] Stephen D. Downing and D. F. Socie, 'Simple rainflow counting algorithms', *International journal of fatigue*, vol. 4, no. 1, pp. 31–40, 1982.

[117] H. Beltran, M. Swierczynski, N. Aparicio, E. Belenguer, Remus Teodorescu, and P. Rodriguez, 'Lithium ion batteries ageing analysis when used in a PV power plant', in *Industrial Electronics (ISIE), 2012 IEEE International Symposium on*, 2012, pp. 1604–1609.

[118] Habiballah Rahimi-Eichi, Unnati Ojha, Federico Baronti, and Mo-Yuen Chow, 'Battery Management System: An Overview of Its Application in the Smart Grid and Electric Vehicles', *IEEE Industrial Electronics Magazine*, vol. 7, no. 2, pp. 4–16, Jun. 2013.

[119] Nalin Chaturvedi, Reinhardt Klein, Jake Christensen, Jasim Ahmed, and Aleksandar Kojic, 'Algorithms for Advanced Battery-Management Systems', *IEEE Control Systems Magazine*, vol. 30, no. 3, pp. 49–68, Jun. 2010.

[120] Martin Winter and Ralph J. Brodd, 'What Are Batteries, Fuel Cells, and Supercapacitors?', *Chemical Reviews*, vol. 104, no. 10, pp. 4245–4270, Oct. 2004.

[121] El Mehdi Laadissi, El Filali Anas, and Malika Zazi, 'Nonlinear black box modeling of a lead acid battery using Hammerstein-Wiener model', *Journal of Theoretical and Applied Information Technology*, vol. 89, no. 2, p. 476, 2016.

[122] J.B. Copetti and F. Chenlo, 'Lead/acid batteries for photovoltaic applications. Test results and modelling. Journal of Power Sources, 47 (1994) 109-118'. 1994.

[123] Hongwen He, Rui Xiong, and Jinxin Fan, 'Evaluation of Lithium-Ion Battery Equivalent Circuit Models for State of Charge Estimation by an Experimental Approach', *Energies*, vol. 4, no. 12, pp. 582–598, Mar. 2011.

[124] Min Chen and Gabriel A. Rincon-Mora, 'Accurate electrical battery model capable of predicting runtime and IV performance', *IEEE transactions on energy conversion*, vol. 21, no. 2, pp. 504–511, 2006.

[125] Habiballah Rahimi-Eichi, Federico Baronti, and Mo-Yuen Chow, 'Online Adaptive Parameter Identification and State-of-Charge Coestimation for Lithium-Polymer Battery Cells', *IEEE Transactions on Industrial Electronics*, vol. 61, no. 4, pp. 2053–2061, Apr. 2014.

[126] Jérémy Dulout, Bruno Jammes, Lionel Séguier, and Corinne Alonso, 'Dimensionnement multi-objectif d'une association batterie – supercondensateur pour une application photovoltaïque', *JNRDM 2016*, Toulouse, p. pp.1-6, Mai-2016.

[127] Javier Silvente Saiz, 'Improving the tactical and operational decision making procedures in chemical supply chains', PhD dissertation, Department of Chemical Engineering, Technical University of Catalonia – Barcelona Tech, 2016.

[128] M. Iqbal, M. Azam, M. Naeem, A.S. Khwaja, and A. Anpalagan, 'Optimization classification, algorithms and tools for renewable energy: A review', *Renewable and Sustainable Energy Reviews*, vol. 39, pp. 640–654, Nov. 2014.

[129] W. D. Kellogg, M. H. Nehrir, G. Venkataramanan, and V. Gerez, 'Generation unit sizing and cost analysis for stand-alone wind, photovoltaic, and hybrid wind/PV systems', *IEEE Transactions on energy conversion*, vol. 13, no. 1, pp. 70–75, 1998.

[130] Lin Xu, Xinbo Ruan, Chengxiong Mao, Buhan Zhang, and Yi Luo, 'An Improved Optimal Sizing Method for Wind-Solar-Battery Hybrid Power System', *IEEE Transactions on Sustainable Energy*, vol. 4, no. 3, pp. 774–785, Jul. 2013.

[131] Tomislav Dragicevic, Hrvoje Pandzic, Davor Skrlec, Igor Kuzle, Josep M. Guerrero, and Daniel S. Kirschen, 'Capacity Optimization of Renewable Energy Sources and Battery Storage in an Autonomous Telecommunication Facility', *IEEE Transactions on Sustainable Energy*, vol. 5, no. 4, pp. 1367–1378, Oct. 2014.

[132] R.T. Marler and J.S. Arora, 'Survey of multi-objective optimization methods for engineering', *Structural and Multidisciplinary Optimization*, vol. 26, no. 6, pp. 369–395, Apr. 2004.

[133] Jürgen Branke, Kalyanmoy Deb, Kaisa Miettinen, and Roman Słowinski (Eds.), Eds., *Multiobjective optimization: interactive and evolutionary approaches*. Berlin ; New York: Springer, 2008.

[134] Yann Riffonneau, 'Gestion des flux énergétiques dans un système photovoltaïque avec stockage connecté au réseau – Application à l'habitat', PhD dissertation, Université Joseph-Fourier-Grenoble I, 2009.

[135] Hao Liang and Weihua Zhuang, 'Stochastic Modeling and Optimization in a Microgrid: A Survey', *Energies*, vol. 7, no. 4, pp. 2027–2050, Mar. 2014.

[136] Ning Xiong, Daniel Molina, Miguel Leon Ortiz, and Francisco Herrera, 'A Walk into Metaheuristics for Engineering Optimization: Principles, Methods and Recent Trends', *International Journal of Computational Intelligence Systems*, vol. 8, no. 4, pp. 606–636, Jul. 2015.

[137] Jesús A. De Loera, Raymond Hemmecke, and Matthias Köppe, 'PARETO OPTIMA OF MULTICRITERIA INTEGER LINEAR PROGRAMS', *Informs Journal on Computing*, vol. 21, no. 1, pp. 39–48, 2008.

[138] Mohamed Cheikh, Bassem Jarboui, Taïcir Loukil, and Patrick Siarry, 'A method for selecting Pareto optimal solutions in multiobjective optimization', *Journal of Informatics and Mathematical Sciences*, vol. 2, no. 1, pp. 51–62, 2010.

[139] Y.A. Katsigiannis, P.S. Georgilakis, and E.S. Karapidakis, 'Multiobjective genetic algorithm solution to the optimum economic and environmental performance problem of small autonomous hybrid power systems with renewables', *IET Renewable Power Generation*, vol. 4, no. 5, p. 404, 2010.

[140] Rodolfo Dufo-López *et al.*, 'Multi-objective optimization minimizing cost and life cycle emissions of stand-alone PV–wind–diesel systems with batteries storage', *Applied Energy*, vol. 88, no. 11, pp. 4033–4041, Nov. 2011.

[141] Dhaker Abbes, André Martinez, and Gérard Champenois, 'Life cycle cost, embodied energy and loss of power supply probability for the optimal design of hybrid power systems', *Mathematics and Computers in Simulation*, vol. 98, pp. 46–62, Apr. 2014.

[142] Subho Upadhyay and M.P. Sharma, 'A review on configurations, control and sizing methodologies of hybrid energy systems', *Renewable and Sustainable Energy Reviews*, vol. 38, pp. 47–63, Oct. 2014.

[143] Wei Zhou, Chengzhi Lou, Zhongshi Li, Lin Lu, and Hongxing Yang, 'Current status of research on optimum sizing of stand-alone hybrid solar–wind power generation systems', *Applied Energy*, vol. 87, no. 2, pp. 380–389, Feb. 2010.

[144] Sunanda Sinha and S.S. Chandel, 'Review of recent trends in optimization techniques for solar photovoltaic–wind based hybrid energy systems', *Renewable and Sustainable Energy Reviews*, vol. 50, pp. 755–769, Oct. 2015.

[145] K. Hirose, T. Shimakage, J. Reilly, and H. Irie, 'The sendai microgrid operational experience in the aftermath of the tohoku earthquake: a case study', *New Energy and Industrial Technology Development Organization*, vol. 308, 2013.

[146] R. Luna-Rubio, M. Trejo-Perea, D. Vargas-Vázquez, and G.J. Ríos-Moreno, 'Optimal sizing of renewable hybrids energy systems: A review of methodologies', *Solar Energy*, vol. 86, no. 4, pp. 1077–1088, Apr. 2012.

[147] A. Hina Fathima and K. Palanisamy, 'Optimization in microgrids with hybrid energy systems – A review', *Renewable and Sustainable Energy Reviews*, vol. 45, pp. 431–446, May 2015.

[148] P. Poonpun and W.T. Jewell, 'Analysis of the Cost per Kilowatt Hour to Store Electricity', *IEEE Transactions on Energy Conversion*, vol. 23, no. 2, pp. 529–534, Jun. 2008.

[149] Hongxing Yang, Zhou Wei, and Lou Chengzhi, 'Optimal design and techno-economic analysis of a hybrid solar–wind power generation system', *Applied Energy*, vol. 86, no. 2, pp. 163–169, Feb. 2009.

[150] Leland T. Blank and Anthony J. Tarquin, *Engineering economy*, 7th ed. New York: McGraw-Hill, 2012.

[151] Donald S. Remer and Armando P. Nieto, 'A compendium and comparison of 25 project evaluation techniques. Part 1: Net present value and rate of return methods', *International Journal of Production Economics*, vol. 42, no. 1, pp. 79–96, 1995.

[152] Christoph Rathgeber, Eberhard Lävemann, and Andreas Hauer, 'Economic top–down evaluation of the costs of energy storages—A simple economic truth in two equations', *Journal of Energy Storage*, vol. 2, pp. 43–46, Aug. 2015.

[153] Benedikt Battke, Tobias S. Schmidt, David Grosspietsch, and Volker H. Hoffmann, 'A review and probabilistic model of lifecycle costs of stationary batteries in multiple applications', *Renewable and Sustainable Energy Reviews*, vol. 25, pp. 240–250, Sep. 2013.

[154] Johannes Weniger, Tjarko Tjaden, and Volker Quaschning, 'Sizing of Residential PV Battery Systems', *Energy Procedia*, vol. 46, pp. 78–87, 2014.

[155] Roger A. Dougal, Shengyi Liu, and Ralph E. White, 'Power and life extension of battery-ultracapacitor hybrids', *IEEE Transactions on components and packaging technologies*, vol. 25, no. 1, pp. 120–131, 2002.

[156] Alon Kuperman and Ilan Aharon, 'Battery-ultracapacitor hybrids for pulsed current loads: A review', *Renewable and Sustainable Energy Reviews*, vol. 15, no. 2, pp. 981–992, Feb. 2011.

[157] Q. Cai, D.J.L. Brett, D. Browning, and N.P. Brandon, 'A sizing-design methodology for hybrid fuel cell power systems and its application to an unmanned underwater vehicle', *Journal of Power Sources*, vol. 195, no. 19, pp. 6559–6569, Oct. 2010.

[158] Yacine Gaoua, 'Modeles mathématiques et techniques d'optimisation non linéaire et combinatoire pour la gestion d'énergie d'un systeme multi-source: vers une implantation temps-réel pour différentes structures électriques de véhicules hybrides', PhD dissertation, École Doctorale Systèmes, Université Toulouse III, 2014.

[159] Nathalie Devillers, Marie-Cécile Péra, Daniel Bienaimé, and Marie-Laure Grojo, 'Influence of the energy management on the sizing of Electrical Energy Storage Systems in an aircraft', *Journal of Power Sources*, vol. 270, pp. 391–402, Dec. 2014.

[160] Fabio Ongaro, Stefano Saggini, and Paolo Mattavelli, 'Li-Ion Battery-Supercapacitor Hybrid Storage System for a Long Lifetime, Photovoltaic-Based Wireless Sensor Network', *IEEE Transactions on Power Electronics*, vol. 27, no. 9, pp. 3944–3952, Sep. 2012.

[161] A. Etxeberria, I. Vechiu, H. Camblong, and J.-M. Vinassa, 'Comparison of three topologies and controls of a hybrid energy storage system for microgrids', *Energy Conversion and Management*, vol. 54, no. 1, pp. 113–121, Feb. 2012.

[162] Valérie Dupé, Bruno Jammes, Lionel Séguier, and Corinne Alonso, 'Accurate power loss model of a boost cell in a multiphase converter for phase management', in *Power Electronics and Applications (EPE'14-ECCE Europe), 2014 16th European Conference on*, 2014, pp. 1–9.

[163] Jérémy Dulout, Amjad Anvari-Moghaddam, Adriana Luna, Bruno Jammes, Corinne Alonso, and Josep M. Guerrero, 'Optimal sizing of a lithium battery energy storage system for grid-connected photovoltaic systems', *IEEE Second International Conference on DC Microgrids (ICDCM 2017)*, pp. 582–587, Jun. 2017.

[164] Manuel Castillo-Cagigal, A. Gutiérrez, F. Monasterio-Huelin, Estefanía Caamaño-Martín, D. Masa, and J. Jiménez-Leube, 'A semi-distributed electric demand-side management system with PV generation for self-consumption enhancement', *Energy Conversion and Management*, vol. 52, no. 7, pp. 2659–2666, 2011.

[165] Angel Barroso, 'Optimisation des systèmes d'éclairage des bâtiments de l'université Toulouse III – Paul Sabatier basée sur un réseau novateur de type bus continu/basse tension', PhD dissertation, École Doctorale GEET, Université Toulouse III, 2017.

[166] Colin J. Humphreys, 'Solid-state lighting', *MRS bulletin*, vol. 33, no. 4, pp. 459–470, 2008.

[167] DOE SSL Program, 'Energy Savings Forecast of Solid-State Lighting in General Illumination Applications, [Accessed September 2017], Available: http://apps1.eere.energy.gov/buildings/publications/pdfs/ssl/energysavingsforecast14.pdf', Aug. 2014.

[168] DOE SSL Program, 'Solid-State Lighting R&D plan', *[Accessed October 2017], Available: https://energy.gov/sites/prod/files/2016/06/f32/ssl_rd-plan_%20jun2016_2.pdf*, Jun. 2016.

[169] Paolo Principi and Roberto Fioretti, 'A comparative life cycle assessment of luminaires for general lighting for the office – compact fluorescent (CFL) vs Light Emitting Diode (LED) – a case study', *Journal of Cleaner Production*, vol. 83, pp. 96–107, Nov. 2014.

[170] DOE SSL Program, 'Life-Cycle Assessment of Energy and Environmental Impacts of LED Lighting Products - Part I: Review of the Life-Cycle Energy Consumption of Incandescent, Compact Fluorescent, and LED Lamps', *technical report, february 2012 updated august 2012*.

[171] Jérémy Dulout *et al.*, 'Multi-objective methodology to find the optimal forward current to supply light emitting diode (LED) lightings', *IEEE Industry Applications Society Annual Meeting (IAS 2016)*, Oct. 2016.

[172] Jérémy Dulout *et al.*, 'Multiobjective optimal design of Light Emitting Diode (LED) lightings', *(Accepted - to be published) IEEE Industry Applications magazine*, pp. 1–9, Jul. 2018.

[173] B. Ackermann, V. Schulz, C. Martiny, A. Hilgers, and X. Zhu, 'Control of LEDs', in *Industry Applications Conference, 2006. 41st IAS Annual Meeting. Conference Record of the 2006 IEEE*, 2006, vol. 5, pp. 2608–2615.

[174] Ray-Lee Lin, Jhong-Yan Tsai, Shun-Yao Liu, and Hsin-Wei Chiang, 'Optimal Design of LED Array Combinations for CCM Single-Loop Control LED Drivers', *IEEE Journal of Emerging and Selected Topics in Power Electronics*, vol. 3, no. 3, pp. 609–616, Sep. 2015.

[175] S.Y. Hui and Y.X. Qin, 'A General Photo-Electro-Thermal Theory for Light Emitting Diode (LED) Systems', *IEEE Transactions on Power Electronics*, vol. 24, no. 8, pp. 1967–1976, Aug. 2009.

[176] U.S. Department of Energy, 'LED Measurement Series: LED Luminaire Reliability', Oct. 2009.

[177] Leena Tähkämö, Marjukka Puolakka, Liisa Halonen, and Georges Zissis, 'Comparison of Life Cycle Assessments of LED Light sources', *Journal of Light & Visual Environment*, vol. 36, no. 2, pp. 44–54, 2012.

[178] UCPTE and UCTE, 'The 50 Year Success Story – Evolution of a European Interconnected Grid', 2009.

[179] Juan Vasquez, Josep Guerrero, Jaume Miret, Miguel Castilla, and Luis Garcia de Vicuna, 'Hierarchical Control of Intelligent Microgrids', *IEEE Industrial Electronics Magazine*, vol. 4, no. 4, pp. 23–29, Dec. 2010.

[180] Omid Palizban, Kimmo Kauhaniemi, and Josep M. Guerrero, 'Microgrids in active network management—Part I: Hierarchical control, energy storage, virtual power plants, and market participation', *Renewable and Sustainable Energy Reviews*, vol. 36, pp. 428–439, Aug. 2014.

[181] Eneko Unamuno and Jon Andoni Barrena, 'Hybrid ac/dc microgrids—Part II: Review and classification of control strategies', *Renewable and Sustainable Energy Reviews*, vol. 52, pp. 1123–1134, Dec. 2015.

[182] J.A.P. Lopes, C.L. Moreira, and A.G. Madureira, 'Defining Control Strategies for MicroGrids Islanded Operation', *IEEE Transactions on Power Systems*, vol. 21, no. 2, pp. 916–924, May 2006.

[183] Yunjie Gu, Xin Xiang, Wuhua Li, and Xiangning He, 'Mode-Adaptive Decentralized Control for Renewable DC Microgrid With Enhanced Reliability and Flexibility', *IEEE Transactions on Power Electronics*, vol. 29, no. 9, pp. 5072–5080, Sep. 2014.

[184] Tomislav Dragicevic, Josep M. Guerrero, Juan C. Vasquez, and Davor Skrlec, 'Supervisory Control of an Adaptive-Droop Regulated DC Microgrid With Battery Management Capability', *IEEE Transactions on Power Electronics*, vol. 29, no. 2, pp. 695–706, Feb. 2014.

[185] Kai Sun, Li Zhang, Yan Xing, and J. M. Guerrero, 'A Distributed Control Strategy Based on DC Bus Signaling for Modular Photovoltaic Generation Systems With Battery Energy Storage', *IEEE Transactions on Power Electronics*, vol. 26, no. 10, pp. 3032–3045, Oct. 2011.

[186] Lexuan Meng *et al.*, 'Review on Control of DC Microgrids and Multiple Microgrid Clusters', *IEEE Journal of Emerging and Selected Topics in Power Electronics*, vol. 5, no. 3, pp. 928–948, Sep. 2017.

[187] Navid Eghtedarpour and Ebrahim Farjah, 'Distributed charge/discharge control of energy storages in a renewable-energy-based DC micro-grid', *IET Renewable Power Generation*, vol. 8, no. 1, pp. 45–57, Jan. 2014.

[188] Yu Zhang, Nikolaos Gatsis, and Georgios B. Giannakis, 'Robust Energy Management for Microgrids With High-Penetration Renewables', *IEEE Transactions on Sustainable Energy*, vol. 4, no. 4, pp. 943–953, Oct. 2013.

[189] Jérémy Dulout, Adriana Luna, Amjad Anvari-Moghaddam, Corinne Alonso, Josep M. Guerrero, and Bruno Jammes, 'Optimal scheduling of a battery-based energy storage system for a microgrid with high penetration of renewable sources', *ELECTRIMACS 2017*, pp. 1–6, Jul. 2017.

[190] energinet.dk, 'Download of market data (Danish electricity grid), https://en.energinet.dk/Electricity/Energy-data', Oct-2017. .

[191] Jérémy Dulout, Corinne Alonso, Lionel Séguier, and Bruno Jammes, 'Development of a photovoltaic low voltage dc microgrid for buildings with energy storage systems', *ELECTRIMACS 2017*, pp. 1–6, Jul. 2017.

[192] G. AlLee and W. Tschudi, 'Edison Redux: 380 Vdc Brings Reliability and Efficiency to Sustainable Data Centers', *IEEE Power and Energy Magazine*, vol. 10, no. 6, pp. 50–59, Nov. 2012.

[193] J. Schonbergerschonberger, R. Duke, and S.D. Round, 'DC-Bus Signaling: A Distributed Control Strategy for a Hybrid Renewable Nanogrid', *IEEE Transactions on Industrial Electronics*, vol. 53, no. 5, pp. 1453–1460, Oct. 2006.

[194] Jérémy Dulout, Bruno Jammes, Lionel Séguier, and Corinne Alonso, 'Control and design of a hybrid energy storage system', *EPE'15 ECCE Europe*, pp. 1–9, Sep. 2015.

[195] F. Huet, 'A review of impedance measurements for determination of the state-of-charge or state-of-health of secondary batteries', *Journal of power sources*, vol. 70, no. 1, pp. 59–69, 1998.

[196] Yaxiao Qin, Deyan Lin, and S.Y. Hui, 'A Simple Method for Comparative Study on the Thermal Performance of LEDs and Fluorescent Lamps', *IEEE Transactions on Power Electronics*, vol. 24, no. 7, pp. 1811–1818, Jul. 2009.

Appendices

Appendix 3.A - Recommended charge/discharge method for batteries

Lead-acid batteries and lithium-ion batteries have to follow some specific operating conditions such as the constant current – constant voltage (CC-CV) charging method. A typical CC-CV charge of a lithium-ion battery is presented in Fig. Appendix 3.1. Typical C-rates for charging lead-acid and lithium-ion batteries are 0.4 C and 1 C, respectively. This enables to charge between 65% and 80% of the total battery nominal capacity. This charge is followed by the constant voltage charging phase which exhibits a current limitation (following an exponential decay). Depending on manufacturers, the battery is fully charged either when a cut-off current equal to 3% of the nominal C-rate is reached or after a given time of processing in this phase such as 2 hours. This second phase is necessary to fully charge a battery but it makes the charge far slower. In this case, the advantage of SCs is that there is not a limiting charging method such as CC-CV, so the full charge of SC can be very fast.

Due to the poor energy efficiency of lead-acid batteries compared to lithium-ion batteries, manufacturers often recommend to apply a charge factor of 1.2. It means that the battery has to be charged 1.2 times more than it has been discharged to recover its initial state of charge. This is mainly due to the bad efficiency during the CV charge when parasitic reactions (such as water electrolysis) occur.
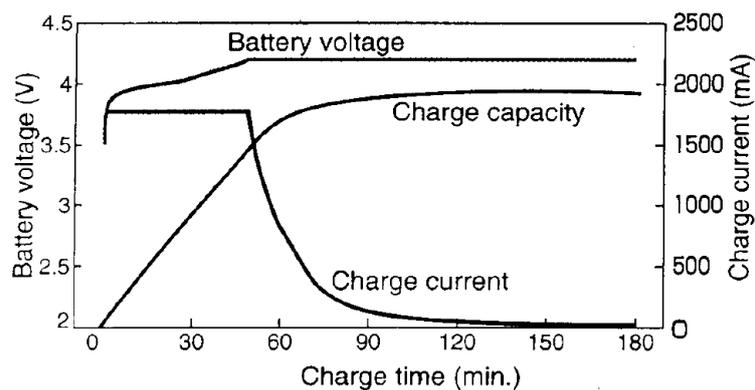

Figure Appendix 3.1 Typical recommended CC–CV charging method applied to a lithium battery

In order to determine when a battery is fully discharged, there is only one stop condition related to a cut-off voltage that is generally given by the manufacturer.

Appendix 3.B - Datasheets of energy storage systems

- **Sealed lead-acid battery (7 Ah 12 V, Yuasa)**

YUASA

YUCEL Y7-12 SPECIFICATION SHEET

Specifications

1) Nominal Voltage	12V
2) Nominal Capacity	
20 hour rate 350 ma to 10.50V	7.0 Ah
10 hour rate 650 ma to 10.50V	6.5 Ah
5 Hour rate 1190 ma to 10.20V	5.95 Ah
1 Hour rate 4200 ma to 9.60V	4.2 Ah
3) Weight (approx.)	2800gm
4) Energy Density (20Hr rate)	91 Wh / litre
5) Specific Energy (10Hr rate)	30 Wh / Kg
6) Internal Resistance (approx.)	30 mΩ (approx)
7) Maximum Discharge Current	40 A
8) Maximum Short Duration Discharge Current	210 A
9) Operating Temperature Range	
Charge:	-15°C to 50°C
Discharge:	-20°C to 60°C
10) Charge Retention at 20°C	
1 month	97%
3 months	91%
6 months	85%
11) Life Expectancy (standby use)	3 to 5 years @ 20°C
12) Sealed Construction	can be operated/charged without leakage
13) Standard Terminal	Faston Tab 187
14) Housing Material	ABS resin

Dimensions

Length	151.0 mm	±1 mm
Width	65.0 mm	±1 mm
Height	97.5 mm	±2 mm

- **Sealed lead-acid battery (1.2 Ah 7 V, Yuasa)**

NP SERIES - NP 1.2-6

Reliability is your Security

Utilizing the latest advance design Oxygen Recombination Technology, Yuasa have applied their 80 years experience in the lead acid battery field to produce the optimum design of Sealed Lead Acid batteries.

FEATURES

- Superb recovery from deep discharge.
- Electrolyte suspension system.
- Gas Recombination.
- Multipurpose: Float or Cyclic use.
- Usable in any orientation.
- Superior energy density.
- Lead calcium grids for extended life.
- Manufactured World wide.
- Application specific designs.

Technical Features

Sealed Construction

Yuasa's unique construction and sealing technique ensures no electrolyte leakage from case or terminals.

Electrolyte Suspension System

All NP batteries utilize Yuasa's unique electrolyte suspension system incorporating a microfine glass mat to retain the maximum amount of electrolyte in the cells. The electrolyte is retained in the separator material and there is no free electrolyte to escape from the cells. No gels or other contaminants are added.
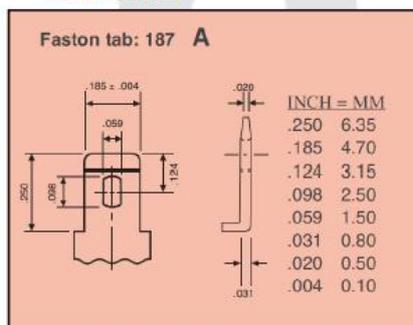
Control of Gas Generation

The design of Yuasa's NP batteries incorporates the very latest oxygen recombination technology to effectively control the generation of gas during normal use.
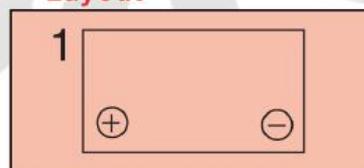
Low Maintenance Operation

Due to the perfectly sealed construction and the recombination of gasses within the cell, the battery is almost maintenance free.

Data Sheet

Terminals

NP batteries are manufactured using a range of terminals which vary in size and type. Please refer to details as shown.

Operation in any Orientation

The combination of sealed construction and Yuasa's unique electrolyte suspension system allows operation in any orientation, with no loss of performance or fear of electrolyte leakage.

Valve Regulated Design

The batteries are equipped with a simple, safe, low pressure venting system which releases excess gas and automatically reseals should there be a build up of gas within the battery due to severe overcharge. Note. On no account should the battery be charged in a sealed container.

General Specifications

Nominal Capacity (Ah)	NP1.2-6
20hr to 1.75vpc 30°C	1.2
10hr to 1.75vpc 20°C	1.1
5hr to 1 .70vpc 20°C	1
1 hr to 1 .60vpc 20°C	0.7
Voltage	6
Energy Density (Wh.L.20hr)	58
Specific Energy (Wh.kg.20hr)	25
Int. Resistance (m.Ohms)	60
Maximum discharge (A)	12
Short Circuit current (A)	36
Dimensions (mm)	
Length	97
Width	25
Height overall	54.5
Weight (Kg)	0.31
Terminal	A
Layout	1
Terminal Torque Nm	-

Terminals

Faston tab: 187 **A**

INCH	= MM
.250	6.35
.185	4.70
.124	3.15
.098	2.50
.059	1.50
.031	0.80
.020	0.50
.004	0.10

Layout

1

$\oplus$ $\ominus$

www.yuasabatteries.com

NP

- **Lithium-ion battery (Samsung INR18650-30Q)**

Specification

SAMSUNG SDI SAMSUNG

Type		Typical INR18650-30Q
Chemistry		NCA
Dimension (mm)	Diameter	18.33 ± 0.07
	Height	64.85 ± 0.15
Weight (g)		45.6
Initial IR (mΩ AC 1kHz)		13.13 ± 2
Initial IR (mΩ DC (10A-1A))		19.94 ± 2
Nominal Voltage (V)		3.61
Charge Method (100mA cut-off)		CC-CV (4.2±0.05V)
Charge Time	Standard (min), 0.5C	134min
	Rapid (min), 4A	68min
Charge Current	Standard current (A)	1.5
	Max. current (A)	4.0
Discharge	End voltage (V)	2.5
	Max. cont. current (A)	15
Rated discharge Capacity	Standard (mAh) (0.2C)	3,040
	rated (mAh) (10A)	2,983

- **Supercapacitor module (16 V 500 F, Maxwell)**

DATASHEET 16V MODULES

FEATURES AND BENEFITS*

- Up to 1,000,000 duty cycles or 10 year DC life
- 16V DC working voltage
- Resistive or active cell balancing available
- Temperature output
- Overvoltage outputs available
- High power density
- Compact, rugged, fully enclosed splash-proof design

TYPICAL APPLICATIONS

- Wind turbine pitch control
- Transportation
- Heavy industrial equipment
- UPS systems

PRODUCT SPECIFICATIONS

ELECTRICAL	BMOD0500 P016 B01
Rated Capacitance	500 F
Minimum Capacitance, initial	500 F
Maximum Capacitance, initial	600 F
Maximum ESR$_{DC}$, initial	2.1 mΩ
Test Current for Capacitance and ESR$_{DC}$	100 A
Rated Voltage	16 V
Absolute Maximum Voltage	17 V
Absolute Maximum Current	1,900 A
Leakage Current at 25°C, maximum (B01 Suffix - VMS 2.0)	5.2 mA
Leakage Current at 25°C, maximum (B02 Suffix - Passive Balancing)	N/A
Maximum Series Voltage	750 V
Capacitance of Individual Cells	3,000 F
Maximum Stored Energy, Individual Cell	3.0 Wh
Number of Cells	6

Appendix 3.C - Rainflow counting method

The rainflow counting method is a useful method that enables to extract a list of cycles with their corresponding cycle depth from a random SOC evolution. The following figures are illustrating how the rainflow counting can be implemented. The presented method is the rainflow algorithm I presented in [116].
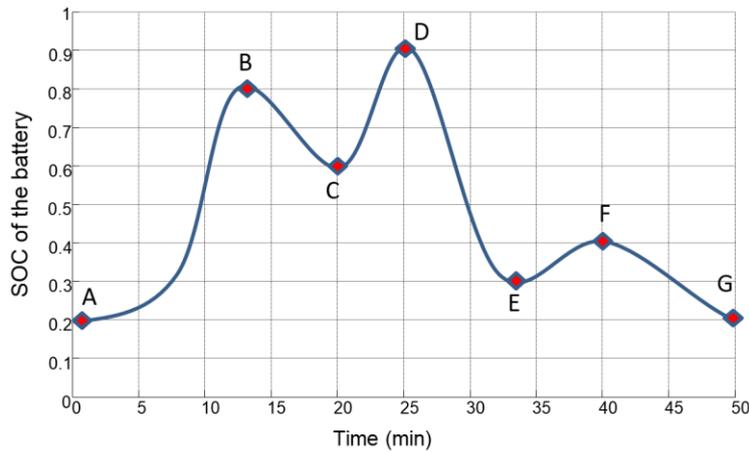

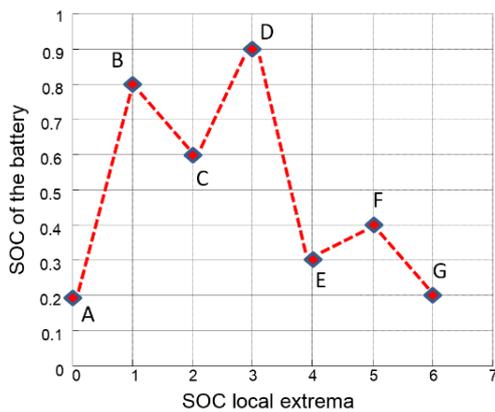*Figure Appendix 3.2 Example of SOC evolution*

Figure Appendix 3.3 List of local extrema obtained from the analysis of SOC evolution

Step 1- The SOC time series has to be transformed into a list of SOC extrema, as presented in Fig. Appendix 3.3.

Step 2- Place in a buffer, one segment (i.e. half-cycle such as [AB], [BC], [CD], etc.) with its respective cycle depth.

Step 3- If the actual segment is not bigger than the previous one, come back to step 2. If the segment is longer than the previous one, then a cycle has been performed with a cycle depth equal to the smaller segment. It is the case for [BC] in Fig. Appendix 3.4.
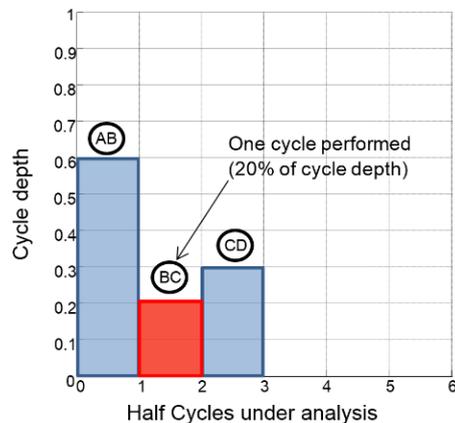

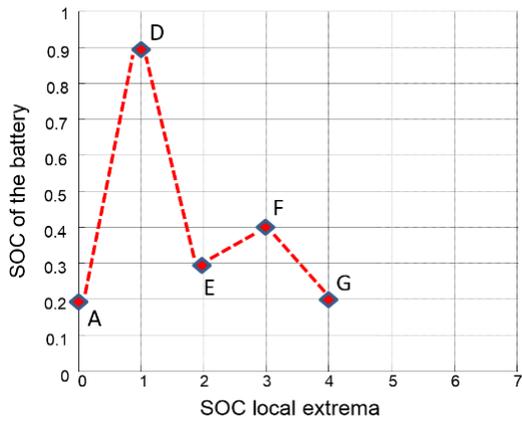*Figure Appendix 3.4 Comparison of half-cycles (buffer)*

Figure Appendix 3.5 Updated list of local extrema

Step 4- Discard the segment that has been used to count a cycle, see Fig. Appendix 3.5. Then come back to step 2.
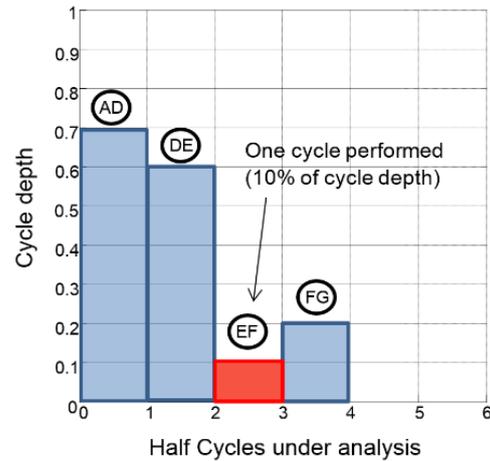

Figure Appendix 3.6 Updated buffer

Continuing the rainflow algorithm, the intermediary results are illustrated in Fig. Appendix 3.6 to 3.8.
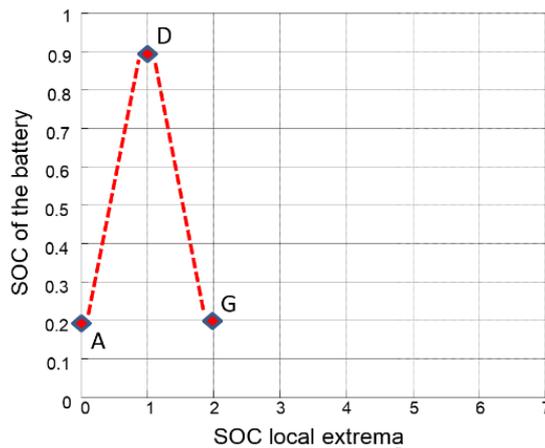

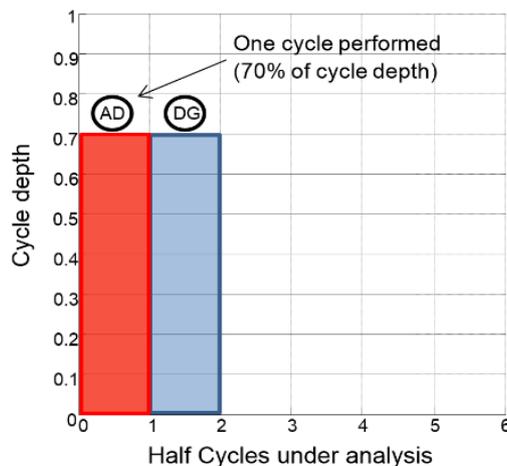Figure Appendix 3.7 Updated list of local extrema (2)

Figure Appendix 3.8 Updated buffer (2)

The final result is presented in Fig. Appendix 3.9, the point G at 0.2 SOC is stored for future processing.
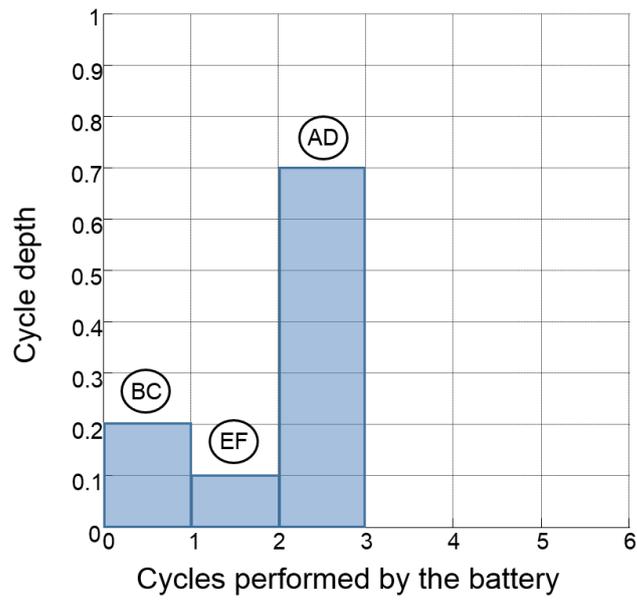

Figure Appendix 3.9 Cycles with their respective cycle depth obtained by rainflow counting algorithm

Appendix 3.D - Electrochemical impedance spectroscopy modelling

A typical equivalent circuit model and electrochemical impedance diagram of a battery are presented in Fig. Appendix 3.2 [120]. The parameter of the model are determined by EIS analysis, which is obtained by applying a sinusoidal excitation signal of small amplitude at a given frequency to the battery. This signal can be either a current (galvanostatic mode) or a voltage (potentiostatic mode), its frequency varies from very low frequencies (< 1 mHz) to high frequencies (> 100 Hz) and its amplitude must be very small to ensure that the AC voltage response of the battery stays close to 10 mV [195]. The impedance response (amplitude and phase shift) of the battery is calculated as follows:

$$Z(f) = \frac{\Delta U}{\Delta I} = \frac{U_{max}\,\sin(2\pi f)}{I_{max}\,\sin(2\pi f + \varphi)} \qquad \text{eq. 3.1}$$

In the equivalent circuit model depicted in Fig. Appendix 3.2-a, C_{DL} represents the charge transfer kinetics (capacitance of the electrical double layer at the electrolyte/electrode interface), $Z_{Electrode}$ reflects the electrode impedance and W is the Warburg impedance that models the diffusion processes of the cell.

In Fig. Appendix 3.2-b, the internal resistance of the battery is obtained when Im(Z) is equal to zero. Two capacitive loops are represented as semi-circles, the smallest one is related to the solid electrolyte interface (SEI) layer and the biggest models the charge transfer process and the electrical double layer capacitance. At low frequencies, the linear part reflects the diffusion process. An inductive part is sometimes represented at higher frequencies than 100 Hz [195].
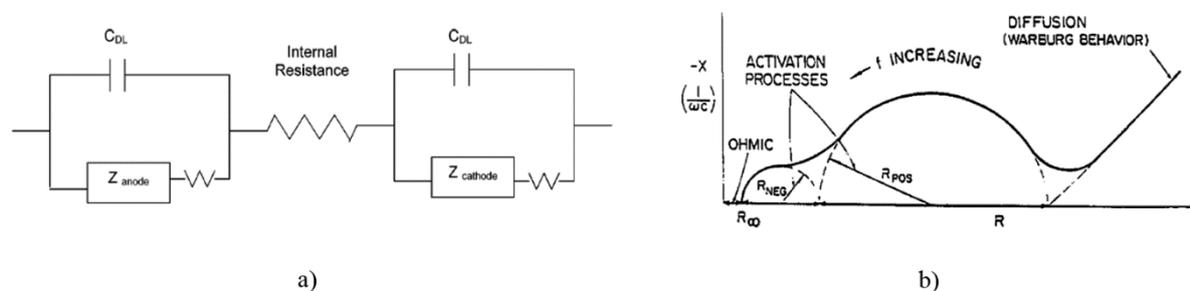

Figure Appendix 3.10 Electrochemical cell modelling by EIS
a) Typical equivalent circuit, b) Impedance spectrum in a Nyquist plot [120]

As for current pulses modelling, in order to have an accurate model of the battery, numerous EIS have to be done (for different SOC, C-rate, etc.). For more information, the parametrization of this model is well presented in [195].

Appendix 3.E – Internal resistance of a lead-acid battery for different C-rates

An illustrative example of relationship between the internal resistance and the C-rate of a lead-acid battery is presented in Fig. Appendix 3.4, based on some experiments done on a Yuasa 6V 1.2 Ah.
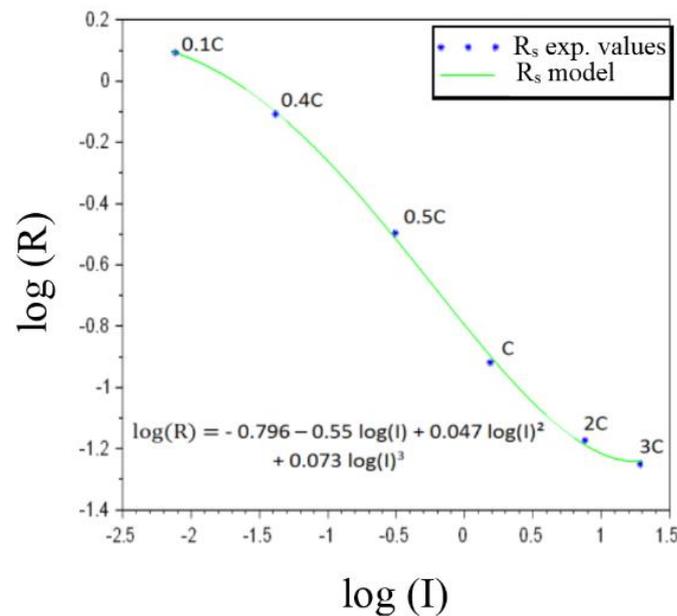

Figure Appendix 3.11 Relationship between internal resistance and C-rate for a lead-acid battery

It appears that the value of internal resistance is really varying depending on the C-rate. In this case, the internal resistance is decreasing for increasing C-rates. We used a log relation in order to find a simpler relationship but a good accuracy is obtained with at least a cubic function (third order polynomial), as presented in Fig. Appendix 3.4.

Appendix 4-A- LED light output

The measurements of LED light output have been performed after thermal stabilization (obtained after 40 minutes). Currents above 700 mA per LED have not been evaluated in order to prevent LED irreversible damage due to a too high junction temperature. Hence, the LED light output has been assessed from 0.1 mA to 700 mA.

According to Fig. Appendix 4.1, it appears that currents from 5 mA to 100 mA are the most effective in terms of luminous efficacy (lm/W).
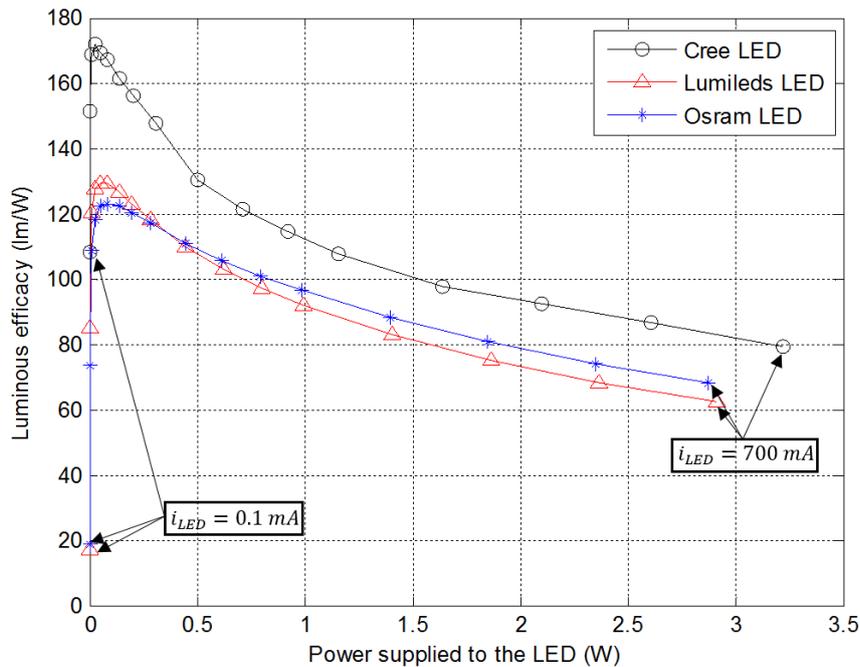

Figure Appendix 4.1 Luminous efficacy vs. Power for three different LEDs

Appendix 4-B- LED Thermal modelling

A complete LED system encompassing PCB and heatsink is presented in Fig. Appendix 4.2-A. An example of LED PCB footprint is illustrated in Fig Appendix 4.2-B.

As shown in Fig Appendix 4.2-C, a complete LED luminaire can be thermally modelled by a simple resistor network (static model). The objective of this study is to estimate the junction temperature of an LED (which is generally not accessible by measurements).
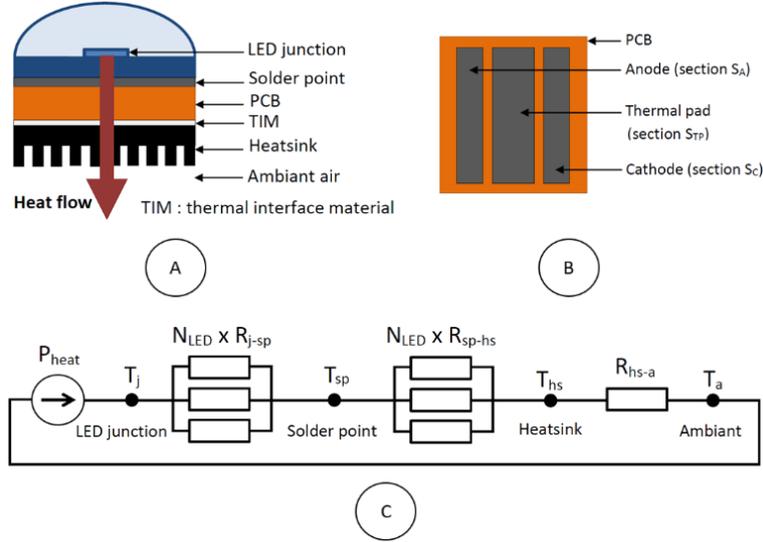

Figure Appendix 4.2 Simplified scheme of an LED system, B- PCB footprint of an LED, C- Thermal model of an LED luminaire

According to the circuit presented in Fig Appendix 4. 2-C, the solder point temperature can be evaluated for every supplied current. When N_{LED} LEDs are mounted on the same heatsink, the solder point temperature is:

$$T_{sp} = T_a + \left(\frac{1}{N_{LED}} R_{sp-hs} + R_{hs-a} \right) P_{heat}$$ eq. App. 1

where T_{sp} and T_a are the solder point and the ambient temperature (°C), respectively. R_{sp-hs} and R_{hs-a} are the thermal resistance between solder point and heatsink and the thermal resistance between heatsink and ambient (°C/W), respectively. P_{heat} is the amount of input power converted by the LED as heat (W). P_{heat} is defined as follows:

$$P_{heat} = \eta_{heat} N_{LED} V_f I_f$$ eq. App. 2

where η_{heat} refers to the power losses coefficient of an LED (0.85 is considered [196]). V_f and I_f are the forward voltage (V) and the forward current (A) of an LED, respectively.

The thermal resistance R_{sp-hs} is equal to the sum of thermal grease and PCB thermal resistances. These thermal resistances are evaluated through their thermal conductivity and their contact area to the LED.

A thermal resistance R_x is calculated as follows:

$$R_x = \frac{L}{k\,A}$$ eq. App. 3

where L is the thickness of the material x (mm), k is the conductivity of the material x (W/mK), A is the contact area (mm²) between the heating device and the material x (grey areas depicted in Fig. Appendix 4.2-B)

The thermal behavior of LED devices have been evaluated with the battery cycler BioLogic BCS-815 and the temperature chamber ESPEC SU-221 (presented in chapter 3). A heatsink with a thermal resistance of 1.2 K/W has been used with a silicone thermal grease (conductivity of 0.9 W/mK). LEDs have been assessed at 25°C with current pulses of 30 minutes from 50 mA to 700 mA by 50 mA. Rests of 30 minutes have been done between two pulses. The voltage across each LED is presented in Fig. Appendix 4.3 (very low dispersion between LEDs from the same manufacturer).
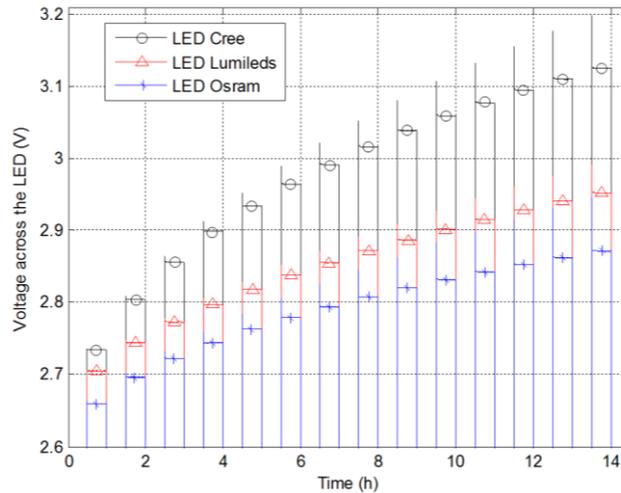

Figure Appendix 4.3 Voltage across each LED for different forward currents

The experimental and modelled solder point temperature are illustrated in Fig. Appendix 4.4.
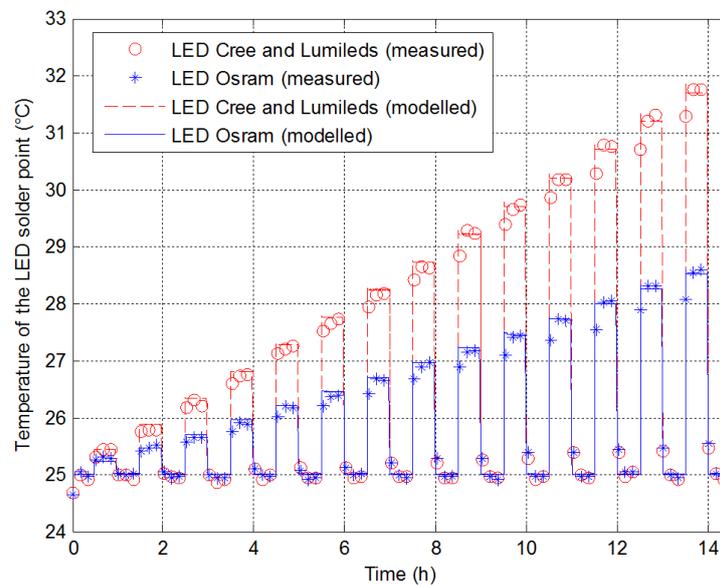

Figure Appendix 4.4 Evolution of LED solder point temperatures

The relationship between the junction temperature and the solder point of an LED is defined as:

$$T_j = T_{sp} + \frac{1}{N_{LED}} R_{j-sp} \, P_{heat} \qquad \text{eq. 4.1}$$

where T_j is the junction temperature of the LED (°C) and R_{j-sp} is the thermal resistance of the LED between junction and solder point (°C/W).

Appendix 4-C- LED lifetime model

According to [176], a simple lifetime model has been defined, as illustrated in Fig Appendix 4.5. The LED aging is considered to be dependant of the junction temperature and the forward current (lifetime is shorter for warmer junction temperature and higher current).
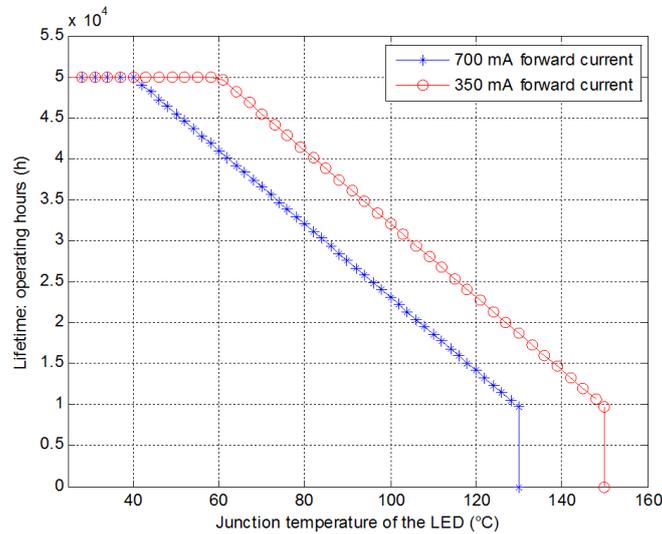
Figure Appendix 4.5 Simplified lifetime model of an LED [176]

The LED lifetime (years) can be calculated as follows:

$$n_{life} = \frac{Lifetime(\text{T}_{jLED}, \text{I}_f)}{T_{op\_year}}$$

<div align="right">eq. App. 4</div>

where $Lifetime(\text{T}_{jLED}, \text{I}_f)$ is the maximum number of operating hours for a given junction temperature and forward current, as described in Fig Appendix 4.5. T_{op_year} is the number of operating hours per year.

Appendix 4-D- Life cycle analysis (LCA) of an LED

Four main life stages have been studied to evaluate the energy consumed over the entire life of the product, as listed below:

- Manufacturing stage: the evaluation of this stage is difficult and needs some assumptions because of the confidentiality of industrial processes. Based on the method presented in [170], this stage represents a large part of the total LCA, as described in chapter 4, Fig. 4.17.

- Transportation stage: it represents less than one percent of the total LCA [170].

- Use stage: major impact on the LCA [169], [170], [177]. Considering a constant luminous flux over lifetime, the energy consumption (in MJ per functional unit) of the use stage is given by the following equation [170]:

$$E_{LCA} = \frac{3.6}{1000} \times P_{LED} \times Lifetime(T_{jLED}, I_f) \times C_{mix} \times N_{equ} \qquad \text{eq. 4.42}$$

where C_{mix} is the secondary to primary energy conversion factor based on the electricity production mix (in 2010 in EU, $C_{mix} = 2.45$ for electricity production [170]). N_{equ} is the number of equivalent LEDs satisfying both luminous flux and lifetime requirements to obtain the desired luminaire.

$$N_{equ} = \frac{F_d \times t_d}{F_{LED} \times Lifetime(T_{jLED}, I_f)} \qquad \text{eq. 4.43}$$

where t_d is the desired number of lighting hours. In this study, $t_d = T_{op\_year}$ because the LCA is assessed for one year of service.

A linear relation between the energy of the use stage LCA and the annual consumption of the luminaire can be written (see [172]):

$$E_{LCA} = \frac{3.6}{1000} \times C_{mix} \times t_d \times P_{Lum} \qquad \text{eq. 4.44}$$

When less than hundred LEDs are needed to make a luminaire, the use stage LCA is by far the main consuming stage of LED life, as shown in chapter 4, Fig. 4.17.

- End-of-life stage: the waste management is a major issue (especially toxic materials). Three scenarios have been assessed in [169] (complete recycling, disposal in a landfill and disposal in an incinerator). Energy that is consumed during the end-of-life stage represents up to 3% of the entire LCA and the difference between the three scenarios accounts for less than 1%. Nevertheless, recycling is the most efficient [169], [177].

Transportation and end-of-life stages have been neglected because of their low impact on the final results of the LCA.

Appendix 5.A- OPzV HOPPECKE batteries (6 V 300 Ah)

power.bloc OPzV

Valve regulated lead-acid batteries

Motive Power Systems
Reserve Power Systems
Special Power Systems
Service

Typical applications of HOPPECKE power.bloc OPzV

■ **Telecommunications**
Mobile phone stations
BTS-stations
Off-grid/on-grid solutions
■ **Traffic systems**
Signalling
Lighting
■ **Security lighting**

Similar to the Illustration

HOPPECKE
POWER FROM INNOVATION

Type overview
Capacities, dimensions and weights

Type	C_{nom}/1.80 V Ah	C_{10}/1.80 V Ah	C_5/1.77 V Ah	C_3/1.75 V Ah	C_1/1.67 V Ah	max.* Weight kg	max.* Length L mm	max.* Width W mm	max.* Height H mm	Fig.
12V 1 power.bloc OPzV 50	50	51	45	40	30	34.0	272	205	383	A
12V 2 power.bloc OPzV 100	100	101	89	80	61	52.0	272	205	383	A
12V 3 power.bloc OPzV 150	150	152	133	119	91	74.0	380	205	383	A
6V 4 power.bloc OPzV 200	200	202	178	159	121	51.0	272	205	383	B
6V 5 power.bloc OPzV 250	250	253	222	199	152	66.0	380	205	383	B
6V 6 power.bloc OPzV 300	300	304	266	239	182	73.0	380	205	383	B

C_{nom} = nominal capacity at 10 h discharge according to DIN 40744
C_{10}, C_5, C_3 and C_1 = Capacity at 10 h, 5 h, 3 h and 1 h discharge
* according to DIN 40744 data to be unterstood as maximum values

Design life: up to 15 years

Appendix 5.B- Supercapacitor module (48 V 165 F, Maxwell)

DATASHEET 48V MODULES

FEATURES AND BENEFITS*

> Up to 1,000,000 duty cycles or 10 year DC life
> 48V DC working voltage
> Active cell balancing
> Temperature output
> Overvoltage outputs available
> High power density

TYPICAL APPLICATIONS

> Hybrid vehicles
> Rail
> Heavy industrial equipment
> UPS systems

PRODUCT SPECIFICATIONS

ELECTRICAL	BMOD0165 P048 BXX
Rated Capacitance	165 F
Minimum Capacitance, initial	165 F
Maximum Capacitance, initial	200 F
Maximum ESR $_{DC,}$ initial	6.3 mΩ
Test Current for Capacitance and ESR $_{DC}$	100 A
Rated Voltage	48 V
Absolute Maximum Voltage	51 V
Absolute Maximum Current	1,900 A
Leakage Current at 25°C, maximum	5.2 mA
Maximum Series Voltage	750 V
Capacitance of Individual Cells	3,000 F
Stored Energy, Individual Cell	3.0 Wh
Number of Cells	18

Appendix 5.C- OPA electrical scheme
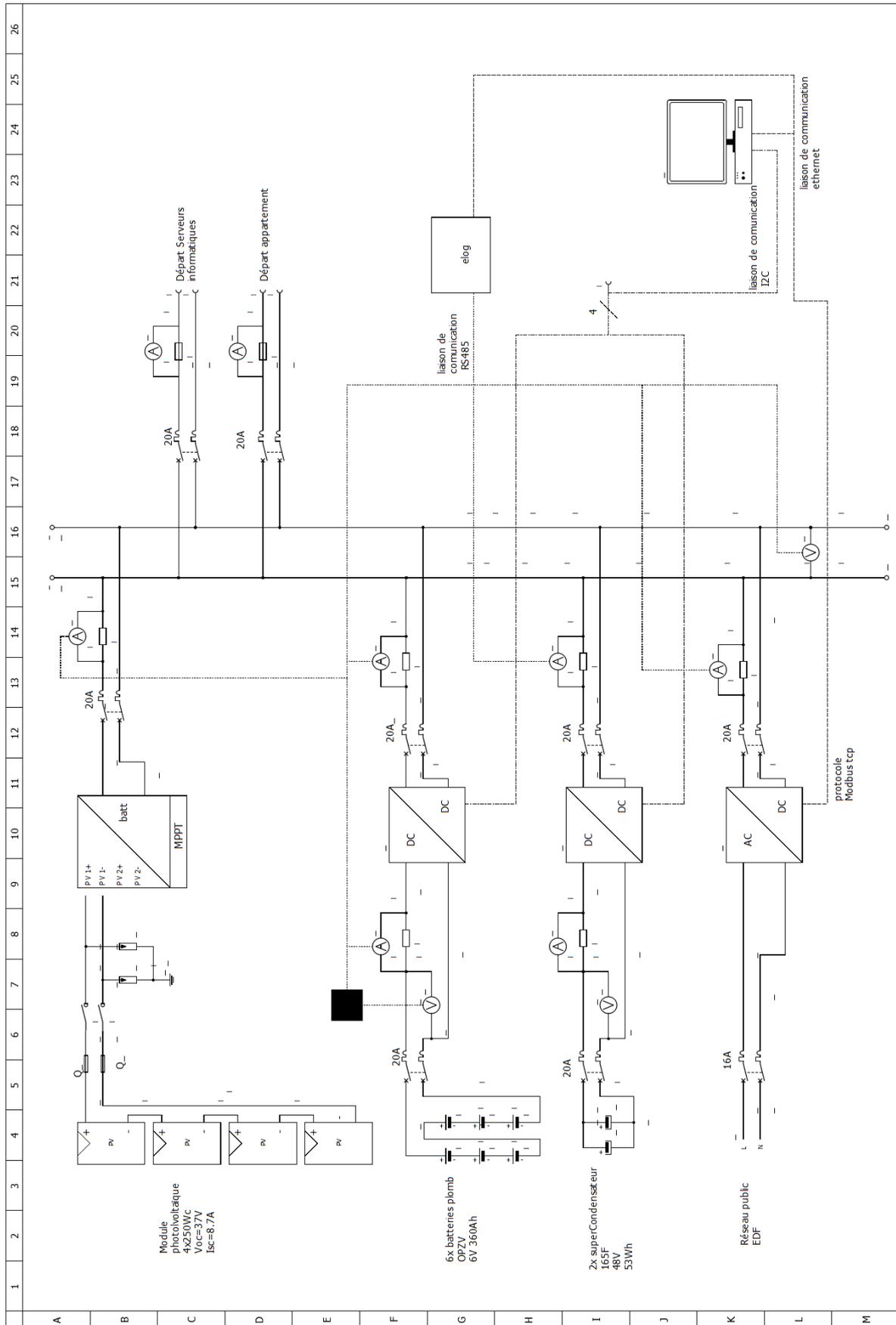
Appendix 5.D- Model of power converters (buck and boost)

This work, aiming at finding the transfer functions of buck and boost converters by taking into account several parasitic resistances, has been published in [194]:
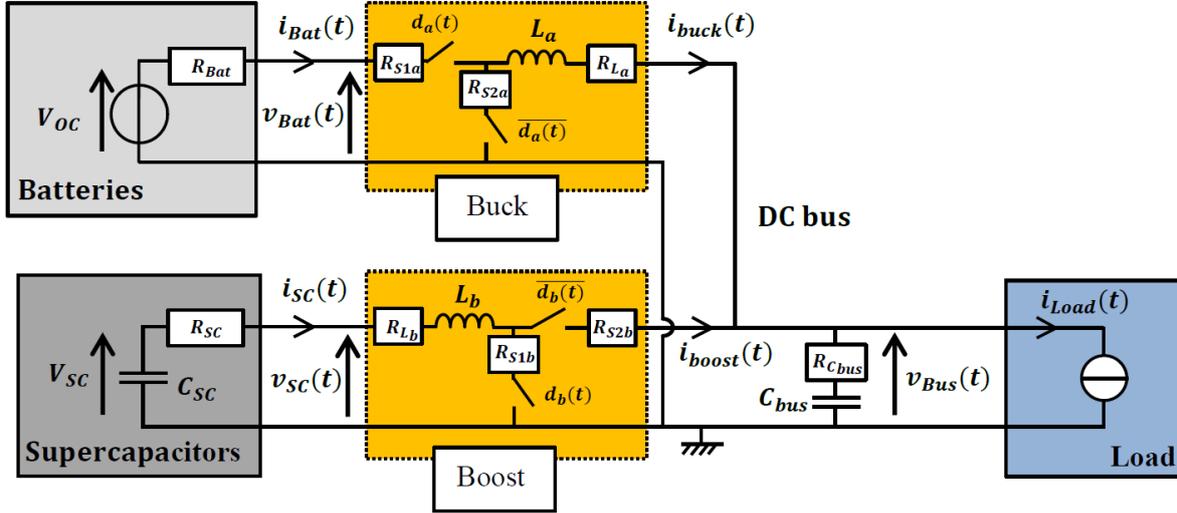

Figure Appendix 5.1 Equivalent circuit model of a hybrid energy storage system connected to a DC load

By linearizing the averaged equations of the converters over a switching time period and around a steady state operating point we get the HESS's average small signal model. For any signal x(t), $\tilde{x}$ is a small variation of x(t) around the nominal value X. The transfer functions of the converters are given by (Ap. 1.b), (Ap. 2.b) and (Ap. 3). For the design of the current loops regulators, we assume that $v_{Bus}(t)$ is constant (its dynamic is very slow compared to the current's dynamic). The regulation of the input current of the buck converter is not commonly used, but it is necessary in our case to deal with the nominal operating conditions of the battery.

By neglecting the variations of the input voltage, we find the following transfer function between $\widetilde{I_{Bat}(s)}$ and $\widetilde{D_a(s)}$ which are respectively the Laplace transform of the input current and the duty cycle of the buck converter:

$$\frac{\widetilde{I_{Bat}(s)}}{\widetilde{D_a(s)}} = \frac{L_a I_{buck}\, s + D_a\, V_{oc} + (R_{S2a} + R_{L_a})\, I_{buck} - (R_{Bat} + R_{S1a}) D_a I_{Bat}}{L_a\, s + (1 - D_a) R_{S2a} + R_{L_a} + (R_{Bat} + R_{S1a})\, D_a} \qquad \text{(Ap. 1.a)}$$

where s is the Laplace variable.

Assuming that $R_{Bat} \gg R_{S1a}$, $R_{L_a} \gg R_{S2a}$ and $R_{L_a} I_{buck} \approx R_{Bat} D_a I_{Bat}$ we can simplify the previous transfer function:

$$\frac{\widetilde{I_{Bat}(s)}}{\widetilde{D_a(s)}} = \frac{L_a I_{buck}\, s + D_a\, V_{oc}}{L_a\, s + R_{L_a} + R_{Bat}\, D_a} \qquad \text{(Ap. 1.b)}$$

By neglecting the variations of the input voltage, we can write:

$$\frac{\widetilde{I_{SC}(s)}}{\widetilde{D_b(s)}} = \frac{V_{bus} - R_{S1b} I_{SC}}{L_b s + D_b R_{S1b} + R_{SC} + R_{L_b} + (1 - D_b)^2 R_{S2b}} \qquad \text{(Ap. 2.a)}$$

Assuming that $R_{SC} \gg R_{S1b}$ and $R_{SC} \gg R_{S2b}$ we can simplify the previous transfer function:

$$\frac{\widetilde{I_{SC}(s)}}{\widetilde{D_b(s)}} = \frac{V_{bus}}{L_b s + R_{SC} + R_{L_b}} \qquad \text{(Ap. 2.b)}$$

Then, we have defined the transfer function of the bus voltage, considering that the current is only delivered by the buck converter:

$$\frac{\widetilde{V_{Bus}(s)}}{\widetilde{I_{Bat}(s)}} = \frac{R_{C_{bus}} C_{bus} s + 1}{D_a C_{bus} s} \qquad \text{(Ap. 3)}$$

We also looked at the transfer function of the bus voltage, considering that the current is only delivered by the boost converter:

$$\frac{\widetilde{V_{Bus}(s)}}{\widetilde{I_{SC}(s)}} = \frac{(1 - D_b) R_{C_{bus}} C_{bus} s + 1 - D_b}{C_{bus} s} \qquad \text{(Ap. 4)}$$

From (Ap.3) and (Ap.4), we can also write:

$$\frac{\widetilde{V_{Bus}(s)}}{\widetilde{I_{Bat}(s)}} = \frac{1}{D_a(1 - D_b)} \frac{\widetilde{v_{Bus}}}{\widetilde{i_{SC}}} = C_f \frac{\widetilde{v_{Bus}}}{\widetilde{i_{SC}}} \qquad \text{(Ap. 5)}$$

where C_f is a dimensionless factor.